PYRENE DERIVATIVES FOR THE MECHANICAL INTERLOCKING OF SWNTs: SYNTHESIS, PROPERTIES, AND POTENTIAL APPLICATIONS

Memoria presentada por

Alejandro López Moreno

Para optar al título de doctor en Química Orgánica

Departamento de Química Orgánica

Universidad Autónoma de Madrid

Madrid, 2016

Memoria presentada para optar al título de doctor en Química Orgánica

Director de tesis:

Dr. Emilio Pérez Álvarez

Tutor académico:

Dr. Giovanni Bottari

A mis padres y a mi hermana.

AGRADECIMIENTOS

En primer lugar, quiero agradecer a Emilio la oportunidad de realizar la tesis con él, la ayuda, el apoyo y todo lo que me ha enseñado, que me ha servido para ver la ciencia con otra luz.

No puedo seguir con otro que no sea David, una persona a la que admiro y el que me metió en esto. Gran científico, mejor amigo. No hay espacio para resumir lo que me has enseñado. Semper fi, chinato.

A Paco, por enseñarme y ayudarme en mis primeros pasos hasta llegar aquí.

Durante 4 años de tesis te encuentras con muchos compañeros pero solo unos pocos resultan ser amigos. Alberto, gracias por las risas, la ayuda, los buenos ratos, el apoyo en los malos y lo que he aprendido de ti. Pero lo importante, gracias por tu amistad. Leo, el ejemplo de que lo bueno viene en frasco pequeño, gracias por las cerves, las charlas, las risas, todo. A Sofía, por ser como eres, única, enorme como compañera, mejor como amiga. No hay adjetivos suficientes para ti. Emerson, o Emerick, como le gusta que le llamen, un tio grande del que no dudo que le irá muy bien, ya tengo el CV preparado. Gracias por los buenos momentos, por aguantarme en los malos, por los cocidos y por tu paciencia en Estrasburgo, ☺

Al resto del piso 2, Tere y Fran (los locos de arriba, gracias por las risas), Belén (la químico-física-orgánica) y Leire, los que pasaron por aquí: Mar, María, Prabhash, Javi; y los nuevos: Zulay, Matías, Enrique, Mariano, Julia (una pena no coincidir más tiempo con vosotros).

A Ricardo, por sus charlas de geopolítica, historia…. y Mourinho.

Al resto de IMDEA Nanociencia, a los muchos de los que he aprendido.

Notes, references, abbreviations and acronyms

In this thesis only published work has been presented. Many projects and results have been left out.

Bibliographic citations have been placed as footnotes in the pages where they were first cited in the section and at the end of each section or chapter; they were added independently at every section or chapter, so they are duplicated in different chapters when necessary.

Throughout this manuscript, abbreviations and acronyms recommended by the American Chemical Society in the Organic Chemistry area (revised in the *Journal of Organic Chemistry* on January **2016**; http://pubs.acs.org/paragonplus/submission/joceah/joceah_authguide.pdf) have been employed. In addition, those indicated below have also been used.

CNT	Carbon nanotube
MWNT	Multi-walled nanotube
SWNTS	Single-walled nanotube
CVD	Chemical Vapor Deposition
SDS	Sodium dodecylsulfate
SDBS	Sodium dodecylbenzenesulfonate
MIM	Mechanically interlocked molecules
MINT	Mechanically interlocked nanotubes
exTTF	π-extended tetrathiafulvalene
AFM	Atomic-force microscopy
PLE	Photoluminescence excitation
PAH	Polycyclic aromatic hydrocarbons
γ-CD	γ–cyclodextrin
PCA	Pyrenecarboxylic acid
PSA	Pyrenesulfonic acid
CYPs	Cytochromes P450

Fc	Ferrocene
NQ	1,4-naphtoquinone
AQ	9,10-anthraquinone
BQ	*para*-benzoquinone
EA	Electron affinity
ZPE	Zero-point energy
TGA	Thermogravimetric analysis
CP	Counterpoise
H	Host
G	Guest
DMA	Dynamic mechanical analysis

ABSTRACT

In this work we presented four main results:

(a) a mild catalytic method to oxidize PAHs and, in particular, pyrene, based on the use of a non-hemo iron catalyst, [Fe(bpmen)$(OTf)_2$], with H_2O_2 as the oxidant. In analogy with the oxidation of pyrene by natural CYPs, the method affords mainly 1,6- and 1,8-pyrenequinones. Furthermore, we studied the electron accepting properties of pyrenequinones both experimentally, through cyclic voltammetry, and theoretically, calculating their EAs.

(b) a simple procedure for the determination of association constants (K_a) between soluble molecules and insoluble and heterogeneous carbon nanotube samples. We report binding constants between five different hosts and two types of SWNTs in four solvents. We have determined numeric values of K_a in the range of $1–10^4$ M^{-1}. The results obtained experimentally were validated through state-of-the-art DFT calculations.

(c) the synthesis of rotaxane-type structures in which SWNTs act as threads, based on the previous works in which the mechanical bond is presented as a new tool for chemical manipulation of SWNTs. We used a U-shaped precursor featuring two derivatives of pyrene as units of a recognition element for SWNTs.

(d) the reinforcement of polymers by mechanically interlocked derivatives of single-walled carbon nanotubes (SWNTs). We compare the mechanical properties of fibers made of polymers and of composites with pristine single-walled carbon nanotubes (SWNTs), mechanically interlocked derivatives of SWNTs (MINTs) and the corresponding supramolecular models.

RESUMEN

En este trabajo se presentan cuatro resultados principales:

(a) un método de oxidación suave de hidrocarburos policíclicos aromáticos, en particular pireno, basado en el uso de un catalizador de hierro no-hemo, [Fe(bpmen)$(OTf)_2$], con H_2O_2 como oxidante. Análogamente a la oxidación llevada a cabo por Citocromos P450, el método da lugar a 1,6- y 1,8-pirenoquinonas. Además, estudiamos las propiedades electroaceptoras de las mismas, experimentalmente, por voltametría cíclica, y teóricamente, calculando sus afinidades electrónicas.

(b) un procedimiento sencillo para la determinación de constantes de asociación (K_a) entre moléculas solubles y de nanotubos de carbono insolubles y heterogéneos. Se presentan las constantes de asociación entre cinco moléculas diferentes y dos tipos de SWNTs en cuatro disolventes. Hemos determinado valores numéricos de K_a en el rango de $1\text{-}10^4$ M^{-1}. Los resultados obtenidos experimentalmente fueron validados mediante cálculos de DFT.

(c) la síntesis de estructura tipo rotaxano basada en nanotubos de carbono. Se usaron un receptor en forma de U compuesto por dos unidades de pireno, con gran afinidad por SWNTs, separadas por un espaciador aromático y decoradas con dos cadenas alquílicas terminadas en dos alquenos. Mediante una reacción de cierre de anillo, se obtuvieron derivados mecánicamente enlazados.

(d) el estudio de las propiedades mecánicas de los nanotubos de carbono mecánicamente enlazados. Se comparan las propiedades de fibras de polímero y de composites preparados con nanotubos sin modificar, MINT y los correspondientes complejos supramoleculares.

TABLE OF CONTENTS

1. INTRODUCTION 3
   1.1. Carbon Nanotubes 3
      1.1.1. Properties 5
      1.1.2. Functionalization of SWNTs 6
         1.1.2.1. Covalent functionalization 6
         1.1.2.2. Non-covalent functionalization 12
         1.1.2.3. Mechanically Interlocked Carbon Nanotubes 16
   1.2. Pyrene 23
      1.2.1. Properties 23
      1.2.2. Functionalization of pyrene 28
         1.2.2.1. Positions 1, 3, 6 and 8 29
         1.2.2.2. Positions 2 and 7 31
         1.2.2.3. Positions 4, 5, 9 and 10 32
   1.3. References 34
2. OBJECTIVES 47
3. Biomimetic oxidation of pyrene and related aromatic hydrocarbons. Unexpected electron accepting abilities of pyrenequinones 51
   3.1. Introduction 51
   3.2. Results and discussion 54
   3.3. Conclusions 61
   3.4. Experimental section 61
   3.5. References 77
4. Determination of association constants towards carbon nanotubes 83
   4.1. Introduction 84
   4.2. Results and discussion 85

4.3. Conclusions 98
4.4. Experimental section 100
4.5. References 123
5. Pyrene-based mechanically interlocked SWNTs 126
5.1. Introduction 126
5.2. Results and discussion 129
5.3. Conclusions 136
5.4. Experimental section 136
5.5. References 161
6. Threading through macrocycles enhances the performance of carbon nanotubes as polymer fillers 165
6.1 Introduction 166
6.2 Results and discussion 169
6.3 Conclusions 177
6.4 Experimental section 178
6.5 References 192
7. CONCLUSIONS 199

INTRODUCTION

1. Introduction

1.1. Carbon nanotubes

With diamond, graphite/graphene, and fullerene, carbon nanotubes (CNTs) are another allotrope form of carbon. Firstly reported by Ijima,[1] multi-walled carbon nanotubes (MWNTs) were discovered in carbon soot of graphite electrodes during an arc-discharge method. CNTs are tubular in shape, made of rolled-up graphene sheets. Those tubes contained at least two or more layers and ranged in outer diameter from 3 nm to 30 nm. Two years later, Ijima[2] reported single-wall carbon nanotubes (SWNTs). The single-wall nanotubes are generally narrower than the multiwall tubes, with diameters in the range 1-2 nm, and tend to be curved rather than straight, due to the presence of defects in their walls.

The structure of carbon nanotubes has been extensively reviewed.[3] SWNTs can be separated in three types: armchair, zigzag, and chiral. The difference in these types of SWNTs is created depending on how the graphene layer is rolled up. The indices *m* and *n* represent the chiral vector, which correspond to the number of unit vectors along the two directions in the honeycomb crystal lattice of graphene. Depending on the values of *m* and *n*. When m = 0, the nanotube is called "zigzag", when m = n, the nanotube is called "armchair", and "chiral nanotubes" encompass all other configurations.

[1] S. Iijima. *Nature*, **1991,** *354*, 56-58.
[2] S. Iijima, T. Ichihashi. *Nature*, **1993**, *363*, 603-605.
[3] (a) M. Terrones. *Annu. Rev. Mater. Res.*, **2003,** *33*, 419-501; (b) M. Zhang, J. Li. *Mater. Today*, **2009,** *12*, 12-18.

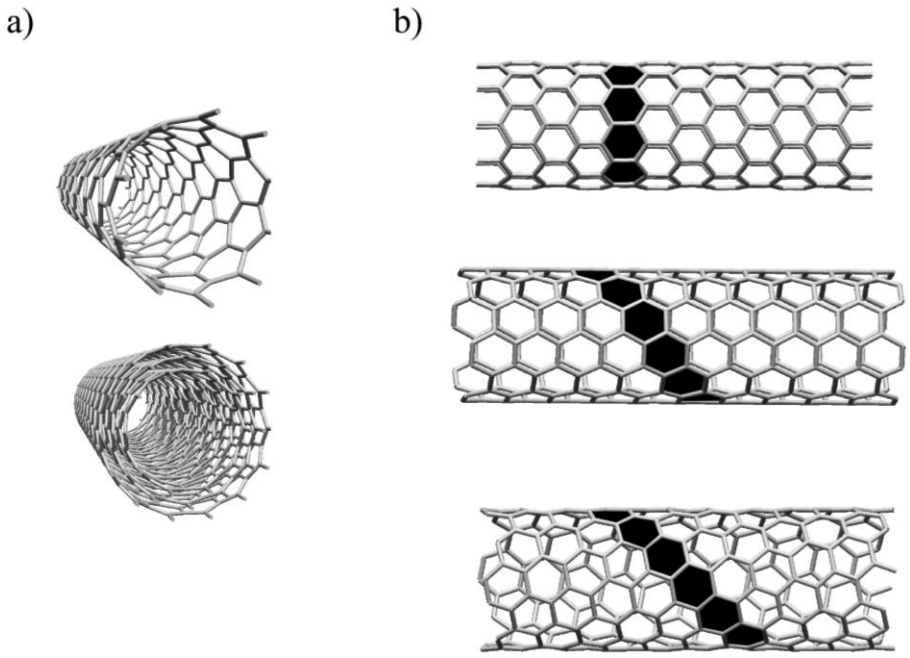

Figure 1. Molecular representations of a) SWCNT (top) and MWCNT (bottom); and b) (10,0) zigzag (top), (6,6) armchair (middle) and (8,4) chiral (bottom) nanotubes.

Different techniques have been developed to produce SWNTs and MWNTs with different structure and morphology. There are three methods commonly used to synthesize nanotubes: arc discharge,[4] laser ablation,[5] and chemical vapor deposition (CVD).[6]

1.1.1. Properties

Carbon nanotubes have outstanding mechanical properties due to the strength of the sp^2 carbon-carbon bonds. Not only these great mechanical

[4] (a) T. W. Ebbesen, P. M. Ajayan. *Nature*, **1992,** *358*, 220-222; (b) C. Journet, W. K. Maser, P. Bernier, A. Loiseau, M. L. de la Chapelle, S. Lefrant, P. Deniard, R. Lee, J. E. Fischer. *Nature*, **1997,** *388*, 756-758.
[5] T. Guo, P. Nikolaev, A. Thess, D. T. Colbert, R. E. Smalley. *Chem. Phys. Lett.*, **1995,** *243*, 49-54.
[6] (a) J. Kong, A. M. Cassell, H. Dai. *Chem. Phys. Lett.*, **1998,** *292*, 567-574; (b) M. Su, B. Zheng, J. Liu. *Chem. Phys. Lett*., **2000,** *322*, 321-326.

properties but also thermal and electronic properties make carbon nanotubes an extraordinary and promising building block for nanotechnology.

CNTs densities can be as low as 1.3 g/cm^3 (one-sixth of that of stainless steel). They present Young's moduli greater than 1TPa and a tensile strength up to 63 GPa, which are 5 and 50 times larger than stainless steel properties, respectively.[7] Additionally, carbon nanotubes have excellent chemical stability and high thermal conductivity (~3000 W/mK).

Their electronic properties are also extraordinary. SWNTs can be metallic or semiconducting depending on the relationship between the axial direction and the unit vectors describing the hexagonal lattice. Semiconducting nanotubes have defined bandgaps that scale inversely with diameter, ranging from approximately 1.8 eV for very small diameter tubes to 0.18 eV for the widest known SWNTs.

These outstanding properties make SWNTs suitable to be used in a wide range of applications such as electrodes,[8] supercapacitors,[9] active materials in field effect transistor,[10] photovoltaic devices,[11] sensors,[12] catalysis,[13]

[7] (a) M.-F. Yu, B. S. Files, S. Arepalli, R. S. Ruoff. . *Phys. Rev. Lett.*, **2000,** *84*, 5552-5555; (b) S. Xie, W. Li, Z. Pan, B. Chang, L. Sun. *J. Phys. Chem. Solids*, **2000,** *61*, 1153-1158.

[8] (a) S. H. Ng, J. Wang, Z. P. Guo, J. Chen, G. X. Wang, H. K. Liu. *Electrochim. Acta*, **2005,** *51*, 23-28; (b) M. J. Kim, D. W. Shin, J.-Y. Kim, S. H. Park, I. t. Han, J. B. Yoo. *Carbon*, **2009,** *47*, 3461-3465; (c) A. L. M. Reddy, M. M. Shaijumon, S. R. Gowda, P. M. Ajayan. *Nano Lett.*, **2009,** *9*, 1002-1006.

[9] (a) W. Lu, L. Qu, K. Henry, L. *J. Power Sources*, **2009,** *189*, 1270-1277; (b) D. N. Futaba, K. Hata, T. Yamada, T. Hiraoka, Y. Hayamizu, Y. Kakudate, O. Tanaike, H. Hatori, M. Yumura, S. Iijima. *Nat Mater*, **2006,** *5*, 987-994; (c) C. Du, N. Pan. *J. Power Sources*, **2006,** *160*, 1487-1494.

[10] A. Wurl, S. Goossen, D. Canevet, M. Sallé, E. M. Pérez, N. Martín, C. Klinke. *J. Phys. Chem. C*, **2012,** *116*, 20062-20066.

[11] (a) M. Bernardi, J. Lohrman, P. V. Kumar, A. Kirkeminde, N. Ferralis, J. C. Grossman, S. Ren. *ACS Nano*, **2012,** *6*, 8896-8903; (b) H. Wang, G. I. Koleilat, P. Liu, G. Jiménez-Osés, Y.-C. Lai, M. Vosgueritchian, Y. Fang, S. Park, K. N. Houk, Z. Bao. *ACS Nano*, **2014,** *8*, 2609-2617.

[12] (a) B. Esser, J. M. Schnorr, T. M. Swager. *Angew. Chem. Int. Ed.*, **2012,** *51*, 5752-5756; (b) A. M. Münzer, Z. P. Michael, A. Star. *ACS Nano*, **2013,** *7*, 7448-7453.

[13] (a) A. Le Goff, V. Artero, B. Jousselme, P. D. Tran, N. Guillet, R. Métayé, A. Fihri, S. Palacin, M. Fontecave. *Science*, **2009,** *326*, 1384-1387; (b) V. Lordi, N. Yao, J. Wei. *Chem. Mater.*, **2001,** *13*, 733-737; (c) L. Jiang, H. Gu, X. Xu, X. Yan. *J. Mol. Catal. A: Chem.*, **2009,** *310*, 144-149; (d) X. Tan, W. Deng, M. Liu, Q. Zhang, Y. Wang. *Chem. Commun.*, **2009**, 7179-7181; (e) J. A. Sullivan, K. A. Flanagan, H. Hain. *Catal. Today*, **2009,** *145*, 108-113.

biomedicine[14] or nanotube-polymer composites, as extensively reviewed Schnorr and Swager.[15]

1.1.2. Functionalization of SWNTs

Despite the fact that pristine SWNTs can be used in many applications, many uses demand their chemical modification in order to purify them, improve their solubility and/or modulate their properties. Nowadays, there are two main general ways of functionalization of SWNTs: covalent functionalization and non-covalent or supramolecular functionalization.

1.1.2.1. Covalent Functionalization

Covalent functionalization is usually an irreversible process. It is based on the formation of a covalent linkage between functional entities and the carbon skeleton of nanotubes. Reactions can be performed at the sidewall or at the defect sites, localized usually at the tips. Due to the importance of this process for the application of carbon nanotubes in different fields, extensive work have been published and reviewed.[16]

Two main routes have been developed for covalent functionalization: amidation or esterification of oxidized SWNTs and addition chemistry to the walls of SWNTs.

In the first case, previous oxidation of the SWNTs is necessary to carry out amidation or esterification reactions. The use of strong acids and ultrasonication or heating produces nanotubes with different oxygenated function.[17] These oxidized SWNTs feature numerous –COOH functionalities

[14] (a) G. Cellot, E. Cilia, S. Cipollone, V. Rancic, A. Sucapane, S. Giordani, L. Gambazzi, H. Markram, M. Grandolfo, D. Scaini, F. Gelain, L. Casalis, M. Prato, M. Giugliano, L. Ballerini. *Nat Nano*, **2009,** *4*, 126-133; (b) M. Adeli, R. Soleyman, Z. Beiranvand, F. Madani. *Chem. Soc. Rev.*, **2013,** *42*, 5231-5256.
[15] J. M. Schnorr, T. M. Swager. *Chem. Mater.*, **2011,** *23*, 646-657.
[16] (a) A. Di Crescenzo, V. Ettorre, A. Fontana. *Beilstein J. Nanotechnol.*, **2014,** *5*, 1675-1690; (b) T. A. Saleh, V. K. Gupta. In *Advanced Carbon Materials and Technology*, John Wiley & Sons, Inc. **2014**; pp 317-330.
[17] J. Liu, A. G. Rinzler, H. Dai, J. H. Hafner, R. K. Bradley, P. J. Boul, A. Lu, T. Iverson, K. Shelimov, C. B. Huffman, F. Rodriguez-Macias, Y.-S. Shon, T. R. Lee, D. T. Colbert, R. E. Smalley. *Science*, **1998,** *280*, 1253-1256.

that can then react via formation of the acid chloride or with activators such as carbodiimides to form amides or esters. Since Haddon *et al.* reported the first work in which amidation reactions are used to produce soluble SWNTs,[18] many works with this kind of modification have been published not only to improve the solubility of SWNTs,[19] but also to combine the interesting properties of carbon nanotubes with other materials[20] or to prepare biosensors by, for example, attaching DNA[21] or carbohydrate ligands.[22]

The esterification of carboxylic functions has been extensively used too. Solubilization of SWNTs in organic solvents was achieved by esterification reactions of porphyrin or alkyl pyrrole[23] units with oxidized SWNTs. The study of fluorescence on porphyrin-SWNTs systems has also been reported by several groups.[24]

The second approach to functionalize the sidewall of SWNTs covalently requires the use of highly reactive agents and it takes advantage of the more reactive parts of carbon nanotubes. Pristine SWNTs presents two regions, caps and sidewalls, with different reactivity. This difference is due to the presence of five-membered rings at the caps of the nanotubes, as in fullerenes, which result in an increase in the sp^3 character of the C-C bonds, and hence enhanced reactivity, and the defects contained by nanotubes on sidewalls. Defects are produced during the synthesis of nanotubes and probably the reactions are

[18] M. A. Hamon, J. Chen, H. Hu, Y. Chen, M. E. Itkis, A. M. Rao, P. C. Eklund, R. C. Haddon. *Adv. Mater.*, **1999,** *11*, 834-840.
[19] B. Zhao, H. Hu, R. C. Haddon. *Adv. Funct. Mater.*, **2004,** *14*, 71-76.
[20] (a) J. L. Delgado, P. de la Cruz, A. Urbina, J. T. López Navarrete, J. Casado, F. Langa. *Carbon*, **2007,** *45*, 2250-2252; (b) S. Giordani, J.-F. Colomer, F. Cattaruzza, J. Alfonsi, M. Meneghetti, M. Prato, D. Bonifazi. *Carbon*, **2009,** *47*, 578-588.
[21] S. E. Baker, W. Cai, T. L. Lasseter, K. P. Weidkamp, R. J. Hamers. *Nano Lett.*, **2002,** *2*, 1413-1417.
[22] L. Gu, T. Elkin, X. Jiang, H. Li, Y. Lin, L. Qu, T.-R. J. Tzeng, R. Joseph, Y.-P. Sun. *Chem. Commun.*, **2005**, 874-876.
[23] S. Cosnier, M. Holzinger. *Electrochim. Acta*, **2008,** *53*, 3948-3954.
[24] (a) H. Li, R. B. Martin, B. A. Harruff, R. A. Carino, L. F. Allard, Y. P. Sun. *Adv. Mater.*, **2004,** *16*, 896-900; (b) D. Baskaran, J. W. Mays, X. P. Zhang, M. S. Bratcher. *J. Am. Chem. Soc.*, **2005,** *127*, 6916-6917.

produced preferably near to these defects.[25] Both pristine and oxidized SWNTs can be used in this approach.

Several types of addition chemistry have been successfully applied to SWNTs, including fluorination, addition of carbenes and nitrenes, 1,3-dipolar cycloadditions, Diels-Alder cycloadditions, nucleophilic addition, free radical additions, reduction and reductive alkylation and direct arylations.[26]

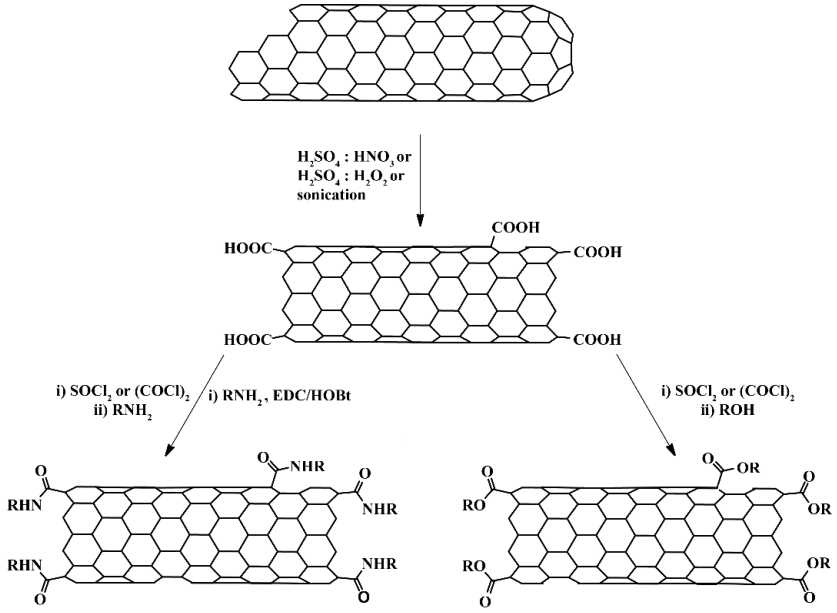

Scheme 1. Covalent functionalization following amidation and esterification reactions.

Margrave *et al.* reported in 1998 the first fluorination of SWNTs with elemental fluorine.[27] This method introduced one fluorine atom per two carbon atoms and it is reversible, the fluorinated SWNTs can be defluorinated with

[25] D. Srivastava, D. W. Brenner, J. D. Schall, K. D. Ausman, M. Yu, R. S. Ruoff. *J. Phys. Chem. B*, **1999,** *103*, 4330-4337.
[26] P. Singh, S. Campidelli, S. Giordani, D. Bonifazi, A. Bianco, M. Prato. *Chem. Soc. Rev.*, **2009,** *38*, 2214-2230.
[27] E. T. Mickelson, C. B. Huffman, A. G. Rinzler, R. E. Smalley, R. H. Hauge, J. L. Margrave. *Chem. Phys. Lett.*, **1998,** *296*, 188-194.

hydrazine. Fluorination enhances the reactivity and further modifications can be produced.

Addition of carbenes, one of the first types of functionalization reported, and addition of nitrenes, follow a similar mechanism and comprehensive studies have been carried out by Haddon[28] and Hirsch.[29]

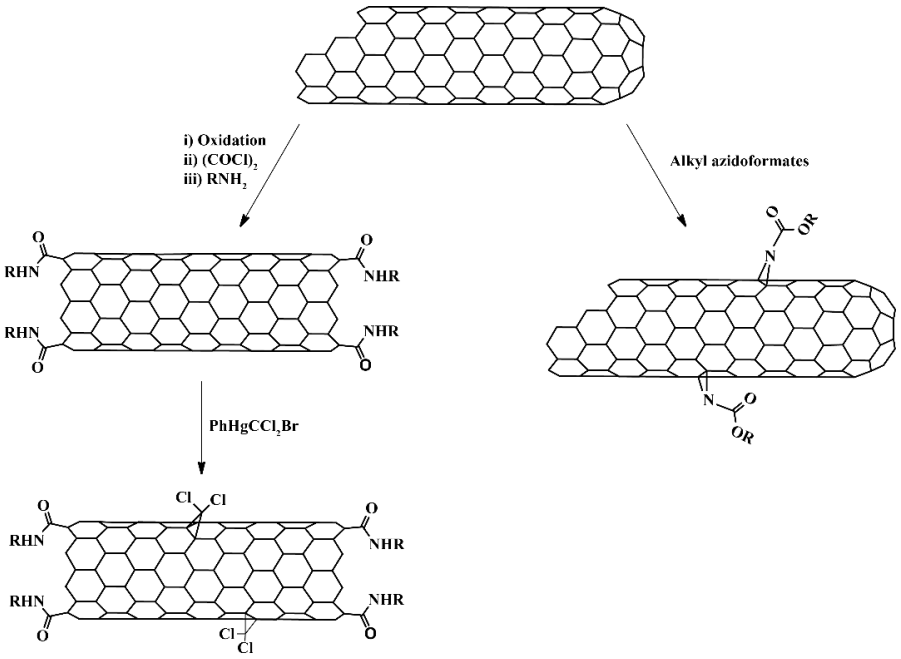

Scheme 2. Carbenes and nitrenes addition to SWNTs.

1,3-dipolar cycloaddition of azomethine ylides, very reactive intermediates, generated *in-situ* by thermal condensation of aldehydes and α-amino acids introduces a large number of pyrrolidine rings fused to the carbon–carbon bonds of CNTs. Prato and coworkers first developed this reaction for

[28] H. Hu, B. Zhao, M. A. Hamon, K. Kamaras, M. E. Itkis, R. C. Haddon. *J. Am. Chem. Soc.*, **2003,** *125*, 14893-14900
[29] M. Holzinger, J. Abraham, P. Whelan, R. Graupner, L. Ley, F. Hennrich, M. Kappes, A. Hirsch. *J. Am. Chem. Soc.*, **2003**, *125*, 8566-8580.

fullerenes,[30] which came to be known as the Prato reaction, and have later extensively studied it for carbon nanotubes.[31]

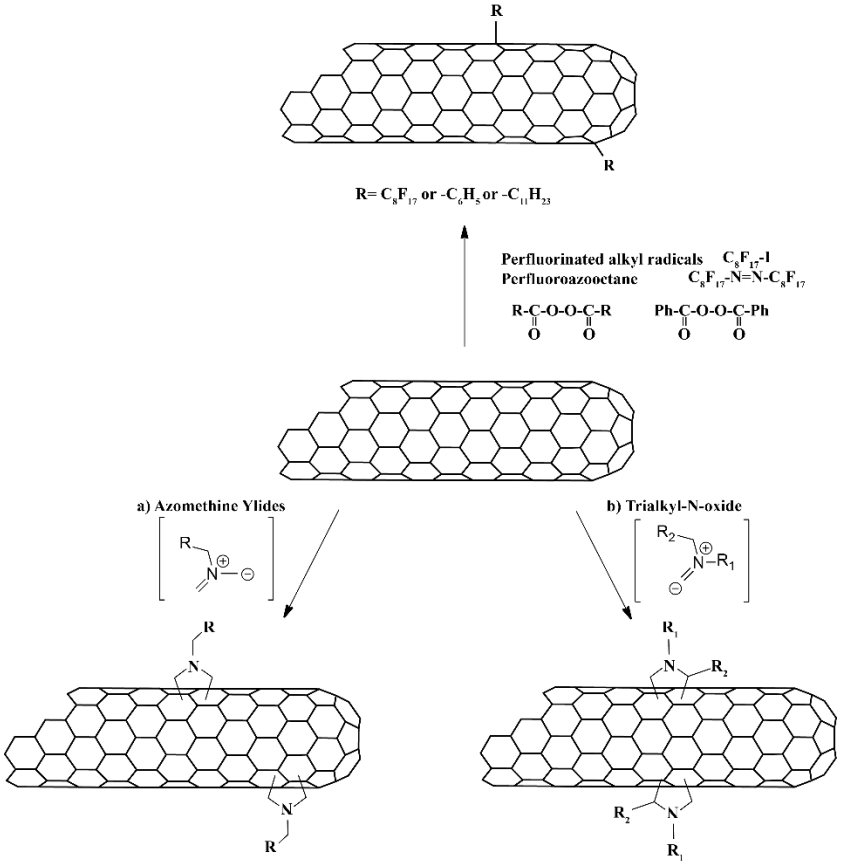

Scheme 3. Radical addition (top) and 1,3-dipolar cycloaddition (bottom) examples.

The modification of short SWNTs by a Diels-Alder cycloaddition in the presence of *o*-quinodimethane has been reported.[32] However, the retro Diels-

[30] M. Maggini, G. Scorrano, M. Prato. *J. Am. Chem. Soc.*, **1993,** *115*, 9798-9799.
[31] (a) A. Callegari, M. Marcaccio, D. Paolucci, F. Paolucci, N. Tagmatarchis, D. Tasis, E. Vazquez, M. Prato. *Chem. Commun.*, **2003**, 2576-2577; (b) D. M. Guldi, M. Marcaccio, D. Paolucci, F. Paolucci, N. Tagmatarchis, D. Tasis, E. Vázquez, M. Prato. *Angew. Chem. Int. Ed.*, **2003,** *42*, 4206-4209; (c) V. Georgakilas, A. Bourlinos, D. Gournis, T. Tsoufis, C. Trapalis, A. Mateo-Alonso, M. Prato. *J. Am. Chem. Soc.*, **2008,** *130*, 8733-8740; (d) M. Prato, K. Kostarelos, A. Bianco. *Acc. Chem. Res.*, **2008,** *41*, 60-68.

Alder occurs too easily to make this type of modification a convenient method for manipulation of carbon nanotubes.

Nucleophilic addition to pristine SWNTs was reported by Coleman *et al.*[33] They carried out the cyclopropanation of SWNTs using diethyl bromomalonate and DBU.

Free-radical additions are also used for SWNTs functionalization. In general, radicals can be produced by inorganic ions and by electrolysis in oxidation-reduction reactions, in a photochemical or thermal way. Numerous methods of SWNTs functionalization using this approach have been reported.[34]

Carbanionic SWNTs can be obtained easily by direct reduction due to the "electron sink" properties of nanotubes, and are suitable intermediates for electrophilic reactions. Birch reduction, napthalenide radical anion mediated reduction or the use of 4,4'-di-*tert*-buthyl biphenyl are some of the methods reported to obtain carbanionic SWNTs.[35]

---

[32] J. L. Delgado, P. de la Cruz, F. Langa, A. Urbina, J. Casado, J. T. López Navarrete. *Chem. Commun.*, **2004**, 1734-1735.
[33] K. S. Coleman, S. R. Bailey, S. Fogden, M. L. H. Green. *J. Am. Chem. Soc.*, **2003,** *125*, 8722-8723.
[34] (a) T. Nakamura, M. Ishihara, T. Ohana, A. Tanaka, Y. Koga. *Chem. Commun.*, **2004**, 1336-1337; (b) H. Peng, L. B. Alemany, J. L. Margrave, V. N. Khabashesku. *J. Am. Chem. Soc.*, **2003,** *125*, 15174-15182; (c) Y. Ying, R. K. Saini, F. Liang, A. K. Sadana, W. E. Billups. *Org. Lett.*, **2003,** *5*, 1471-1473; (d) L. Wei, Y. Zhang. *Chem. Phys. Lett.*, **2007,** *446*, 142-144.
[35] (a) S. Pekker, J. P. Salvetat, E. Jakab, J. M. Bonard, L. Forró. *J. Phys. Chem. B*, **2001,** *105*, 7938-7943; (b) A. Pénicaud, P. Poulin, A. Derré, E. Anglaret, P. Petit. *J. Am. Chem. Soc.*, **2005,** *127*, 8-9; (c) A. García-Gallastegui, I. Obieta, I. Bustero, G. Imbuluzqueta, J. Arbiol, J. I. Miranda, J. M. Aizpurua. *Chem. Mater.*, **2008,** *20*, 4433-4438.

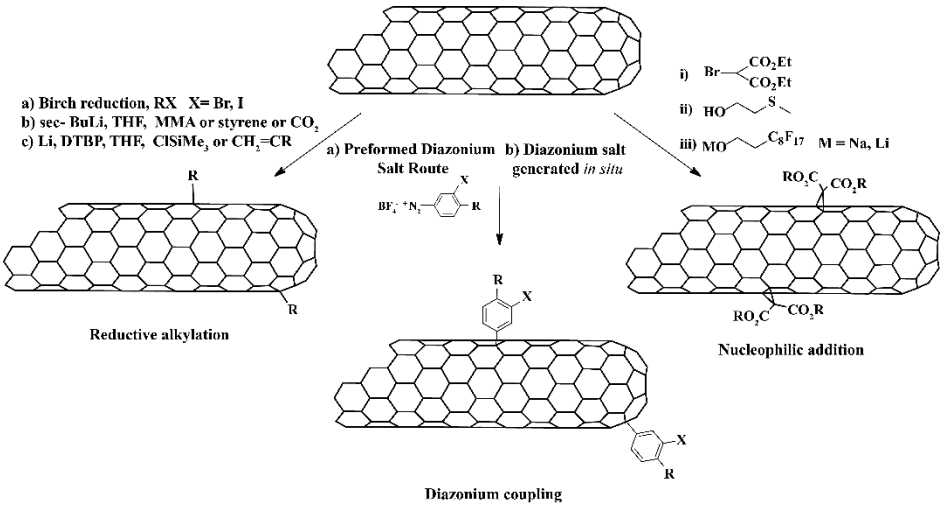

Scheme 4. Functionalization using reductive alkylation, diazonium coupling reactions and nucleophilic addition.

Direct arylations were firstly reported by Tour's group, who presented the synthesis of several aryl diazonium salts and their addition to SWNTs.[36]

1.1.2.2. Non-covalent Functionalization

Non-covalent functionalization is based on van der Waals forces, hydrogen bonds, electrostatic forces and π-π stacking interactions. Non-covalent functionalization has the advantage that it can be carried out under relatively mild reaction conditions. Also, it does not introduce perturbations in the electronic structure of the nanotubes and the perfect graphitic structure of the nanotube can be maintained. However, because of the very nature of this type of functionalization, involving weak forces, it is not well suited for some applications. The non-covalent functionalization is a reversible process, which occurs under equilibrium conditions, so that attachment and detachment of the

[36] C. A. Dyke, J. M. Tour. *J. Phys. Chem. A*, **2004,** *108*, 11151-11159.

adsorbed molecules always take place simultaneously. The ratio between the rates of attachment and detachment (the association constant) can be tuned by varying the solvent, temperature, etc.

In recent years, a big number of CNTs surface modifiers, including small molecules and polymers,[37] have been developed and utilized to non-covalently functionalize them.

Surfactants, such as sodium dodecylsulfate (SDS) and dodecyltrimethylammonium bromide, have two main parts, which interact differently with carbon nanotubes. The hydrophobic tails tend to be adsorbed onto nanotubes surfaces by nonspecific hydrophobic interactions while the hydrophilic heads interact with the media, so that stable suspensions of carbon nanotubes can be obtained in certain solvents. Using these surfactants, metal nanoparticles,[38] inorganic oxides[39] and other components have been attached to CNTs.

Aromatic molecules are capable of forming specific and directional π-π stacking interactions with carbon nanotubes. This is evident comparing two surfactants with same alkyl length but different structure. It has been proven that sodium dodecylbenzenesulfonate (SDBS) is more effective to solubilize nanotubes as a result of the presence of a phenyl ring. Aromatic molecules have been widely used to modify CNTs.

[37] (a) A. Di Crescenzo, V. Ettorre, A. Fontana. *Beilstein J. Nanotechnol*, **2014,** *5*, 1675-1690; (b) H. Li, S. I. Song, G. Y. Song, I. Kim. *J. Nanosci. Nanotechnol.*, **2014,** *14*, 1425-1440; (c) P. Bilalis, D. Katsigiannopoulos, A. Avgeropoulos, G. Sakellariou. *RSC Adv.*, **2014,** *4*, 2911-2934; (d) E. M. Pérez, N. Martín. *Chem. Soc. Rev.*, **2015,** *44*, 6425-6433.
[38] C.-L. Lee, Y.-C. Ju, P.-T. Chou, Y.-C. Huang, L.-C. Kuo, J.-C. Oung. *Electrochem. Commun.*, **2005,** *7*, 453-458.
[39] C. Zamora-Ledezma, L. Añez, J. Primera, P. Silva, S. Etienne-Calas, E. Anglaret. *Carbon*, **2008,** *46*, 1253-1255.

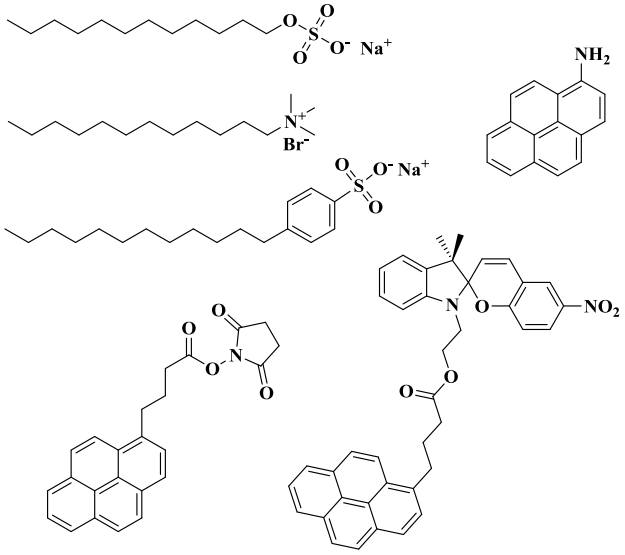

Figure 2. Molecular structures molecules used to functionalize non-covalently carbon nanotubes.

Eder *et al.*[40] reported the use of benzene alcohol to functionalize CNTs because of its ability to keep the particle size small and to provide better interaction with the hydrophobic nanotubes.

Molecules containing polyaromatic components demonstrate stronger affinity toward the basal plane of CNTs resulting in more stable solution or suspension. Several works have been published reporting the use of pyrene derivatives such as 1-aminopyrene,[41] 1-pyrenebutanoic acid succinimidyl ester[42] or pyrene-carrying ammonium ion.[43]

With respect to small molecules, polymer grafting presents the advantage to make carbon nanotubes soluble in a wide range of solvents depending on the polymer, even when the degree of functionalization is small. Thus, non-

[40] D. Eder, A. H. Windle. *J. Mater. Chem.*, **2008,** *18*, 2036-2043.
[41] X. L. Li, Y. Q. Liu, L. Fu, L. C. Cao, D. C. Wei, Y. Wang. *Adv. Funct. Mater.*, **2006,** *16*, 2431-2437.
[42] R. J. Chen, Y. Zhang, D. Wang, H. Dai. *J. Am. Chem. Soc.*, **2001,** *123*, 3838-3839.
[43] N. Nakashima, Y. Tomonari, H. Murakami. *Chem. Lett.*, **2002,** *31*, 638-639.

covalent functionalization of CNTs with polymers permits the dispersion of the tubes in aqueous or non-aqueous solvents without changing their structure.

Both linear homopolymer and linear block copolymers have been used to functionalize CNTs. Homopolymers generally have aromatics motifs along the chains and/or functional moieties on their chain ends. Sometimes, additional ionic moieties are required.[44] Meanwhile, steric repulsion among polymer-decorated tubes can be employed for stabilization of CNT dispersions[45] and block-copolymers are one of the most efficient steric stabilizers. It has been reported that the solubility of nanotubes can be effectively tuned by the composition of the copolymer.[46]

As-obtained SWNTs present a mixture of chiralities, and, therefore, of electronic properties. Linear polymers have been used to separate or enrich mixtures of SWNTs of with different sizes or chiralities. Regioregular poly(3-alkylthiophene)s,[47] aromatic polymers like poly(9,9-dioctylfluorenyl- 2,7-diyl)[48], even, DNA[49] have been used to sort SWNTs.

Although the conventional linear polymers and block copolymers have been extensively used, there are two drawbacks derived from the properties of such polymers: (1) amphiphilic block copolymers generally result in the formation of free micelles that are difficult to remove from the SWNTs walls, and (2) the polyelectrolytes are very sensitive to the media, limiting the work

[44] (a) A. Carrillo, J. A. Swartz, J. M. Gamba, R. S. Kane, N. Chakrapani, B. Wei, P. M. Ajayan. *Nano Lett.*, **2003,** *3*, 1437-1440; (b) M. A. Correa-Duarte, N. Sobal, L. M. Liz-Marzán, M. Giersig. *Adv. Mater.*, **2004,** *16*, 2179-2184; (c) K. Welsher, Z. Liu, S. P. Sherlock, J. T. Robinson, Z. Chen, D. Daranciang, H. Dai. *Nat. Nanotechnol.*, **2009,** *4*, 773-780.

[45] (a) R. Bandyopadhyaya, E. Nativ-Roth, O. Regev, R. Yerushalmi-Rozen. Nano Letters, **2002**, *2*, 25-28; (b) R. Shvartzman-Cohen, E. Nativ-Roth, E. Baskaran, Y. Levi-Kalisman, I. Szleifer, R. Yerushalmi-Rozen. J. Am. Chem. Soc., **2004**, *126*, 14850-14857.

[46] (a) J. Zou, L. Liu, H. Chen, S. I. Khondaker, R. D. McCullough, Q. Huo, L. Zhai. *Adv. Mater.*, **2008,** *20*, 2055-2060; (b) K. T. Kim, W. H. Jo. *J. Polym. Sci., Part A: Polym. Chem.*, **2010,** *48*, 4184-4191; (c) J. Zou, H. Chen, A. Chunder, Y. Yu, Q. Huo, L. Zhai. *Adv. Mater.*, **2008,** *20*, 3337-3341.

[47] (a) H. Wang, G. I. Koleilat, P. Liu, G. Jiménez-Osés, Y.-C. Lai, M. Vosgueritchian, Y. Fang, S. Park, K. N. Houk, Z. Bao. *ACS Nano*, **2014,** *8*, 2609-2617; (b) H. W. Lee, Y. Yoon, S. Park, J. H. Oh, S. Hong, L. S. Liyanage, H. Wang, S. Morishita, N. Patil, Y. J. Park, J. J. Park, A. Spakowitz, G. Galli, F. Gygi, P. H. S. Wong, J. B. H. Tok, J. M. Kim, Z. Bao. *Nat. Commun.*, **2011,** *2*, 541.

[48] A. Nish, J.-Y. Hwang, J. Doig, R. J. Nicholas. *Nat. Nanotechnol.*, **2007,** *2*, 640-646.

[49] X. Tu, S. Manohar, A. Jagota, M. Zheng. *Nature*, **2009,** *460*, 250-253.

conditions. Dendritic polymers have been developed to avoid those shortcomings.[50] For example, Li *et al.*[49a] used a multi-pyrene terminated hyperbranched polyglycidol (pHBP) to debundle MWNTs. This 3D dendritic architecture provides numerous interactions with nanotubes through π-π stacking and it can be easily removed using solvents.

1.1.2.3. Mechanically Interlocked Carbon Nanotubes

Mechanically interlocked molecules (MIMs) are formed by two or more separate components that are linked together mechanically. They are not connected through covalent bonds but cannot be separated without breaking a covalent bond. For example, catenanes and rotaxanes are MIMs. Catenanes are architectures where two or more macrocycles are interlocked as links in a chain. Rotaxanes present one or more macrocycles trapped onto a linear component, the thread, by bulky substituents at its ends, known as stoppers.

[50] (a) H. Li, J. K. Jo, L. Zhang, C.-S. Ha, H. Suh, I. Kim. *Adv. Funct. Mater.*, **2010,** *20*, (22), 3864-3873; (b) H. Li, L. Han, J. J. Cooper-White, I. Kim. *Nanoscale*, **2012,** *4*, 1355-1361; (c) Li, J. J. Cooper-White. *Nanoscale*, **2013,** *5*, 2915-2920.

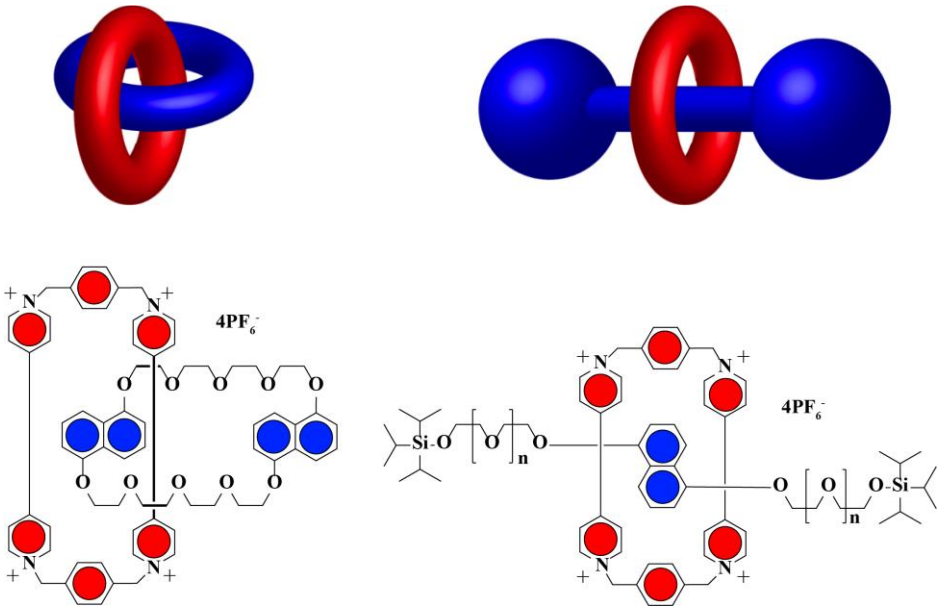

Figure 3. Cartoon and chemical structure of a catenane[51] and a rotaxane[52].

Because of their properties, these types of molecular architectures have been extensively studied not only as candidates for the construction of molecular machinery,[53] but also in the production of mechanically interlocked materials such as polymers[54] or metallic organic frameworks.[55]

In 2014, our group reported the first strategy for the synthesis of mechanically interlocked derivatives of SWNTs (MINTs).[56] This new tool for the chemical manipulation of SWNTs combined the advantages of the other types of functionalization, *i.e.* kinetically stable products while maintaining the structure of the SWNTs.

[51] P. R. Ashton, C. L. Brown, E. J. T. Chrystal, T. T. Goodnow, A. E. Kaifer, K. P. Parry, D. Philp, A. M. Z. Slawin, N. Spencer, J. F. Stoddart, D. J. Williams. *J. Chem. Soc., Chem. Commun.*, **1991**, 634-639.
[52] J. A. Bravo, F. M. Raymo, J. F. Stoddart, A. J. P. White, D. J. Williams. *Eur. J. Org. Chem.*, **1998**, 2565-2571.
[53] E. R. Kay, D. A. Leigh, F. Zerbetto. *Angew. Chem. Int. Ed.*, **2007,** *46*, 72-191.
[54] L. Fang, M. A. Olson, D. Benitez, E. Tkatchouk, W. A. Goddard III, J. F. Stoddart. *Chem. Soc. Rev.*, **2010,** *39*, 17-29.
[55] Q. Li, C.-H. Sue, S. Basu, A. K. Shveyd, W. Zhang, G. Barin, L. Fang, A. A. Sarjeant, J. F. Stoddart, O. M. Yaghi. *Angew. Chem. Int. Ed.*, **2010,** *49*, 6751-6755.
[56] A. de Juan, Y. Pouillon, L. Ruiz-González, A. Torres-Pardo, S. Casado, N. Martín, Á. Rubio, E. M. Pérez. *Angew. Chem. Int. Ed.*, **2014,** *53*, 5394-5400.

MINTs are rotaxane-type structure in which SWNTs act as threads and macrocycles are formed around them by a clipping strategy. A U-shape precursor with two recognition units for nanotubes and alkene-terminated alkyl chains is attached to SWNTs by non-covalent interactions and the MINTs are formed through a ring closing metathesis reaction.

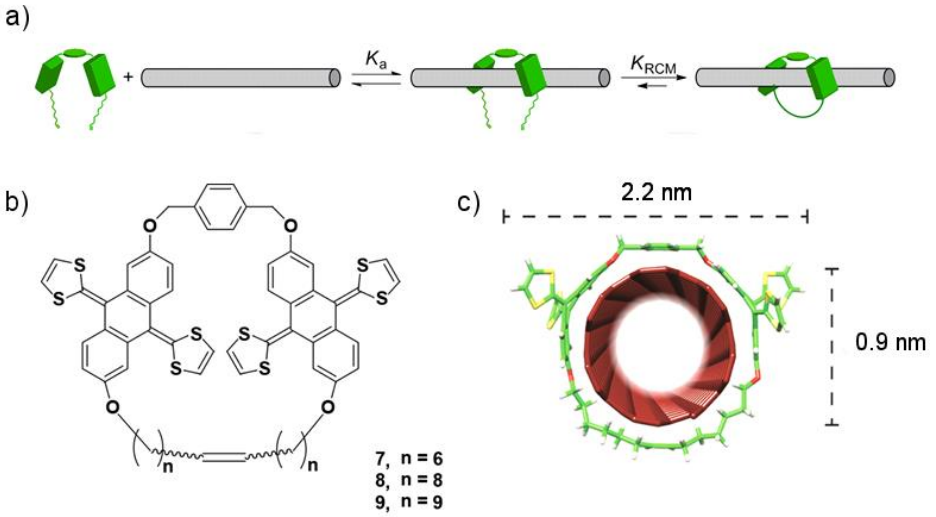

Figure 4. a) Representation of the clipping strategy for the synthesis of MINTs; b) Chemical structure of macrocycles based on exTTF units; c) Energy-minimized (MMFF94) molecular model of a MINT pseudorotaxane.

Owing to their well-known positive non-covalent interactions with carbon materials as fullerenes[57] and SWNTs,[58] π-extended derivatives of tetrathiafulvalene (exTTF) were used as recognition motifs for the preparation of U-shapes and macrocycles (Figure 4). A comprehensive collection of

[57] (a) D. Canevet, M. Gallego, H. Isla, A. de Juan, E. M. Pérez, N. Martín. *J. Am. Chem. Soc.*, **2011,** *133*, 3184-3190; (b) H. Isla, M. Gallego, E. M. Pérez, R. Viruela, E. Ortí, N. Martín. *J. Am. Chem. Soc.*, **2010,** *132*, 1772-1773.
[58] C. Romero-Nieto, R. García, M. Á. Herranz, C. Ehli, M. Ruppert, A. Hirsch, D. M. Guldi, N. Martín. *J. Am. Chem. Soc.*, **2012,** *134*, 9183-9192.

control experiments and characterization by Raman, UV-vis-NIR, PLE spectroscopy, NMR, HR-TEM and AFM, provide the confirmation of interlocked nature of the MINT.

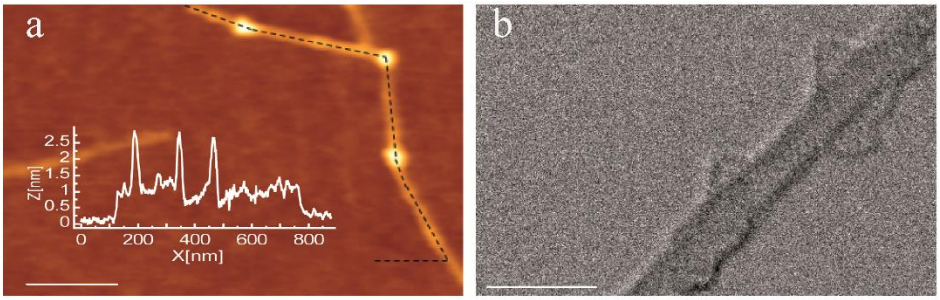

Figure 5. a) AFM topography image of a spin-casted suspension of MINT in TCE. Inset shows the profile along the dashed black line. b) HR-STEM bright-field image of a single SWNTs surrounded by two macrocycles. Scale bars are 100 nm for a) and 2 nm for b).

The high stability of MINTs was demonstrated through extensive washes after heating at reflux in tetrachloroethane (b.p. 146 ºC). Even under these harsh conditions, the macrocycles stay attached to the SWNTs, proving that the dethreading process is highly improbable.

Studying the degree of functionalization as a function of the initial concentration of the U-shape precursor, we confirmed that MINT-forming reaction proceeds via a U-shape·SWNTs complex. Increasing the concentration of U-shape the degree of functionalization increases until the saturation, as is shown in Figure 6, which can be taken as the saturation of the binding equilibrium between SWNT and the U-shape. As concentrations of bound U-shape and total U-shape, data could be fit to 1:1 binding isotherm using Equation (1) and extracting the concentration of free U-shape from TGA data.

(1) $$\frac{[\mathbf{1}]_{bound}}{[\mathbf{1}]_{total}} = \frac{k_a[\mathbf{1}]_{free}}{1+k_a[\mathbf{1}]_{free}}$$

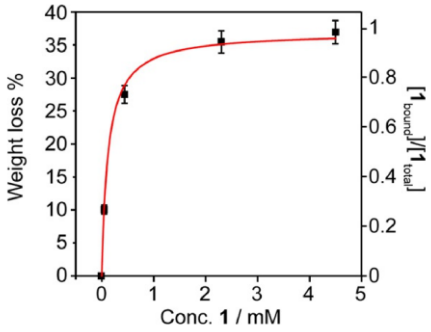

Figure 6. Degree of functionalization with increasing concentration of U-shaped (catalyst and solvent adsorption subtracted), and its fit to calculate the approximate binding constant between U-shape and SWNTs.

Bis-alkenes such as U-shape can cyclize via RCM, which proceeds with pseudo-first-order kinetics, or poly/oligomerize, following second-order kinetics. From analysis of conversion-time data, the rate-determining step was confirmed to be the RCM, which discards significant participation of oligomers formed in-situ.[59]

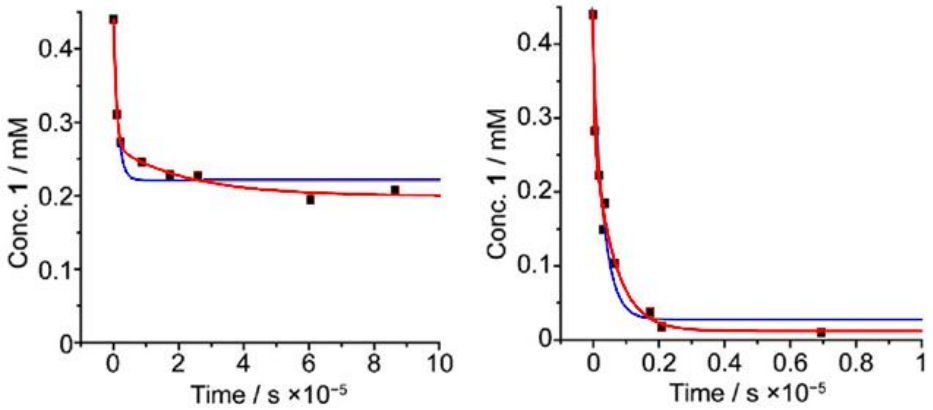

Figure 7. Left) Kinetic data for the formation of MINT, and its fit to a monoexponential (blue) and biexponential (red) decay. Right) Kinetic data for the formation of macrocycle, and its fit to a monoexponential (blue) and biexponential (red) decay.

[59] A. de Juan, M. Mar Bernal, E. M. Pérez. *ChemPlusChem*, **2015,** *80*, 1153-1157.

More recently, we have established that the properties of MINTs are significantly different from those of supramolecular-modified SWNTs. The electronic properties of exTTF-based MINTs were investigated both in the ground state and upon excitation performing a complete study by Raman spectroscopy, steady state absorption and femtosecond transient absorption spectroscopy.[60] Although there is no charge-transfer between exTTF and SWNTs in the ground state, efficient photoinduced charge-transfer between exTTF and SWNTs was found. Moreover, in this work, we proved that the MINT-forming reaction is diameter-selective, as is shown in Figure 8. In RBM zone of Raman spectra is observed a decrease in the intensity of the RBMs corresponding to (6,5) and (6,4) SWNTs (311 and 331 cm^{-1}) after MINT reaction. In the 3D NIR spectra, a clear quenching is produced for (6,5)-SWNTs signal.

[60] E. Martínez-Periñán, A. de Juan, Y. Pouillon, C. Schierl, V. Strauss, N. Martín, A. Rubio, D. M. Guldi, E. Lorenzo, E. M. Pérez. *Nanoscale*, **2016,** *8*, 9254-9264.

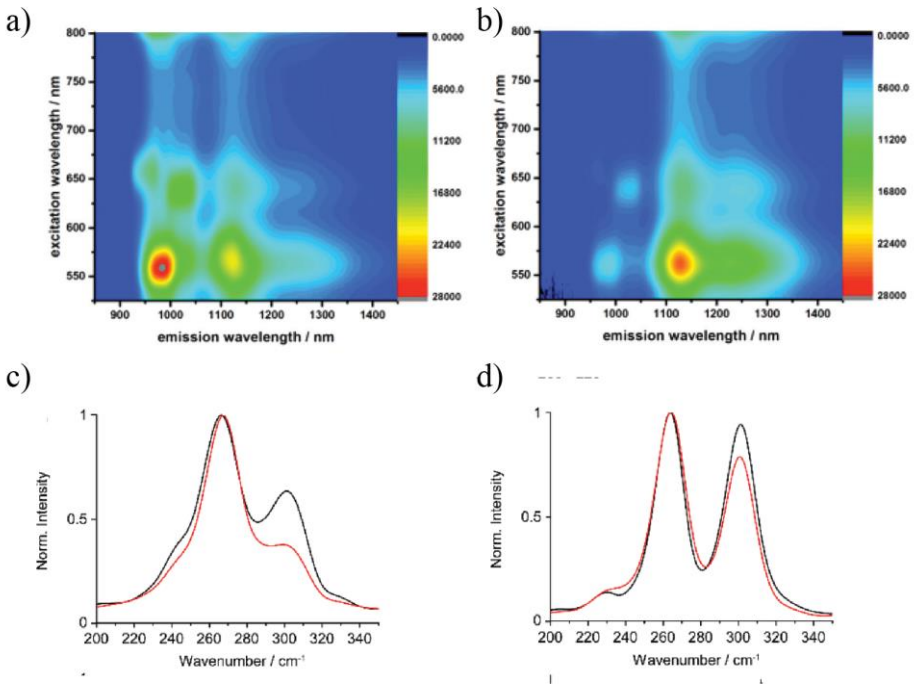

Figure 8. Top: 3D NIR fluorescence spectra of a) (6,5)-enriched SWNTs and b) MINT-(6,5) in D_2O/SDBS (1 wt%) measured with an OD of 0.35 at 570 nm. Bottom: Comparison of the RBMs of SWNTs (black) and MINT-(6,5) (red) with c) λ_{exc} = 532 nm and d) λ_{exc} = 785 nm.

By cyclic voltammetry, through analysis of the scan rate dependence yield were found differences between charge-transfer constants for MINT and supramolecular model, 21.4 s^{-1} and 26.1 s^{-1} respectively, which confirmed the different nature of the interactions.

The extension of this type of functionalization of carbon nanotubes, using other recognition motifs such as polycyclic aromatic hydrocarbons or porphyrins, is promising. The further study of the optical, electrical, thermal or mechanical properties of the new MINTs and the comparison not only with

pristine nanotubes but also with the corresponding covalent and supramolecular models results an interesting challenge.

1.2. Pyrene

This work investigates the synthesis of pyrene derivatives for their interfacing with carbon nanotubes through mechanical interlocking. I will now describe the physical and chemical properties of pyrene and provide examples of its noncovalent interactions with SWNTs.

1.2.1. Properties

Pyrene is a polycyclic aromatic hydrocarbon (PAH) with planar structure constituted by four fused aromatic rings.

Pyrene has exceptional photophysical properties, with a long fluorescence lifetime in solution as monomer and the possibility of the formation of an excimer by π-π stacking of two pyrene units, which has three distinctive properties: 1) an emission between 410-480 nm; 2) high intensity ratio excimer/monomer; and 3) the excimer is observed even at low concentrations. These characteristics combined with the high quantum yield [61] and the sensitivity of the excitation spectra to environmental changes make pyrene one of most studied chromophores. Pyrene derivatives present charge-transfer behavior, with pyrene acting as electron-donor or as electron-acceptor depending on the substituent(s) attached.

Thanks to the previously mentioned absorption/emission properties and its aromatic surface, pyrene has been extensively used as fluorophore in molecular recognition[62] or structural biology[63] and in the supramolecular association of

[61] G. v. Bünau. J. B. Birks: Photophysics of Aromatic Molecules. Wiley-Interscience, London. 704 Seiten. Preis: 210s. *Berichte der Bunsengesellschaft für physikalische Chemie*, **1970,** *74*, 1294-1295.
[62] S. Karuppannan, J.-C. Chambron. *Chem. Asian J.*, **2011,** *6*, 964-984.
[63] G. Bains, A. B. Patel, V. Narayanaswami. *Molecules*, **2011,** *16*, 7909.

carbon nanotubes[64] and graphene.[65] Some representative examples of pyrene applications for its optical properties and for its association with carbon materials are presented below.

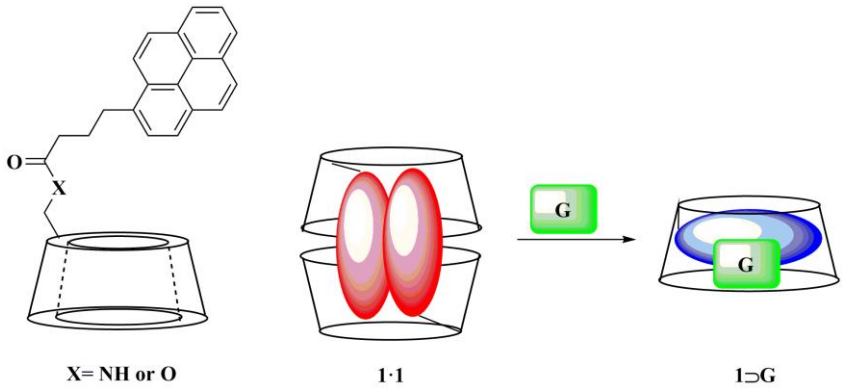

Scheme 5. Mechanism of pyrene functionalized γ-CD as sensor.

Pyrene derivatives have been incorporated into sensors to detect external substrates due to its sensitivity to local environmental changes. Often, these systems contain two or more pyrene moieties. Generally, monomer emission is observed from the pyrenes but in the presence of external substrates some conformational changes are produced in the sensor, the pyrene units are closer and excimer emission is observed. The monomer/excimer ratio determine the amount of external substrate.[66] Pyrene excimer luminescence is activated by γ–cyclodextrin (γ–CD). Based on this, Ueno and co-workers[67] found that γ–CD with a pyrenyl group anchored at the lower rim formed the self-inclusion dimer 1·1 in 10% dimethyl sulfoxide (DMSO) aqueous solution, which exhibited excimer emission. Addition of various organic guest species, such as terpenes

[64] C. Ehli, G. M. A. Rahman, N. Jux, D. Balbinot, D. M. Guldi, F. Paolucci, M. Marcaccio, D. Paolucci, M. Melle-Franco, F. Zerbetto, S. Campidelli, M. Prato. *J. Am. Chem. Soc.*, **2006,** *128*, 11222-11231.
[65] G. Zeng, Y. Xing, J. Gao, Z. Wang, X. Zhang. *Langmuir*, **2010,** *26*, 15022-15026.
[66] (a) S. Karuppannan, J.-C. Chambron. *Chem. Asian J.*, **2011,** *6*, 964-984; (b) E. Manandhar, K. J. Wallace. *Inorg. Chim. Acta*, **2012,** *381*, 15-43.
[67] (a) A. Ueno, I. Suzuki, T. Osa. *J. Chem. Soc., Chem. Commun.*, **1988**, 1373-1374; (b) A. Ueno, I. Suzuki, T. Osa. *J. Am. Chem. Soc.*, **1989,** *111*, 6391-6397.

and steroids, to 1·1 produced the dissociation of the dimer. As a result, the excimer emission disappeared, whereas the monomer emission increased.

Numerous works have been published using pyrene as sensor for metals such as Cu^{+},[68] Ag^{+},[69] Hg^{2+},[70] or Pb^{2+},[71] some of them very important in environmental and biological systems because of their well-known toxicity. The mechanism of these sensors is based on a complexation-induced dimerization, where the metal induces a folding which produces the dimerization and consequently the excimer emission.

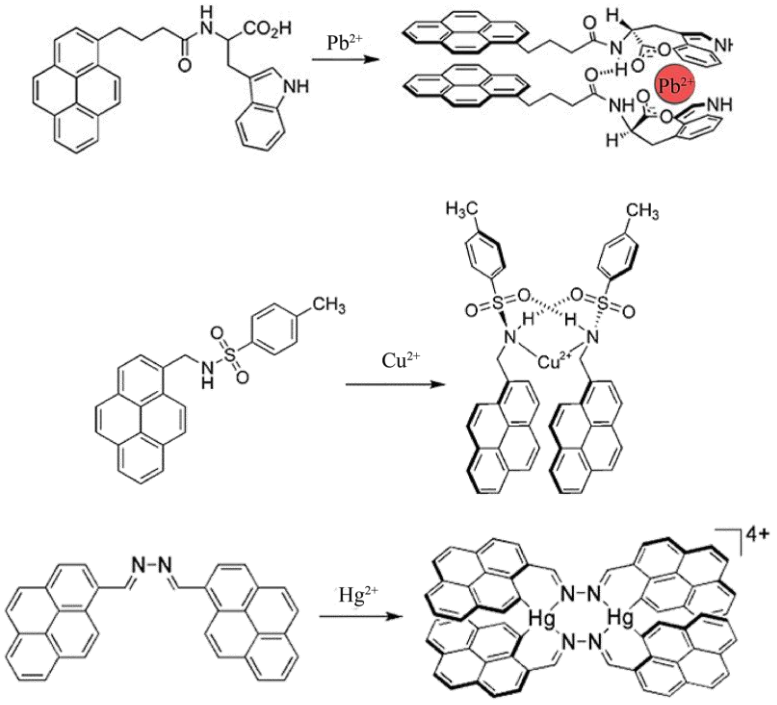

Figure 9. Structures of monomers/dimers in pyrene based metals sensors.

[68] H. S. Jung, M. Park, D. Y. Han, E. Kim, C. Lee, S. Ham, J. S. Kim. *Org. Lett.*, **2009,** *11*, 3378-3381.
[69] R.-H. Yang, W.-H. Chan, A. W. M. Lee, P.-F. Xia, H.-K. Zhang. *J. Am. Chem. Soc.*, **2003,** *125*, 2884-2885.
[70] R. Martínez, A. Espinosa, A. Tárraga, P. Molina. *Org. Lett.*, **2005,** *7*, 5869-5872.
[71] L.-J. Ma, Y.-F. Liu, Y. Wu. *Chem. Commun.*, **2006**, 2702-2704.

Other interesting biological systems have also been quantified using pyrene-based sensors, for example DNA,[72] glucose[73] or heparine.[74]

For its planar structure and its ability to undergo π-π stacking interactions, pyrene is extensively used as recognition motif for carbon nanotubes and graphene. Pyrene has been used in the liquid-phase exfoliation of graphene as well as in the preparation of sensors based on graphene.[75] For the exfoliation of graphene in aqueous solutions, pyrene derivatives such as pyrenecarboxylic acid (PCA) and pyrenesulfonic acid (PSA) have been used.[76]

Polymers with units of pyrene of pyrene derivatives have been developed. Compared with pyrene derivative small molecule, the corresponding polymer is a more efficient dispersant. The long chain provides more sites for solvation and sufficient spatial volume to repel nanocarbons from each other for stabilization.[77] Pyrene-terminal polymers are preferable to maximize the number of chains attached achieving concentrations from 67 $\mu g \cdot mL^{-1}$ up to 40 $mg \cdot mL^{-1}$ of graphene nanosheets with polystyrene and polymethylmethaacrylate.[78]

Pyrene and its derivatives present a high affinity for carbon nanotubes[79] and it has been used for the functionalization of nanotubes by noncovalent approaches. Numerous efforts have been made for the solubilization of carbon

[72] K. Yamana, Y. Fukunaga, Y. Ohtani, S. Sato, M. Nakamura, W. J. Kim, T. Akaike, A. Maruyama. *Chem. Commun*., **2005**, 2509-2511.
[73] C. Yu, V. W.-W. Yam. *Chem. Commun*., **2009**, 1347-1349.
[74] L. Zeng, P. Wang, H. Zhang, X. Zhuang, Q. Dai, W. Liu. *Org. Lett*., **2009,** *11*, 4294-4297.
[75] (a) K. Paek, H. Yang, J. Lee, J. Park, B. J. Kim. *ACS Nano*, **2014,** *8*, 2848-2856; (b) X. Mao, H. Su, D. Tian, H. Li, R. Yang. *ACS Appl. Mater. Interfaces*, **2013,** *5*, 592-597; (c) C. Yu, Y. Guo, H. Liu, N. Yan, Z. Xu, G. Yu, Y. Fang, Y. Liu. *Chem. Commun.*, **2013,** *49*, 6492-6494.
[76] (a) M. Zhang, R. R. Parajuli, D. Mastrogiovanni, B. Dai, P. Lo, W. Cheung, R. Brukh, P. L. Chiu, T. Zhou, Z. Liu, E. Garfunkel, H. He. *Small*, **2010,** *6*, 1100-1107; (b) D. Parviz, S. Das, H. S. T. Ahmed, F. Irin, S. Bhattacharia, M. J. Green. *ACS Nano*, **2012,** *6*, 8857-8867; (c) X. An, T. Simmons, R. Shah, C. Wolfe, K. M. Lewis, M. Washington, S. K. Nayak, S. Talapatra, S. Kar. *Nano Lett.*, **2010,** *10*, 4295-4301.
[77] H. Wang, Z. Chen, L. Xin, J. Cui, S. Zhao, Y. Yan. *J. Polym. Sci., Part A: Polym. Chem.*, **2015,** *53*, 2175-2185.
[78] K. D. Papadimitriou, E. N. Skountzos, S. S. Gkermpoura, I. Polyzos, V. G. Mavrantzas, C. Galiotis, C. Tsitsilianis. *ACS Macro Lett.*, **2016,** *5*, 24-29.
[79] K. Yang, L. Zhu, B. Xing. *Environ. Sci. Technol.*, **2006,** *40*, 1855-1861 .

nanotubes using pyrene derivatives. Nakashima *et al.*[80] and Tomonari *et al.*[81] achieved the solubilization of SWNTs in water using a pyrene-carrying ammonium ion, a water-soluble amphiphile. Pyrene-containing polymers have been synthesized to improve the solubility of SWNTs not only in water but also in organic solvents.[82] The use of this type of polymers is not only limited to solubilize nanotubes. As example, Yuan *et al.*[83] synthesized pyrene-containing poly(phenylacetylene)s which interacts with SWNTs and the nanohybrids presented the combined properties of the constituents, allowing, in addition the preparation of films and its use in photovoltaic devices.

The great affinity of pyrene for carbon nanomaterials can be used to attach nanoparticles[84] in order to prepare donor-acceptor nanohybrids which can be used as integrative components at electrode surfaces.

Most of the uses described above require the chemical functionalization of pyrene. Pyrene is a particularly stable PAH, so its chemistry often requires harsh conditions. A brief summary of the possibilities to functionalize pyrene is detailed below.

[80] N. Nakashima, Y. Tomonari, H. Murakami. *Chem. Lett.*, **2002,** *31*, 638-639.
[81] Y. Tomonari, H. Murakami, N. Nakashima. *Chem. - Eur. J.*, **2006,** *12*, 4027-4034.
[82] G. J. Bahun, C. Wang, A. Adronov. *J. Polym. Sci., Part A: Polym. Chem.*, **2006,** *44*, 1941-1951, (b) Petrov, F. Stassin, C. Pagnoulle, R. Jerome. *Chem. Commun.*, **2003**, 2904-2905.
[83] W. Z. Yuan, J. Z. Sun, Y. Dong, M. Häussler, F. Yang, H. P. Xu, A. Qin, J. W. Y. Lam, Q. Zheng, B. Z. Tang. *Macromolecules*, **2006,** *39*, 8011-8020.
[84] (a) D. M. Guldi, G. M. A. Rahman, V. Sgobba, N. A. Kotov, D. Bonifazi, M. Prato. *J. Am. Chem. Soc.*, **2006,** *128*, 2315-2323; (b) L. Hu, Y. L. Zhao, K. Ryu, C. Zhou, J. F. Stoddart, G. Grüner. *Adv. Mater.*, **2008,** *20*, 939-946.

1.2.2. Functionalization of pyrene

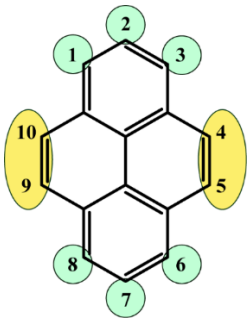

Scheme 6. Structure of pyrene. K regions are marked as yellow.

The functionalization of pyrene has been extensively reviewed and studied for different applications.[85] Pyrene can be functionalized by electrophiles, oxidants and reducing agents and transition metal mediated C-H activation. Positions 1-, 3-, 6-, and 8- are significantly more active than the other positions (the 4-, 5-, 9-, and 10-positions or the 2- and 7-positions) with relative energy with respect of substitution of the 1-, 3-, 6-, and 8-positions lower by 9 kcalmol^{-1} than the K region positions and 20 kcal·mol^{-1} lower than 2- and 7-positions.[86] Then, the electrophilic substitution of pyrene takes place preferentially at the 1-, 8-, 6-, and 3-positions, following that order.[87] Therefore, 1-substituted pyrenes and 1,3,6,8-tetrasubstituted pyrenes can be easily prepared by direct electrophilic substitution. The relatively simple purification make this approach useful to incorporate pyrene to different molecular architectures. In contrast, despite of the enormous advantages of have pure disubstituted pyrenes derivatives, the selective preparation of them in the 1-, 3-, 6- and 8- positions is not simple and the products are often

[85] (a) T. M. Figueira-Duarte, K. Müllen. *Chem. Rev.*, **2011,** *111*, 7260-7314; (b) J. M. Casas-Solvas, J. D. Howgego, A. P. Davis. *Org. Biomol. Chem.*, **2014,** *12*, 212-232; (c) X. Feng, J.-Y. Hu, C. Redshaw, T. Yamato. *Chem. - Eur. J.*, **2016,** *22*, 11898-11916.
[86] M. J. S. Dewar, R. D. Dennington. *J. Am. Chem. Soc.*, **1989,** *111*, 3804-3808.
[87] H. Cerfontain, K. Laali, H. J. A. Lambrechts. *Recl. Trav. Chim. Pays-Bas*, **1983,** *102*, 210-214.

difficult to isolate. Substitution at the 2- and 7-positions represents a challenge, as these positions are not directly accessible by electrophilic substitution of pyrene, and multistep synthesis have been required, until the publication of an iridium catalyzed direct conversion of pyrene with bis(pinacolato)diboron in 2005.[88]

1.2.2.1. Positions 1, 3, 6 and 8

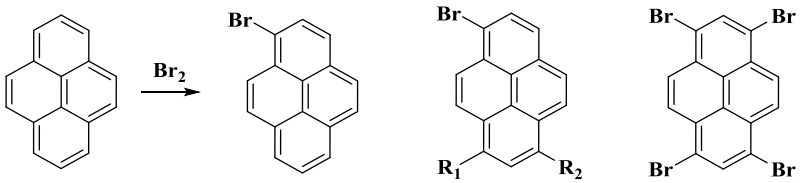

Scheme 7. Bromination of pyrene.

In 1937, Vollmann *et al.* reported the first synthesis of mono-, double-, tri or tetra-substituted pyrene derivatives.[89] Controlling the amount of Br_2, bromination can be directed to an isomer mixture of 1,6- and 1,8-dibromopyrene, which cannot be separated by chromatographic column. Fractional crystallization is used to isolate the isomers.[90] Chloropyrene derivatives have also been reported.[88]

As an alternative to the bromination, the nitration of pyrene to obtain a mixture of nitro derivatives has been described. The subsequent reduction of the nitro groups leads to a separable mixture of isomers of aminopyrenes.[91]

[88] D. N. Coventry, A. S. Batsanov, A. E. Goeta, J. A. K. Howard, T. B. Marder, R. N. Perutz. *Chem. Commun.*, **2005**, 2172-2174.
[89] H. Vollmann, H. Becker, M. Corell, H. Streeck**.** *Justus Liebigs Ann. Chem.,* **1937,** *531*, 1-159.
[90] J. Grimshaw, J. Trocha-Grimshaw. *J. Chem. Soc., Perkin Trans. 1*, **1972**, 1622-1623.
[91] (a) H. Vollmann, H. Becker, M. Corell, H. Streeck. *Justus Liebigs Ann. Chem.,* **1937,** *531*, 1-159; (b) Y. Hashimoto, K. Shudo. *Chem. Pharm. Bull.*, **1984,** *32*, 1992-1994.

Aminopyrenes and its derivatives have been widely used to modify carbon materials,[92] as intermediates for photoconductive materials for electrophotography[93] or electroluminescent devices. [94]

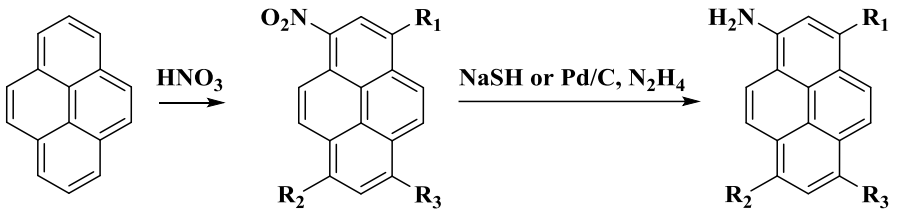

R_1= H, R_2= H, R_3= H
R_1= NO_2, R_2= H, R_3= H
R_1= H, R_2= NO_2, R_3= H
R_1= H, R_2= H, R_3= NO_2

R_1= H, R_2= H, R_3= H
R_1= NH_2, R_2= H, R_3= H
R_1= H, R_2= NH_2, R_3= H
R_1= H, R_2= H, R_3= NH_2

Scheme 8. Obtention of aminopyrene derivatives.

Pyrene can be oxidized to form mixtures of 1,6 and 1,8 pyrenediones by several microorganisms under aerobic conditions.[95] In a synthetic laboratory setting, a similar outcome can be obtained using extreme conditions, namely $K_2Cr_2O_7$ or $Na_2Cr_2O_7 \cdot 2H_2O$ in strong acids.[96] The resulting mixture is difficult to separate by chromatographic column.

[92] (a) E. Y. L. Teo, H. N. Lim, R. Jose, K. F. Chong. *RSC Adv.*, **2015,** *5*, 38111-38116; (b) S. Wang, X. Wang, S. P. Jiang. *Langmuir*, **2008,** *24*, 10505-10512.
[93] C. Tanaka, M. Sasaki, T. Aruga, T. Shimada, H. Adachi. US5344985 A. **1994**.
[94] T. Eida, M. Fukuda, K. Nishimura. JP 2011023614. **2011**.
[95] (a) A. L. Launen, J. L. Pinto, M. M. Moore. *Appl. Microbiol. Biotechnol.*, **1999,** *51*, 510-515; (b) L. Bezalel, Y. Hadar, P. P. Fu, J. P. Freeman, C. E. Cerniglia. *Appl. Environ. Microbiol.*, **1996,** *62*, 2554-2559.
[96] A. J. Fatiadi. *J. Chromatogr. A*, **1965,** *20*, 319-324.

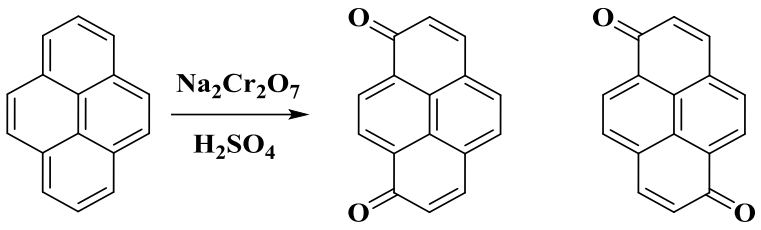

Scheme 9. Oxidation of pyrene to pyrenequinones.

1.2.1.2. Positions 2 and 7

As a result of the previously mentioned problems associated with synthesizing 2- and 2,7-derivatives by traditional aromatic substitution routes, alternative synthetic strategies must be employed, like the oxidation of substituted [2.2]metacyclophanes,[97] photochemical ring-closure of 2,2'-divinylbiphenyls[98] or the electrophilic aromatic substitution of 4,5,9,10-tetrahydropyrene, followed by subsequent dehydrogenation.

A tert-butyl group can be introduced in the positions 2- and 2,7- by treatment of pyrene with aluminum chloride ($AlCl_3$) and tert-butyl chloride.[99] The site-selectivity is determined by steric effects.

[97] H. Irngartinger, R. G. H. Kirrstetter, C. Krieger, H. Rodewald, H. A. Staab. *Tetrahedron Lett.*, **1977,** *18*, 1425-1428.
[98] M. Kreyenschmidt, M. Baumgarten, N. Tyutyulkov, K. Müllen. *Angew. Chem. Int. Ed.*, **1994,** *33*, 1957-1959.
[99] T. Yamato, A. Miyazawa, M. Tashiro. *Chem. Ber.*, **1993,** *126*, 2505-2511.

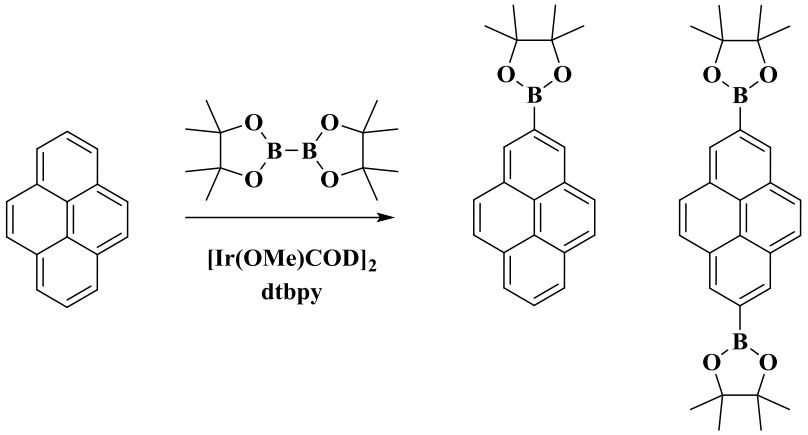

Scheme 10. Borylation of pyrene.

Recently, a one-step synthesis was reported to obtain pyrene-2,7-bis(boronate)ester in very good yields using an *in situ* prepared iridium-based catalyst.[100]

1.2.1.3. Positions 4, 5, 9 and 10

According to Clar's rule for PAHs, the resonance structure with the largest number of disjoint aromatic π-sextets, *i.e.* benzene-like moieties, is the most important for characterization of properties. Considering this rule, pyrene can be represented with two aromatic rings and two double bonds in the K-region, which makes this region to show alkene-like character. For example, reagents which act on double bonds like palladium on charcoal for reduction,[101] or osmium or ruthenium tetraoxide[102] for oxidation, also transform pyrene at the 4,5,9,10 positions.

[100] D. N. Coventry, A. S. Batsanov, A. E. Goeta, J. A. K. Howard, T. B. Marder, R. N. Perutz. *Chem. Commun.*, **2005**, 2172-2174.
[101] P. P. Fu, H. M. Lee, R. G. Harvey. *J. Org. Chem.*, **1980,** *45*, 2797-2803.
[102] (a) F. G. Oberender, J. A. Dixon. *J. Org. Chem.*, **1959,** *24*, 1226-1229; (b) C. J. R. Bataille, T. J. Donohoe. *Chem. Soc. Rev.*, **2011,** *40*, 114-128.

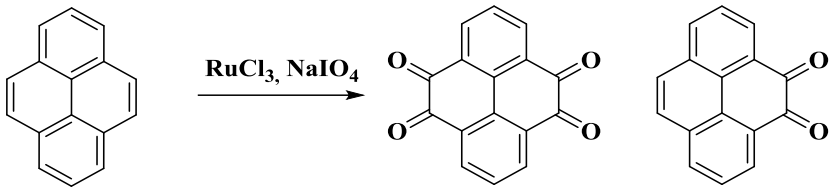

Scheme 11. Oxidation of pyrene to pyrene-4,5,9,10-tetraone and pyrene-4,5-dione.

Another approach to functionalize the 4,5,9,10-positions of the pyrene ring is the bromination of 2,7-di-tertbutylpyrene, which has the active positions blocked, and with an excess of bromine 4,5,9,10-tetrabromo-2,7-di-tert-butylpyrene is obtained.[103]

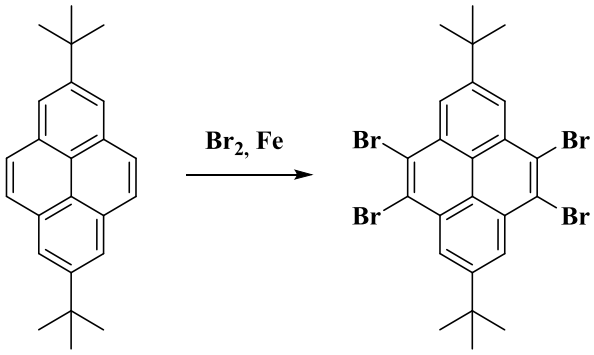

Scheme 12. Bromination of 2,7-di-tert-butylpyrenepyrene to 4,5,9,10-tetrabromo-2,7-di-tert-butylpyrenepyrene.

These two modifications allow the extension of the conjugated system by condensation[104] or the use of the tetrabromo derivative as building block for pyrene-fused pyrazaacenes.[105]

[103] T. Yamato, M. Fujimoto, A. Miyazawa, K. Matsuo. *J. Chem. Soc., Perkin Trans. 1*, **1997**, 1201-1208.
[104] A. Mateo-Alonso, N. Kulisic, G. Valenti, M. Marcaccio, F. Paolucci, M. Prato. *Chem. Asian J.*, **2010,** *5*, 482-485.
[105] A. Mateo-Alonso. *Chem. Soc. Rev.*, **2014,** *43*, 6311-6324.

1.3. References

1. S. Iijima. Helical microtubules of graphitic carbon. *Nature*, **1991**, *354*, 56-58.
2. S. Iijima, T. Ichihashi. Single-shell carbon nanotubes of 1-nm diameter. *Nature*, **1993**, *363*, 603-605
3. (a) M. Terrones. Science and Technology of the Twenty-First Century: Synthesis, Properties, and Applications of Carbon Nanotubes. *Annu. Rev. Mater. Res.*, **2003,** *33*, 419-501; (b) M. Zhang, J. Li. Carbon nanotube in different shapes. *Mater. Today*, **2009**, *12*, 12-18.
4. (a) T. W. Ebbesen, P. M. Ajayan. Large-scale synthesis of carbon nanotubes. *Nature*, **1992**, *358*, 220-222; (b) C. Journet, W. K. Maser, P. Bernier, A. Loiseau, M. L. de la Chapelle, S. Lefrant, P. Deniard, R. Lee, J. E. Fischer. Large-scale production of single-walled carbon nanotubes by the electric-arc technique. *Nature*, **1997**, *388*, 756-758.
5. T. Guo, P. Nikolaev, A. Thess, D. T. Colbert, R. E. Smalley. Catalytic growth of single-walled manotubes by laser vaporization. *Chem. Phys. Lett.*, **1995**, *243*, 49-54.
6. (a) J. Kong, A. M. Cassell, H. Dai. Chemical vapor deposition of methane for single-walled carbon nanotubes. *Chem. Phys. Lett.*, **1998**, *292*, 567-574; (b) M. Su, B. Zheng, J. Liu. A scalable CVD method for the synthesis of single-walled carbon nanotubes with high catalyst productivity. *Chem. Phys. Lett.*, **2000**, *322*, 321-326.
7. (a) M.-F. Yu, B. S. Files, S. Arepalli, R. S. Ruoff. Tensile Loading of Ropes of Single Wall Carbon Nanotubes and their Mechanical Properties. *Phys. Rev. Lett.*, **2000**, *84*, 5552-5555; (b) S. Xie, W. Li, Z. Pan, B. Chang, L. Sun. Mechanical and physical properties on carbon nanotube. *J. Phys. Chem. Solids*, **2000**, *61*, 1153-1158.
8. (a) S. H. Ng, J. Wang, Z. P. Guo, J. Chen, G. X. Wang, H. K. Liu. Single wall carbon nanotube paper as anode for lithium-ion battery. *Electrochim. Acta*, **2005**, *51*, 23-28; (b) M. J. Kim, D. W. Shin, J.-Y. Kim, S. H. Park, I. t. Han, J. B. Yoo. The production of a flexible electroluminescent device on polyethylene terephthalate films using transparent conducting carbon nanotube electrode. *Carbon*, **2009**, *47*, 3461-3465; (c) A. L. M. Reddy, M. M. Shaijumon, S. R. Gowda, P. M. Ajayan. Coaxial MnO_2/Carbon Nanotube Array Electrodes for High-Performance Lithium Batteries. *Nano Lett.*, **2009**, *9*, 1002-1006.
9. (a) W. Lu, L. Qu, K. Henry, L. Dai. High performance electrochemical capacitors from aligned carbon nanotube electrodes and ionic liquid electrolytes. *J. Power Sources*, **2009**, *189*, 1270-1277; (b) D. N. Futaba, K. Hata, T. Yamada, T. Hiraoka, Y. Hayamizu, Y. Kakudate, O. Tanaike, H. Hatori, M. Yumura, S. Iijima. Shape-engineerable and highly densely packed single-walled carbon nanotubes and their application as super-capacitor electrodes. *Nat. Mater.*, **2006**, *5*, 987-994; (c) C. Du, N. Pan. Supercapacitors using carbon nanotubes films by electrophoretic deposition. *J. Power Sources*, **2006**, *160*, 1487-1494.

10. A. Wurl, S. Goossen, D. Canevet, M. Sallé, E. M. Pérez, N. Martín, C. Klinke. Supramolecular Interaction of Single-Walled Carbon Nanotubes with a Functional TTF-Based Mediator Probed by Field-Effect Transistor Devices. *J. Phys, Chem. C*, **2012**, *116*, 20062-20066.
11. (a) M. Bernardi, J. Lohrman, P. V. Kumar, A. Kirkeminde, N. Ferralis, J. C. Grossman, S. Ren. Nanocarbon-Based Photovoltaics. *ACS Nano*, **2012**, *6*, 8896-8903; (b) H. Wang, G. I. Koleilat, P. Liu, G. Jiménez-Osés, Y.-C. Lai, M. Vosgueritchian, Y. Fang, S. Park, K. N. Houk, Z. Bao. High-Yield Sorting of Small-Diameter Carbon Nanotubes for Solar Cells and Transistors. *ACS Nano*, **2014**, *8*, 2609-2617.
12. (a) B. Esser, J. M. Schnorr, T. M. Swager. Selective Detection of Ethylene Gas Using Carbon Nanotube-based Devices: Utility in Determination of Fruit Ripeness. *Angew. Chem. Int. Ed.*, **2012**, *51*, 5752-5756; (b) A. M. Münzer, Z. P. Michael, A. Star. Carbon Nanotubes for the Label-Free Detection of Biomarkers. *ACS Nano*, **2013**, *7*, 7448-7453.
13. (a) A. Le Goff, V. Artero, B. Jousselme, P. D. Tran, N. Guillet, R. Métayé, A. Fihri, S. Palacin, M. Fontecave. From Hydrogenases to Noble Metal–Free Catalytic Nanomaterials for H_2 Production and Uptake, *Science*, **2009**, *326*, 1384-1387; (b) V. Lordi, N. Yao, J. Wei. Method for Supporting Platinum on Single-Walled Carbon Nanotubes for a Selective Hydrogenation Catalyst. *Chem. Mater.*, **2001**, *13*, 733-737; (c) L. Jiang, H. Gu, X. Xu, X. Yan. Selective hydrogenation of o-chloronitrobenzene (o-CNB) over supported Pt and Pd catalysts obtained by laser vaporization deposition of bulk metals. *J. Mol. Catal. A: Chem.*, **2009**, *310*, 144-149; (d) X. Tan, W. Deng, M. Liu, Q. Zhang, Y. Wang. Carbon nanotube-supported gold nanoparticles as efficient catalysts for selective oxidation of cellobiose into gluconic acid in aqueous medium. *Chem. Commun.*, **2009**, 7179-7181; (e) J. A. Sullivan, K. A. Flanagan, H. Hain. Suzuki coupling activity of an aqueous phase Pd nanoparticle dispersion and a carbon nanotube/Pd nanoparticle composite. *Catal. Today*, **2009**, *145*, 108-113.
14. (a) G. Cellot, E. Cilia, S. Cipollone, V. Rancic, A. Sucapane, S. Giordani, L. Gambazzi, H. Markram, M. Grandolfo, D. Scaini, F. Gelain, L. Casalis, M. Prato, M. Giugliano, L. Ballerini. Carbon nanotubes might improve neuronal performance by favouring electrical shortcuts. *Nat. Nanotechnol.*, **2009**, *4*, 126-133; (b) M. Adeli, R. Soleyman, Z. Beiranvand, F. Madani. Carbon nanotubes in cancer therapy: a more precise look at the role of carbon nanotube-polymer interactions. *Chem. Soc. Rev.*, **2013**, *42*, 5231-5256.
15. J. M. Schnorr, T. M. Swager. Emerging Applications of Carbon Nanotubes. *Chem. Mater.*, **2011**, *23*, 646-657.
16. (a) A. Di Crescenzo, V. Ettorre, A. Fontana. Non-covalent and reversible functionalization of carbon nanotubes. *Beilstein J. Nanotechnol.*, **2014**, *5*, 1675-1690; (b) A. Saleh, V. K. Gupta. Covalent and Non-Covalent Functionalization of Carbon Nanotubes. In *Advanced Carbon Materials and Technology*, John Wiley & Sons, Inc. **2014**; pp 317-330.

17. J. Liu, A. G. Rinzler, H. Dai, J. H. Hafner, R. K. Bradley, P. J. Boul, A. Lu, T. Iverson, K. Shelimov, C. B. Huffman, F. Rodriguez-Macias, Y.-S. Shon, T. R. Lee, D. T. Colbert, R. E. Smalley. Fullerene Pipes. *Science*, **1998**, *280*, 1253-1256.
18. M. A. Hamon, J. Chen, H. Hu, Y. Chen, M. E. Itkis, A. M. Rao, P. C. Eklund, R. C. Haddon. Dissolution of Single-Walled Carbon Nanotubes. *Adv. Mater.*, **1999**, *11*, 834-840.
19. B. Zhao, H. Hu, R. C. Haddon. Synthesis and Properties of a Water-Soluble Single-Walled Carbon Nanotube–Poly(m-aminobenzene sulfonic acid) Graft Copolymer. *Adv. Funct. Mater.*, **2004**, *14*, 71-76.
20. (a) J. L. Delgado, P. de la Cruz, A. Urbina, J. T. López Navarrete, J. Casado, F. Langa. The first synthesis of a conjugated hybrid of C60–fullerene and a single-wall carbon nanotube. *Carbon*, **2007**, *45*, 2250-2252; (b) S. Giordani, J.-F. Colomer, F. Cattaruzza, J. Alfonsi, M. Meneghetti, M. Prato, D. Bonifazi. Multifunctional hybrid materials composed of [60]fullerene-based functionalized-single-walled carbon nanotubes. *Carbon*, **2009**, *47*, 578-588.
21. S. E. Baker, W. Cai, T. L. Lasseter, K. P. Weidkamp, R. J. Hamers. Covalently Bonded Adducts of Deoxyribonucleic Acid (DNA) Oligonucleotides with Single-Wall Carbon Nanotubes: Synthesis and Hybridization. *Nano Lett.*, **2002**, *2*, 1413-1417.
22. L. Gu, T. Elkin, X. Jiang, H. Li, Y. Lin, L. Qu, T.-R. J. Tzeng, R. Joseph, Y.-P. Sun. Single-walled carbon nanotubes displaying multivalent ligands for capturing pathogens. *Chem. Commun.*, **2005**, 874-876.
23. S. Cosnier, M. Holzinger. Design of carbon nanotube-polymer frameworks by electropolymerization of SWCNT-pyrrole derivatives. *Electrochim. Acta*, **2008**, *53*, 3948-3954.
24. (a) H. Li, R. B. Martin, B. A. Harruff, R. A. Carino, L. F. Allard, Y. P. Sun. Single-Walled Carbon Nanotubes Tethered with Porphyrins: Synthesis and Photophysical Properties. *Adv. Mater.*, **2004**, *16*, 896-900; (b) D. Baskaran, J. W. Mays, X. P. Zhang, M. S. Bratcher. Carbon Nanotubes with Covalently Linked Porphyrin Antennae: Photoinduced Electron Transfer. *J. Am. Chem. Soc.*, **2005**, *127*, 6916-6917.
25. D. Srivastava, D. W. Brenner, J. D. Schall, K. D. Ausman, M. Yu, R. S. Ruoff. Predictions of Enhanced Chemical Reactivity at Regions of Local Conformational Strain on Carbon Nanotubes: Kinky Chemistry. *J. Phys. Chem. B*, **1999**, *103*, 4330-4337.
26. P. Singh, S. Campidelli, S. Giordani, D. Bonifazi, A. Bianco, M. Prato. Organic functionalization and characterization of single-walled carbon nanotubes. *Chem. Soc. Rev.*, **2009**, *38*, 2214-2230.
27. E. T. Mickelson, C. B. Huffman, A. G. Rinzler, R. E. Smalley, R. H. Hauge, J. L. Margrave. Fluorination of single-wall carbon nanotubes. *Chem. Phys. Lett.*, **1998**, *296*, 188-194.

28. H. Hu, B. Zhao, M. A. Hamon, K. Kamaras, M. E. Itkis, R. C. Haddon. Sidewall Functionalization of Single-Walled Carbon Nanotubes by Addition of Dichlorocarbene. *J. Am. Chem. Soc.*, **2003**, *125*, 14893-14900.
29. M. Holzinger, J. Abraham, P. Whelan, R. Graupner, L. Ley, F. Hennrich, M. Kappes, A. Hirsch. Functionalization of Single-Walled Carbon Nanotubes with (R-)Oxycarbonyl Nitrenes. *J. Am. Chem. Soc.*, **2003**, *125*, 8566-8580.
30. M. Maggini, G. Scorrano, M. Prato. Addition of azomethine ylides to C60: synthesis, characterization, and functionalization of fullerene pyrrolidines. *J. Am. Chem. Soc.*, **1993**, *115*, 9798-9799.
31. (a) A. Callegari, M. Marcaccio, D. Paolucci, F. Paolucci, N. Tagmatarchis, D. Tasis, E. Vazquez, M. Prato. Anion recognition by functionalized single wall carbon nanotubes. *Chem. Commun.*, **2003**, 2576-2577; (b) D. M. Guldi, M. Marcaccio, D. Paolucci, F. Paolucci, N. Tagmatarchis, D. Tasis, E. Vázquez, M. Prato. Single-Wall Carbon Nanotube–Ferrocene Nanohybrids: Observing Intramolecular Electron Transfer in Functionalized SWNTs. *Angew. Chem. Int. Ed.*, **2003**, *42*, 4206-4209; (c) V. Georgakilas, A. Bourlinos, D. Gournis, T. Tsoufis, C. Trapalis, A. Mateo-Alonso, M. Prato. Multipurpose Organically Modified Carbon Nanotubes: From Functionalization to Nanotube Composites. *J. Am. Chem. Soc.*, **2008**, *130*, 8733-8740; (d) M. Prato, K. Kostarelos, A. Bianco. Functionalized Carbon Nanotubes in Drug Design and Discovery. *Acc. Chem. Res.*, **2008**, *41*, 60-68.
32. J. L. Delgado, P. de la Cruz, F. Langa, A. Urbina, J. Casado, J. T. López Navarrete. Microwave-assisted sidewall functionalization of single-wall carbon nanotubes by Diels-Alder cycloaddition. *Chem. Commun.*, **2004**, 1734-1735.
33. K. S. Coleman, S. R. Bailey, S. Fogden, M. L. H. Green. Functionalization of Single-Walled Carbon Nanotubes via the Bingel Reaction. *J. Am. Chem. Soc.*, **2003**, *125*, 8722-8723.
34. (a) T. Nakamura, M. Ishihara, T. Ohana, A. Tanaka, Y. Koga. Sidewall modification of single-walled carbon nanotubes using photolysis of perfluoroazooctane. *Chem. Commun.*, **2004**, 1336-1337; (b) H. Peng, L. B. Alemany, J. L. Margrave, V. N. Khabashesku. Sidewall Carboxylic Acid Functionalization of Single-Walled Carbon Nanotubes. *J. Am. Chem. Soc.*, **2003**, *125*, 15174-15182; (c) Y. Ying, R. K. Saini, F. Liang, A. K. Sadana, W. E. Billups. Functionalization of Carbon Nanotubes by Free Radicals. *Org. Lett.*, **2003**, *5*, 1471-1473; (d) L. Wei, Y. Zhang. Covalent sidewall functionalization of single-walled carbon nanotubes via one-electron reduction of benzophenone by potassium. *Chem. Phys. Lett.*, **2007**, *446*, 142-144.
35. (a) S. Pekker, J. P. Salvetat, E. Jakab, J. M. Bonard, L. Forró. Hydrogenation of Carbon Nanotubes and Graphite in Liquid Ammonia. *J. Phys. Chem. B*, **2001**, *105*, 7938-7943; (b) A. Pénicaud, P. Poulin, A. Derré, E. Anglaret, P. Petit. Spontaneous Dissolution of a Single-Wall Carbon Nanotube Salt. *J. Am. Chem. Soc.*, **2005**, *127*, 8-9; (c) A. García-Gallastegui, I. Obieta, I. Bustero, G. Imbuluzqueta, J. Arbiol, J. I. Miranda, J. M. Aizpurua. Reductive Functionalization of Single-Walled Carbon

Nanotubes with Lithium Metal Catalyzed by Electron Carrier Additives. *Chem. Mater.*, **2008**, *20*, 4433-4438.
36. C. A. Dyke, J. M. Tour. Covalent Functionalization of Single-Walled Carbon Nanotubes for Materials Applications. *J. Phys. Chem. A*, **2004**, *108*, 11151-11159.
37. (a) A. Di Crescenzo, V. Ettorre, A. Fontana. Non-covalent and reversible functionalization of carbon nanotubes. *Beilstein J. Nanotechnol.*, **2014**, *5*, 1675-1690; (b) H. Li, S. I. Song, G. Y. Song, I. Kim. Non-Covalently Functionalized Carbon Nanostructures for Synthesizing Carbon-Based Hybrid Nanomaterials. *J. Nanosci. Nanotechnol.*, **2014**, *14*, 1425-1440; (c) P. Bilalis, D. Katsigiannopoulos, A. Avgeropoulos, G. Sakellariou. Non-covalent functionalization of carbon nanotubes with polymers. *RSC Adv.*, **2014**, *4*, 2911-2934; (d) E. M. Pérez, N. Martín. π-π interactions in carbon nanostructures. *Chem. Soc. Rev*., **2015**, *44*, 6425-6433.
38. C.-L. Lee, Y.-C. Ju, P.-T. Chou, Y.-C. Huang, L.-C. Kuo, J.-C. Oung. Preparation of Pt nanoparticles on carbon nanotubes and graphite nanofibers via self-regulated reduction of surfactants and their application as electrochemical catalyst. *Electrochem. Commun.*, **2005**, *7*, 453-458.
39. C. Zamora-Ledezma, L. Añez, J. Primera, P. Silva, S. Etienne-Calas, E. Anglaret. Photoluminescent single wall carbon nanotube–silica composite gels. *Carbon*, **2008**, *46*, 1253-1255.
40. D. Eder, A. H. Windle. Morphology control of CNT-TiO_2 hybrid materials and rutile nanotubes. *J. Mater. Chem.*, **2008**, *18*, 2036-2043.
41. X. L. Li, Y. Q. Liu, L. Fu, L. C. Cao, D. C. Wei, Y. Wang. Efficient Synthesis of Carbon Nanotube–Nanoparticle Hybrids. *Adv. Funct. Mater.*, **2006**, *16*, 2431-2437.
42. R. J. Chen, Y. Zhang, D. Wang, H. Dai. Noncovalent Sidewall Functionalization of Single-Walled Carbon Nanotubes for Protein Immobilization. *J. Am. Chem. Soc.*, **2001**, *123*, 3838-3839.
43. N. Nakashima, Y. Tomonari, Murakami. Water-Soluble Single-Walled Carbon Nanotubes via Noncovalent Sidewall-Functionalization with a Pyrene-Carrying Ammonium Ion. *Chem. Lett.*, **2002**, *31*, 638-639.
44. (a) A. Carrillo, J. A. Swartz, J. M. Gamba, R. S. Kane, N. Chakrapani, B. Wei, P. M. Ajayan. Noncovalent Functionalization of Graphite and Carbon Nanotubes with Polymer Multilayers and Gold Nanoparticles. *Nano Lett.*, **2003**, *3*, 1437-1440; (b) M. A. Correa-Duarte, N. Sobal, L. M. Liz-Marzán, M. Giersig. Linear Assemblies of Silica-Coated Gold Nanoparticles Using Carbon Nanotubes as Templates. *Adv. Mater.*, **2004**, *16*, 2179-2184; (c) K. Welsher, Z. Liu, S. P. Sherlock, J. T. Robinson, Z. Chen, D. Daranciang, H. Dai. A route to brightly fluorescent carbon nanotubes for near-infrared imaging in mice. *Nat. Nanotechnol.*, **2009**, *4*, 773-780.
45. (a) R. Bandyopadhyaya, E. Nativ-Roth, O. Regev, R. Yerushalmi-Rozen. Stabilization of Individual Carbon Nanotubes in Aqueous Solutions. Nano Lett., **2002**, *2*, 25-28; (b) R. Shvartzman-Cohen, E. Nativ-Roth, E. Baskaran, Y. Levi-Kalisman, I. Szleifer, R. Yerushalmi-Rozen. Selective Dispersion of Single-Walled Carbon

Nanotubes in the Presence of Polymers: the Role of Molecular and Colloidal Length Scales. *J. Am. Chem. Soc.*, **2004**, *126*, 14850-14857.
46. (a) J. Zou, L. Liu, H. Chen, S. I. Khondaker, R. D. McCullough, Q. Huo, L. Zhai. Dispersion of Pristine Carbon Nanotubes Using Conjugated Block Copolymers. *Adv. Mater.*, **2008**, *20*, 2055-2060; (b) K. T. Kim, W. H. Jo. Noncovalent functionalization of multiwalled carbon nanotubes using graft copolymer with naphthalene and its application as a reinforcing filler for poly(styrene-co-acrylonitrile). *J. Polym. Sci., Part A: Polym. Chem.*, **2010**, *48*, 4184-4191; (c) J. Zou, H. Chen, A. Chunder, Y. Yu, Q. Huo, L. Zhai. Preparation of a Superhydrophobic and Conductive Nanocomposite Coating from a Carbon-Nanotube-Conjugated Block Copolymer Dispersion. *Adv. Mater.*, **2008**, *20*, 3337-3341.
47. (a) H. Wang, G. I. Koleilat, P. Liu, G. Jiménez-Osés, Y.-C. Lai, M. Vosgueritchian, Y. Fang, S. Park, K. N. Houk, Z. Bao. High-Yield Sorting of Small-Diameter Carbon Nanotubes for Solar Cells and Transistors. *ACS Nano*, **2014**, *8*, 2609-2617; (b) H. W. Lee, Y. Yoon, S. Park, J. H. Oh, S. Hong, L. S. Liyanage, H. Wang, S. Morishita, N. Patil, Y. J. Park, J. J. Park, A. Spakowitz, G. Galli, F. Gygi, P. H. S. Wong, J. B. H. Tok, J. M. Kim, Z. Bao. Selective dispersion of high purity semiconducting single-walled carbon nanotubes with regioregular poly(3-alkylthiophene)s. *Nat. Commun.*, **2011**, *2*, 541.
48. A. Nish, J.-Y. Hwang, J. Doig, R. J. Nicholas. Highly selective dispersion of single-walled carbon nanotubes using aromatic polymers. *Nat. Nanotechnol.*, **2007**, *2*, 640-646.
49. X. Tu, S. Manohar, A. Jagota, M. Zheng. DNA sequence motifs for structure-specific recognition and separation of carbon nanotubes. *Nature*, **2009**, *460*, 250-253.
50. (a) H. Li, J. K. Jo, L. Zhang, C.-S. Ha, H. Suh, I. Kim. A General and Efficient Route to Fabricate Carbon Nanotube-Metal Nanoparticles and Carbon Nanotube-Inorganic Oxides Hybrids. *Adv. Funct. Mater.*, **2010**, *20*, 3864-3873; (b) H. Li, L. Han, J. J. Cooper-White, I. Kim. A general and efficient method for decorating graphene sheets with metal nanoparticles based on the non-covalently functionalized graphene sheets with hyperbranched polymers. *Nanoscale*, **2012**, *4*, 1355-1361; (c) H. Li, J. J. Cooper-White. Hyperbranched polymer mediated fabrication of water soluble carbon nanotube-metal nanoparticle hybrids. *Nanoscale*, **2013**, *5*, 2915-2920.
51. P. R. Ashton, C. L. Brown, E. J. T. Chrystal, T. T. Goodnow, A. E. Kaifer, K. P. Parry, D. Philp, A. M. Z. Slawin, N. Spencer, J. F. Stoddart, D. J. Williams. The self-assembly of a highly ordered [2]catenane. *J. Chem. Soc., Chem. Commun.*, **1991**, 634-639.
52. J. A. Bravo, F. M. Raymo, J. F. Stoddart, A. J. P. White, D. J. Williams. High Yielding Template-Directed Syntheses of [2]Rotaxanes. *Eur. J. Org. Chem.*, **1998**, 2565-2571.
53. E. R. Kay, D. A. Leigh, F. Zerbetto. Synthetic Molecular Motors and Mechanical Machines. *Angew. Chem. Int. Ed.*, **2007**, *46*, 72-191.

54. L. Fang, M. A. Olson, D. Benitez, E. Tkatchouk, W. A. Goddard Iii, J. F. Stoddart. Mechanically bonded macromolecules. *Chem. Soc. Rev.*, **2010**, *39*, 17-29.
55. Q. Li, C.-H. Sue, S. Basu, A. K. Shveyd, W. Zhang, G. Barin, L. Fang, A. A. Sarjeant, J. F. Stoddart, O. M. Yaghi. A Catenated Strut in a Catenated Metal–Organic Framework. *Angew. Chem. Int. Ed.*, **2010**, *49*, 6751-6755.
56. A. de Juan, Y. Pouillon, L. Ruiz-González, A. Torres-Pardo, S. Casado, N. Martín, Á. Rubio, E. M. Pérez. Mechanically Interlocked Single-Wall Carbon Nanotubes. *Angew. Chem. Int. Ed.*, **2014**, *53*, 5394-5400.
57. (a) D. Canevet, M. Gallego, H. Isla, A. de Juan, E. M. Pérez, N. Martín. Macrocyclic Hosts for Fullerenes: Extreme Changes in Binding Abilities with Small Structural Variations. *J. Am. Chem. Soc.*, **2011**, *133*, 3184-3190; (b) H. Isla, M. Gallego, E. M. Pérez, R. Viruela, E. Ortí, N. Martín. A Bis-exTTF Macrocyclic Receptor That Associates C60 with Micromolar Affinity. *J. Am. Chem. Soc.*, **2010**, *132*, 1772-1773.
58. C. Romero-Nieto, R. García, M. Á. Herranz, C. Ehli, M. Ruppert, A. Hirsch, D. M. Guldi, N. Martín. Tetrathiafulvalene-Based Nanotweezers—Noncovalent Binding of Carbon Nanotubes in Aqueous Media with Charge Transfer Implications. *J. Am. Chem. Soc.*, **2012**, *134*, 9183-9192.
59. A. de Juan, M. Mar Bernal, E. M. Pérez. Optimization and Insights into the Mechanism of Formation of Mechanically Interlocked Derivatives of Single-Walled Carbon Nanotubes. *ChemPlusChem*, **2015**, *80*, 1153-1157.
60. E. Martínez-Periñan, A. de Juan, Y. Pouillon, C. Schierl, V. Strauss, N. Martín, A. Rubio, D. M. Guldi, E. Lorenzo, E. M. Pérez. The mechanical bond on carbon nanotubes: diameter-selective functionalization and effects on physical properties. *Nanoscale*, **2016**, *8*, 9254-9264.
61. G. v. Bünau. J. B. Birks: Photophysics of Aromatic Molecules. Wiley-Interscience, London. 704 Seiten. Preis: 210s. *Berichte der Bunsengesellschaft für physikalische Chemie*, **1970**, *74*, 1294-1295.
62. S. Karuppannan, J.-C. Chambron. Supramolecular Chemical Sensors Based on Pyrene Monomer–Excimer Dual Luminescence. *Chem. Asian J.*, **2011**, *6*, 964-984
63. G. Bains, A. B. Patel, V. Narayanaswami. Pyrene: A Probe to Study Protein Conformation and Conformational Changes. *Molecules*, **2011**, *16*, 7909.
64. C. Ehli, G. M. A. Rahman, N. Jux, D. Balbinot, D. M. Guldi, F. Paolucci, M. Marcaccio, D. Paolucci, M. Melle-Franco, F. Zerbetto, S. Campidelli, M. Prato. Interactions in Single Wall Carbon Nanotubes/Pyrene/Porphyrin Nanohybrids. *J. Am. Chem. Soc.*, **2006**, *128*, 11222-11231.
65. G. Zeng, Y. Xing, J. Gao, Z. Wang, X. Zhang. Unconventional Layer-by-Layer Assembly of Graphene Multilayer Films for Enzyme-Based Glucose and Maltose Biosensing. *Langmuir*, **2010**, *26*, 15022-15026.
66. (a) S. Karuppannan, J.-C. Chambron. Supramolecular Chemical Sensors Based on Pyrene Monomer–Excimer Dual Luminescence. *Chem. Asian J.*, **2011**, *6*, 964-984; (b)

E. Manandhar, K. J. Wallace. Host–guest chemistry of pyrene-based molecular receptors. *Inorg. Chim. Acta*, **2012**, *381*, 15-43.
67. (a) A. Ueno, I. Suzuki, T. Osa. Formation of pyrene excimer in an association dimer of pyrene-appended γ-cyclodextrin. *J. Chem. Soc., Chem. Commun.*, **1988**, 1373-1374; (b) A. Ueno, I. Suzuki, T. Osa. Association dimers, excimers, and inclusion complexes of pyrene-appended γ-cyclodextrins. *J. Am. Chem. Soc.*, **1989**, *111*, 6391-6397.
68. H. S. Jung, M. Park, D. Y. Han, E. Kim, C. Lee, S. Ham, J. S. Kim. Cu^{2+} Ion-Induced Self-Assembly of Pyrenylquinoline with a Pyrenyl Excimer Formation. *Org. Lett.*, **2009**, *11*, 3378-3381.
69. R.-H. Yang, W.-H. Chan, A. W. M. Lee, P.-F. Xia, H.-K. Zhang. A Ratiometric Fluorescent Sensor for AgI with High Selectivity and Sensitivity. *J. Am. Chem. Soc.*, **2003**, *125*, 2884-2885.
70. R. Martínez, A. Espinosa, A. Tárraga, P. Molina. New Hg^{2+} and Cu^{2+} Selective Chromo- and Fluoroionophore Based on a Bichromophoric Azine. *Org. Lett.*, **2005**, *7*, 5869-5872.
71. L.-J. Ma, Y.-F. Liu, Y. Wu. A tryptophan-containing fluoroionophore sensor with high sensitivity to and selectivity for lead ion in water. *Chem. Commun.*, **2006**, 2702-2704.
72. K. Yamana, Y. Fukunaga, Y. Ohtani, S. Sato, M. Nakamura, W. J. Kim, T. Akaike, A. Maruyama. DNA mismatch detection using a pyrene-excimer-forming probe. *Chem. Commun.*, **2005**, 2509-2511.
73. C. Yu, V. W.-W. Yam. Glucose sensing via polyanion formation and induced pyrene excimer emission. *Chem. Commun.*, **2009**, 1347-1349.
74. (a) K. Paek, H. Yang, J. Lee, J. Park, B. J. Kim. Efficient Colorimetric pH Sensor Based on Responsive Polymer–Quantum Dot Integrated Graphene Oxide. *ACS Nano*, **2014,** *8*, 2848-2856; (b) X. Mao, H. Su, D. Tian, H. Li, R. Yang. Bipyrene-Functionalized Graphene as a "Turn-On" Fluorescence Sensor for Manganese (II) Ions in Living cells. *ACS Appl. Mater. Interfaces*, **2013,** *5*, 592-597; (c) C. Yu, Y. Guo, H. Liu, N. Yan, Z. Xu, G. Yu, Y. Fang, Y. Liu. Ultrasensitive and selective sensing of heavy metal ions with modified graphene. *Chem. Commun.*, **2013,** *49*, 6492-6494.
75. L. Zeng, P. Wang, H. Zhang, X. Zhuang, Q. Dai, W. Liu. Highly Selective and Sensitive Heparin Probing from Supramolecular Assembly of Pyrene Derivatives. *Org. Lett.*, **2009**, *11*, 4294-4297.
76. (a) M. Zhang, R. R. Parajuli, D. Mastrogiovanni, B. Dai, P. Lo, W. Cheung, R. Brukh, P. L. Chiu, T. Zhou, Z. Liu, E. Garfunkel, H. He. Production of Graphene Sheets by Direct Dispersion with Aromatic Healing Agents. *Small*, **2010**, *6*, 1100-1107; (b) D. Parviz, S. Das, H. S. T. Ahmed, F. Irin, S. Bhattacharia, M. J. Green. Dispersions of Non-Covalently Functionalized Graphene with Minimal Stabilizer. *ACS Nano*, **2012**, *6*, 8857-8867; (c) X. An, T. Simmons, R. Shah, C. Wolfe, K. M. Lewis, M. Washington, S. K. Nayak, S. Talapatra, S. Kar. Stable Aqueous Dispersions of

Noncovalently Functionalized Graphene from Graphite and their Multifunctional High-Performance Applications. *Nano Lett.*, **2010**, *10*, 4295-4301.
77. H. Wang, Z. Chen, L. Xin, J. Cui, S. Zhao, Y. Yan. Synthesis of pyrene-capped polystyrene by free radical polymerization and its application in direct exfoliation of graphite into graphene nanosheets. *J. Polym. Sci., Part A: Polym. Chem.*, **2015**, *53*, 2175-2185.
78. K. D. Papadimitriou, E. N. Skountzos, S. S. Gkermpoura, I. Polyzos, V. G. Mavrantzas, C. Galiotis, C. Tsitsilianis. Molecular Modeling Combined with Advanced Chemistry for the Rational Design of Efficient Graphene Dispersing Agents. *ACS Macro Lett.*, **2016**, *5*, 24-29.
79. K. Yang, L. Zhu, B. Xing. Adsorption of Polycyclic Aromatic Hydrocarbons by Carbon Nanomaterials. *Environ. Sci. Technol*, **2006**, *40*, 1855-1861.
80. N. Nakashima, Y. Tomonari, H. Murakami. Water-Soluble Single-Walled Carbon Nanotubes via Noncovalent Sidewall-Functionalization with a Pyrene-Carrying Ammonium Ion. *Chem. Lett.*, **2002**, *31*, 638-639.
81. Y. Tomonari, H. Murakami, N. Nakashima. Solubilization of Single-Walled Carbon Nanotubes by using Polycyclic Aromatic Ammonium Amphiphiles in Water—Strategy for the Design of High-Performance Solubilizers. *Chem. - Eur. J.*, **2006**, *12*, 4027-4034.
82. (a) G. J. Bahun, C. Wang, A. Adronov. Solubilizing single-walled carbon nanotubes with pyrene-functionalized block copolymers. *J. Polym. Sci., Part A: Polym. Chem.*, **2006**, *44*, 1941-1951; (b) P. Petrov, F. Stassin, C. Pagnoulle, R. Jerome. Noncovalent functionalization of multi-walled carbon nanotubes by pyrene containing polymers. *Chem. Commun.*, **2003**, 2904-2905.
83. W. Z. Yuan, J. Z. Sun, Y. Dong, M. Häussler, F. Yang, H. P. Xu, A. Qin, J. W. Y. Lam, Q. Zheng, B. Z. Tang. Wrapping Carbon Nanotubes in Pyrene-Containing Poly(phenylacetylene) Chains: Solubility, Stability, Light Emission, and Surface Photovoltaic Properties. *Macromolecules*, **2006**, *39*, 8011-8020.
84. (a) D. M. Guldi, G. M. A. Rahman, V. Sgobba, N. A. Kotov, D. Bonifazi, M. Prato. CNT−CdTe Versatile Donor−Acceptor Nanohybrids. *J. Am. Chem. Soc.*, **2006**, *128*, 2315-2323; (b) L. Hu, Y. L. Zhao, K. Ryu, C. Zhou, J. F. Stoddart, G. Grüner. Light-Induced Charge Transfer in Pyrene/CdSe-SWNT Hybrids. *Adv. Mater.*, **2008**, *20*, 939-946.
85. (a) T. M. Figueira-Duarte, K. Müllen. Pyrene-Based Materials for Organic Electronics. *Chem. Rev.*, **2011**, *111*, 7260-7314; (b) J. M. Casas-Solvas, J. D. Howgego, A. P. Davis. Synthesis of substituted pyrenes by indirect methods. *Org. Biomol. Chem.*, **2014**, *12* 212-232; (c) X. Feng, J.-Y. Hu, C. Redshaw, T. Yamato. Functionalization of Pyrene to Prepare Luminescent Materials—Typical Examples of Synthetic Methodology. *Chem. - Eur. J.*, **2016**, *22*, 11898-11916.

86. M. J. S. Dewar, R. D. Dennington. DEWAR-PI study of electrophilic substitution in selected polycyclic fluoranthene hydrocarbons. *J. Am. Chem. Soc.*, **1989**, *111*, 3804-3808.
87. H. Cerfontain, K. Laali, H. J. A. Lambrechts. Aromatic sulfonation 86. Sulfonation of pyrene, 1-methylpyrene and perylene. *Recl. Trav. Chim. Pays-Bas*, **1983**, *102*, 210-214.
88. D. N. Coventry, A. S. Batsanov, A. E. Goeta, J. A. K. Howard, T. B. Marder, R. N. Perutz. Selective Ir-catalysed borylation of polycyclic aromatic hydrocarbons: structures of naphthalene-2,6-bis(boronate), pyrene-2,7-bis(boronate) and perylene-2,5,8,11-tetra(boronate) esters. *Chem. Commun.*, **2005**, 2172-2174.
89. H. Vollmann, H. Becker, M. Corell, H. Streeck. Beiträge zur Kenntnis des Pyrens und seiner Derivate. *Justus Liebigs Ann, Chem.*, **1937**, *531*,1-159.
90. J. Grimshaw, J. Trocha-Grimshaw. Characterisation of 1,6- and 1,8-dibromopyrenes. *J. Chem. Soc., Perkin Trans. 1*, **1972**, 1622-1623.
91. (a) H. Vollmann, H. Becker, M. Corell, H. Streeck. Beiträge zur Kenntnis des Pyrens und seiner Derivate. *Justus Liebigs Ann, Chem.*, **1937**, *531*,1-159; (b) Y. Hashimoto, K. Shudo. Preparation of Pure Isomers of Dinitropyrenes. *Chem. Pharm. Bull.* , **1984**, *32*, 1992-1994.
92. (a) E. Y. L. Teo, H. N. Lim, R. Jose, K. F. Chong. Aminopyrene functionalized reduced graphene oxide as a supercapacitor electrode. *RSC Adv.*, **2015**, *5*, 38111-38116; (b) S. Wang, X. Wang, S. P. Jiang. PtRu Nanoparticles Supported on 1-Aminopyrene-Functionalized Multiwalled Carbon Nanotubes and Their Electrocatalytic Activity for Methanol Oxidation. *Langmuir*, **2008**, *24*, 10505-10512.
93. C. Tanaka, M. Sasaki, T. Aruga, T. Shimada, H. Adachi. US5344985 A. **1994**.
94. T. Eida, M. Fukuda, K. Nishimura. JP 2011023614. **2011**.
95. (a) A. L. Launen, J. L. Pinto, M. M. Moore. Optimization of pyrene oxidation by Penicillium janthinellum using response-surface methodology. *Appl. Microbiol. Biotechnol.*, **1999**, *51*, 510-515; (b) L. Bezalel, Y. Hadar, P. P. Fu, J. P. Freeman, C. E. Cerniglia. Initial Oxidation Products in the Metabolism of Pyrene, Anthracene, Fluorene, and Dibenzothiophene by the White Rot Fungus Pleurotus ostreatus. *Appl. Environ. Microbiol.*, **1996**, *62*, 2554-2559.
96. A. J. Fatiadi. Separation of pyrenediones by column. *J. Chromatogr. A*, **1965**, *20*, 319-324.
97. H. Irngartinger, R. G. H. Kirrstetter, C. Krieger, H. Rodewald, H. A. Staab. Synthese und struktur von [2.2](2,7)pyrenophan. *Tetrahedron Lett.*, **1977**, *18*, 1425-1428.
98. M. Kreyenschmidt, M. Baumgarten, N. Tyutyulkov, K. Müllen. 2,2′-Bipyrenyl and para-Terpyrenyl—A New Type of Electronically Decoupled Oligoarylene. *Angew. Chem. Int. Ed.*, **1994**, *33*, 1957-1959.

99. T. Yamato, A. Miyazawa, M. Tashiro. Medium-Sized Cyclophanes, 29. Synthesis and Desulfurization of 2,11-Dithia[3]metacyclo- and 2,11-Dithia[3]paracyclo[3](4,9)pyrenophanes. *Chem. Ber.*, **1993**, *126*, 2505-2511.
100. D. N. Coventry, A. S. Batsanov, A. E. Goeta, J. A. K. Howard, T. B. Marder, R. N. Perutz. Selective Ir-catalysed borylation of polycyclic aromatic hydrocarbons: structures of naphthalene-2,6-bis(boronate), pyrene-2,7-bis(boronate) and perylene-2,5,8,11-tetra(boronate) esters. *Chem. Commun.*, **2005**, 2172-2174.
101. P. P. Fu, H. M. Lee, R. G. Harvey. Regioselective catalytic hydrogenation of polycyclic aromatic hydrocarbons under mild conditions. *J. Org. Chem.*, **1980**, *45*, 2797-2803.
102. (a) F. G. Oberender, J. A. Dixon. Osmium and Ruthenium Tetroxide-Catalyzed Oxidations of Pyrene1. *J. Org. Chem.*, **1959**, *24*, 1226-1229; (b) C. J. R. Bataille, T. J. Donohoe. Osmium-free direct *syn*-dihydroxylation of alkenes. *Chem. Soc. Rev.*, **2011**, *40*,114-128.
103. T. Yamato, M. Fujimoto, A. Miyazawa, K. Matsuo. Selective preparation of polycyclic aromatic hydrocarbons. Part 5.1 Bromination of 2,7-di-tert-butylpyrene and conversion into pyrenoquinones and their pyrenoquinhydrones. *J. Chem. Soc., Perkin Trans. 1*, **1997**, 1201-1208.
104. A. Mateo-Alonso, N. Kulisic, G. Valenti, M. Marcaccio, F. Paolucci, M. Prato. Facile Synthesis of Highly Stable Tetraazaheptacene and Tetraazaoctacene Dyes. *Chem. Asian J.*, **2010**, *5*, 482-485.
105. A. Mateo-Alonso. Pyrene-fused pyrazaacenes: from small molecules to nanoribbons. *Chem. Soc. Rev.*, **2014**, *43*, 6311-6324.

OBJECTIVES

2. Objectives

The present thesis addresses four main objectives:

i. We will explore new reactions to obtain pyrene derivatives and we will study their electronic properties properties.
ii. We will study the association of pyrene derivatives with SWNTs.
iii. We will prepare pyrene-based U-shaped molecules and macrocycles to use them in the modification of carbon nanotubes through mechanical bond.
iv. We will compare the properties of MINTs to those of supramolecular compounds of identical chemical composition.

As part of this work we will characterize and study:

v. the electron acceptor properties of pyrenequinones by electrochemistry and theoretical calculations.
vi. the association of pyrene derivatives with different types of SWNTs, determining the association constants using thermogravimetric analysis.
vii. the new pyrene-based MINTs through an extensive spectroscopic and microscopic characterization using thermogravimetric analysis, UV-vis-NIR spectroscopy, photoluminescence of excitation, Raman spectroscopy or transmission electron microscopy.
viii. the mechanical properties of MINTs incorporated into polystyrene fibers by electrospinning, and its comparison to supramolecular models.

RESULTS

3. Biomimetic oxidation of pyrene and related aromatic hydrocarbons. Unexpected electron accepting abilities of pyrenequinones

Alejandro López-Moreno, David Clemente-Tejeda, Joaquín Calbo, Atena Naeimi, Francisco Bermejo, Enrique Ortí, and Emilio M. Pérez, *Chem. Commun.*, **2014**, *50*, 9372-9375.

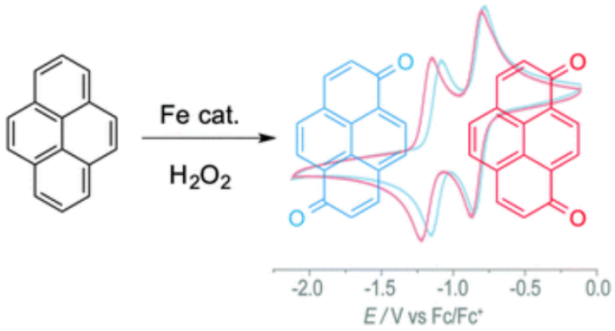

We present a mild catalytic method to oxidize PAHs and, in particular, pyrene. The pyrenediones are much better electron acceptors than benzoquinone in the gas phase and present similar accepting abilities in solution.

3.1. Introduction

Polycyclic aromatic hydrocarbons (PAHs) have attracted a great deal of attention in areas of research as diverse as biochemistry,[1] astrochemistry,[2] and materials science.[3] In this last field, PAHs have received part of the shock wave

[1] D. W. Nebert, T. P. Dalton, A. B. Okey, F. J. González. *J. Biol. Chem.*, **2004,** *279*, 23847-23850.
[2] A. G. G. M. Tielens. *Annu. Rev. Astron. Astrophys.*, **2008,** *46*, 289-337.
[3] (a) J. Wu, W. Pisula, K. Müllen. *Chem. Rev.*, **2007,** *107*, 718-747; (b) M. D. Watson, A. Fechtenkoetter, K. Müllen. *Chem. Rev.*, **2001,** *101*, 1267-1300.

from the recent explosion of research on graphene,[4,5] due to their structural similarities.[6] Among PAHs, pyrene is probably one of the best-known organic chromophores. Its unique absorption and, in particular, its monomer/excimer emission properties have made it the fluorophore of choice for applications ranging from molecular recognition[7] to structural biology.[8] Due to its extended aromatic surface, it has also been utilized in the supramolecular association of carbon nanotubes[9] and graphene.[10] Therefore, synthetic methodologies for the structural variation of pyrene are in high demand.[11] Given their intrinsic stability, the chemical modification of pristine PAHs often relies on harsh conditions, like the utilization of strong oxidizing agents and/or acids. For instance, pyrene can be nitrated with HNO_3/CH_3COOH,[12] brominated with Br_2[13] or sulfonylated with SO_3.[14] In Nature, PAHs are metabolized by cytochrome P450 enzymes (CYPs) to form oxygen-containing electrophilic species, which are known to be

[4] See *Acc. Chem. Res.*, **2013,** *46*, 1-189, special issue on graphene and references cited therein.
[5] (a) J. K. Wassei, R. B. Kaner. *Acc. Chem. Res.*, **2013,** *46*, 2244-2253; (b) L. Rodríguez-Pérez, M. A. Herranz, N. Martin. *Chem. Commun.*, **2013,** *49*, 3721-3735; (c) E. V. Iski, E. N. Yitamben, L. Gao, N. P. Guisinger. *Adv. Funct. Mater.*, **2013,** *23*, 2554-2564; (d) C. K. Chua, M. Pumera. *Chem. Soc. Rev.*, **2013,** *42*, 3222-3233; (e) K. S. Novoselov, V. I. Fal'ko, L. Colombo, P. R. Gellert, M. G. Schwab, K. Kim. *Nature*, **2012,** *490*, 192-200; (f) Y. Zhu, S. Murali, W. Cai, X. Li, J. W. Suk, J. R. Potts, R. S. Ruoff. *Adv. Mater.*, **2010,** *22*, 3906-3924; (g) M. J. Allen, V. C. Tung, R. B. Kaner. *Chem. Rev.*, **2010,** *110*, 132-145.
[6] (a) A. Konishi, Y. Hirao, K. Matsumoto, H. Kurata, R. Kishi, Y. Shigeta, M. Nakano, K. Tokunaga, K. Kamada, T. Kubo. *J. Am. Chem. Soc.*, **2013,** *135*, 1430-1437; (b) C.-N. Feng, M.-Y. Kuo, Y.-T. Wu. *Angew. Chem., Int. Ed.*, **2013,** *52*, 7791-7794; (c) R. Yamaguchi, S. Hiroto, H. Shinokubo. *Org. Lett.*, **2012,** *14*, 2472-2475; (d) D. J. Jones, B. Purushothaman, S. Ji, A. B. Holmes, W. W. H. Wong. *Chem. Commun.*, **2012,** *48*, 8066-8068; (e) L. Chen, Y. Hernandez, X. Feng, K. Müllen. *Angew. Chem., Int. Ed.*, **2012,** *51*, 7640-7654; (f) J. M. Alonso, A. E. Díaz-Álvarez, A. Criado, D. Pérez, D. Peña, E. Guitián. *Angew. Chem., Int. Ed.*, **2012,** *51*, 173-177; (g) X. Yang, X. Dou, A. Rouhanipour, L. Zhi, H. J. Raeder, K. Müllen. *J. Am. Chem. Soc.*, **2008,** *130*, 4216-4217; (h) Z. Liu, R. C. Larock. *Angew. Chem., Int. Ed.*, **2007,** *46*, 2535-2538; (i) X. Feng, J. Wu, M. Ai, W. Pisula, L. Zhi, J. P. Rabe, K. Müllen. *Angew. Chem., Int. Ed.*, **2007,** *46*, 3033-3036; (j) M. Kastler, J. Schmidt, W. Pisula, D. Sebastiani, K. Müllen. *J. Am. Chem. Soc.*, **2006,** *128*, 9526-9534; (k) X. Feng, J. Wu, V. Enkelmann, K. Müllen. *Org. Lett.*, **2006,** *8*, 1145-1148; (l) M. C. Bonifacio, C. R. Robertson, J.-Y. Jung, B. T. King. *J. Org. Chem.*, **2005,** *70*, 8522-8526; (m) Z. Wang, Z. Tomovic, M. Kastler, R. Pretsch, F. Negri, V. Enkelmann, K. Müllen. *J. Am. Chem. Soc.*, **2004,** *126*, 7794-7795.
[7] S. Karuppannan, J.-C. Chambron. *Chem. - Asian J.*, **2011,** *6*, 964-984.
[8] G. Bains, A. B. Patel, V. Narayanaswami. *Molecules*, **2011,** *16*, 7909-7935.
[9] F. D'Souza, A. S. D. Sandanayaka, O. Ito. *J. of Phys. Chem. Lett.*, **2010,** *1*, 2586-2593.
[10] J. A. Mann, J. Rodríguez-López, H. D. Abruña, W. R. Dichtel. *J. Am. Chem. Soc.*, **2011**, *133*, 17614-17617.
[11] (a) A. Mateo-Alonso. *Chem. Soc. Rev.*, **2014,** *43*, 6311-6324; (b) S.-i. Kawano, M. Baumgarten, D. Chercka, V. Enkelmann, K. Müllen. *Chem. Commun.*, **2013,** *49*, 5058-5060.
[12] Y. Hashimoto, K. Shudo. *Chem. Pharm. Bull.*, **1984,** *32*,1992-1997.
[13] S. Bernhardt, M. Kastler, V. Enkelmann, M. Baumgarten, K. Müllen. *Chem. - Eur. J.*, **2006,** *12*, 6117-6128.
[14] A. R. Katritzky, M. S. Kim, D. Fedoseyenko, K. Widyan, M. Siskin, M. Francisco. *Tetrahedron*, **2009,** *65*, 1111-1114.

carcinogenic.[15] Taking pyrene as an example, it is considered to be a priority environmental pollutant by the United States Environment Protection Agency, and its oxidation is an established method for its detoxification.[16] Pyrene can be oxidized to form mixtures of 1,6 and 1,8-pyrenediones (**1** and **2** in **Table 1**) by several microorganisms under aerobic conditions.[17] In a synthetic laboratory setting, a similar outcome can be obtained using extreme conditions, namely $K_2Cr_2O_7$ in 4M H_2SO_4 under reflux for 3 hours, which yields a modest 40% of the mixture of both diones.[18] Alternatively, $Na_2Cr_2O_7 \cdot 2H_2O$ in acetic anhydride and acetic acid can also be utilized to oxidize pyrene at room temperature. This last method requires 24 hours of reaction time and extensive purification to yield 31% and 18% of **1** and **2**, respectively.[19] Here, we present a mild and fast method to oxidize pyrene to the corresponding quinoid 1,6- and 1,8-diketones with hydrogen peroxide, utilizing a non-hemo iron complex as the catalyst. This type of complexes have been successfully utilized as catalysts in the C–H oxidation of a variety of substrates,[20] including alkanes,[21] alkenes[22] and a few arenes[23] under relatively mild, environmentally friendly conditions, typically utilizing H_2O_2 as an oxidant.

---

[15] W. Xue, D. Warshawsky. *Toxicol. Appl. Pharmacol.*, **2005,** *206*, 73-93.
[16] P. Barathi, A. Senthil Kumar. *Langmuir*, **2013,** *29*, 10617-10623.
[17] (a) L. A. Launen, L. J. Pinto, M. M. Moore. *Appl. Microbiol. Biotechnol.*, **1999,** *51*, 510-515; (b) T. Wunder, S. Kremer, O. Sterner, H. Anke. *Appl. Microbiol. Biotechnol.*, **1994,** *42*, 636-641; (c) M. Lambert, S. Kremer, O. Sterner, H. Anke. *Appl. Environ. Microbiol.*, **1994,** *60*, 3597-601.
[18] A. J. Fatiadi. *J. Chromatogr.*, **1965,** *20*, 319-324.
[19] H. Cho, R. G. Harvey. *J. Chem. Soc., Perkin Trans. 1*, **1976**, 836-839.
[20] E. P. Talsi, K. P. Bryliakov. *Coord. Chem. Rev.*, **2012,** *256*, 1418-1434.
[21] (a) Y. Hitomi, K. Arakawa, T. Funabiki, M. Kodera. *Angew. Chem., Int. Ed.*, **2012,** *51*, 3448-3452; (b) L. Gómez, I. Garcia-Bosch, A. Company, J. Benet-Buchholz, A. Polo, X. Sala, X. Ribas, M. Costas. *Angew. Chem. Int. Ed.*, **2009,** *48*, 5720-5723; (c) P. E. Gormisky, M. C. White. *J. Am. Chem. Soc.*, **2013,** *135*, 14052-14055; (d) M. S. Chen, M. C. White. *Science*, **2007,** *318*, 783-787.
[22] (a) P. Spannring, V. Yazerski, P. C. A. Bruijnincx, B. M. Weckhuysen, R. J. M. Klein Gebbink. *Chem. - Eur. J.*, **2013,** *19*, 15012-15018; (b) B. F. Perandones, E. del Rio Nieto, C. Godard, S. Castillon, P. De Frutos, C. Claver. *ChemCatChem*, **2013,** *5*, 1092-1095; (c) D. Clemente-Tejeda, A. López-Moreno, F. A. Bermejo. *Tetrahedron*, **2013,** *69*, 2977-2986; (d) I. Garcia-Bosch, Z. Codola, I. Prat, X. Ribas, J. Lloret-Fillol, M. Costas. *Chem. - Eur. J.*, **2012,** *18*, 13269-13273; (e) S. M. Barry, H. Mueller-Bunz, P. J. Rutledge. *Org. Biomol. Chem.*, **2012,** *10*, 7372-7381; (f) M. S. Chen, M. C. White. *Science*, **2010,** *327*, 566-571.
[23] (a) P. Liu, Y. Liu, E. L.-M. Wong, S. Xiang, C.-M. Che. *Chem. Sci.*, **2011,** *2*, 2187-2195; (b) I. Prat, A. Company, V. Postils, X. Ribas, L. Que, Jr., J. M. Luis, M. Costas. *Chem. - Eur. J.*, **2013,** *19*, 6724-6738.

3.2. Results and discussion

We decided to investigate the oxidation of pyrene utilizing the following non-hemo iron catalysts: [Fe(bpmen)$(OTf)_2$], [Fe(bpycen)$(OTf)_2$], and [Fe$(pymcy)_2(OTf)_2$], where bpmen = *N,N'*-bis-(2-pyridylmethyl)-*N,N'* dimethyl-1,2-ethylenediamine, bpycen = *N,N'*-bis(pyridin-2-ylmethylene)ethane-1,2-diimine, pymcy = N-(pyridin-2-ylmethylene)cyclohexanamine, and OTf = trifluoromethanesulfonate (see **Figure S2** in the experimental section for the structures).

Table 1 Non-hemo iron catalyzed oxidation of pyrene.

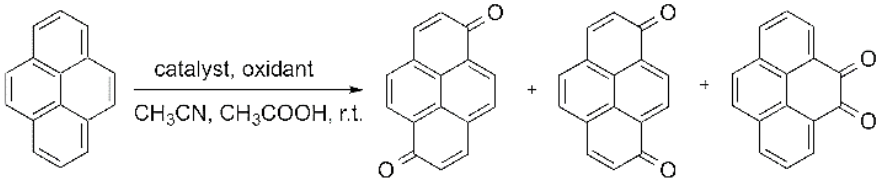

Entry	Catalyst (mol %)	Oxidant (eq.)	Yield (%)[a]		
			1	**2**	**3**
1	Fe$(pymcy)_2(OTf)_2$	H_2O_2 (3 eq.)	-	-	-
2	Fe(bpycen)$(OTf)_2$ (15%)	H_2O_2 (3 eq.)	-	-	-
3	Fe(bpmen)$(OTf)_2$ (5%)	H_2O_2 (3 eq.)	14	8	-
4	Fe(bpmen)$(OTf)_2$ (10%)	H_2O_2 (3 eq.)	17	9	-
5	Fe(bpmen)$(OTf)_2$ (15%)	H_2O_2 (3 eq.)	29	16	5
6	Fe(bpmen)$(OTf)_2$ (20%)	H_2O_2 (3 eq.)	15	9	-

[a] Isolated yields, after column chromatography.

Table 1 summarizes the reaction conditions we have tested in this work. In all cases, pyrene was dissolved in a 0.33 M CH_3COOH solution in CH_3CN, to

which three separate additions containing one third of the total catalyst and H_2O_2 in CH_3CN were added at 10 min intervals. After the last addition, the solution was allowed to stir at room temperature for 10 more minutes and quenched with a saturated $NaHCO_3$ aqueous solution.[24] No oxidation products were observed in the presence of the imine-based catalysts $[Fe(pymcy)_2(OTf)_2]$ or $[Fe(bpycen)(OTf)_2]$ (entries 1 and 2 in **Table 1**). However, the reaction was immediately apparent when utilizing $[Fe(bpmen)(OTf)_2]$ (entries 3–6 in **Table 1**). In analogy with the biooxidation by CYPs, the main products detected by HPLC analysis were 1,6 and 1,8-pyrenediones (**1** and **2** in **Table 1**) with some residual 4,5-pyrenedione (**3** in **Table 1**) detectable in some of the runs. All products showed spectroscopic and analytical properties (^{1}H NMR, ^{13}C NMR, and MALDI-TOF) consistent with their structure and the data reported in the literature (see the experimental section). Under optimized conditions (entry 5 in **Table 1**), 29%, 16% and 5% isolated yields for **1**, **2**, and **3** were obtained, respectively. Adding more catalyst (entry 6 in **Table 1**) resulted in complex mixtures of oxidation and decreased yields for **1** and **2**. Although the isolated yields were relatively modest, the mild method proposed here compares well to the much stronger oxidation conditions reported earlier.[18,19] Other small PAHs, like naphthalene and anthracene also produce the corresponding 1,4-naphtoquinone (NQ) and 9,10-anthraquinone (AQ), in modest to good yields (32% and 85%, respectively, entries 2 and 3 in **Table 2**). In both cases conversion was completed by TLC, but naphthalene yielded a mixture of oxidation products where 1,4-naphthoquinone was the main component. Unsurprisingly, the oxidation of anthracene proceeded cleanly to yield 9,10-anthraquinone. However, other substrates, such as benzene and phenanthrene (entries 1 and 4 in **Table 2**), did not show signs of reaction by TLC analysis.

[24] D. Clemente-Tejeda, A. López-Moreno, F. A. Bermejo. *Tetrahedron*, **2012,** *68*, 9249-9255.

Table 2 Fe(bpmen)$(OTf)_2$ catalyzed oxidation of other PAHs.[a]

Entry	Reagent	Product	Conversion	Yield[b]
1	Benzene	-	-	-
2	Naphthalene	1,4-Naphthoquinone	100 %	32 %
3	Anthracene	9,10-Anthraquinone	100 %	85 %
4	Phenanthrene	-	-	-

[a] All reactions were run under the conditions described in entry 5 of Table 1 and the main text. [b] Isolated yields, after column chromatography.

Quinones are key electron acceptors in both biology and industry. For instance, coenzyme Q10, which features a *p*-benzoquinone (BQ) core as a redox unit, is involved in the electron transport chain in aerobic respiration, and doubles as an antioxidant inhibiting both the initiation and the propagation of lipid and protein oxidations.[25] From an industrial point of view, 2-alkylanthraquinones have been utilized to produce hydrogen peroxide since the 1940s, and indeed the anthraquinone method still monopolises the large scale production of H_2O_2.[26] Despite these facts, research on pyrenequinones has focused on their environmental interest and their use as photosensitizers in the production of singlet oxygen for photodynamic therapy.[27] Surprisingly, the electron-accepting properties of pyrenequinones have hardly been investigated.[28] Figure 1 displays the cyclic voltammograms of **1** and **2** in CH_3CN. Both quinones show two reversible reduction waves at half-wave potentials $E_{1/2}^1$ = 0.82 V and $E_{1/2}^2$ = 1.12 V for **1** and $E_{1/2}^1$ = 0.84 V and $E_{1/2}^2$ = 1.19 V for **2**, with respect to ferrocene/ferricenium. For comparison, BQ undergoes reduction at $E_{1/2}^1$ = 0.88 V and $E_{1/2}^2$= 1.47 V, NQ at $E_{1/2}^1$ = 1.06 V and $E_{1/2}^2$ = 1.63 V and AQ

[25] L. Ernster, G. Dallner. *Biochim. Biophys. Acta, Mol. Basis Dis.*, **1995,** *1271*, 195-204.
[26] J. M. Campos-Martín, G. Blanco-Brieva, J. L. G. Fierro. *Angew. Chem., Int. Ed.*, **2006,** *45*, 6962-6984.
[27] J. Arnbjerg, M. J. Paterson, C. B. Nielsen, M. Jørgensen, O. Christiansen, P. R. Ogilby. *J. Phys. Chem. A,* **2007,** *111*, 5756-5767.
[28] E. J. Moriconi, B. Rakoczy, W. F. O'Connor. *J. Org. Chem.*, **1962,** *27*, 2772-2776.

at $E_{1/2}^1$ = 1.31 V and $E_{1/2}^2$ = 1.89 V under identical experimental conditions (**Figure S3** of experimental section). The cathodic shift of the first reduction potential along the BQ, NQ, and AQ series can be easily rationalized in terms of the energy and topology calculated for the LUMO (**Figure 2**). The LUMO is mainly localized on the quinoid ring and suffers a destabilization along the BQ, NQ, and AQ series due to the additional antibonding interactions arising from the inclusion of lateral benzene rings. In contrast, the LUMOs of **1** and **2** stand close in energy with respect to the LUMO of BQ because they resemble two BQ LUMOs with no additional destabilizing interactions. This explains, to a first approximation, the similar values obtained for the first reduction potential of **1**, **2**, and BQ.

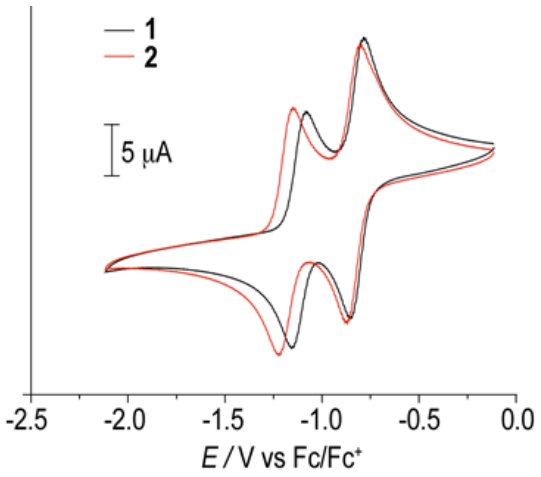

Figure 1. Cyclic voltammograms of **1** (black) and **2** (red) in CH_3CN at room temperature. Glassy carbon was employed as the working electrode, $Ag/AgNO_3$ as the reference electrode, and 0.1 M $TBAPF_6$ as the electrolyte.

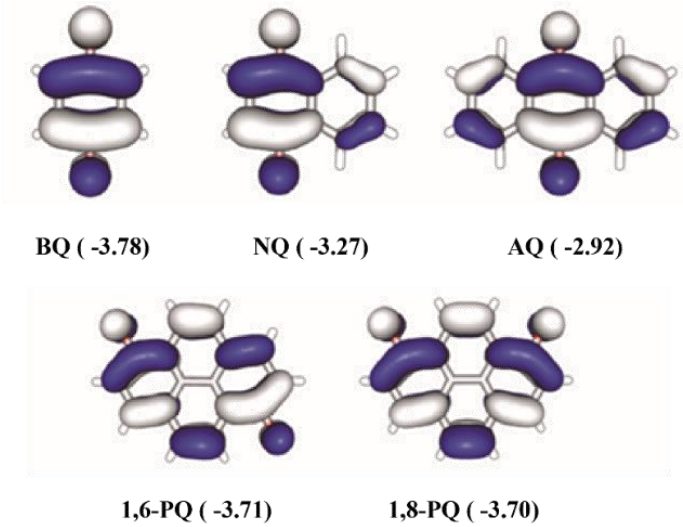

Figure 2. Topology and energy (in eV) calculated for the lowest-unoccupied molecular orbital (LUMO).

Although the measurement of reduction potentials is usually considered to be a valid method to evaluate the electron acceptor ability of molecules, their electron affinity (EA) is a direct measurement of it. **Table 3** gives the adiabatic EA values computed at room temperature using the G3(MP2) procedure (see the experimental section for full computational details). The G3(MP2) method provides an EA of 1.92 eV for BQ in very good agreement with the experimental value of 1.91 eV.[29] Likewise, the EA values calculated for NQ (1.83 eV) and AQ (1.66 eV) reproduce accurately the experimental values of 1.81 and 1.59 eV, respectively.[29] Therefore, the electron-accepting ability decreases with the size of the system along the BQ, NQ, and AQ series. In contrast, the EA values calculated for **1** (2.32 eV) and **2** (2.34 eV) indicate that the pyrenediones are remarkably stronger electron acceptors than BQ.

[29] E. C. M. Chen, W. E. Wentworth. *Mol. Cryst. Liq. Cryst.*, **1989,** *171*, 271-285.

Table 3 Thermochemical (in eV) and electrochemical (in V) data calculated for the one-electron attachment $A + e^- \rightarrow A^-$ reaction. Experimental first half-wave reduction potentials are also included.

	BQ	NQ	AQ	**1**	**2**
$EA_{298K,\ theor}$ [a]	1.92	1.83	1.66	2.32	2.34
$EA_{298K,\ exp}$ [b]	1.91	1.81	1.59	-	-
$\Delta G_{g,298K}$ [c]	–2.07	–1.97	–1.80	–2.48	–2.49
$\Delta\Delta G_{solv}$	–2.02	–1.91	–1.81	–1.62	–1.62
ΔG_{red}	–4.09	–3.88	–3.61	–4.09	–4.12
$E^1_{1/2,theor}$ [d]	–0.90	–1.11	–1.37	–0.89	–0.87
$E^1_{1/2,exp}$	–0.88	–1.06	–1.31	–0.82	–0.84

[a] Zero-point energy and thermal corrections are included. [b] Experimental values extracted from reference 29. [c] Corrected values taking into account the free electron as an ideal monoatomic gas, 5/2 RT,[30] and the correction for the change in the standard state from 1 atm to 1 $mol \cdot L^{-1}$.[31] [d] E_{ref} = 4.99 V (reduction potential of Fc^+/Fc).[32]

To rationalize the apparent mismatch between the theoretical EAs, calculated in gas phase, and the experimental $E_{1/2}$ values, measured in CH_3CN, the first half-wave reduction potentials were estimated theoretically using the expression[33]

$$E_{1/2} = \Delta G_{red}/(nF) + E_{ref}$$

where ΔG_{red} is the free energy difference for the one-electron attachment reaction in solution (i.e. $\Delta G_{red} = \Delta Gg + \Delta\Delta G_{solv.}$), n is the number of electrons

[30] J. E. Bartmess. *J. Phys. Chem.*, **1994,** *98*, 6420-6424.
[31] M. D. Liptak, K. C. Gross, P. G. Seybold, S. Feldgus, G. C. Shields. *J. Am. Chem. Soc.*, **2002,** *124*, 6421-6427.
[32] M. Namazian, C. Y. Lin, M. L. Coote. *J. Chem. Theory Comput.*, **2010,** *6*, 2721-2725.
[33] M. Namazian, M. L. Coote. *J. Phys. Chem. A*, **2007,** *111*, 7227-7232.

transferred (n = 1 in this case), F is the Faraday constant and Δ_{ref} is the potential of the reference electrode. The free energy difference in gas phase (ΔG_g) and the free energy of solvation ($\Delta\Delta G_{solv}$) were computed at the G3(MP2) level and using a continuum solvation model (PCM with acetonitrile), respectively (see the experimental section). ΔG_g follows the same trend as the EA values (**Table 3**) because entropy effects are computed to be as small as 0.5 cal mol^{-1} K^{-1}. The origin of the larger EAs calculated for **1** and **2** compared to BQ stems from the larger π-electron delocalization in the LUMO of the formers at nearly the same molecular orbital energy (**Figure 2**). On the other hand, the $\Delta\Delta G_{solv}$ stabilization term is computed to be 0.4 eV larger for BQ than for **1** and **2**. The decrease (in absolute value) of the $\Delta\Delta G_{solv}$ term along the BQ > NQ > AQ > **1** = **2** series (**Table 3**) is mainly due to the fact that solvation effects stabilize to a larger extent the anion of BQ (2.25 eV) than the anions of NQ (2.13 eV), AQ (2.03 eV), **1** (1.94 eV) and **2** (1.95 eV) (**Table S1**, experimental section). EA and solvation stability differences between BQ and the two pyrenediones cancel each other and result in similar ΔG_{red} values for the three systems (**Table 3**). The final theoretical $E_{1/2}$ values are computed to be 0.90, 0.89 and 0.87 V for BQ, **1** and **2**, respectively, in very good agreement with the experimental data. Accurate values are also predicted for NQ and AQ (**Table 3**). Calculations therefore support the electron-acceptor capabilities measured in solution for pyrenediones **1** and **2**, and ascribe $E_{1/2}$ values similar to BQ due to the cancellation of two competing terms: (i) the larger EAs computed for **1** and **2** in gas phase and (ii) the less stabilizing solvation term ($\Delta\Delta G_{sol}$) in the pyrenediones. This result contrasts with the empirical linear-regression procedure usually employed to relate $E_{1/2}$ and EA ($E_{1/2} = EA - \Delta\Delta G_{solv.} + E_{ref}$), where $\Delta\Delta G_{solv}$ is considered to be constant for a given family of structurally similar compounds.[34]

[34] R. S. Ruoff, K. M. Kadish, P. Boulas, E. C. M. Chen. *J. Phys. Chem.*, **1995,** *99*, 8843-8850.

3.3. Conclusion

In conclusion, we have described a mild oxidation method for pyrene and other small PAHs, based on the use of a non-hemo iron catalyst, [Fe(bpmen)$(OTf)_2$], with H_2O_2 as the oxidant. Our method affords mainly 1,6- and 1,8-pyrenediones, in analogy with the oxidation of pyrene by natural CYPs. Although modest, the isolated yields of pyrenequinones are synthetically useful, and comparable to those recently reported for the catalytic oxidation of smaller PAHs.[35] To the best of our knowledge, this constitutes the first example of Fe-catalyzed C–H oxidation of PAHs. The electron accepting properties of both pyrenequinones were investigated experimentally through cyclic voltammetry, which showed that **1** and **2** are slightly better acceptors than BQ in solution. A detailed theoretical investigation revealed that the pyrenequinones show much higher EAs than BQ, approximately by 0.4 eV. By calculating the theoretical reduction potentials in solution, we showed that the difference in EA is cancelled out by a significantly decreased $\Delta\Delta G_{solv}$ in the case of **1** and **2** with respect to BQ. Our results suggest that the commonly accepted practice of assuming that $\Delta\Delta G_{solv}$ remains constant for a family of structurally related compounds,[34] such as the quinones under study, can sometimes lead to significant errors.

3.4. Experimental section

General Consideration: NMR spectra were recorded with BRUKER AVANCE III-HD NANOBAY 300MHz and BRUKER DRX 500MHz. Mass spectra were measured with ULTRAFLEX III (MALDI-TOF/TOF). Electrochemistry was measured with Potentiostat Autolab PGSTAT 30.

All materials used for synthesis were obtained from Sigma-Aldrich or Alfa Aesar. All organic solvents for synthesis were of analytical grade and were

[35] P. Kumari, R. Nagpal, S. M. S. Chauhan. *Catal. Commun.*, **2012,** *29*, 15-20.

obtained commercially. They were used without further purification. All reactions were monitored by thin-layer chromatography (TLC) with Merck silica gel plates (60F-254) under irradiation by UV-lamp (254 nm). Scharlau silica gel (230-400 mesh) was used in the column-chromatography purification.

Experimental procedure (5% of catalyst)

A 100 mL round bottom flask was charged with 0.5 mL of CH_2Cl_2, 1.5 mL of a 0.33 M CH_3COOH solution in CH_3CN, $Fe(bpmen)(OTf)_2$ (9 mg, 0.016 mmol, 1.6 mol %) and pyrene (200 mg, 1 mmol, 1.0 equiv). The solution was stirred vigorously at room temperature. A solution of H_2O_2 (30 wt %, 0.136 mL, 1.2 mmol, 1.2 equiv) in CH_3CN (8 mL, 0.13 M) was added dropwise via syringe. After stirring for 10 min, 1 mL of a 0.5 M CH_3COOH solution in CH_3CN and $Fe(bpmen)(OTf)_2$ (9 mg, 0.016 mmol, 1.6 mol %) were added. This was followed by the dropwise addition of H_2O_2 (30 wt %, 0.136 mL, 1.2 mmol, 1.2 equiv) in CH_3CN (8 mL, 0.13 M). A third addition was performed for a total of 5 mol % $Fe(bpmen)(OTf)_2$, 1.5 equiv of CH_3COOH, and 3.6 equivalents of H_2O_2. After the last 10 min of stirring, a $NaHCO_3$ saturated aqueous solution was added and the mixture was extracted with ethyl acetate. The combined organic layers were dried over anhydrous Mg_2SO_4, evaporated under reduced pressure and purified by chromatographic column (H:AcOEt 7:3) to obtain 121 mg of pyrene, 32 mg (14%) of 1,6-pyrenedione and 18.2 mg (8%) of 1,8-pyrenedione.

Experimental procedure (10% of catalyst)

A 100 mL round bottom flask was charged with 0.5 mL of CH_2Cl_2, 1.5 mL of a 0.33 M CH_3COOH solution in CH_3CN, $Fe(bpmen)(OTf)_2$ (20 mg, 0.033 mmol, 3.3 mol %), and pyrene (200 mg, 1 mmol, 1.0 equiv). The solution was stirred vigorously at room temperature. A solution of H_2O_2 (30 wt %, 0.136 mL, 1.2 mmol, 1.2 equiv) in CH_3CN (8 mL, 0.13 M) was added dropwise via syringe. After stirring for 10 min, 1 mL of a 0.5 M CH_3COOH solution in CH_3CN and $Fe(bpmen)(OTf)_2$ (20 mg, 0.033 mmol, 3.3 mol %) were added. This was

followed by the dropwise addition of H_2O_2 (30 wt %, 0.136 mL, 1.2 mmol, 1.2 equiv) in CH_3CN (8 mL, 0.13 M). A third addition was performed for a total of 10 mol % Fe(bpmen)$(OTf)_2$, 1.5 equiv of CH_3COOH and 3.6 equiv of H_2O_2. After the last 10 min of stirring, a $NaHCO_3$ saturated aqueous solution was added and the mixture was extracted with ethyl acetate. The combined organic layers were dried over anhydrous Mg_2SO_4, evaporated under reduced pressure and purified by chromatographic column (H:AcOEt 7:3) to obtain 98 mg of pyrene, 40 mg (17%) of 1,6-pyrenedione and 20 mg (9%) of 1,8-pyrenedione.

Experimental procedure (15% of catalyst)

A 100 mL round bottom flask was charged with 0.5 mL of CH_2Cl_2, 1.5 mL of a 0.33 M CH_3COOH solution in CH_3CN, Fe(bpmen)$(OTf)_2$ (31.2 mg, 0.05 mmol, 5 mol %) and pyrene (200 mg, 1 mmol, 1.0 equiv). The solution was stirred vigorously at room temperature. A solution of H_2O_2 (30 wt %, 0.136 mL, 1.2 mmol, 1.2 equiv) in CH_3CN (8 mL, 0.13 M) was added dropwise via syringe. After stirring for 10 min, 1 mL of a 0.5 M CH_3COOH solution in CH_3CN and Fe(bpmen)$(OTf)_2$ (31.2 mg, 0.05 mmol, 5 mol %) were added. This was followed by the dropwise addition of H_2O_2 (30 wt %, 0.136 mL, 1.2 mmol, 1.2 equiv) in CH_3CN (8 mL, 0.13 M). A third addition was performed for a total of 15 mol % Fe(bpmen)(OTf)2, 1.5 equiv of CH_3COOH and 3.6 equiv of H_2O_2. After the last 10 min of stirring, a $NaHCO_3$ saturated aqueous solution was added and the mixture was extracted with ethyl acetate. The combined organic layers were dried over anhydrous Mg_2SO_4, evaporated under reduced pressure and purified by chromatographic column (H:AcOEt 7:3) to obtain 62 mg of pyrene, 68 mg (29%) of 1,6-pyrenedione, 36.5 mg (16%) of 1,8-pyrenedione and 11 mg (5%) of 4,5-pyrenedione.

Experimental procedure (20% of catalyst)

A 100 mL round bottom flask was charged with 0.5 mL of CH_2Cl_2, 1.5 mL of a 0.33 M CH_3COOH solution in CH_3CN, Fe(bpmen)$(OTf)_2$ (42 mg, 0.067 mmol, 6.7 mol %), and pyrene (200 mg, 1 mmol, 1.0 equiv). The solution was stirred vigorously at room temperature. A solution of H_2O_2 (30 wt %, 0.136 mL, 1.2 mmol, 1.2 equiv) in CH_3CN (8 mL, 0.13 M) was added dropwise via syringe. After stirring for 10 min, 1 mL of a 0.5 M CH_3COOH solution in CH_3CN and Fe(bpmen)$(OTf)_2$ (42 mg, 0.067 mmol, 6.7 mol %) were added. This was followed by the dropwise addition of H_2O_2 (30 wt %, 0.136 mL, 1.2 mmol, 1.2 equiv) in CH_3CN (8 mL, 0.13 M). A third addition was performed for a total of 20 mol % Fe(bpmen)(OTf)2, 1.5 equiv of CH_3COOH and 3.6 equiv of H_2O_2. After the last 10 min of stirring, a $NaHCO_3$ saturated aqueous solution was added and the mixture was extracted with ethyl acetate. The combined organic layers were dried over anhydrous Mg_2SO_4, evaporated under reduced pressure and purified by chromatographic column (H:AcOEt 7:3) to obtain 43 mg of pyrene, 34 mg (15%) of 1,6-pyrenedione and 20.2 mg (9%) of 1,8-pyrenedione.

The reactions of anthracene, naphthalene and benzene were carried out using the 15% of catalyst procedure.

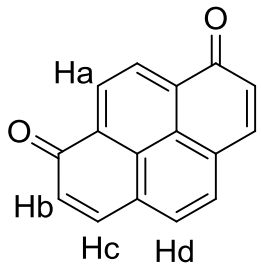

^{1}H NMR (300 MHz, $CDCl_3$) δ 8.64 (s, 2H, Ha), 7.67 (d, 2H, J = 9.8 Hz, Hc), 7.67 (s, 2H, Hd), 6.68 (d, 2H, J = 9.8 Hz, Hb).

^{13}C NMR (125 MHz, $CDCl_3$) δ 185.2, 141.5, 132.3, 131.2, 131.1, 129.6, 129.5, 127.6.

MS m/z: calcd. for $C_{16}H_8O_2$ [M+2H$^+$] 234.06, found MALDI-TOF 234.1

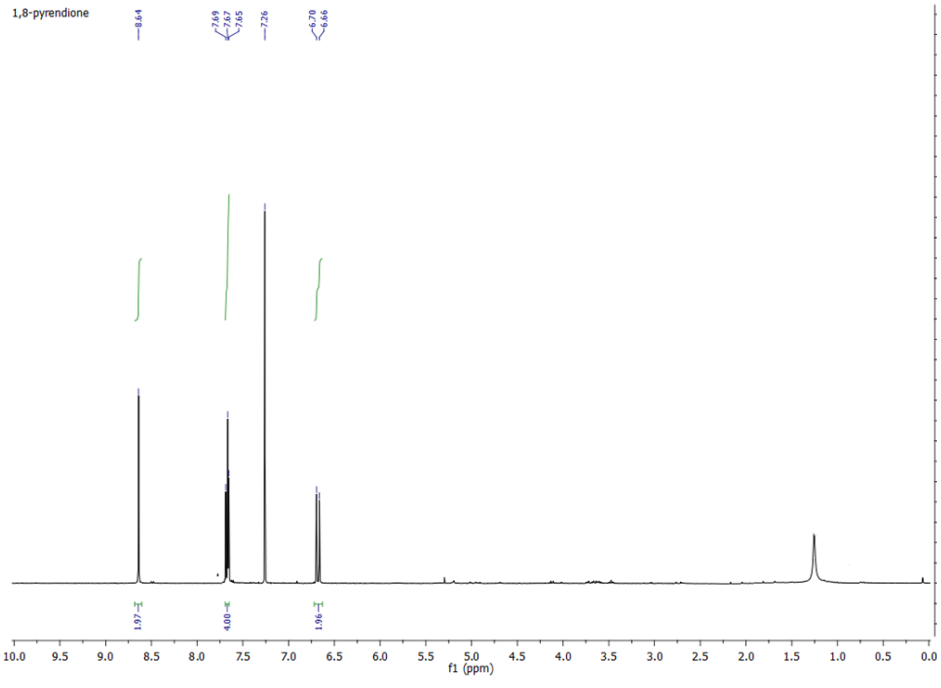

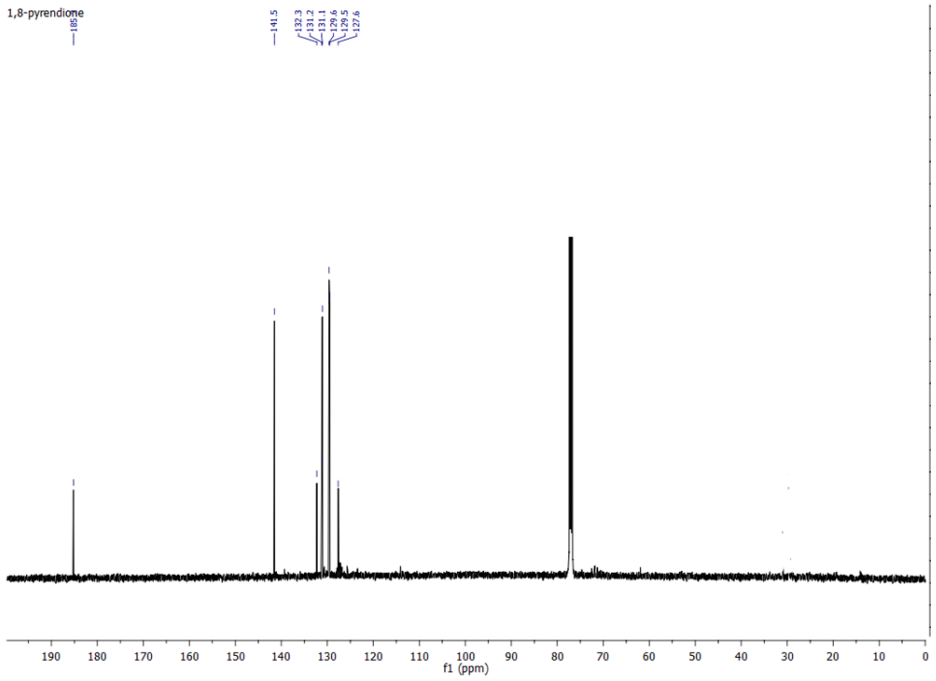
1,8-pyrendiome
185.1
141.5
132.3
131.2
131.1
129.6
129.5
127.6
190 180 170 160 150 140 130 120 110 100 90 80 70 60 50 40 30 20 10 0
f1 (ppm)

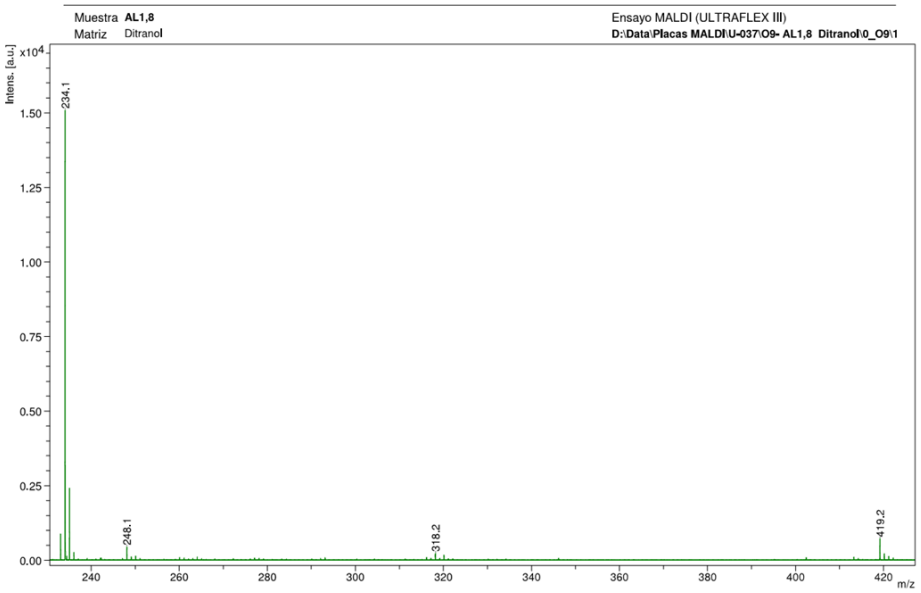
Muestra AL1,8
Matriz Ditranol
Ensayo MALDI (ULTRAFLEX III)
D:\Data\Placas MALDI\U-037\O9- AL1,8 Ditranol\0_O9\1
Intens. [a.u.]
x10^4
1.50
1.25
1.00
0.75
0.50
0.25
0.00
234.1
248.1
318.2
419.2
240 260 280 300 320 340 360 380 400 420
m/z

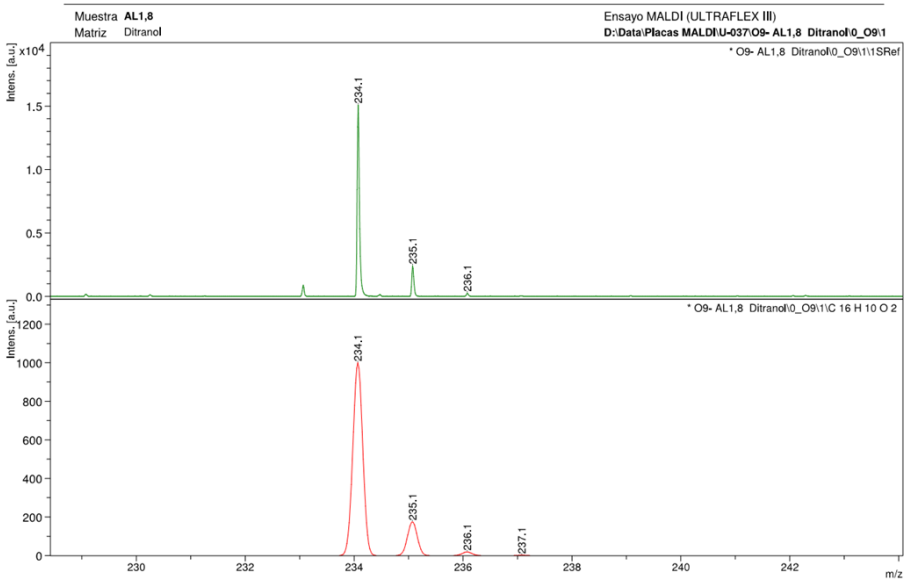

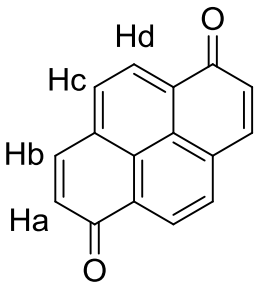

^{1}H NMR (300 MHz, $CDCl_3$) δ 8.49 (d, J = 7.5 Hz, 2H, Hd), 7.83 (d, J = 7.5 Hz, 2H, Hc), 7.68 (d, J = 9.8 Hz, 2H, Hb), 6.71 (d, J = 9.8 Hz, 2H, Ha).

^{13}C NMR (75 MHz, $CDCl_3$) δ 185.5, 141.2, 133.9, 130.9, 130.8, 130.4, 130.2, 127.7.

MS m/z: calcd. for $C_{16}H_8O_2$ [M+2H$^+$] 234.06 found MALDI-TOF 234.1

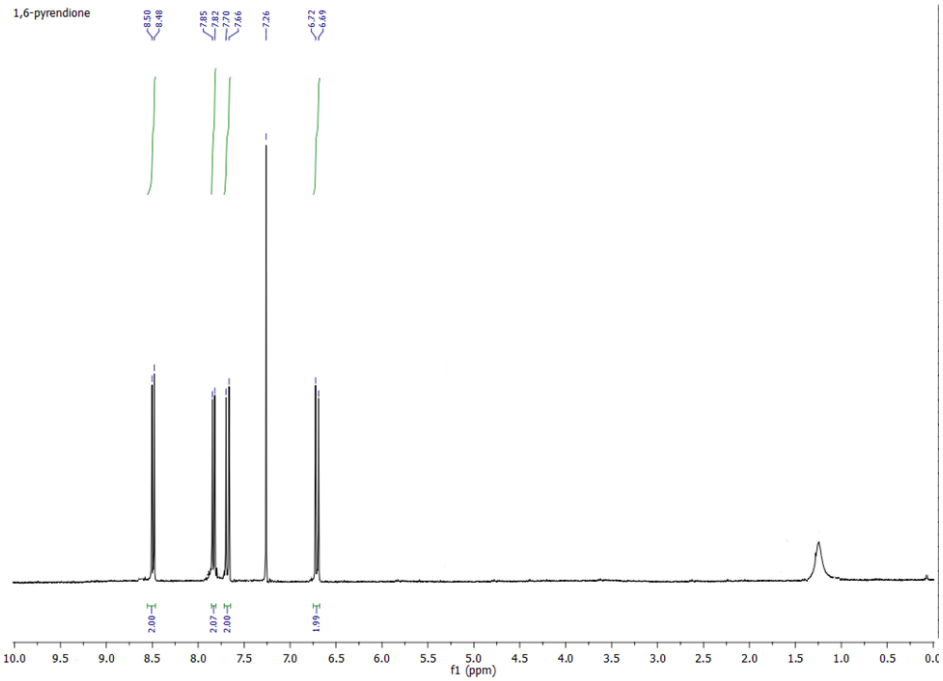
1,6-pyrendione
8.50
8.48
7.85
7.82
7.70
7.66
7.26
6.72
6.69
2.00
2.07
2.08
1.99
f1 (ppm)

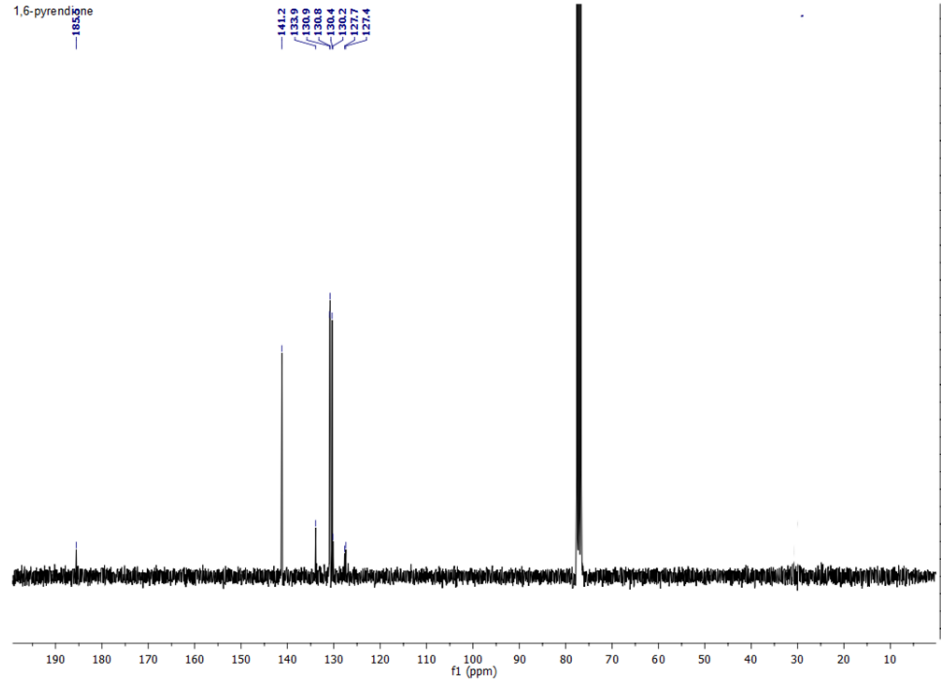
1,6-pyrendione
185.5
141.2
133.9
130.9
130.8
130.4
130.2
127.7
127.4
f1 (ppm)

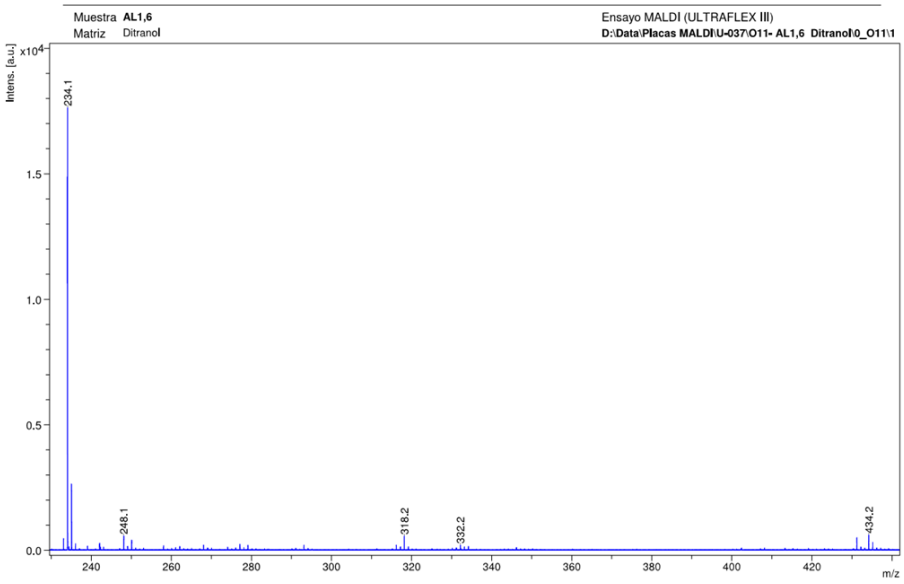
Muestra AL1,6
Matriz Ditranol
Ensayo MALDI (ULTRAFLEX III)
D:\Data\Placas MALDI\U-037\O11- AL1,6 Ditranol\0_O11\1
Intens. [a.u.]
x10^4
234.1
248.1
318.2
332.2
434.2
m/z

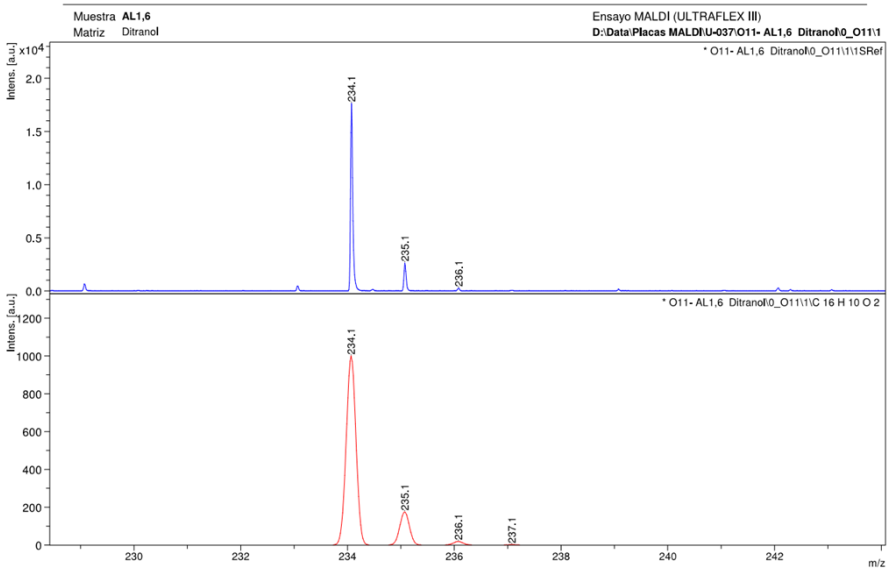
Muestra AL1,6
Matriz Ditranol
Ensayo MALDI (ULTRAFLEX III)
D:\Data\Placas MALDI\U-037\O11- AL1,6 Ditranol\0_O11\1
* O11- AL1,6 Ditranol\0_O11\1\1\1SRef
* O11- AL1,6 Ditranol\0_O11\1\1\C 16 H 10 O 2
Intens. [a.u.]
234.1
235.1
236.1
237.1
m/z

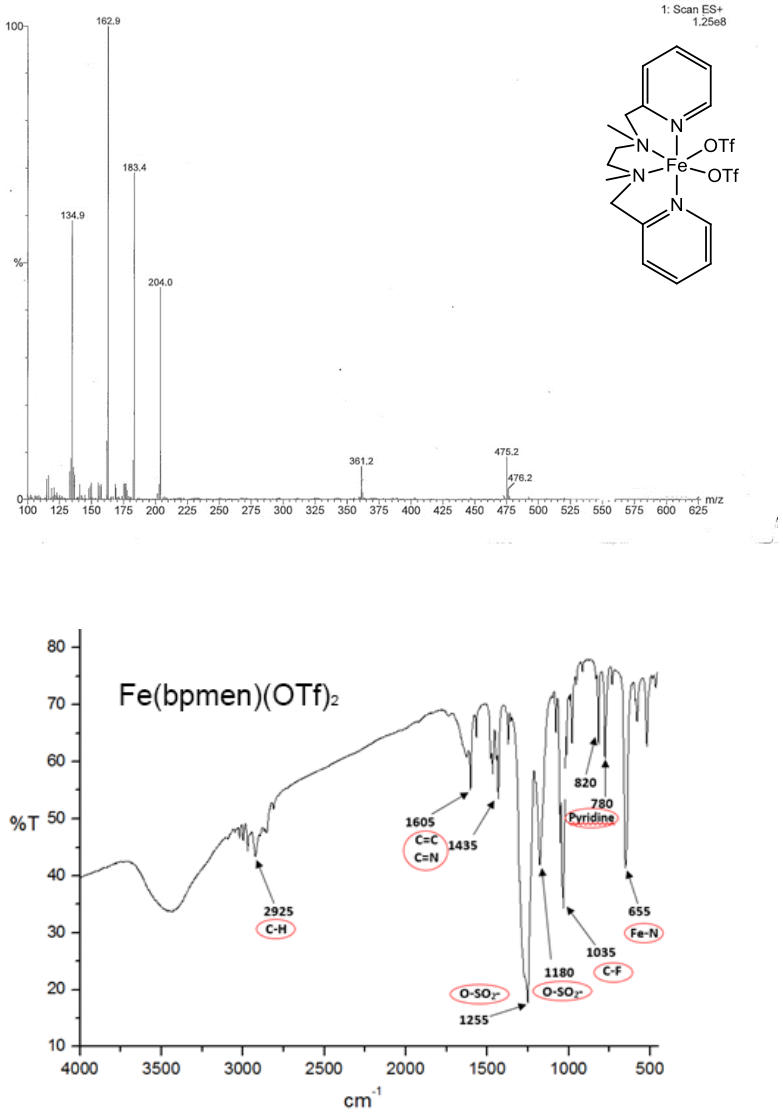

Figure S1. IR spectra of catalyst Fe(bpmen)$(OTf)_2$.

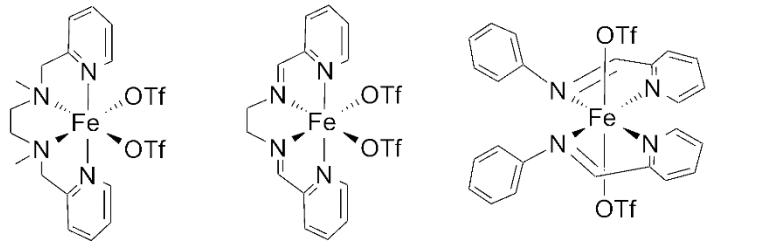

Fe(bpmen)$(OTf)_2$ Fe(bpycen)$(OTf)_2$ Fe(pymcy)$_2$$(OTf)_2$

bpmen = N,N'-bis-(2-pyridylmethyl)-N,N'-dimethyl-1,2-ethylenediamine

bpycen = N,N'-bis(pyridin-2-ylmethylene)ethane-1,2-diimine

pymcy = N-(pyridin-2-ylmethylene)cyclohexanamine

Figure S2. Iron Catalysts. Fe(bpmen)$(OTf)_2$ was synthetized following previous work.[24] Fe(bpycen)$(OTf)_2$ and Fe(pymcy)$_2$$(OTf)_2$ were synthetized following previous work.[36]

[36] P. Shejwalkar, N. P. Rath, E. B. Bauer. *Dalton Trans.*, **2011,** *40*, 7617-7631.

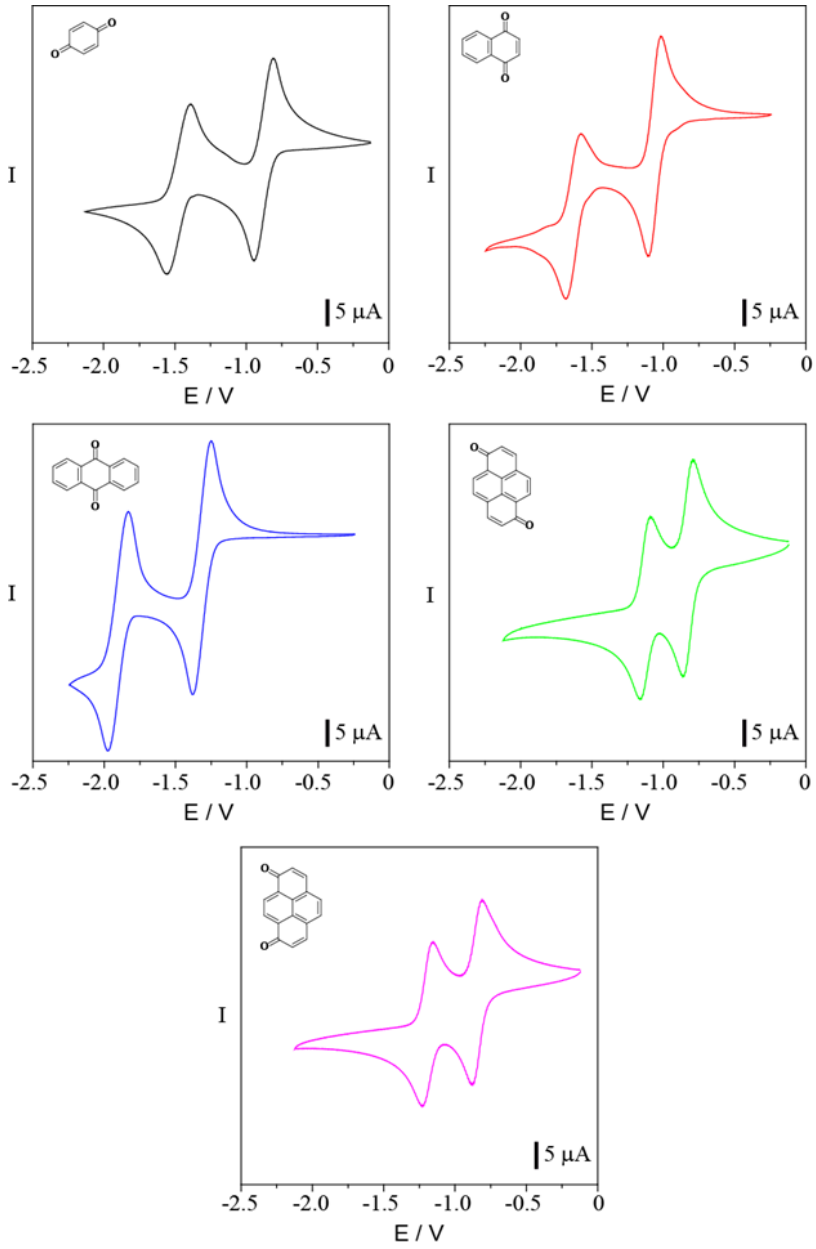

Figure S3. Cyclic voltammograms in acetonitrile at room temperature. Glassy carbon was employed as the working electrode. $Ag/AgNO_3$ as the electrode and 0.1 M $TBAPF_6$ as the electrolyte. Potential is displayed vs Fc/Fc^+.

Computational details

All the calculations were carried out using the Gaussian 09 (version D01) program package.[37] Full-geometry optimization of both neutral and anion species of parent *p*-benzoquinone (*p*-BQ) and pyrenediones **1** and **2** was performed with the Becke's three parameter B3LYP exchange-correlation functional[38],[39] and the cc-pVTZ Dunning's basis set.[40] The anions were calculated as open-shell doublet systems using the unrestricted UB3LYP approach. Even though no special symmetry restriction was imposed during the optimization process, minimum-energy conformations of C2h and C2v symmetry were obtained for **1** and **2**, respectively, in both neutral and reduced states. To calculate the free energy of solvation ($\Delta\Delta G_{solv}$) of the one-electron attachment $A + e^- \rightarrow A^-$ reaction, single-point B3LYP/cc-pVTZ energy calculations were performed for *p*-BQ and the two pyrenediones in the presence of the solvent (acetonitrile, $\varepsilon = 35.688$) within the SCRF (self-consistent reaction field) theory using the polarized continuum model (PCM).[41],[42] The PCM model considers the solvent as a continuous medium with a dielectric constant ε, and represents the solute by means of a cavity built with a number of interlaced spheres. Other continuum solvation models such as the conductor-like PCM

[37] *Gaussian 09, Revision A.02,* M. J. Frisch, G. W. Trucks, H. B. Schlegel, G. E. Scuseria, M. A. Robb, J. R. Cheeseman, G. Scalmani, V. Barone, B. Mennucci, G. A. Petersson, H. Nakatsuji, M. Caricato, X. Li, H. P. Hratchian, A. F. Izmaylov, J. Bloino, G. Zheng, J. L. Sonnenberg, M. Hada, M. Ehara, K. Toyota, R. Fukuda, J. Hasegawa, M. Ishida, T. Nakajima, Y. Honda, O. Kitao, H. Nakai, T. Vreven, J. A. Montgomery Jr., J. E. Peralta, F. Ogliaro, M. J. Bearpark, J. Heyd, E. N. Brothers, K. N. Kudin, V. N. Staroverov, R. Kobayashi, J. Normand, K. Raghavachari, A. P. Rendell, J. C. Burant, S. S. Iyengar, J. Tomasi, M. Cossi, N. Rega, N. J. Millam, M. Klene, J. E. Knox, J. B. Cross, V. Bakken, C. Adamo, J. Jaramillo, R. Gomperts, R. E. Stratmann, O. Yazyev, A. J. Austin, R. Cammi, C. Pomelli, J. W. Ochterski, R. L. Martin, K. Morokuma, V. G. Zakrzewski, G. A. Voth, P. Salvador, J. J. Dannenberg, S. Dapprich, A. D. Daniels, Ö. Farkas, J. B. Foresman, J. V. Ortiz, J. Cioslowski, D. J. Fox. Gaussian, Inc.,Wallingford CT, **2009**.
[38] A. D. Becke. *J. Chem. Phys*, **1993,** *98*, 5648-5652.
[39] C. Lee, W. Yang, R. G. Parr. *Phys. Rev. B*, **1988,** *37*, 785-789.
[40] R. A. Kendall, T. H. Dunning, R. J. Harrison. *J. Chem. Phys.*, **1992,** *96*, 6796-6806.
[41] J. Tomasi, M. Persico. *Chem. Rev.*, **1994,** *94*, 2027-2094.
[42] J. Tomasi, B. Mennucci, R. Cammi. *Chem. Rev.*, **2005,** *105*, 2999-3094.

(CPCM)[43],[44] and SMD[45] were used to compare the effect of the solvation model on the free energy of solvation.

Table S1 presents the thermochemical and electrochemical data calculated for the one-electron attachment $A + e^- \rightarrow A^-$ process depicted in **Figure S4**, where A stands for *p*-BQ and pyrenediones **1** and **2**. Thermodynamic data were computed both at the B3LYP/cc-pVTZ level and by means of the more accurate Gaussian-3 theory using reduced Moller-Plesset order (G3(MP2)).[46] The G3(MP2) theory is based on MP2(full)/6-31G(d)-optimized geometries using all electrons and a series of single-point energy calculations at higher levels of theory. An accurate estimation of the total energy is performed by a QCISD(T)/6-31G(d) calculation followed by a series of corrections according to the formula:

$$E_0[G3(MP2)] = QCISD(T)/6\text{-}31G(d) + \Delta E_{MP2} + \Delta E(SO) + E(ZPE) + E(HLC)$$

where the correction at the second-order Moller-Plesset level is given by

$$\Delta E_{MP2} = [E(MP2/G3MP2large)] - [E(MP2/6\text{-}31G(d))],$$

the spin-orbit correction, $\Delta E(SO)$, is included for atomic species only and the zero-point correction, E(ZPE), is obtained from scaled (0.8929) HF/6-31G(d) frequencies. Finally, a higher level correction, E(HLC), is added to take into account remaining deficiencies in the energy calculations.

Table S2 compares the solvation free energy differences ($\Delta\Delta G_{solv}$) between the neutral and the anion species of *p*-BQ, **1** and **2** computed at the B3LYP/cc-pVTZ level using different solvation models. The three models employed lead to identical trends with similar relative values.

[43] M. Cossi, N. Rega, G. Scalmani, V. Barone. *J. Comput. Chem.*, **2003,** *24*, 669-681.
[44] V. Barone, M. Cossi. *J. Phys. Chem. A*, **1998,** *102*, 1995-2001.
[45] A. V. Marenich, C. J. Cramer, D. G. Truhlar. *J. Phys. Chem. B*, **2009,** *113*, 6378-6396.
[46] L. A. Curtiss, P. C. Redfern, K. Raghavachari, V. Rassolov, J. A. Pople. *J. Chem. Phys.*, **1999,** *110*, 4703-4709.

Table S1. Thermochemical (in eV) and electrochemical (in V) data calculated for the one-electron attachment $A + e^- \rightarrow A^-$ process depicted in Figure S4.

	B3LYP/cc-pVTZ			G3(MP2)		
	BQ	**1**	**2**	BQ	**1**	**2**
EA[a]	1.943	2.312	2.302	1.852	2.230	2.254
EA + ZPE[b]	1.993	2.374	2.366	1.916	2.322	2.341
EA + ZPE + 298K[c]	1.999	2.376	2.368	1.923	2.324	2.344
$\Delta H_{g,298K}$[d]	–1.999	–2.376	–2.368	–1.923	–2.324	–2.344
$\Delta S_{g,298K}$[e]	0.017	0.693	0.715	–0.347	0.453	0.322
$\Delta G_{g,298K}$[f]	–2.000	–2.385	–2.377	–1.919	–2.330	–2.348
$\Delta G_{g,corrected}$[g]	–2.146	–2.531	–2.523	–2.065	–2.476	–2.494
$\Delta G_{solv}(A)$[h]	–0.223	–0.323	–0.331			
$\Delta G_{solv}(A^-)$[h]	–2.245	–1.940	–1.954			
$\Delta\Delta G_{solv}$[i]	–2.023	–1.617	–1.623	–2.023	–1.617	–1.623
ΔG_{red}[j]	–4.169	–4.148	–4.146	–4.088	–4.093	–4.117
$E_{1/2,absolute}$[k]	4.169	4.148	4.146	4.088	4.093	4.117
$E_{1/2,relative}$[l]	–0.819	–0.840	–0.842	–0.900	–0.895	–0.871

[a] Adiabatic electron affinities calculated as the energy difference between the total energies computed for the neutral and the anion species at their respective fully-optimized geometries.

[b] Adiabatic electron affinities including the zero-point energy (ZPE).

[c] Adiabatic electron affinities including the ZPE and the correction at 298 K to the internal thermal energy ($E_{tot} = E_{trans} + E_{rot} + E_{vib} + E_{elec}$).

[d] Enthalpy difference between the anion and the neutral species for the one-electron attachment reaction depicted in Figure S4.

[e] Entropy difference for the one-electron attachment reaction. Values expressed in cal/K·mol.

[f] Free energy difference for the one-electron attachment reaction in gas phase. $\Delta G_{g,298K} = \Delta H_{g,298K} - T\Delta S_{g,298K}$

[g] Corrected values taking into account the free electron as an ideal monoatomic gas, 5/2 RT,[30] and the correction for the change in standard state from 1 atm to 1 mol·L^{-1},[31] according to the following formula:[33] $\Delta G_{g,corrected} = \Delta G_{g,298K} - 5/2\ RT + RT\ \ln 24.46$.

[h] Free energy of solvation for the neutral (A) and the anion (A^-) species (see Figure S4). Values are calculated at the B3LYP/cc-pVTZ level using the polarized continuum model (PCM) with acetonitrile as solvent. Minimum-energy geometries in gas phase at the same level of theory are employed.

[i] Free energy of solvation for the one-electron attachment reaction defined as follows: $\Delta\Delta G_{solv} = \Delta G_{solv}(A^-) - \Delta G_{solv}(A)$.

[j] Free energy difference in solution for the thermodynamic cycle shown in Figure S4. $\Delta G_{red} = \Delta G_{g,298K} + \Delta\Delta G_{solv}$

[k] Absolute first half-wave reduction potentials. $E_{1/2} = \Delta G_{red}/(-1 \times F)$

[l] First half-wave reduction potentials with respect to ferrocene/ferricenium. E_{ref} = –4.99 V (reduction potential of Fc/Fc^+).[32]

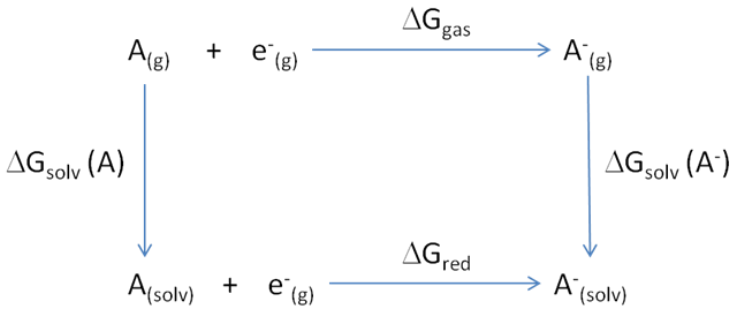

$$\Delta\Delta G_{solv} = \Delta G_{solv}(A^-) - \Delta G_{solv}(A)$$

Figure S4. Thermodynamic cycle for the analysis of solution effects on the one-electron attachment $A + e^- \rightarrow A^-$ reaction.

Table S2. Solvation free energy differences ($\Delta\Delta G_{solv}$) in eV between the neutral and the anion species of *p*-BQ, **1** and **2** computed at the B3LYP/cc-pVTZ level using different solvation models and the B3LYP/cc-pVTZ minimum-energy geometries.

	p-BQ	**1**	**2**
PCM	–2.023	–1.617	–1.623
CPCM	–2.022	–1.618	–1.625
SMD	–1.823	–1.447	–1.455

3.5. References

1. D. W. Nebert, T. P. Dalton, A. B. Okey, F. J. Gonzalez. Role of Aryl Hydrocarbon Receptor-mediated Induction of the CYP1 Enzymes in Environmental Toxicity and Cancer. *J. Biol. Chem.*, **2004,** *279*, 23847-23850.
2. A. G. G. M. Tielens. Interstellar Polycyclic Aromatic Hydrocarbon Molecules. *Annu. Rev. Astron. Astrophys.*, **2008,** *46*, 289-337.
3. (a) J. Wu, W. Pisula, K. Müllen. Graphenes as Potential Material for Electronics. *Chem. Rev.*, **2007,** *107*, 718-747; (b) M. D. Watson, A. Fechtenkoetter, K. Müllen. Big Is Beautiful-"Aromaticity" Revisited from the Viewpoint of Macromolecular and Supramolecular Benzene Chemistry. *Chem. Rev.*, **2001,** *101*, 1267-1300.
4. See *Acc. Chem. Res.*, **2013,** *46*, 1-189, special issue on graphene and references cited therein.
5. (a) J. K. Wassei, R. B. Kaner. Oh, the Places You'll Go with Graphene. *Acc. Chem. Res.*, **2013,** *46*, 2244-2253; (b) L. Rodríguez-Pérez, M. Á. Herranz, N. Martín. The chemistry of pristine graphene. *Chem. Commun.*, **2013,** *49*, 3721-3735; (c) E. V. Iski, E. N. Yitamben, L. Gao, N. P. Guisinger. Graphene at the Atomic-Scale: Synthesis, Characterization, and Modification. *Adv. Funct. Mater.*, **2013,** *23*, 2554-2564; (d) C. K. Chua, M. Pumera. Covalent chemistry on graphene. *Chem. Soc. Rev.*, **2013,** *42*, 3222-3233; (e) K. S. Novoselov, V. I. Fal'ko, L. Colombo, P. R. Gellert, M. G. Schwab, K. Kim. A roadmap for graphene. *Nature*, **2012,** *490*, 192-200; (f) Y. Zhu, S. Murali, W. Cai, X. Li, J. W. Suk, J. R. Potts, R. S. Ruoff. Graphene and Graphene Oxide: synthesis, Properties, and Applications. *Adv. Mater.*, **2010,** *22*, 3906-3924; (g) M. J. Allen, V. C. Tung, R. B. Kaner. Honeycomb Carbon: A Review of Graphene. *Chem. Rev.*, **2010,** *110*, 132-145.

6. (a) A. Konishi, Y. Hirao, K. Matsumoto, H. Kurata, R. Kishi, Y. Shigeta, M. Nakano, K. Tokunaga, K. Kamada, T. Kubo. Synthesis and Characterization of Quarteranthene: Elucidating the Characteristics of the Edge State of Graphene. *J. Am. Chem. Soc.*, **2013,** *135*, 1430-1437; (b) C.-N. Feng, M.-Y. Kuo, Y.-T. Wu. Nanoribbons at the Molecular Level. Synthesis, Structural Analysis, and Properties of [8]Circulenes. *Angew. Chem., Int. Ed.*, **2013,** *52*, 7791-7794; (c) R. Yamaguchi, S. Hiroto, H. Shinokubo. Synthesis of Oxygen-Substituted Hexa-*peri*-hexabenzocoronenes through Ir-Catalyzed Direct Borylation. *Org. Lett.*, **2012,** *14*, 2472-2475; (d) D. J. Jones, B. Purushothaman, S. Ji, A. B. Holmes, W. W. H. Wong. Synthesis of electron-poor hexa-*peri*-hexabenzocoronenes. *Chem. Commun.*, **2012,** *48*, 8066-8068; (e) L. Chen, Y. Hernandez, X. Feng, K. Müllen. From Nanographene and Graphene Nanoribbons to Graphene Sheets: Chemical Synthesis. *Angew. Chem., Int. Ed.*, **2012,** *51*, 7640-7654; (f) J. M. Alonso, A. E. Díaz-Álvarez, A. Criado, D. Pérez, D. Peña, E. Guitián. [16]Cloverphene: a Clover-Shaped *cata*-Condensed Nanographene with Sixteen Fused Benzene Rings. *Angew. Chem., Int. Ed.*, **2012,** *51*, 173-177; (g) X. Yang, X. Dou, A. Rouhanipour, L. Zhi, H. J. Raeder, K. Müllen. Two-Dimensional Graphene Nanoribbons. *J. Am. Chem. Soc.*, **2008,** *130*, 4216-4217; (h) Z. Liu, R. C. Larock. Palladium-Catalyzed, Sequential, Three-Component Cross-Coupling of Aryl Halides, Alkynes, and Arynes. *Angew. Chem., Int. Ed.*, **2007,** *46*, 2535-2538; (i) X. Feng, J. Wu, M. Ai, W. Pisula, L. Zhi, J. P. Rabe, K. Müllen. Triangle-Shaped Polycyclic Aromatic Hydrocarbons. *Angew. Chem., Int. Ed.*, **2007,** *46*, 3033-3036; (j) M. Kastler, J. Schmidt, W. Pisula, D. Sebastiani, K. Müllen. From Armchair to Zigzag Peripheries in Nanographenes. *J. Am. Chem. Soc.*, **2006,** *128*, 9526-9534; (k) X. Feng, J. Wu, V. Enkelmann, K. Müllen. Hexa-*peri*-hexabenzocoronenes by Efficient Oxidative Cyclodehydrogenation: The Role of the Oligophenylene Precursors. *Org. Lett.*, **2006,** *8*, 1145-1148; (l) M. C. Bonifacio, C. R. Robertson, J.-Y. Jung, B. T. King. Polycyclic Aromatic Hydrocarbons by Ring-Closing Metathesis. *J. Org. Chem.*, **2005,** *70*, 8522-8526; (m) Z. Wang, Z. Tomovic, M. Kastler, R. Pretsch, F. Negri, V. Enkelmann, K. Müllen. Graphitic Molecules with Partial "Zig/Zag" Periphery. *J. Am. Chem. Soc.*, **2004,** *126*, 7794-7795.

7. S. Karuppannan, J.-C. Chambron. Supramolecular Chemical Sensors Based on Pyrene Monomer-Excimer Dual Luminescence. *Chem. - Asian J.*, **2011,** *6*, 964-984.

8. G. Bains, A. B. Patel, V. Narayanaswami. Pyrene: A Probe to Study Protein Conformation and Conformational Changes. *Molecules*, **2011,** *16*, 7909-7935.

9. F. D'Souza, A. S. D. Sandanayaka, O. Ito. SWNT-Based Supramolecular Nanoarchitectures with Photosensitizing Donor and Acceptor Molecules. *J. of Phys. Chem. Lett.*, **2010,** *1*, 2586-2593.

10. J. A. Mann, J. Rodríguez-López, H. D. Abruña, W. R. Dichtel. Multivalent Binding Motifs for the Noncovalent Functionalization of Graphene. *J. Am. Chem. Soc.*, **2011**, *133*, 17614-17617.

11. (a) A. Mateo-Alonso. Pyrene-fused pyrazaacenes: from small molecules to nanoribbons. *Chem. Soc. Rev.*, **2014,** *43*, 6311-6324; (b) S.-i. Kawano, M. Baumgarten,

D. Chercka, V. Enkelmann, K. Müllen. Electron donors and acceptors based on 2,7-functionalized pyrene-4,5,9,10-tetraone. *Chem. Commun.*, **2013,** *49*, 5058-5060.
12. Y. Hashimoto, K. Shudo. Preparation of Pure Isomers of Dinitropyrenes. *Chem. Pharm. Bull.*, **1984,** *32*,1992-1997.
13. S. Bernhardt, M. Kastler, V. Enkelmann, M. Baumgarten, K. Müllen. Pyrene as Chromophore and Electrophore: Encapsulation in a Rigid Polyphenylene Shell. *Chem. - Eur. J.*, **2006,** *12*, 6117-6128.
14. A. R. Katritzky, M. S. Kim, D. Fedoseyenko, K. Widyan, M. Siskin, M. Francisco. The sulfonation of aromatic and heteroaromatic polycyclic compounds. *Tetrahedron*, **2009,** *65*, 1111-1114.
15. W. Xue, D. Warshawsky. Metabolic activation of polycyclic and heterocyclic aromatic hydrocarbons and DNA damage: A review. *Toxicol. Appl. Pharmacol.*, **2005,** *206*, 73-93.
16. P. Barathi, A. Senthil Kumar. Electrochemical Conversion of Unreactive Pyrene to Highly Redox-Active 1,2-Quinone Derivatives on a Carbon Nanotube-Modified Gold Electrode Surface and Its Selective Hydrogen Peroxide Sensing. *Langmuir*, **2013,** *29*, 10617-10623.
17. (a) L. A. Launen, L. J. Pinto, M. M. Moore. Optimization of pyrene oxidation by *Penicillium janthinellum* using response-surface methodology. *Appl. Microbiol. Biotechnol.*, **1999,** *51*, 510-515; (b) T. Wunder, S. Kremer, O. Sterner, H. Anke. Metabolism of the polycyclic aromatic hydrocarbon pyrene by *Aspergillus niger* SK 9317. *Appl. Microbiol. Biotechnol.*, **1994,** *42*, 636-641; (c) M. Lambert, S. Kremer, O. Sterner, H. Anke. Metabolism of Pyrene by the Basidiomycete *Crinipellis stipitaria* and Identification of Pyrenequinones and Their Hydroxylated Precursors in Strain JK375. *Appl. Environ. Microbiol.*, **1994,** *60*, 3597-601.
18. A. J. Fatiadi. Separation of pyrenediones by column chromatography. *J. Chromatogr.*, **1965,** *20*, 319-324.
19. H. Cho, R. G. Harvey. Synthesis of hydroquinone diacetates from polycyclic aromatic quinones. *J. Chem. Soc., Perkin Trans. 1*, **1976**, 836-839.
20. E. P. Talsi, K. P. Bryliakov. Chemo- and stereoselective C-H oxidations and epoxidations/*cis*-dihydroxylations with H_2O_2, catalyzed by non-heme iron and manganese complexes. *Coord. Chem. Rev.*, **2012,** *256*, 1418-1434.
21. (a) Y. Hitomi, K. Arakawa, T. Funabiki, M. Kodera. An Iron(III)-Monoamidate Complex Catalyst for Selective Hydroxylation of Alkane C-H Bonds with Hydrogen Peroxide. *Angew. Chem., Int. Ed.*, **2012,** *51*, 3448-3452; (b) L. Gómez, I. Garcia-Bosch, A. Company, J. Benet-Buchholz, A. Polo, X. Sala, X. Ribas, M. Costas. Stereospecific C—H Oxidation with H_2O_2 Catalyzed by a Chemically Robust Site-Isolated Iron Catalyst. *Angew. Chem. Int. Ed.*, **2009,** *48*, 5720-5723; (c) P. E. Gormisky, M. C. White. Catalyst-Controlled Aliphatic C-H Oxidations with a Predictive Model for Site-Selectivity. *J. Am. Chem. Soc.*, **2013,** *135*, 14052-14055; (d) M. S. Chen, M. C. White.

A Predictably Selective Aliphatic C-H Oxidation Reaction for Complex Molecule Synthesis. *Science*, **2007,** *318*, 783-787.
22. (a) P. Spannring, V. Yazerski, P. C. A. Bruijnincx, B. M. Weckhuysen, R. J. M. Klein Gebbink. Fe-Catalyzed One-Pot Oxidative Cleavage of Unsaturated Fatty Acids into Aldehydes with Hydrogen Peroxide and Sodium Periodate. *Chem. - Eur. J.*, **2013,** *19*, 15012-15018; (b) B. F. Perandones, E. del Río Nieto, C. Godard, S. Castillón, P. De Frutos, C. Claver. Fe-Catalyzed Olefin Epoxidation with Tridentate Non-Heme Ligands and Hydrogen Peroxide as the Oxidant. *ChemCatChem*, **2013,** *5*, 1092-1095; (c) D. Clemente-Tejeda, A. López-Moreno, F. A. Bermejo. Non-heme iron catalysis in C=C, C-H, and CH_2 oxidation reactions. Oxidative transformations on terpenoids catalyzed by Fe(bpmen)$(OTf)_2$. *Tetrahedron*, **2013,** *69*, 2977-2986; (d) I. Garcia-Bosch, Z. Codola, I. Prat, X. Ribas, J. Lloret-Fillol, M. Costas. Iron-Catalyzed C-H Hydroxylation and Olefin cis-Dihydroxylation Using a Single-Electron Oxidant and Water as the Oxygen-Atom Source. *Chem. - Eur. J.*, **2012,** *18*, 13269-13273; (e) S. M. Barry, H. Mueller-Bunz, P. J. Rutledge. Investigating the oxidation of alkenes by non-heme iron enzyme mimics. *Org. Biomol. Chem.*, **2012,** *10*, 7372-7381; (f) M. S. Chen, M. C. White. Combined Effects on Selectivity in Fe-Catalyzed Methylene Oxidation. *Science*, **2010,** *327*, 566-571.
23. (a) P. Liu, Y. Liu, E. L.-M. Wong, S. Xiang, C.-M. Che. Iron oligopyridine complexes as efficient catalysts for practical oxidation of arenes, alkanes, tertiary amines and *N*-acyl cyclic amines with Oxone. *Chem. Sci.*, **2011,** *2*, 2187-2195; (b) I. Prat, A. Company, V. Postils, X. Ribas, L. Que, Jr., J. M. Luis, M. Costas. The Mechanism of Stereospecific C-H Oxidation by Fe(Pytacn) Complexes: Bioinspired Non-Heme Iron Catalysts Containing *cis*-Labile Exchangeable Sites. *Chem. - Eur. J.*, **2013,** *19*, 6724-6738.
24. D. Clemente-Tejeda, A. López-Moreno, F. A. Bermejo. Oxidation of unsaturated steroid ketones with hydrogen peroxide catalyzed by Fe(bpmen)$(OTf)_2$. New methodology to access biologically active steroids by chemo-, and stereoselective processes. *Tetrahedron*, **2012,** *68*, 9249-9255.
25. L. Ernster, G. Dallner. Biochemical, physiological and medical aspects of ubiquinone function. *Biochim. Biophys. Acta, Mol. Basis Dis.*, **1995,** *1271*, 195-204.
26. J. M. Campos-Martín, G. Blanco-Brieva, J. L. G. Fierro. Hydrogen Peroxide Synthesis: An Outlook Beyond the Anthraquinone Process. *Angew. Chem., Int. Ed.*, **2006,** *45*, 6962-6984.
27. J. Arnbjerg, M. J. Paterson, C. B. Nielsen, M. Jørgensen, O. Christiansen, P. R. Ogilby. One- and Two-Photon Photosensitized Singlet Oxygen Production: Characterization of Aromatic Ketones as Sensitizer Standards. *J. Phys. Chem. A*, **2007,** *111*, 5756-5767.
28. E. J. Moriconi, B. Rakoczy, W. F. O'Connor. Oxidation-Reduction Potentials and Absorption Spectra of Polycyclic Aromatic Quinones. *J. Org. Chem.*, **1962,** *27*, 2772-2776.

29. E. C. M. Chen, W. E. Wentworth. Experimental Determination of Electron Affinities of Organic Molecules. *Mol. Cryst. Liq. Cryst.*, **1989,** *171*, 271-285.
30. J. E. Bartmess. Thermodynamics of the Electron and the Proton. *J. Phys. Chem.*, **1994,** *98*, 6420-6424.
31. M. D. Liptak, K. C. Gross, P. G. Seybold, S. Feldgus, G. C. Shields. Absolute pK_a Determinations for Substituted Phenols. *J. Am. Chem. Soc.*, **2002,** *124*, 6421-6427.
32. M. Namazian, C. Y. Lin, M. L. Coote. Benchmark Calculations of Absolute Reduction Potential of Ferricinium/Ferrocene Couple in Nonaqueous Solutions. *J. Chem. Theory Comput.*, **2010,** *6*, 2721-2725.
33. M. Namazian, M. L. Coote. Accurate Calculation of Absolute One-Electron Redox Potentials of Some *para*-Quinone Derivatives in Acetonitrile. *J. Phys. Chem. A*, **2007,** *111*, 7227-7232.
34. R. S. Ruoff, K. M. Kadish, P. Boulas, E. C. M. Chen. Relationship between the Electron Affinities and Half-Wave Reduction Potentials of Fullerenes, Aromatic Hydrocarbons, and Metal Complexes. *J. Phys. Chem.*, **1995,** *99*, 8843-8850.
35. P. Kumari, R. Nagpal, S. M. S. Chauhan. Efficient oxidation of polycyclic aromatic hydrocarbons with H_2O_2 catalyzed by 5,10,15-triarylcorrolatoiron (IV) chloride in ionic liquids. *Catal. Commun.*, **2012,** *29*, 15-20.
36. P. Shejwalkar, N. P. Rath, E. B. Bauer. New iron(ii) α-iminopyridine complexes and their catalytic activity in the oxidation of activated methylene groups and secondary alcohols to ketones. *Dalton Trans.*, **2011,** *40*, 7617-7631.
37. *Gaussian 09, Revision A.02*, M. J. Frisch, G. W. Trucks, H. B. Schlegel, G. E. Scuseria, M. A. Robb, J. R. Cheeseman, G. Scalmani, V. Barone, B. Mennucci, G. A. Petersson, H. Nakatsuji, M. Caricato, X. Li, H. P. Hratchian, A. F. Izmaylov, J. Bloino, G. Zheng, J. L. Sonnenberg, M. Hada, M. Ehara, K. Toyota, R. Fukuda, J. Hasegawa, M. Ishida, T. Nakajima, Y. Honda, O. Kitao, H. Nakai, T. Vreven, J. A. Montgomery Jr., J. E. Peralta, F. Ogliaro, M. J. Bearpark, J. Heyd, E. N. Brothers, K. N. Kudin, V. N. Staroverov, R. Kobayashi, J. Normand, K. Raghavachari, A. P. Rendell, J. C. Burant, S. S. Iyengar, J. Tomasi, M. Cossi, N. Rega, N. J. Millam, M. Klene, J. E. Knox, J. B. Cross, V. Bakken, C. Adamo, J. Jaramillo, R. Gomperts, R. E. Stratmann, O. Yazyev, A. J. Austin, R. Cammi, C. Pomelli, J. W. Ochterski, R. L. Martin, K. Morokuma, V. G. Zakrzewski, G. A. Voth, P. Salvador, J. J. Dannenberg, S. Dapprich, A. D. Daniels, Ö. Farkas, J. B. Foresman, J. V. Ortiz, J. Cioslowski, D. J. Fox. Gaussian, Inc.,Wallingford CT, **2009**.
38. A. D. Becke. Density-functional thermochemistry. III. The role of exact exchange. *J. Chem. Phys*, **1993,** *98*, 5648-5652.
39. C. Lee, W. Yang, R. G. Parr. Development of the Colle-Salvetti correlation-energy formula into a functional of the electron density. *Phys. Rev. B*, **1988,** *37*, 785-789.
40. R. A. Kendall, T. H. Dunning, R. J. Harrison. Electron affinities of the first-row atoms revisited. Systematic basis sets and wave functions. *J. Chem. Phys.*, **1992,** *96*, 6796-6806.

41. J. Tomasi, M. Persico. Molecular Interactions in Solution: An Overview of Methods Based on Continuous Distributions of the Solvent. *Chem. Rev.*, **1994,** *94*, 2027-2094.
42. J. Tomasi, B. Mennucci, R. Cammi. Quantum Mechanical Continuum Solvation Models. *Chem. Rev.*, **2005,** *105*, 2999-3094.
43 M. Cossi, N. Rega, G. Scalmani, V. Barone. Energies, structures, and electronic properties of molecules in solution with the C-PCM solvation model. *J. Comput. Chem.*, **2003,** *24*, 669-681.
44. V. Barone, M. Cossi. Quantum Calculation of Molecular Energies and Energy Gradients in Solution by a Conductor Solvent Model. *J. Phys. Chem. A*, **1998,** *102*, 1995-2001.
45. A. V. Marenich, C. J. Cramer, D. G. Truhlar. Universal Solvation Model Based on Solute Electron Density and on a Continuum Model of the Solvent Defined by the Bulk Dielectric Constant and Atomic Surface Tensions. *J. Phys. Chem. B*, **2009,** *113*, 6378-6396.
46. L. A. Curtiss, P. C. Redfern, K. Raghavachari, V. Rassolov, J. A. Pople. Gaussian-3 theory using reduced Mo/ller-Plesset order. *J. Chem. Phys.*, **1999,** *110*, 4703-4709.

4. Determination of association constants towards carbon nanotubes

Alberto de Juan, Alejandro López-Moreno, Joaquín Calbo, Enrique Ortí, and Emilio M. Pérez, *Chem. Sci.*, **2015**, *6*, 7008-7014.

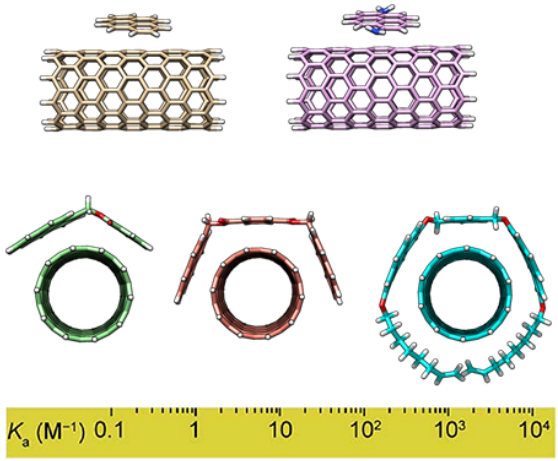

Single-walled carbon nanotubes (SWNTs) are one of the most promising nanomaterials and their supramolecular chemistry has attracted a lot of attention. However, despite well over a decade of research, there is no standard method for the quantification of their noncovalent chemistry in solution/ suspension. Here, we describe a simple procedure for the determination of association constants (K_a) between soluble molecules and insoluble and heterogeneous carbon nanotube samples. To test the scope of the method, we report binding constants between five different hosts and two types of SWNTs in four solvents. We have determined numeric values of K_a in the range of 1–10^4 M^{-1}. Solvent effects as well as structural changes in both the host and guest result in noticeable changes of K_a. The results obtained experimentally were validated through state-of-the-art DFT calculations. The generalization of quantitative and comparable association constants data should significantly help advance the supramolecular chemistry of carbon nanotubes.

4.1. Introduction

Materials with at least one of their dimensions in the nanometer range, such as graphene,[1] carbon nanotubes,[2] quantum dots,[3] metal nanoparticles,[4] few layer transition metal chalcogenides[5] etc., are expected to revolutionize technology[6] and have certainly transformed science already.[7] In particular, the extreme aspect ratio and extraordinary physical properties of single-walled carbon nanotubes (SWNTs) have attracted a great deal of attention.[8] Chemical modifications are usually necessary to take full advantage of their properties and/or to modulate them.[9] A particularly attractive strategy is to utilize noncovalent forces to yield supramolecular constructs, since it guarantees the structural integrity of the nanotube, and changing the structure of the host, its concentration, the solvent, and/or temperature can modulate the stability of the associates.[10] In this respect, the quantification of the supramolecular interactions is of paramount importance. From the experimental point of view, skillfully designed atomic force microscopy experiments have allowed for the measurement of interaction forces between single molecules and SWNTs.[11] A kinetic model for the measurement of chirality-specific interactions of SWNTs

[1] (a) A. K. Geim, K. S. Novoselov. *Nat. Mater.*, **2007,** *6*, 183-191; (b) A. K. Geim. *Science*, **2009,** *324*, 1530-1534; (c) C. N. R. Rao, A. K. Sood, K. S. Subrahmanyam, A. Govindaraj. *Angew. Chem., Int. Ed.*, **2009,** *48*, 7752-7777.
[2] D. Tasis, N. Tagmatarchis, A. Bianco, M. Prato. *Chem. Rev.*, **2006,** *106*, 1105-1136.
[3] J. Y. Kim, O. Voznyy, D. Zhitomirsky, E. H. Sargent. *Adv. Mater.*, **2013,** *25*, 4986-5010.
[4] M. V. Kovalenko, L. Manna, A. Cabot, Z. Hens, D. V. Talapin, C. R. Kagan, V. I. Klimov, A. L. Rogach, P. Reiss, D. J. Milliron, P. Guyot-Sionnnest, G. Konstantatos, W. J. Parak, T. Hyeon, B. A. Korgel, C. B. Murray, W. Heiss. *ACS Nano*, **2015,** *9*, 1012-1057.
[5] N. P. Dasgupta, X. Meng, J. W. Elam, A. B. F. Martinson. *Acc. Chem. Res.*, **2015,** *48*, 341-348.
[6] M. F. L. De Volder, S. H. Tawfick, R. H. Baughman, A. J. Hart. *Science*, **2013,** *339*, 535-539.
[7] From a purely bibliometric point of view, there are 73 journals listed under Nanoscience and Nanotechnology in the Journal of Citations Reports, of which the first seven have impact factors larger than 10. Ijima's first report on carbon nanotubes (S. Ijima, *Nature*, **1991**, *354*, 56-58) has been cited more than 22600 times. Data from Scifinder, August 2015.
[8] P. Avouris, Z. Chen, V. Perebeinos. *Nat. Nanotechnol.*, **2007,** *2*, 605-615.
[9] (a) P. Singh, S. Campidelli, S. Giordani, D. Bonifazi, A. Bianco, M. Prato. *Chem. Soc. Rev.*, **2009,** *38*, 2214-2230, (b) A. Hirsch. *Angew. Chem. Int. Ed.*, **2002,** *41*, 1853-1859.
[10] (a) N. Martín, J. –F. Nierengarten. *Supramolecular Chemistry of Fullerenes and Carbon Nanotubes*. **2012**; (b) Y.-L. Zhao, J. F. Stoddart. *Acc. Chem. Res.*, **2009,** *42*, 1161-1171.
[11] S. Iliafar, J. Mittal, D. Vezenov, A. Jagota. *J. Am. Chem. Soc.*, **2014,** *136*, 12947-12957.

with hydrogels has also been reported.[12] In silico investigations are far more abundant, and a wide variety of DFT methods have been tested.[13] However, the overwhelming majority of publications on noncovalent chemistry of nanotubes do not report quantitative data.[10, 14] This is in sharp contrast with the literature on soluble host–guest systems, in which the determination of the association constant (K_a) is hardly ever overlooked, and comparison of the K_a data is the main tool to understand molecular recognition events. Needless to say, the lack of quantitative and comparable information represents a major obstacle in the progress of the supramolecular chemistry of SWNTs.

Here, we describe a simple method for the determination of association constants between insoluble and heterogeneous nanotube samples and soluble molecules. To prove its validity, we have determined the association constants of five molecules towards two types of SWNTs in four different solvents.

4.2. Results and discussion

Due to the heterogeneous nature of most samples and the characteristic insolubility of SWNTs, it is virtually impossible to calculate their molar concentration in solution. This has hampered the determination of association constants in SWNT-based supramolecular systems, with a few notable exceptions based on approximations to apply standard spectroscopic titration methods.[15] However, it is known that association constants can be calculated from the fraction of occupied binding sites and the concentration of the host–guest complex, the free host, or the free guest species only.[16] This method is not

[12] K. Tvrdy, R. M. Jain, R. Han, A. J. Hilmer, T. P. McNicholas, M. S. Strano. *ACS Nano*, **2013,** *7*, 1779-1789.
[13] D. Umadevi, S. Panigrahi, G. N. Sastry. *Acc. Chem. Res.*, **2014,** *47*, 2574-2581.
[14] E. M. Pérez, N. Martín. *Chem. Soc. Rev.*, **2015,** *44*, 6425-6433.
[15] (a) P. Salice, A. Gambarin, N. Daldosso, F. Mancin, E. Menna. *J. Phys. Chem. C*, **2014,** *118*, 27028-27038, (b) H. Oh, J. Sim, S.-Y. Ju. *Langmuir*, **2013,** *29*, 11154-11162, (c) J. K. Sprafke, S. D. Stranks, J. H. Warner, R. J. Nicholas, H. L. Anderson. *Angew. Chem. Int. Ed.*, **2011,** *50*, 2313-2316.
[16] (a) K. A. Connors. *Binding Constants. The Measurement of Molecular Complex Stability*. **1987**; (b) P. Thordarson. *Chem. Soc. Rev.*, **2011,** *40*, 1305-1323.

usually applied to soluble host–guest systems because the total concentration of host and guest are known quantities and the calculation of the concentration of free species is problematic.[16b] We take advantage of the insolubility of the carbonaceous material to measure the concentration of bound and free species.

The experimental procedure is described graphically in Scheme 1 and can be summarized as follows: SWNTs (1 mg mL^{-1}, unless stated otherwise) are suspended in a solution of known concentration of the host molecule in a given solvent, and the mixture stirred for 2 hours to allow it to reach equilibrium. After this time, the suspension is filtered through a 0.2 μm-pore polytetrafluoroethylene membrane, retaining the host–SWNT complex. The solid is analysed through TGA (N_2, 50 °C min^{-1}) to quantify the amount of host in the complex, from which the concentration of free species is calculated by subtraction. Specifically, we measure the weight loss up to 600 °C, where all of the associated host has been desorbed and the nanotubes are still intact. From the degree of functionalization and the mass of the sample analysed, we calculate the total mass of host in the complex, from which its initial concentration in the equilibrium is immediate. Alternatively, the concentration of free species can be directly measured in the filtrate.[‡] The same procedure is repeated for several initial concentrations of the host molecule, ranging from 0 to near saturation in the solvent under study. A blank experiment to determine the adsorbed/encapsulated solvent was run in all cases, and the data subtracted. All the experiments were performed at room temperature.

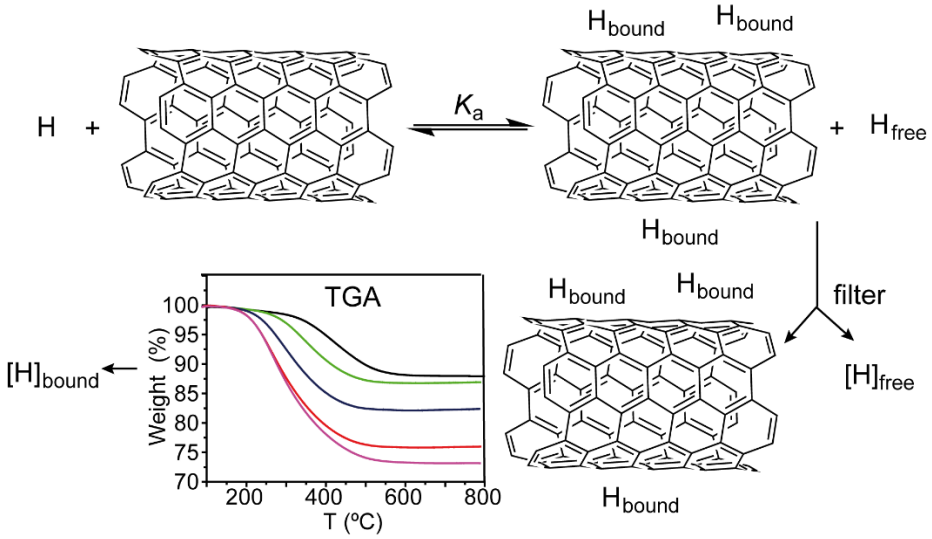

Scheme 1. Procedure for the measurement of $[H]_{bound}$ and $[H]_{free}$. A known concentration of host molecule H and SWNTs are allowed to reach equilibrium, and then complexed and free species are physically separated through filtration. The concentration of $[H]_{bound}$ is measured by TGA (typical results for a titration experiment are shown, see the experimental section for full data set). The concentration of $[H]_{free}$ can then be calculated by subtraction or directly measured in the filtrate.

The binding isotherms are obtained by plotting the degree of functionalization against the concentration of free host, and were analyzed using a standard 1:1 isotherm:[16b]

$$\theta = \frac{S\ x\ K_a\ x\ [H]_{free}}{1 +\ K_a\ x\ [H]_{free}}$$

where θ is the fraction of occupied binding sites and S represents the maximum functionalization at saturation, when θ equals 1. In this case, the 1:1 stoichiometry does not refer to the host:SWNT molar ratio, but to the number of occupied binding sites on SWNT, so that it is necessarily 1:1. In this respect, the

binding isotherm is both formally and conceptually equivalent to the Langmuir isotherm,[17] widely used for the quantification of the adsorption of gases onto solid surfaces.

Pyrene is by far the most widely used supramolecular partner for SWNTs, so we based our investigations on pyrene and its derivatives. **Figure 1** shows the chemical structure of the hosts for SWNTs used in the present work. First, we titrated **1** against plasma-purified SWNTs (pp-SWNTs, 98% purity, 0.8–1.6 nm in diameter) in tetrahydrofuran (THF), dimethylformamide (DMF), tetrachloroethane (TCE), and methanol (MeOH) at room temperature. **Figure 2** shows results of these titrations, where each data point is the average of three separate experiments.

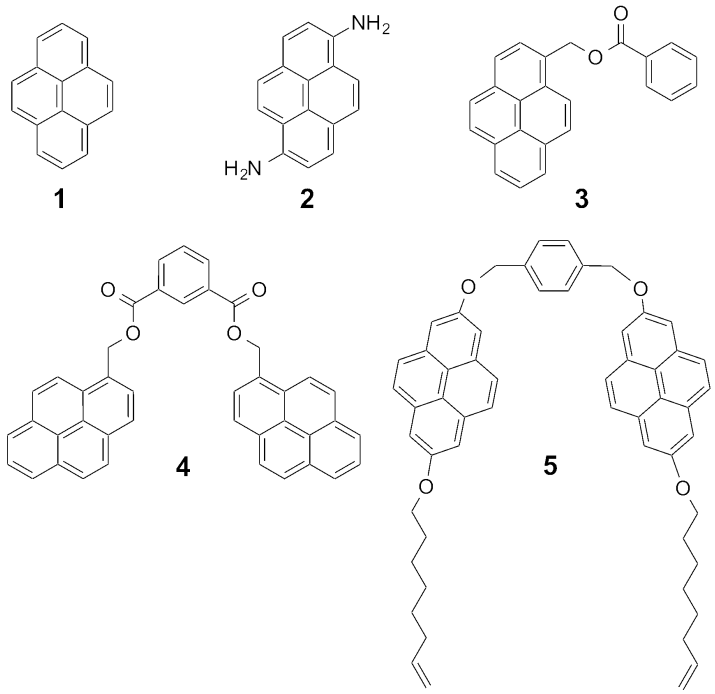

Figure 1 Structure of the hosts for SWNTs used in this work.

[17] I. Langmuir. *J. Am. Chem. Soc.*, **1918,** *40*, 1361-1402.

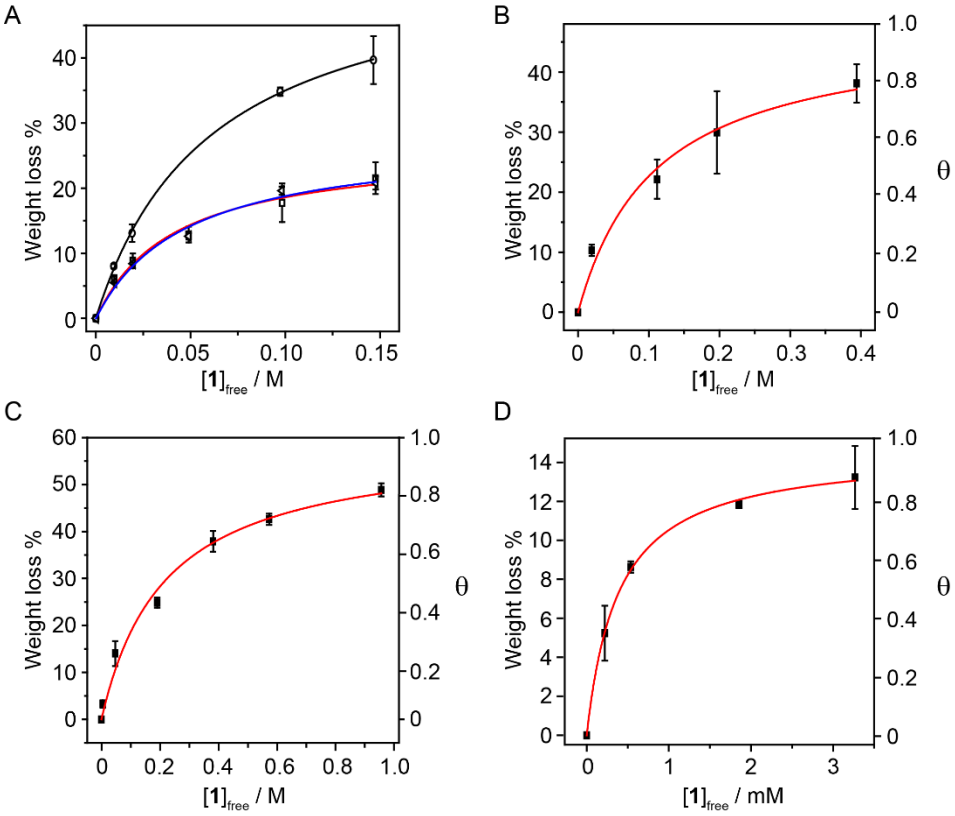

Figure 2. Titrations of pyrene vs. pp-SWNTs in (a) THF at 0.1 mg mL^{-1} of SWNTs (circles and black line, K_a = 16.4 ± 0.8 M^{-1}, r^2 = 0.999); 1 mg mL^{-1} of SWNTs (squares and red line, K_a = 24 ± 6 M^{-1}, r^2 = 0.979); and 10 mg mL^{-1} of SWNTs (triangles and blue line, K_a = 21 ± 4 M^{-1}, r^2 = 0.985); (b) DMF (K_a = 9 ± 3 M^{-1}, r^2 = 0.978); (c) TCE (K_a = 4.5 ± 0.9 M^{-1}, r^2 = 0.987); (d) MeOH (K_a = (2.6 ± 0.2) × 10^3 M^{-1}, r^2 = 0.998). Each data point is the average of three separate experiments, and the error bars represent the standard deviation. Solid lines represent the fit.

As a first test of the experimental validity of our approach, we decided to get data for titrations with significant variations in the concentration of SWNTs. In particular, we used 0.1, 1 and 10 mg mL^{-1} of nanotubes in THF (**Figure 2a**), which afforded K_a = 16.4 ± 0.8 M^{-1}, [§] 24 ± 6 M^{-1}, and 21 ± 4 M^{-1}, respectively. We were pleased to find that all values for K_a are identical within experimental

error. The main variability comes from the degree of functionalization at saturation, which is significantly larger for the more dilute sample. This reflects a more efficient disaggregation of the nanotubes, which in turn results in an increase in the availability of binding sites for **1**. Therefore, the method works correctly for samples with significantly different degrees of aggregation of the SWNTs.

With regards to the effect of the solvent, the association constants increase with decreasing ability to solvate SWNTs, showing that solvophobic interactions play a relevant role in the binding event. In DMF and TCE, solvents commonly used to disperse SWNTs, the binding constants are very small: $K_a = 9 \pm 3$ and 4.5 ± 0.9 M^{-1}, respectively (**Figure 2b and c**). In THF there is an increase of one order of magnitude, to $K_a = 24 \pm 6$ M^{-1} (**Figure 2a**), which is further amplified in MeOH, a notoriously bad solvent for SWNTs, to reach millimolar affinity with $K_a = (2.6 \pm 0.2) \times 10^3$ M^{-1} (**Figure 2d**).

In order to investigate whether the method is sufficiently sensitive to detect small changes in the structure of the nanotubes, we carried out titrations of **1** *vs.* (6,5)-enriched SWNTs (93% purity, 0.7–0.9 nm in diameter) in THF, DMF, TCE and MeOH at room temperature. The association constant towards (6,5)-SWNTs are: $K_a = 41 \pm 8$ M^{-1} in THF, 1.6 ± 0.4 M^{-1} in DMF, 1.6 ± 0.1 M^{-1} in TCE, and $(1.0 \pm 0.1) \times 10^3$ M^{-1} in MeOH (**Figure 3**). Therefore, with the only exception of THF, in which some unexpected solvent effect takes place, the association constants are smaller than those towards pp-SWNTs. Considering the planar geometry of pyrene, it is expected to establish stronger van der Waals interactions with nanotubes of larger diameter, a tendency that is corroborated by DFT calculations (see below). These results confirm that the method is sensitive enough to such subtle differences in the structure of the nanotube as a decrease in the average diameter of the sample.

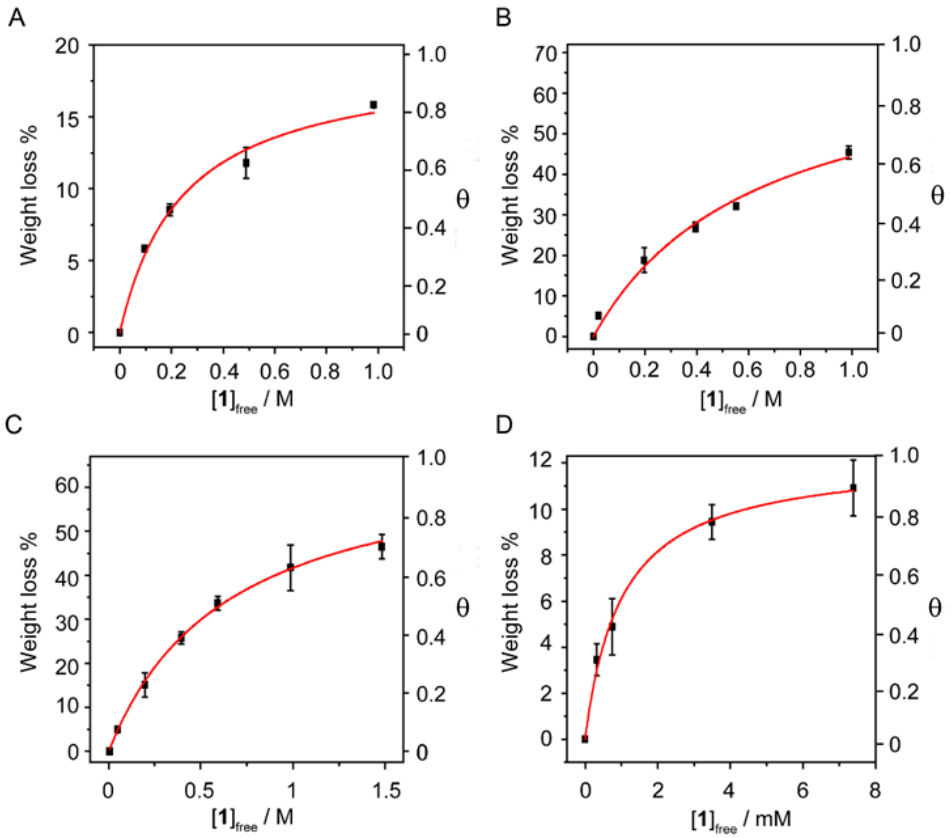

Figure 3. Titrations of **1** *vs.* (6,5)-SWNTs in (a) THF (K_a = 41 ± 8 M^{-1}, r^2 = 0.987); (b) DMF (K_a = 1.6 ± 0.4 M^{-1}, r^2 = 0.985); (c) TCE (K_a = 1.6 ± 0.1 M^{-1}, r^2 = 0.998); (d) MeOH (K_a = (1.0 ± 0.1) × 10^3 M^{-1}, r^2 = 0.994). Each data point is the average of three separate experiments, and the error bars represent the standard deviation. Solid red lines represent the fit.

The method is also sensitive towards the structure of the host. To get experimental evidence, we designed a collection of hosts composed by 1,6-diaminopyrene (**2**), the benzoic and isophthalic esters of pyrene-1-methanol (**3** and **4**, respectively), and bis-pyrene U-shape molecule **5**, which we have used

in the synthesis of mechanically interlocked derivatives of SWNTs.[18] Hosts **3**–**5** were titrated *vs.* pp-SWNTs in THF at room temperature, while we used DMF for the titration of **2** for solubility reasons.

Both electron-rich conjugated compounds and amines are known to interact strongly with SWNTs, so we expected **2** to show a significantly larger association constant compared to pyrene. This is indeed the case, as we calculated K_a = (2.2 ± 0.5) × 10^2 M^{-1} for the **2**·pp-SWNTs associate (**Figure 4a**), which is more than two orders of magnitude larger than the K_a of **1** in the same solvent. Addition of an extra aromatic ring in **3** also results in a significant increase in binding constant with respect to pyrene, reaching K_a = (9 ± 3) × 10 M^{-1} in THF (**Figure 4b**). Bivalent tweezers-like hosts are a particularly popular design for the supramolecular association of SWNTs and fullerenes, as they typically show very good affinity at a relatively low synthetic cost.[19] Indeed, **4** shows K_a = (6.5 ± 0.6) × 10^3 M^{-1} towards pp-SWNTs in THF (**Figure 4c**). Finally, we decided to get an insight into the association of U-shaped molecule **5**, which associates pp-SWNTs with K_a = (7 ± 2) × 10^3 M^{-1} (**Figure 4d**), slightly larger than that of **4**.

[18] (a) A. de Juan, Y. Pouillon, L. Ruiz-González, A. Torres-Pardo, S. Casado, N. Martín, A. Rubio, E. M. Pérez. *Angew. Chem., Int. Ed.*, **2014,** *53*, 5394-5400, (b) A. de Juan, E. M. Pérez. *Nanoscale*, **2013,** *5*, 7141-7148, (c) A. López-Moreno, E. M. Pérez. *Chem. Commun.*, **2015,** *51*, (25), 5421-5424, (d) A. de Juan, M. Mar Bernal, E. M. Pérez. *ChemPlusChem*, **2015,** *80*, 1153-1157.
[19] E. M. Pérez, N. Martín. *Pure Appl. Chem.*, **2010**, *82*, 523-533.

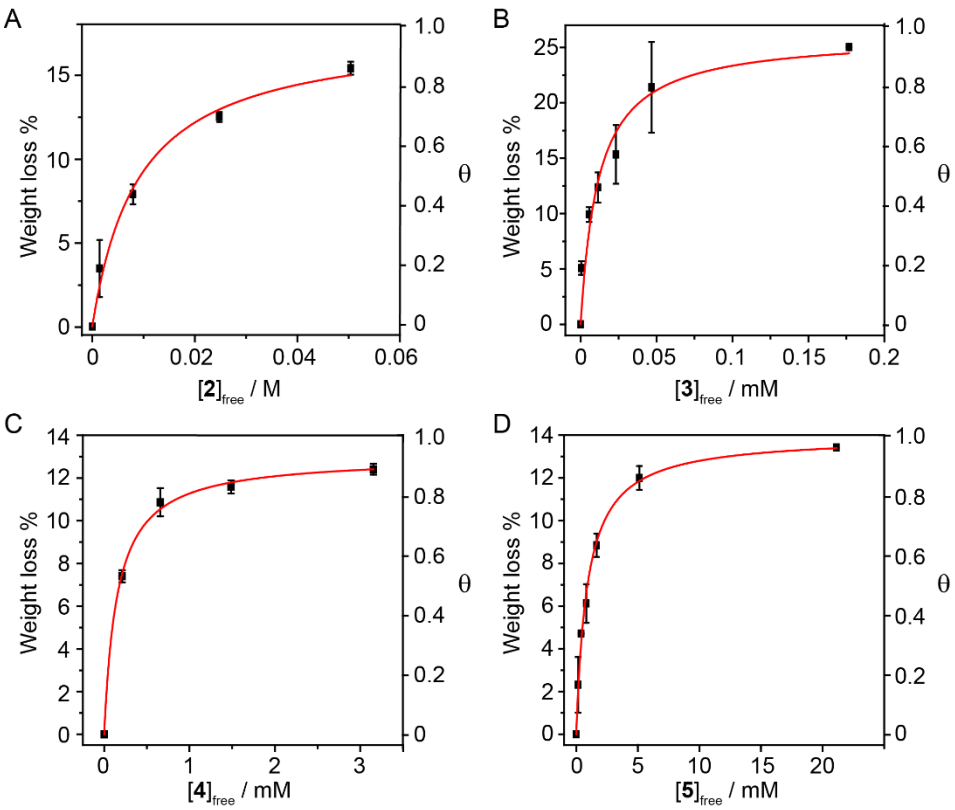

Figure 4. Titrations of the following hosts *vs.* pp-SWNTs (a) **2** in DMF (K_a = (2.2 ± 0.5) × 10^2 M^{-1}, r^2 = 0.986); (b) **3** in THF (K_a = (9 ± 3) × 10 M^{-1}, r^2= 0.937); (c) **4** in THF (K_a = (6.5 ± 0.6) × 10^3 M^{-1}, r^2 = 0.998); **5** in THF (K_a = (7 ± 2) × 10^3, r^2 = 0.951). Each data point is the average of three separate experiments, and the error bars represent the standard deviation. Solid red lines represent the fit.

Note that **4** and **5** feature two pyrene binding motifs each, and might show multivalency and/or cooperativity phenomena.[20] Since our method is based on measuring the concentration of the complex by desorbing it completely, it would not be valid to determine stepwise association constants. A possible approach to

[20] For detailed discussion on the subject, see: C. A. Hunter, H. L. Anderson. *Angew. Chem. Int. Ed.*, **2009,** *48*, 7488-7499.

investigate such issues would be to utilize the Hill equation.[21] Considering the clearly hyperbolic shape of the binding isotherms, we have determined average binding constants only.

To validate our experimental results, theoretical calculations were performed for the list of host–guest nanotube assemblies under the density functional theory (DFT) framework. The atom pair-wise Grimme's dispersion correction in its latest version (D3)[22] was coupled to the hybrid density functional of Perdew–Burke–Hernzerhof (PBE0)[23] through the Becke-Johnson damping function[24] and including the three-body dispersion correction (E^{ABC}).[25] The double-zeta Pople's 6-31G** basis set[26] was employed throughout and the basis set superposition error (BSSE) was corrected according to the counterpoise (CP) scheme of Boys and Bernardi.[27] The intensity of the interaction between host and guest was calculated by means of two different quantities. The interaction energy (E_{int}) is defined as the energy difference between the host–guest complex (HG) and the individual moieties separately (H and G), with all of them at the geometry of the complex:

$$E_{\text{int}} = E_{\text{HG}}^{\text{HG}} - E_{\text{H}}^{\text{HG}} - E_{\text{G}}^{\text{HG}}$$

where $E_X{}^Y$ is the energy of fragment *X* at the geometry of *Y*.

Otherwise, the binding (or association) energy (E_{bind}) was calculated taking into account the relaxation of the separate monomers and, therefore, considering

[21] For applications of the Hill equation to multifunctional synthetic pores, see: (a) Y. Baudry, G. Bollot, V. Gorteau, S. Litvinchuk, J. Mareda, M. Nishihara, D. Pasini, F. Perret, D. Ronan, N. Sakai, M. R. Shah, A. Som, N. Sordé, P. Talukdar, D. H. Tran, S. Matile. *Adv. Funct. Mater.*, **2006,** *16*, 169-179; For an application of the Hill equation to the association of fullerenes, see: (b) E. M. Pérez, L. Sánchez, G. Fernández, N. Martín. *J. Am. Chem. Soc.*, **2006,** *128*, 7172-7173; Ercolani has argued against the use of the Hill equation for self-assembly processes: (c) G. Ercolani. *J. Am. Chem. Soc.*, **2003,** *125*, 16097-16103.
[22] S. Grimme, J. Antony, S. Ehrlich, H. Krieg. *J. Chem. Phys.*, **2010,** *132*, 154104/1-154104/19.
[23] C. Adamo, V. Barone. *J. Chem. Phys.*, **1999,** *110*, 6158-6170.
[24] S. Grimme, S. Ehrlich, L. Goerigk. *J. Comput. Chem.*, **2011,** *32*, 1456-1465.
[25] S. Grimme. *Chem. - Eur. J.*, **2012,** *18*, 9955-9964.
[26] M. M. Francl, W. J. Pietro, W. J. Hehre, J. S. Binkley, M. S. Gordon, D. J. DeFrees, J. A. Pople. *J. Chem. Phys.*, **1982,** *77*, 3654-3665.
[27] S. F. Boys, F. Bernardi. *Mol. Phys.*, **1970,** *19*, 553-566.

the deformation energy required to transform the host/guest moieties from their minimum-energy geometries to the geometry acquired in the assembly:

$$E_{\text{bind}} = E_{\text{def}} + E_{\text{int}}$$

where:

$$E_{\text{def}} = (E_{\text{H}}^{\text{HG}} - E_{\text{H}}^{\text{H}}) + (E_{\text{G}}^{\text{HG}} - E_{\text{G}}^{\text{G}})$$

As a general model for the pp-SWNTs we have utilized a fragment of a zig-zag (10,0)-SWNT. The effect of the length of the nanotube into the intermolecular interaction was assessed by increasing the SWNT size in a **1**·SWNT complex, showing that the association energy is nearly converged with sizes slightly larger than the host length (see **Table S2** and **Figure S21**).

Figure 5 displays the minimum-energy geometries for the **1–5** hosts assembled with the pp-SWNT model of $C_{160}H_{20}$ computed at the PBE0-D3/6-31G** level of theory in gas phase. Among the different closely energetic conformations of **1** over pp-SWNT, the diagonal arrangement is found to be the most stable, with close π–π contacts in the range of 3.2–3.5 Å. The interaction energy of **1**·pp-SWNT is computed at −15.24 kcal mol^{-1}, which is slightly reduced to −14.84 kcal mol^{-1} for the binding energy as a consequence of the deformation energy penalty (0.59 kcal mol^{-1}). Moving from the pyrene system to 1,6-diaminopyrene (**2**), additional n–π interactions arise from close nitrogen···nanotube contacts (approximately at 4.0 Å). The E_{int} of **2**·pp-SWNT is calculated 1.3 kcal mol^{-1} larger than for **1**·pp-SWNT, but this difference is not maintained in the binding energy (**Table 1**). The deformation energy, calculated to be 2.83 kcal mol^{-1} for **2**·pp-SWNT, explains this trend. The inclusion of an extra aromatic ring in **3** results in a significant increase of the interaction energy up to −23.68 kcal mol^{-1}, with close π–π benzene···SWNTs (3.5 Å) and C═O···SWNTs (3.2 Å) contacts. Bivalent tweezers-like hosts further improve the supramolecular affinity *vs.* pp-SWNT with E_{int} as large as −38.78 and −63.23

kcal mol^{-1} in **4** and **5**, respectively. The binding energy in host **4** (−36.42 kcal mol^{-1}) is indeed approximately the sum of E_{bind} for its constituting moieties **1** and **3** (−14.84 + (−21.52) = −36.36 kcal mol^{-1}), which supports the theoretical approach undertaken. Whereas the E_{def} of **4** is computed similar to **2** and **3**, it amounts 20.46 kcal mol^{-1} for **5** due to the accommodation of the alkoxy chains around the nanotube (**Figure 4**). This disposition confers **5**·pp-SWNT an increased E_{bind} of −42.78 kcal mol^{-1} due to close CH···π contacts calculated in the range of 2.7–3.2 Å, which contribution to the total binding energy amounts 6 kcal mol^{-1}.

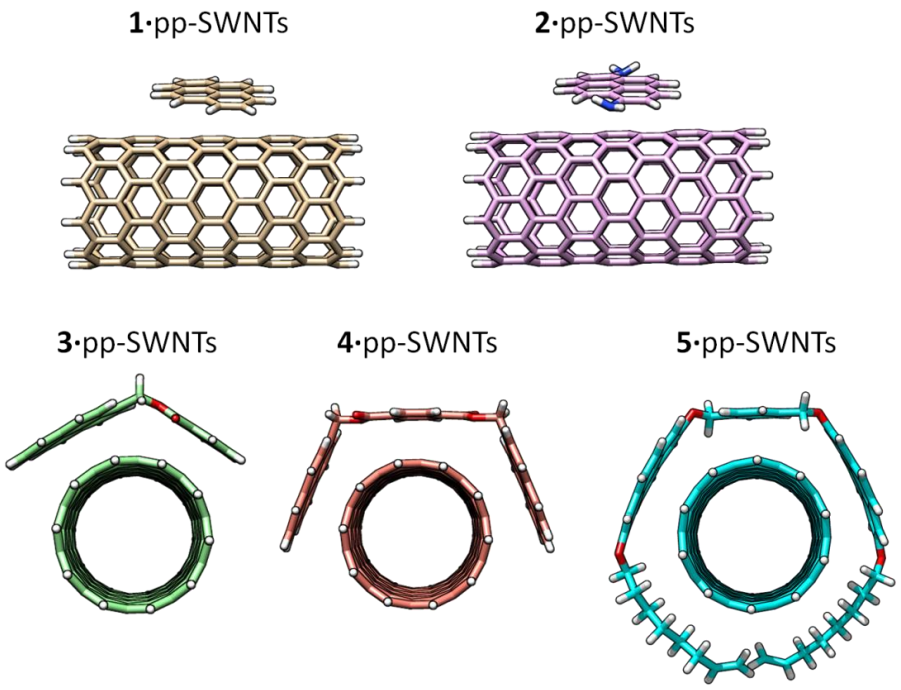

Figure 5. Minimum-energy geometry for the supramolecular assemblies formed by hosts **1–5** *vs.* the pp-SWNTs model calculated at the PBE0-D3/6-31G** level of theory.

Table 1 Energy parameters (kcal mol^{-1}) of the interaction between hosts **1–5** and guest SWNTs at the CP-corrected PBE0-D3/6-31G**+E^{ABC} level

System	E_{int}	E_{def}	E_{bind}	CA (Å^2)[a]
1·(6,5)-SWNTs	−13.85	0.81	−13.04	42.20
1·pp-SWNTs	−15.24	0.59	−14.84	42.70
2·pp-SWNTs	−16.53	2.83	−13.70	47.25
3·pp-SWNTs	−23.68	2.16	−21.52	75.30
4·pp-SWNTs	−38.78	2.36	−36.42	126.85
5·pp-SWNTs	−63.23	20.46	−42.78	188.55

[a]The intermolecular contact area (CA) was calculated using the UCSF Chimera 1.7 software according to the formula: (area of the host + area of the guest – area of the complex)/2, where the area refers to solvent-excluded molecular surfaces, composed of probe contact, toroidal, and reentrant surface.

Finally, the influence of the structure of the nanotube in the stability of the host–guest assembly was assessed by comparing the associates of pp-SWNT and (6,5)-SWNT with pyrene **1**. The E_{int} of **1**·(6,5)-SWNT was computed at −13.85 kcal mol^{-1}, which is 1.4 kcal mol^{-1} smaller than the E_{int} of **1**·pp-SWNT. The minimum energy structures calculated for the supramolecular complexes between pyrene and the two types of nanotubes (**Figure S22**) reveal subtle differences in terms of intermolecular contacts. The diameter of (6,5)-SWNT is computed at 7.5 Å, slightly smaller than for the pp-SWNT model (7.9 Å), which provokes a less efficient supramolecular assembly with pyrene. The deformation energy of **1**·(6,5)-SWNT is computed somewhat larger than **1**·pp-SWNT (**Table 1**), suggesting that the pyrene core is required to have a larger deformation to accommodate over the more-curved nanotube surface of (6,5)-SWNT. Moreover,

the intermolecular contact area for **1**·(6,5)-SWNT is calculated to be 0.5 Å^2 smaller than in **1**·pp-SWNT.

Most remarkably, the calculated E_{bind} energies and the experimentally determined K_a values show excellent quantitative agreement, despite the fact that desolvation and solvation energies are not included in our calculations. A plot of the ln K_a *vs.* $-E_{bind}$ for molecules **1**, **3**, **4**, and **5**, towards pp-SWNTs in THF at room temperature, the largest set for which we have extracted comparable K_a data, is shown in **Figure 6**. Fixing the intercept to 0, the data fit well (r^2 = 0.984) to a straight line of slope 0.22 ± 0.01. Therefore, our analysis shows that the ΔG_{bind} determined experimentally is proportional to the calculated E_{bind}.

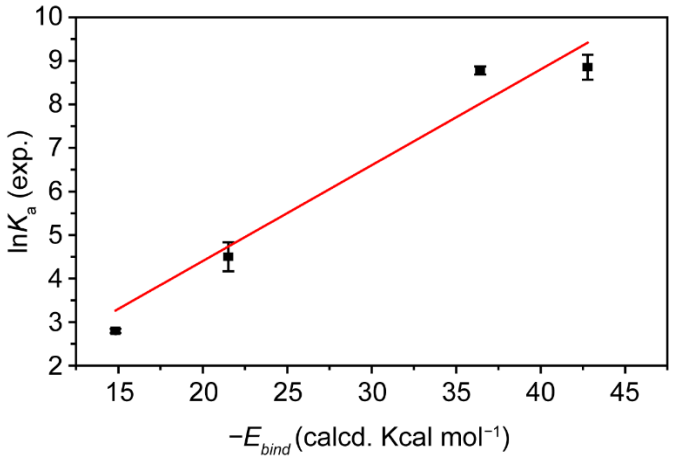

Figure 6. Plot of ln K_a *vs.* $-E_{bind}$, comparing the experimental and calculated data.

4.3. Conclusions

In summary, we have described a simple method for the determination of association constants between soluble molecules and insoluble and

heterogeneous nanomaterials. The method is based on the measurement of the concentration of free host, and therefore does not require any approximation. The quantitative measurements were carried out using TGA data only, so in principle, *any* host molecule can be evaluated regardless of its spectroscopic properties.

To illustrate the scope and limitations of this methodology, we have tested five different hosts and two types of SWNTs in four different solvents for a total of 17 binding constant determinations. The data fit well to the binding isotherm in all cases, with a minimum r^2 of 0.937 (**Table S1**). The method is sensitive to solvent effects, as well as to small structural changes in both the SWNT and the host. The numeric values of K_a span over approximately four orders of magnitude, showing that the method is valid both for very small and large binding constants. Our data were validated by DFT calculations, which correctly reproduce the trends observed experimentally.

Although the main objective of the present work was to develop a standard method for the determination of binding constants towards carbon nanotubes, several interesting observations can be made with the present data set of K_a. Perhaps the most relevant conclusion is that our results back the utilization of a single unit of pyrene as a noncovalent anchor to SWNTs in polar protic solvents,[28] but caution against assuming that it will "adsorb irreversibly" to the nanotubes in any organic solvent,[29] as the association constants can be as low as 1 M^{-1}. This is particularly relevant in cases where the pyrene-SWNT supramolecular construct will be subjected to further modifications after association. In this respect, using two pyrene units connected to form a tweezers-like receptor seems a valid alternative.

Taking into account the simplicity of the methodology described, we sincerely hope that the determination of association constants will become routine

[28] N. Nakashima, Y. Tomonari, H. Murakami. *Chem. Lett.*, **2002,** *31*, 638-639.
[29] R. J. Chen, Y. Zhang, D. Wang, H. Dai. *J. Am. Chem. Soc.*, **2001,** *123*, 3838-3839.

for anyone interested in the supramolecular chemistry of carbon nanotubes. The generalization of such quantitative data will undoubtedly produce a significant leap in our understanding of their noncovalent chemistry.

The techniques and methods described here should also be applicable to other insoluble nanomaterials, such as few-layer graphene. We are currently working towards the extension of this method to such nanomaterials.

Notes

‡ Somewhat counterintuitively, we find the direct measurement of $[H]_{free}$ in the filtrate more problematic experimentally. We believe the main reasons behind this are variations in the volume of solvent during the filtration process and spectral overlap of the hosts with the carbonaceous impurities present in the filtrate.

§ Considering that each data point consists of three separate experiments, we have reported errors directly as obtained from the fitting software. Based on our previous experience determining association constants, an experimental error within 20% can be expected.

4.4. Experimental section

Synthesis and characterization

General. Reagents were used as purchased. All air-sensitive reactions were carried out under argon atmosphere. Flash chromatography was performed using silica gel (Merck, Kieselgel 60, 230-240 mesh, or Scharlau 60, 230-240 mesh). Analytical thin layer chromatographies (TLC) were performed using aluminium-coated Merck Kieselgel 60 F254 plates. The NMR experiments were performed on a Bruker Avance 400 spectrometer (Magnet Ascend 400), operating at a frequency of 400 MHz and Bruker Avance 300 spectrometer (Magnet Ascend 400), operating at a frequency of 300 MHz at 298 K, unless otherwise stated,

using partially deuterated solvents as internal standards. Coupling constants (J) are denoted in Hz and chemical shifts (δ) in ppm. Multiplicities are denoted as follows: s = singlet, d = doublet, t = triplet, m = multiplet, b = broad. Fast atom bombardment (FAB) ionization experiments were recorded on a Waters VG AutoSpec spectrometer and Matrix-assisted Laser desorption ionization (coupled to a Time-Of-Flight analyzer) experiments (MALDI-TOF) were recorded on a HP1100MSD spectrometer and a Bruker REFLEX spectrometer, respectively. Thermogravimetric analyses (TGA) were performed using a TA Instruments TGAQ500 with a ramp of 50 °C/min under nitrogen from 100 to 1000 °C.

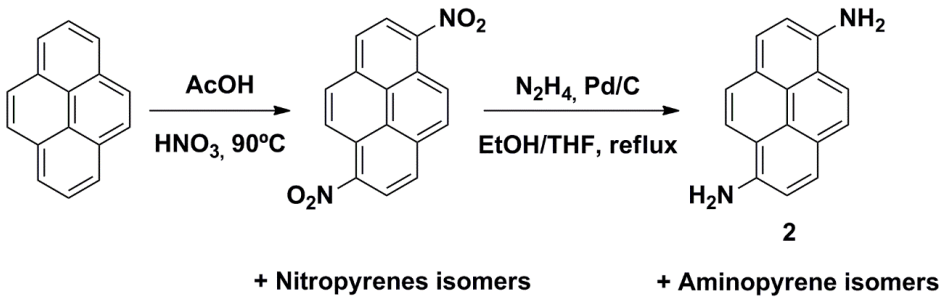

Nitropyrenes were synthetized as described in *Chem. Pharm. Bull.*, **1984**, *32*, 1992-1997.

Nitropyrenes (1.45 g) were dissolved in a mixture of ethanol and tetrahydrofuran (2:1, 12 mL) and palladium on activated charcoal (27 mg) was added over the solution. The mixture was refluxed, hydrazine (1.8 mL, 37 mmol) was added and then refluxed for 12 h. The mixture was filtered and the solvent was removed under vacuum. The aminopyrenes were purified by column chromatography (silica gel, 10% Ethyl acetate in dichloromethane).

Rf (10% Ethyl acetate in dichloromethane) values were 0.9 for 1-aminopyrene (Compound **8c**, 20%), 0.6 for 1,6-diaminopyrene (Compound **2**, 25%), 0.4 for 1,3- diaminopyrene and 0.3 for 1,8-diaminopyrene.

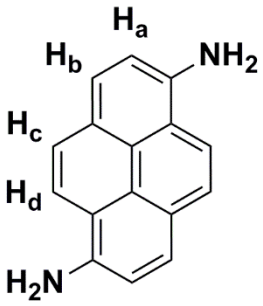

Compound **2**. ^{1}H NMR (300 MHz, DMSO-d6) δ 7.80 (d, *J* = 9.2 Hz, 2H, H_c), 7.75 (d, *J* = 8.2 Hz, 2H, H_b), 7.68 (d, *J* = 9.2 Hz, 2H, H_d), 7.26 (d, *J* = 8.2 Hz, 2H, H_a), 5.92 (s, 4H, NH_2). ^{13}C NMR (75 MHz, DMSO-d6) δ 142.8, 127.1, 125.5, 124.3, 123.1, 117.3, 116.6, 113.4. MS *m/z* calculated for $C_{16}H_{12}N_2$ [M^+] 232.1 found MALDI-TOF 232.1.

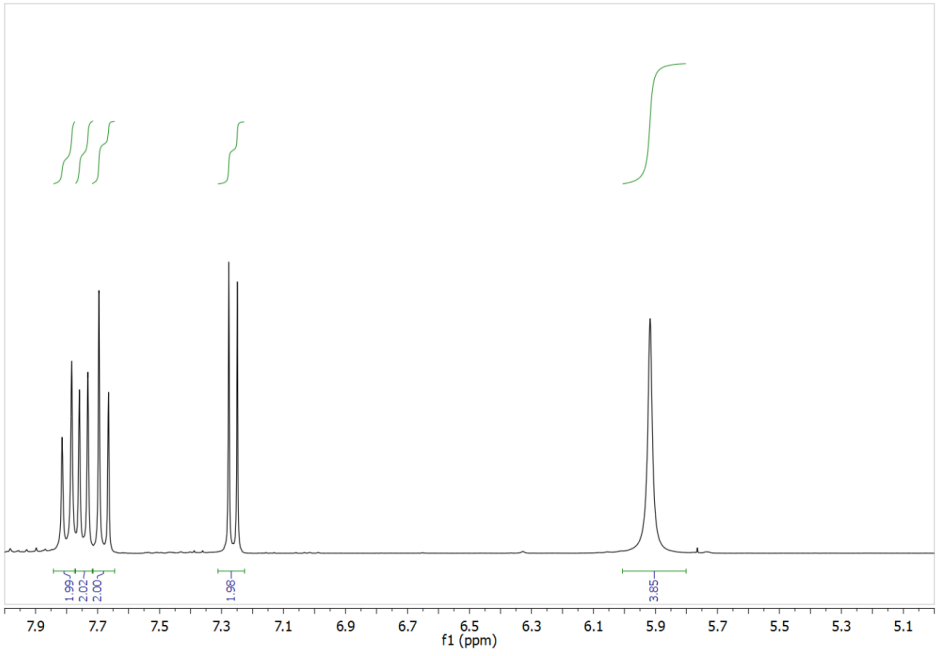

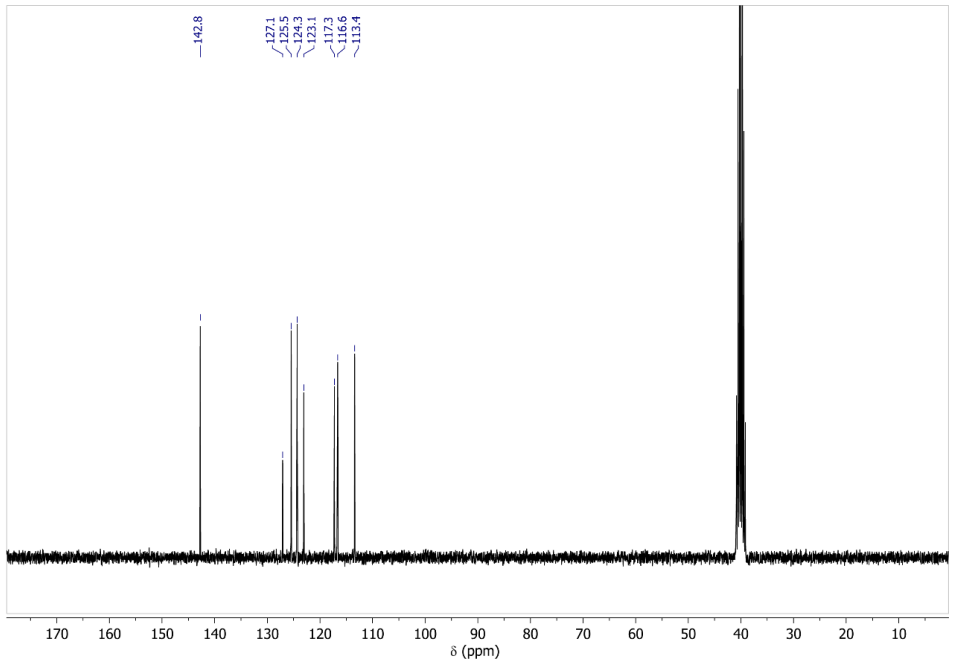
142.8
127.1
125.5
124.3
123.1
117.3
116.6
113.4
170 160 150 140 130 120 110 100 90 80 70 60 50 40 30 20 10
δ (ppm)

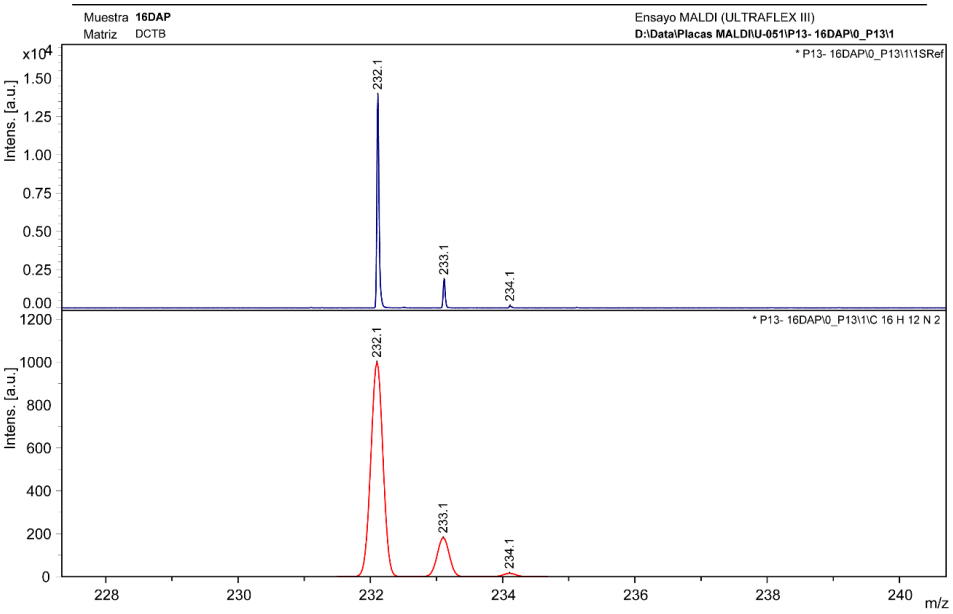
Muestra 16DAP
Matriz DCTB
Ensayo MALDI (ULTRAFLEX III)
D:\Data\Placas MALDI\U-051\P13- 16DAP\0_P13\1
* P13- 16DAP\0_P13\1\1SRef
x10^4
Intens. [a.u.]
232.1
233.1
234.1
* P13- 16DAP\0_P13\1\C 16 H 12 N 2
228 230 232 234 236 238 240
m/z

Synthesis of compounds 3 and 4

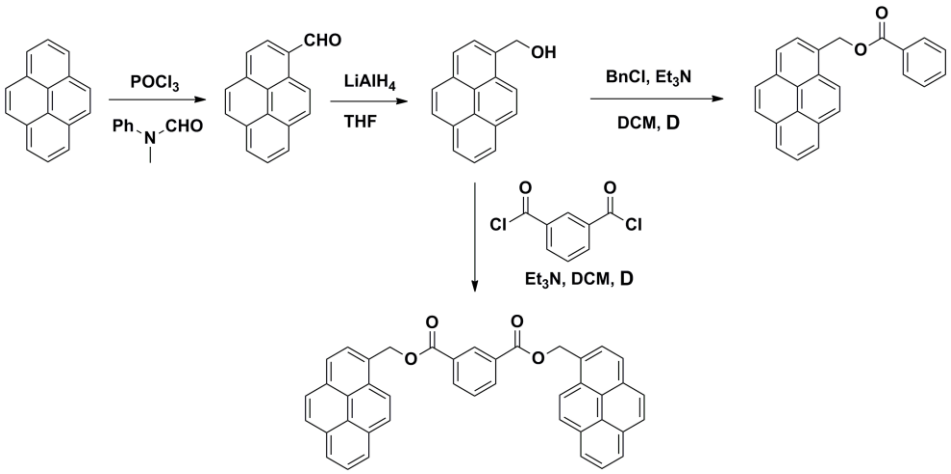

1-pyrenemethanol was synthetized as described in *Chem. - Eur. J.* **2010**, *16*, 9154.

Compound **3.** 1-pyrenemethanol (1.05 g, 4.48 mmol) was dissolved in chloroform (40 mL) and triethylamine (0.93 mL, 6.72 mmol) was added. Then benzoyl chloride (0.94 g, 6.72 mmol) was added and the mixture was refluxed for 3 h. After this time the solvent was removed under vacuum and hexane was added. The product was recovered by filtration and washed several times with hexane to obtain compound **3** in quantitative yield.

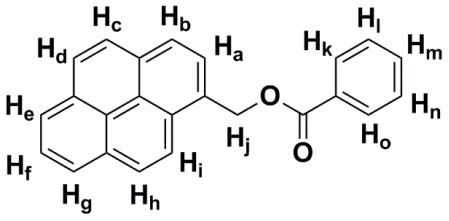

Compound **3.** ^{1}H NMR (300 MHz, $CDCl_3$) δ 8.38 (d, *J* = 9.2 Hz, 1H, H_e), 8.24 – 8.15 (m, 5H, $H_{b+g+f+k+o}$), 8.10 – 7.99 (m, 5H, $H_{a+c+i+h+d}$), 7.59 – 7.47 (m, 1H, H_m), 7.43 – 7.35 (m, 2H, H_{l+n}) 6.08 (s, 2H, H_j).^{13}C NMR (75 MHz, $CDCl_3$) δ 166.6, 133.1, 131.8, 131.3, 130.8, 130.2, 129.8, 129.7, 129.0, 128.4, 128.4, 127.9, 127.8, 127.4, 126.2, 125.6, 125.5, 125.0, 124.7, 123.0, 65.4. MS *m/z* calculated for $C_{24}H_{16}O_2$ [M^+] 336.1 found MALDI-TOF 336.2.

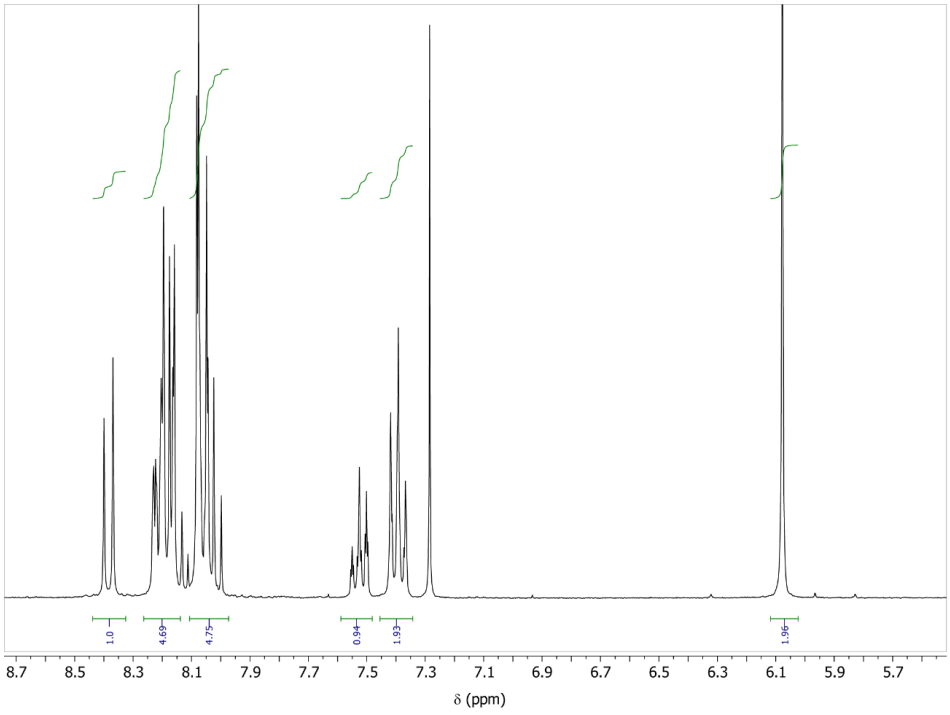

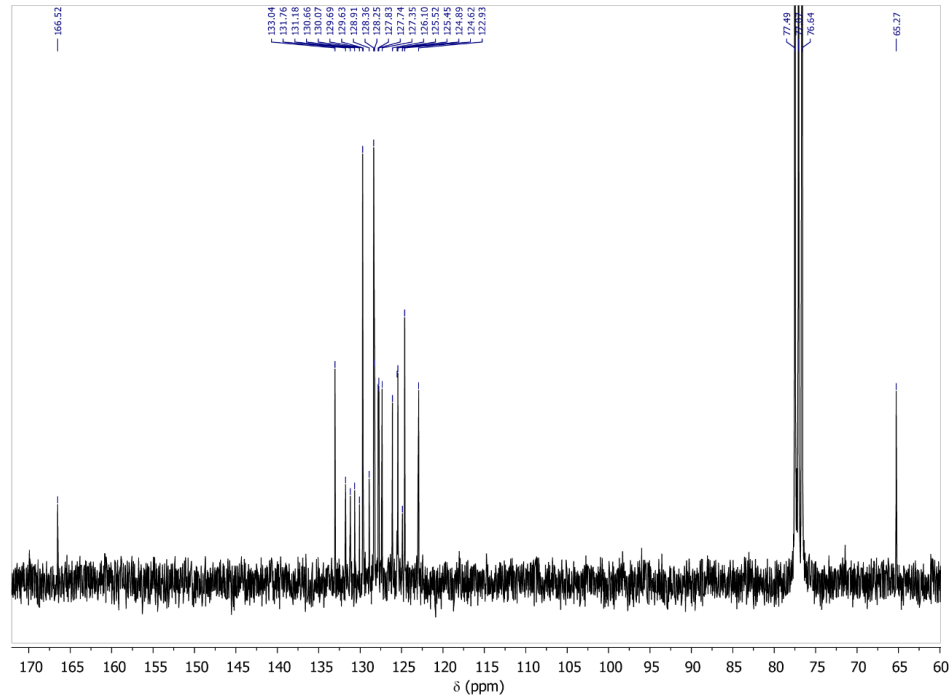
166.52
133.04
131.76
131.18
130.66
130.07
129.69
129.63
128.91
128.36
128.25
127.83
127.74
127.35
126.10
125.52
125.45
124.89
123.62
122.93
77.49
76.64
65.27
170 165 160 155 150 145 140 135 130 125 120 115 110 105 100 95 90 85 80 75 70 65 60
δ (ppm)

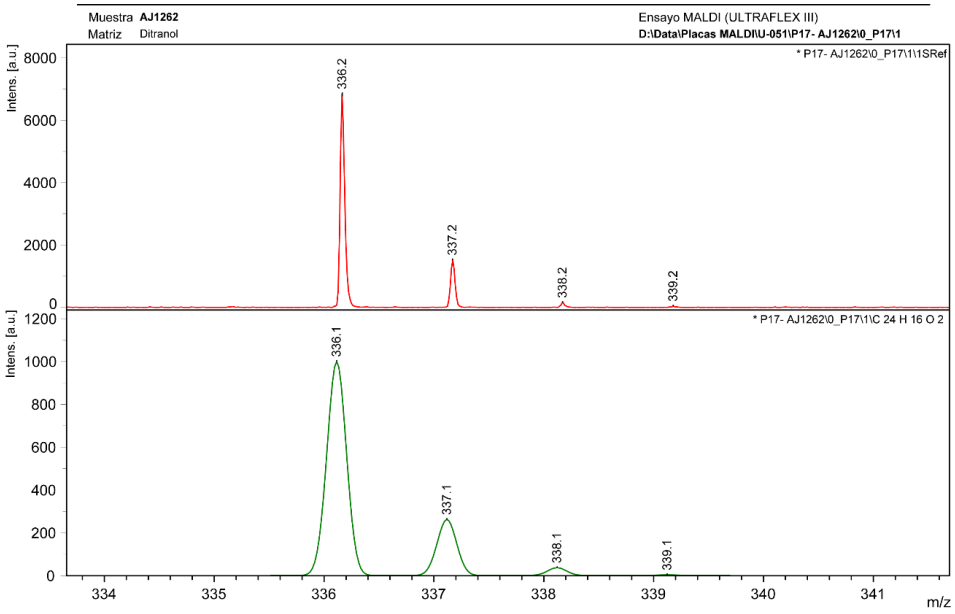
Muestra AJ1262
Matriz Ditranol
Ensayo MALDI (ULTRAFLEX III)
D:\Data\Placas MALDI\U-051\P17- AJ1262\0_P17\1
* P17- AJ1262\0_P17\1\1SRef
Intens. [a.u.]
8000
6000
4000
2000
0
336.2
337.2
338.2
339.2
* P17- AJ1262\0_P17\1\C 24 H 16 O 2
1200
1000
800
600
400
200
0
336.1
337.1
338.1
339.1
334 335 336 337 338 339 340 341
m/z

Compound **4.** 1-pyrenemethanol (1 g, 4.27 mmol) was dissolved in chloroform (20 mL) and triethylamine (0.6 mL, 4.27 mmol) was added. Isophtaloyl dichloride (0.21 g, 1.07 mmol) was added and the mixture was refluxed for 4h. After this time an additional 30 mL of chloroform were added, and the solution washed sequentially with 50 mL of hydrochloric acid 2N, 50 mL of 5% $NaHCO_3$ aqueous solution and water. The organic layer was separated, dried over Na_2SO_4 and the solvent removed under vacuum to obtain a solid. Compound **4** (65%) was purified by column chromatography (silica gel, dichloromethane).

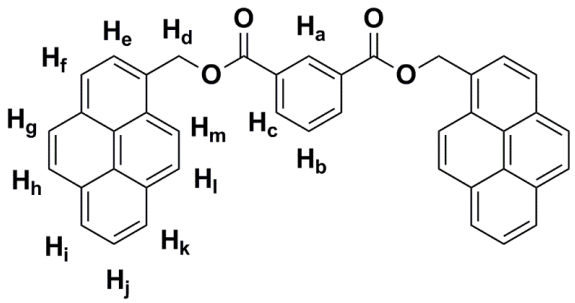

Compound **4**.^{1}H NMR (400 MHz, $CDCl_3$) δ 8.80 (t, *J* = 1.2 Hz, 1H, H_a), 8.37-8.34 (m, 2H, H_i), 8.24 – 8.16 (m, 4H, H_{f+c}), 8.18 (d, *J* = 7.6 Hz, 2H, H_k), 8.15 – 8.11 (m, 6H, H_{j+h+g}), 8.11 – 8.09 (m, 2H, H_m), 8.08 – 8.00 (m, 4H, H_{e+l}), 7.45 (t, *J* = 7.8 Hz, 1H, H_b), 6.09 (s, 4H, H_d). ^{13}C NMR (101 MHz, $CDCl_3$) δ 165.7, 134.1, 131.8, 131.2, 131.0, 130.7, 130.6, 129.6, 128.6, 128.6, 128.3, 127.9, 127.8, 127.4, 126.1, 125.6, 125.5, 124.9, 124.6, 124.6, 122.8, 77.3, 65.6. MS *m/z* calculated for $C_{42}H_{26}O_4$ [M^+] 594.2 found FAB 594.2.

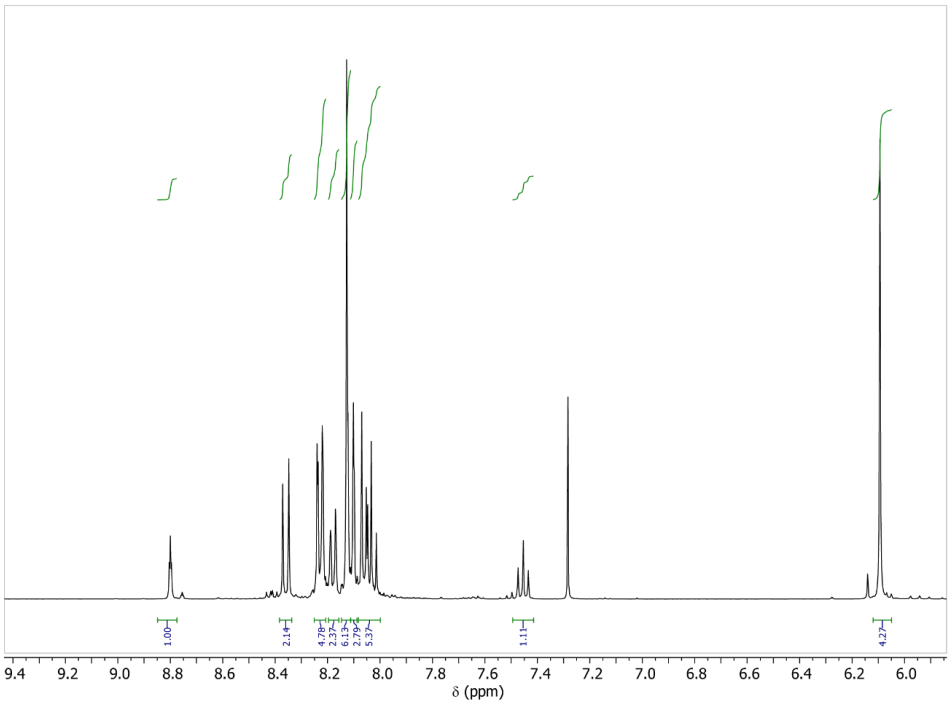
1.00
2.14
4.78
2.37
6.13
2.79
5.37
1.11
4.27
9.4 9.2 9.0 8.8 8.6 8.4 8.2 8.0 7.8 7.6 7.4 7.2 7.0 6.8 6.6 6.4 6.2 6.0
δ (ppm)

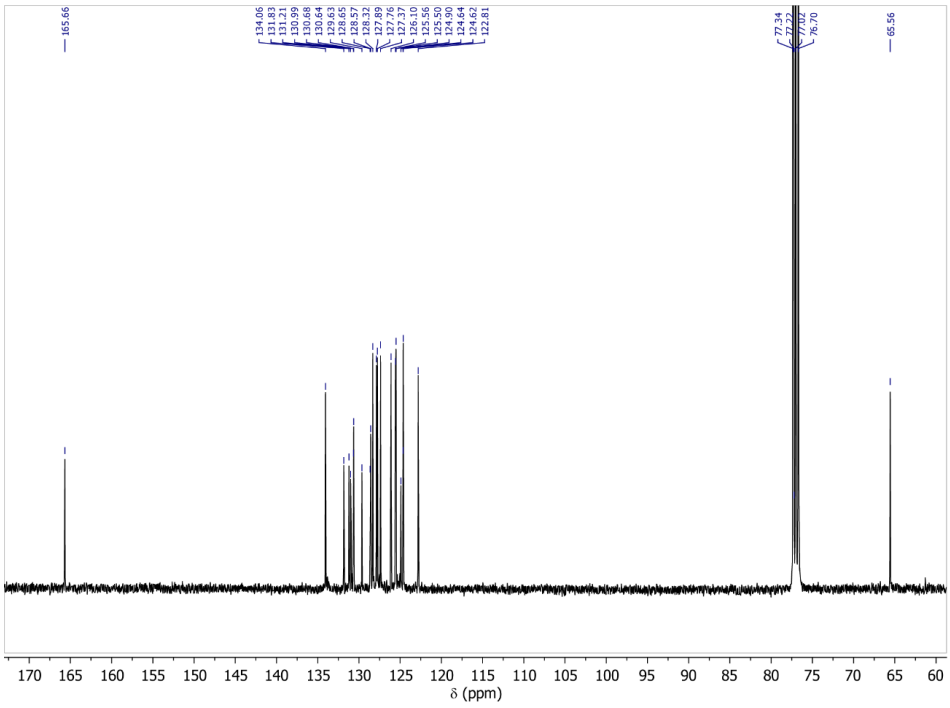
165.66
134.06
131.83
131.21
130.99
130.68
130.64
129.63
128.65
128.57
128.32
127.89
127.76
127.37
126.10
125.56
125.50
124.90
124.64
124.62
122.81
77.34
77.22
77.02
76.70
65.56
170 165 160 155 150 145 140 135 130 125 120 115 110 105 100 95 90 85 80 75 70 65 60
δ (ppm)

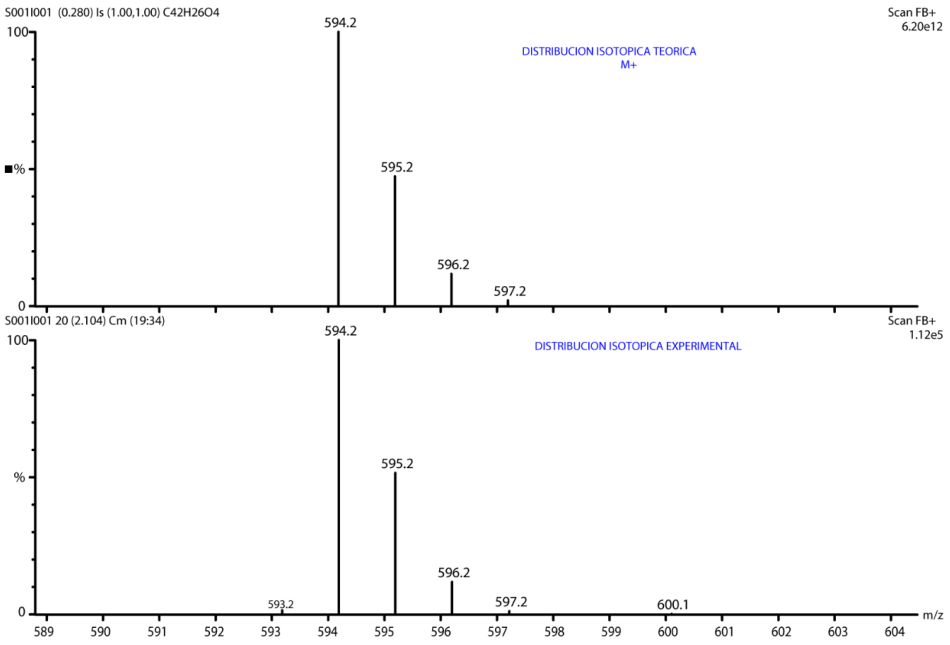

Synthesis of compound 5

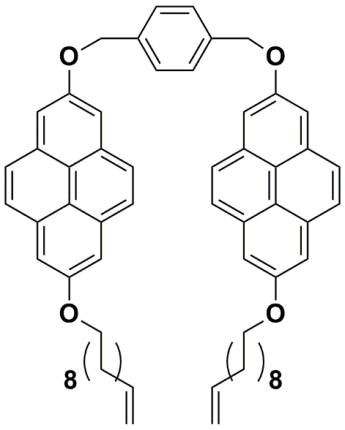

5

Compound **5** was synthetized as described in *Chem. Commun.* **2015**, *51*, 5421.

General procedure for titration

The titration curve for each host is formed using the TGA results of independent incubation experiments performed with different host concentration.

Each experiment proceeds as follows: the host molecule was dissolved in the corresponding solvent. Carbon nanotubes were added (1 mg mL^{-1}) and the suspension was stirred for 2 h at room temperature. Then, the mixture was filtered through a 0.2 µm-pore size polytetrafluorethylene membrane. The solid obtained was dried under vacuum and characterized by thermogravimetric analysis (N_2, ramp of 50 ºC min^{-1}, weight loss was measured from 100 ºC to 600 ºC).

Each independent experiment for each host concentration was repeated 3 times and the different results were averaged. A blank to determine the solvent adsorbed on or encapsulated in the carbon nanotube was carried out, and subtracted in the data analysis.

Thermogravimetric analysis

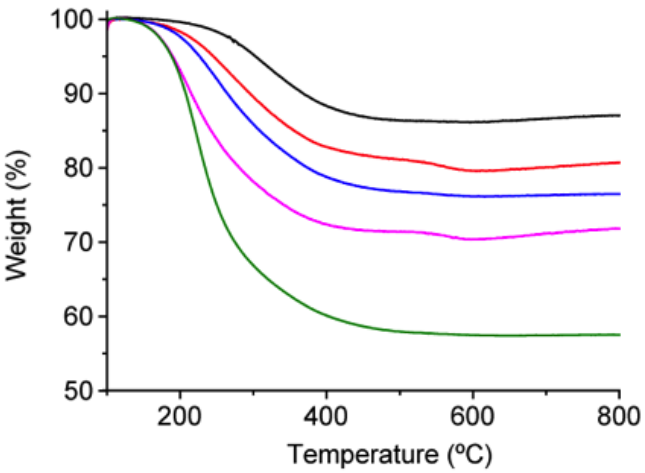

Figure S1. TG analysis of titration of **1** *vs* pp-SWNTs in THF at 0.1 mg mL^{-1} of SWNTs.

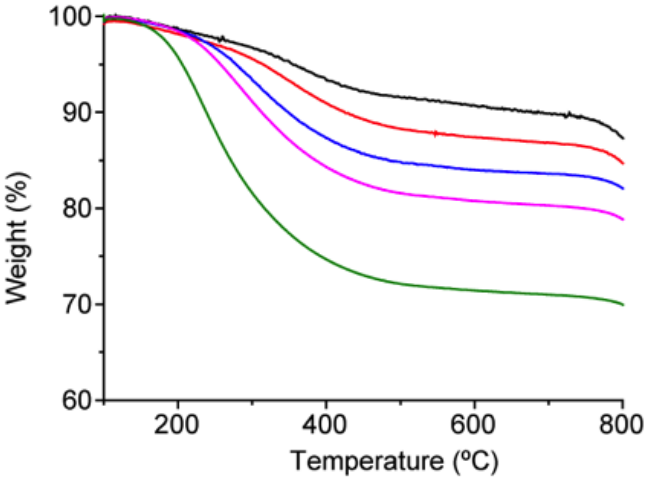

Figure S2. TG analysis of titration of **1** *vs* pp-SWNTs in THF at 1 mg mL^{-1} of SWNTs.

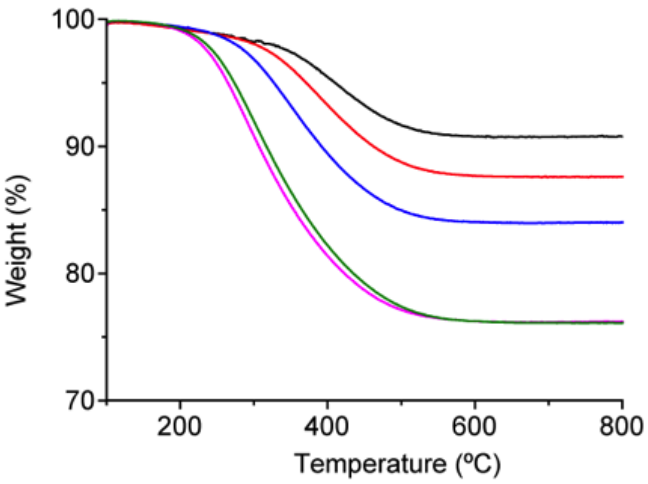

Figure S3. TG analysis of titration of **1** *vs* pp-SWNTs in THF at 10 mg mL^{-1} of SWNTs.

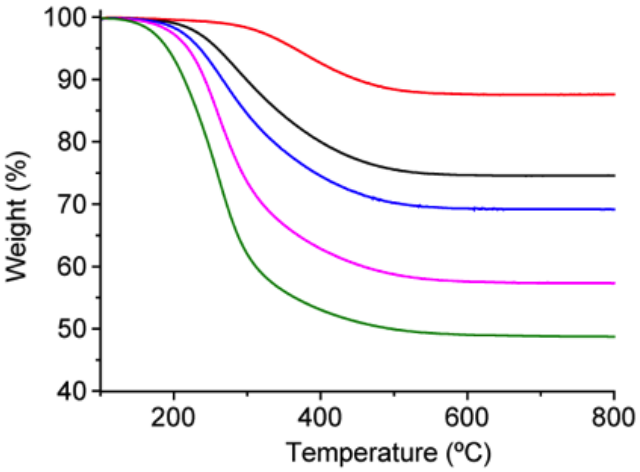

Figure S4. TG analysis of titration of **1** *vs* pp-SWNTs in DMF at 1 mg mL^{-1} of SWNTs.

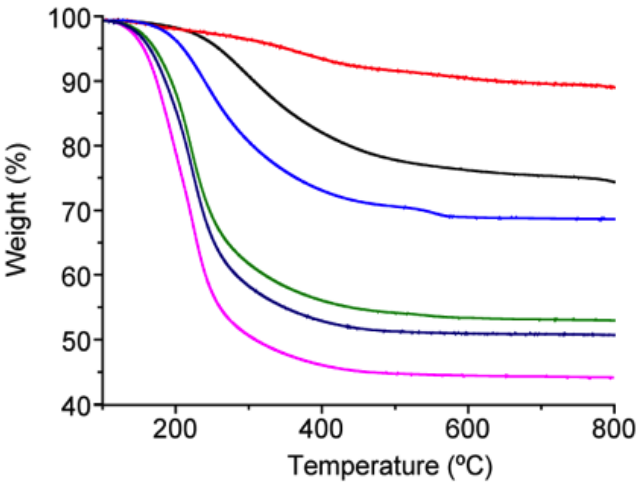

Figure S5. TG analysis of titration of **1** *vs* pp-SWNTs in TCE at 1 mg mL^{-1} of SWNTs.

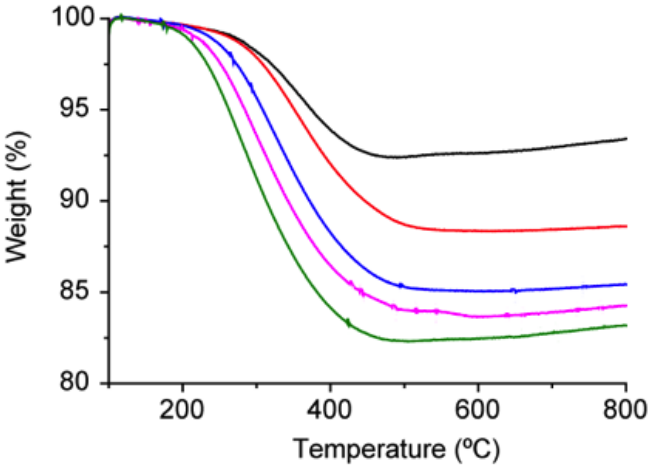

Figure S6. TG analysis of titration of **1** *vs* pp-SWNTs in MeOH at 1 mg mL^{-1} of SWNTs.

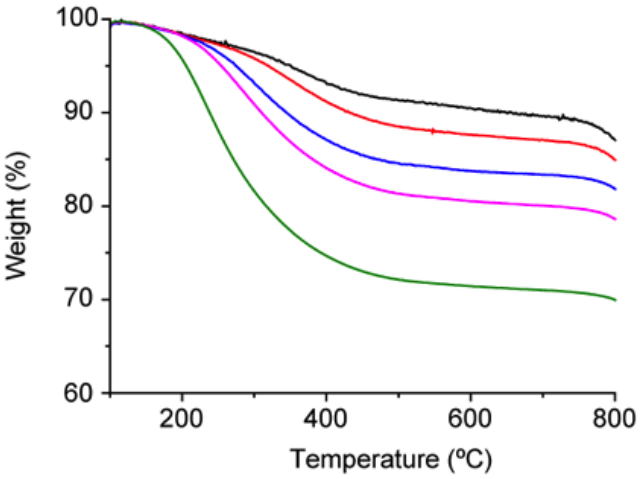

Figure S7. TG analysis of titration of **1** *vs* (6,5)-SWNTs in THF at 1 mg mL^{-1} of SWNTs.

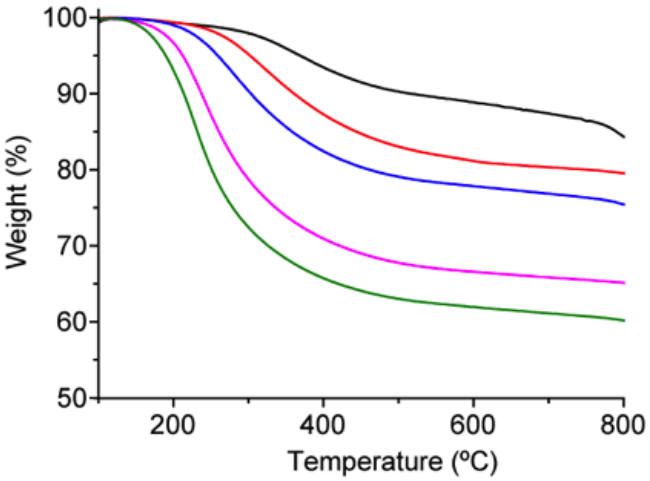

Figure S8. TG analysis of titration of **1** *vs* (6,5)-SWNTs in DMF at 1 mg mL^{-1} of SWNTs.

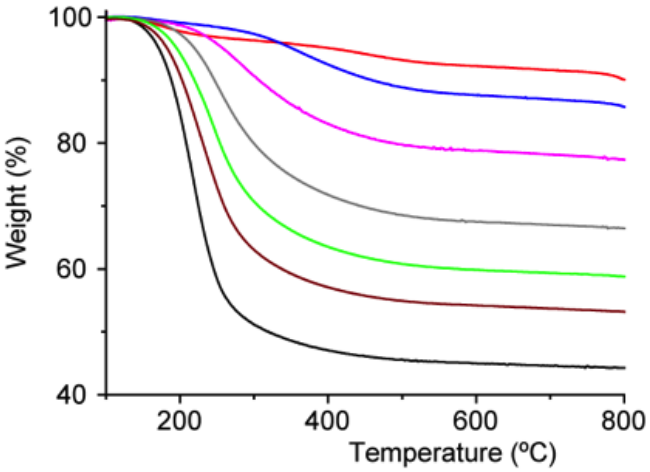

Figure S9. TG analysis of titration of **1** *vs* (6,5)-SWNTs in TCE at 1 mg mL^{-1} of SWNTs.

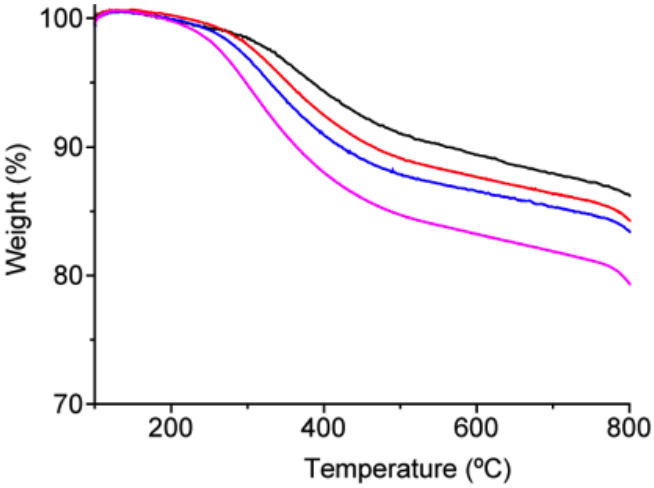

Figure S10. TG analysis of titration of **1** *vs* (6,5)-SWNTs in MeOH at 1 mg mL^{-1} of SWNTs.

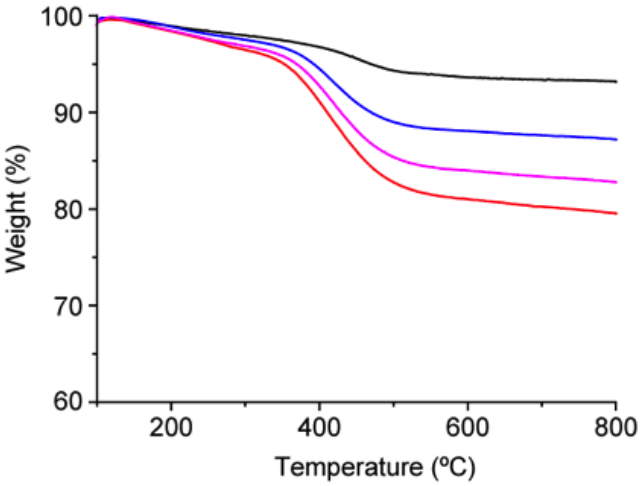

Figure S11. TG analysis of titration of **2** *vs* pp-SWNTs in DMF at 1 mg mL^{-1} of SWNTs.

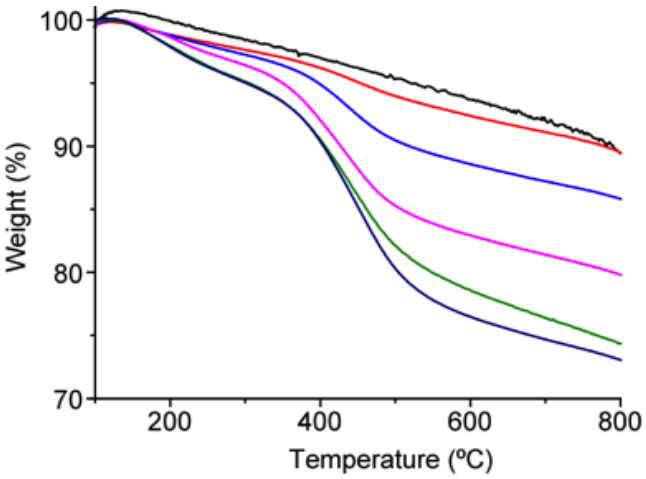

Figure S12. TG analysis of titration of **2** *vs* (6,5)-SWNTs in DMF at 1 mg mL^{-1} of SWNTs.

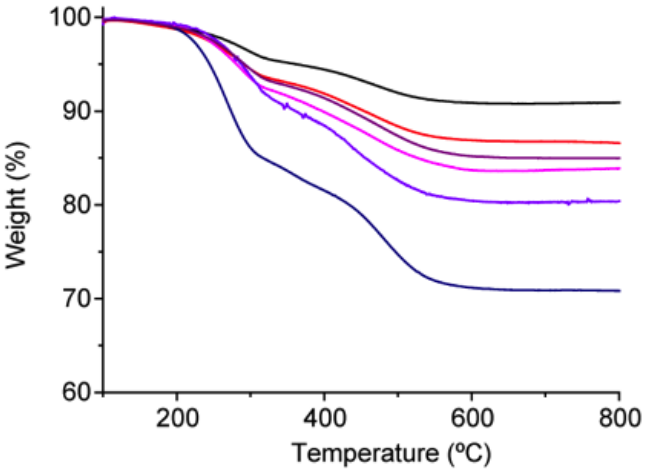

Figure S13. TG analysis of titration of **3** *vs* pp-SWNTs in THF at 1 mg mL^{-1} of SWNTs.

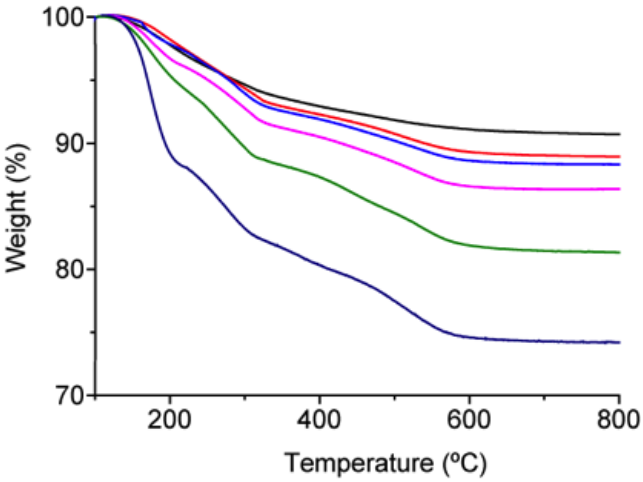

Figure S14. TG analysis of titration of **3** *vs* pp-SWNTs in TCE at 1 mg mL^{-1} of SWNTs.

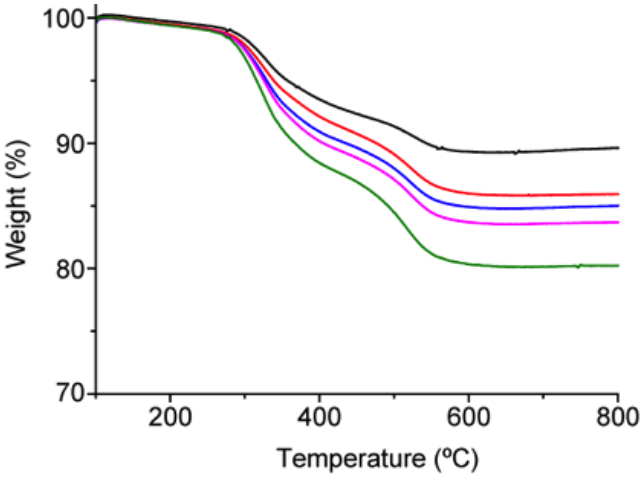

Figure S15. TG analysis of titration of **4** *vs* pp-SWNTs in THF at 1 mg mL^{-1} of SWNTs.

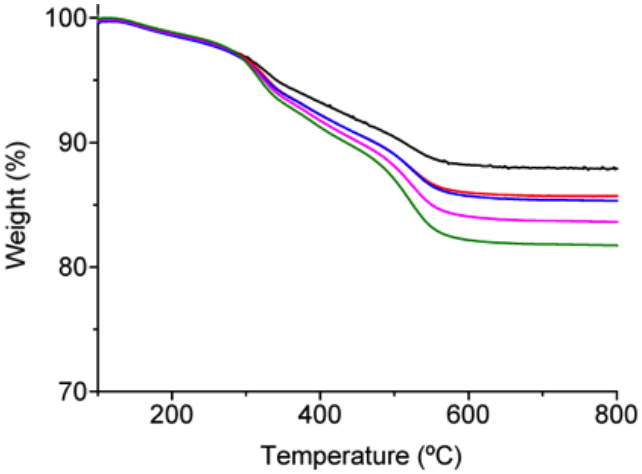

Figure S16. TG analysis of titration of **4** *vs* pp-SWNTs in TCE at 1 mg mL^{-1} of SWNTs.

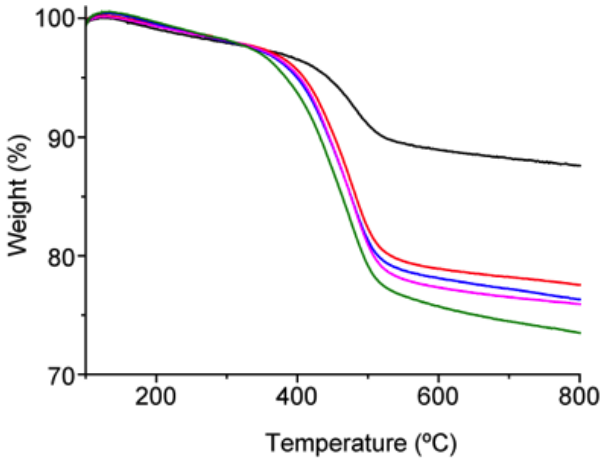

Figure S17. TG analysis of titration of **5** *vs* pp-SWNTs in THF at 1 mg mL^{-1} of SWNTs.

Table S1. Summary of results obtained from titrations at 298 K.

	Solvent	K_a (M^{-1})	Error (M^{-1})	Saturation (%)	r^2
1·pp-SWNTs	THF[a]	16.4	0.8	56	0.999
1·pp-SWNTs	THF	24	6	26	0.979
1·pp-SWNTs	THF[b]	21	4	28	0.985
1·pp-SWNTs	DMF	9	3	47	0.978
1·pp-SWNTs	TCE	4.5	0.9	59	0.987
1·pp-SWNTs	MeOH	2.6×10^3	0.2×10^3	15	0.998
1·(6,5)-SWNTs	THF	41	8	19	0.987
1·(6,5)-SWNTs	DMF	1.6	0.4	73	0.985
1·(6,5)-SWNTs	TCE	1.6	0.1	67	0.998
1·(6,5)-SWNTs	MeOH	1.0×10^3	0.1×10^3	12	0.994
2·pp-SWNTs	DMF	2.2×10^2	0.5×10^2	18	0.986
2·(6,5)-SWNTs	DMF	29	3	27	0.995
3·pp-SWNTs	THF	9 x 10	3 x 10	26	0.937
3·pp-SWNTs	TCE	20	5	24	0.965
4·pp-SWNTs	THF	6.5×10^3	0.6×10^3	13	0.998
4·pp-SWNTs	TCE	4×10^3	1×10^3	9	0.986
5·pp-SWNTs	THF	7×10^3	2×10^3	21	0.951

[a] 0.1 mg mL^{-1} of pp-SWNTs

[b] 10 mg mL^{-1} of pp-SWNTs

Adsorption isotherms not shown in the main text

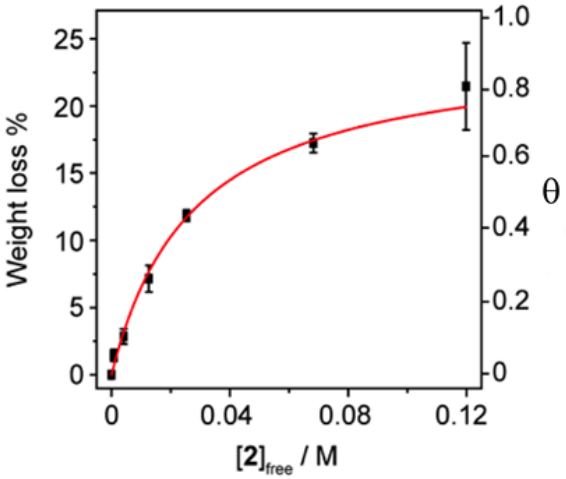

Figure S18. Titration of **2** *vs* (6,5) SWNTs in DMF at 298 K (K_a = 29 ± 3 M^{-1}, r^2 = 0.995)

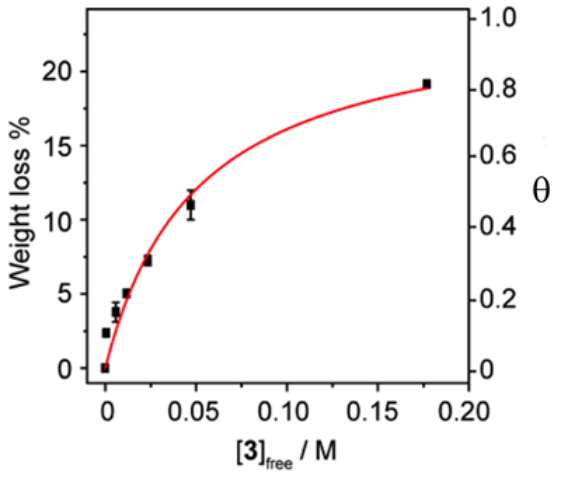

Figure S19. Titration of **3** *vs* pp-SWNTs in TCE at 298 K (K_a = 20 ± 5 M^{-1}, r^2 = 0.965)

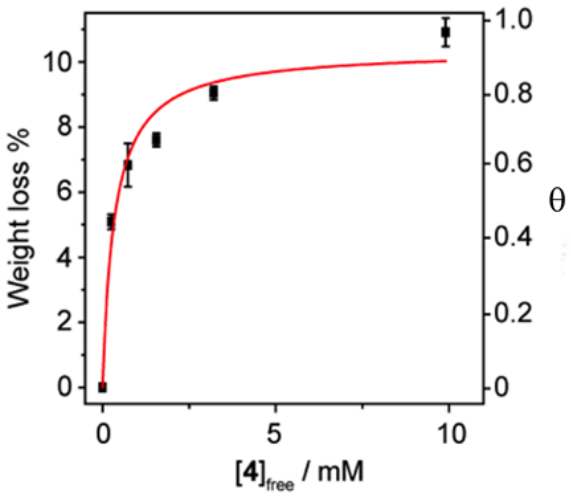

Figure S20. Titration of **4** *vs* pp-SWNTs in TCE at 298 K (K_a = 2.9± 0.8 × 10^3 M^{-1}, r^2 = 0.960).

Theoretical calculations

Table S2. Binding energy (kcal/mol) depending on the nanotube length for the parallel and perpendicular dispositions of the supramolecular **1**·pp-SWNT complex calculated at the PBE0-D3/6-31G** level of theory.

		Binding energy (kcal/mol)	
		Semi-rigid	Fully relaxed
parallel	**1**·$C_{40}H_{20}$	-11.05	-11.25
	1·$C_{80}H_{20}$	-17.80	-18.11
	1·$C_{120}H_{20}$	-21.79	-21.76
	1·$C_{200}H_{20}$	-21.18	-21.42
perpendicular	**1**·$C_{40}H_{20}$	-10.88	-11.12
	1·$C_{80}H_{20}$	-16.40	-17.11
	1·$C_{120}H_{20}$	-19.46	-19.60
	1·$C_{200}H_{20}$	-18.85	-17.97

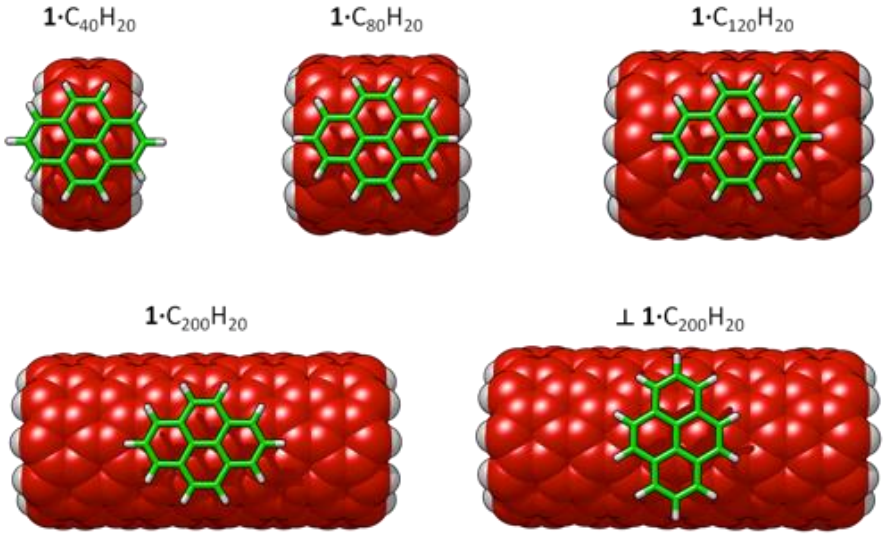

Figure S21. Minimum-energy geometries of parallel **1**·pp-SWNT assemblies and the perpendicular ⊥**1**·$C_{200}H_{20}$ calculated at the PBE0-D3/6-31G** level from a semi-rigid optimization with fixed intramolecular parameters.

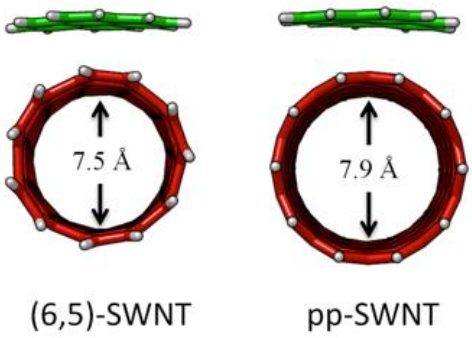

Figure S22. Side view of the supramolecular complex formed by pyrene and two types of SWNTs.

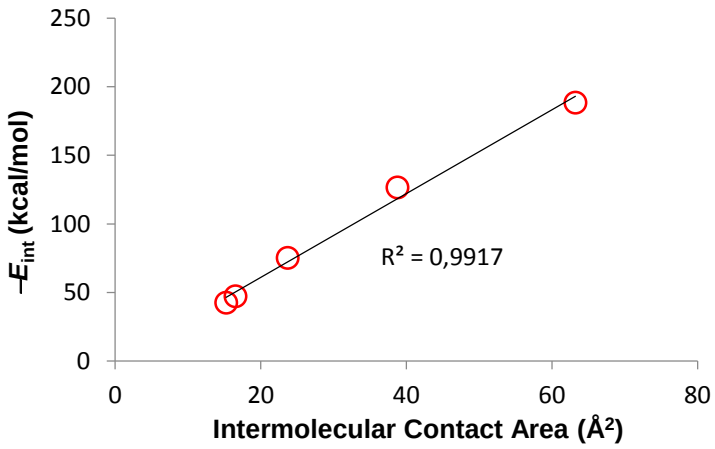

Figure S23. Relationship between the intermolecular contact area and the interaction energy for the **host**·pp-SWNTs assemblies.

4.5. References

1. (a) A. K. Geim, K. S. Novoselov. The rise of graphene. *Nat. Mater.*, **2007,** *6*, 183-191; (b) A. K. Geim. Graphene: Status and Prospects. *Science*, **2009,** *324*, 1530-1534; (c) C. N. R. Rao, A. K. Sood, K. S. Subrahmanyam, A. Govindaraj. Graphene: The New Two-Dimensional Nanomaterial. *Angew. Chem., Int. Ed.*, **2009,** *48*, 7752-7777.

2. D. Tasis, N. Tagmatarchis, A. Bianco, M. Prato. Chemistry of Carbon Nanotubes. *Chem. Rev.*, **2006,** *106*, 1105-1136.

3. J. Y. Kim, O. Voznyy, D. Zhitomirsky, E. H. Sargent. 25th Anniversary Article: Colloidal Quantum Dot Materials and Devices: A Quarter-Century of Advances. *Adv. Mater.*, **2013,** *25*, 4986-5010.

4. M. V. Kovalenko, L. Manna, A. Cabot, Z. Hens, D. V. Talapin, C. R. Kagan, V. I. Klimov, A. L. Rogach, P. Reiss, D. J. Milliron, P. Guyot-Sionnnest, G. Konstantatos, W. J. Parak, T. Hyeon, B. A. Korgel, C. B. Murray, W. Heiss. Prospects of Nanoscience with Nanocrystals. *ACS Nano*, **2015,** *9*, 1012-1057.

5. N. P. Dasgupta, X. Meng, J. W. Elam, A. B. F. Martinson. Atomic Layer Deposition of Metal Sulfide Materials. *Acc. Chem. Res.*, **2015,** *48*, 341-348.

6. M. F. L. De Volder, S. H. Tawfick, R. H. Baughman, A. J. Hart. Carbon Nanotubes: Present and Future Commercial Applications. *Science*, **2013,** *339*, 535-539.

7. P. Avouris, Z. Chen, V. Perebeinos. Carbon-based electronics. *Nat. Nanotechnol.*, **2007,** *2*, 605-615.

8. (a) P. Singh, S. Campidelli, S. Giordani, D. Bonifazi, A. Bianco, M. Prato. Organic functionalization and characterization of single-walled carbon nanotubes. *Chem. Soc. Rev.*, **2009,** *38*, 2214-2230; (b) A. Hirsch. Functionalization of Single-Walled Carbon Nanotubes. *Angew. Chem. Int. Ed.*, **2002,** *41*, 1853-1859.
9. (a) *Supramolecular Chemistry of Fullerenes and Carbon Nanotubes*, ed. N. Martín, J. –F. Nierengarten, Wiley-VCH Verlag GmbH & Co. KGaA, **2012**; (b) Y.-L. Zhao, J. F. Stoddart. Noncovalent Functionalization of Single-Walled Carbon Nanotubes. *Acc. Chem. Res.*, **2009,** *42*, 1161-1171.
10. S. Iliafar, J. Mittal, D. Vezenov, A. Jagota. Interaction of Single-Stranded DNA with Curved Carbon Nanotube Is Much Stronger Than with Flat Graphite. *J. Am. Chem. Soc.*, **2014,** *136*, 12947-12957.
11. K. Tvrdy, R. M. Jain, R. Han, A. J. Hilmer, T. P. McNicholas, M. S. Strano. A Kinetic Model for the Deterministic Prediction of Gel-Based Single-Chirality Single-Walled Carbon Nanotube Separation. *ACS Nano*, **2013,** *7*, 1779-1789.
12. D. Umadevi, S. Panigrahi, G. N. Sastry. Noncovalent Interaction of Carbon Nanostructures. *Acc. Chem. Res.*, **2014,** *47*, 2574-2581.
13. E. M. Pérez, N. Martín. π-π interactions in carbon nanostructures. *Chem. Soc. Rev.*, **2015,** *44*, 6425-6433.
14. (a) P. Salice, A. Gambarin, N. Daldosso, F. Mancin, E. Menna. Noncovalent Interaction between Single-Walled Carbon Nanotubes and Pyrene-Functionalized Gold Nanoparticles in Water-Soluble Nanohybrids. *J. Phys. Chem. C*, **2014,** *118*, 27028-27038; (b) H. Oh, J. Sim, S.-Y. Ju. Binding Affinities and Thermodynamics of Noncovalent Functionalization of Carbon Nanotubes with Surfactants. *Langmuir*, **2013,** *29*, 11154-11162; (c) J. K. Sprafke, S. D. Stranks, J. H. Warner, R. J. Nicholas, H. L. Anderson. Noncovalent Binding of Carbon Nanotubes by Porphyrin Oligomers. *Angew. Chem. Int. Ed.*, **2011,** *50*, 2313-2316.
15. (a) K. A. Connors. *Binding Constants. The Measurement of Molecular Complex Stability*. John Wiley & sons: New York, **1987**; (b) P. Thordarson. Determining association constants from titration experiments in supramolecular chemistry. *Chem. Soc. Rev.*, **2011,** *40*, (3), 1305-1323.
16. I. Langmuir. The adsorption of gases on plane surfaces of glass, mica and platinum. *J. Am. Chem. Soc.*, **1918,** *40*, 1361-1402.
17. (a) A. de Juan, Y. Pouillon, L. Ruiz-González, A. Torres-Pardo, S. Casado, N. Martín, Á. Rubio, E. M. Pérez. Mechanically Interlocked Single-Wall Carbon Nanotubes. *Angew. Chem., Int. Ed.*, **2014,** *53*, 5394-5400; (b) A. de Juan, E. M. Pérez. Getting tubed: mechanical bond in endohedral derivatives of carbon nanotubes?, *Nanoscale*, **2013,** *5*, 7141-7148; (c) A. López-Moreno, E. M. Pérez. Pyrene-based mechanically interlocked SWNTs. *Chem. Commun.*, **2015,** *51*, 5421-5424; (d) A. de Juan, M. Mar Bernal, E. M. Pérez. Optimization and Insights into the Mechanism of Formation of Mechanically Interlocked Derivatives of Single-Walled Carbon Nanotubes. *ChemPlusChem*, **2015,** *80*, 1153-1157.

18. E. M. Pérez, N. Martín. Molecular tweezers for fullerenes. *Pure Appl. Chem.*, **2010**, *82*, 523-533.
19. C. A. Hunter, H. L. Anderson. What is Cooperativity?, *Angew. Chem. Int. Ed.*, **2009,** *48*, 7488-7499.
20. (a) Y. Baudry, G. Bollot, V. Gorteau, S. Litvinchuk, J. Mareda, M. Nishihara, D. Pasini, F. Perret, D. Ronan, N. Sakai, M. R. Shah, A. Som, N. Sordé, P. Talukdar, D. H. Tran, S. Matile. Molecular Recognition by Synthetic Multifunctional Pores in Practice: Are Structural Studies Really Helpful?, *Adv. Funct. Mater.*, **2006,** *16*, 169-179; (b) E. M. Pérez, L. Sánchez, G. Fernández, N. Martín. exTTF as a Building Block for Fullerene Receptors. Unexpected Solvent-Dependent Positive Homotropic Cooperativity. *J. Am. Chem. Soc.*, **2006,** *128*, 7172-7173; (c) G. Ercolani. Assessment of Cooperativity in Self-Assembly. *J. Am. Chem. Soc.*, **2003,** *125*, 16097-16103.
21. S. Grimme, J. Antony, S. Ehrlich, H. Krieg. A consistent and accurate ab initio parametrization of density functional dispersion correction (DFT-D) for the 94 elements H-Pu. *J. Chem. Phys.*, **2010,** *132*, 154104.
22. C. Adamo, V. Barone. Toward reliable density functional methods without adjustable parameters: The PBE0 model. *J. Chem. Phys.*, **1999,** *110*, 6158-6170.
23. S. Grimme, S. Ehrlich, L. Goerigk. Effect of the damping function in dispersion corrected density functional theory. *J. Comput. Chem.*, **2011,** *32*, 1456-1465.
24. S. Grimme. Supramolecular Binding Thermodynamics by Dispersion-Corrected Density Functional Theory. *Chem. - Eur. J.*, **2012,** *18*, 9955-9964.
25. M. M. Francl, W. J. Pietro, W. J. Hehre, J. S. Binkley, M. S. Gordon, D. J. DeFrees, J. A. Pople. Self-consistent molecular orbital methods. XXIII. A polarization-type basis set for second-row elements. *J. Chem. Phys.*, **1982,** *77*, 3654-3665.
26. S. F. Boys, F. Bernardi. The calculation of small molecular interactions by the differences of separate total energies. Some procedures with reduced errors. *Mol. Phys.*, **1970,** *19*, 553-566.
27. S. F. Boys, F. Bernardi. The calculation of small molecular interactions by the differences of separate total energies. Some procedures with reduced errors. *Mol. Phys.*, **1970,** *19*, 553-566.
28. N. Nakashima, Y. Tomonari, H. Murakami. Water-Soluble Single-Walled Carbon Nanotubes via Noncovalent Sidewall-Functionalization with a Pyrene-Carrying Ammonium Ion. *Chem. Lett.*, **2002,** *31*, 638-639.
29. R. J. Chen, Y. Zhang, D. Wang, H. Dai. Noncovalent Sidewall Functionalization of Single-Walled Carbon Nanotubes for Protein Immobilization. *J. Am. Chem. Soc.*, **2001,** *123*, 3838-3839.

5. Pyrene-based mechanically interlocked SWNTs

Alejandro López-Moreno and Emilio M. Pérez, *Chem. Commun.* **2015,** *51*, 5421-5424.

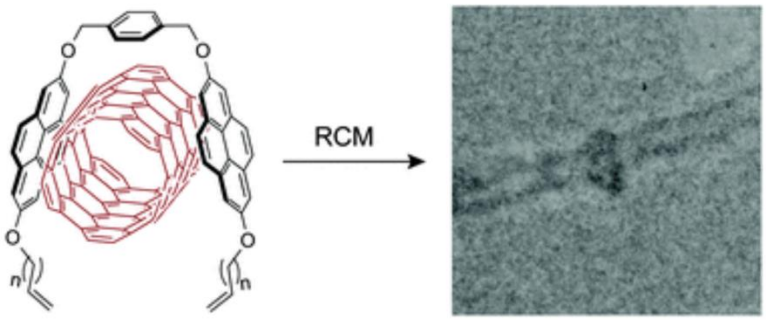

The synthesis of rotaxane-type species composed of pyrene macrocycles and SWNTs as linear components is described. Pyrene-SWNT interactions help template the ring-closing metathesis of U-shape precursors around the nanotubes.

5.1. Introduction

Single-walled carbon nanotubes (SWNTs) are rolled-up graphene sheets, forming tubules of diameters typically around 1 nm. SWNTs can be semiconducting or metallic depending on the direction of the honeycomb pattern along which the graphene sheet is rolled.[1] Metallic SWNTs show ballistic electron transport.[2] Semiconducting SWNTs have structurally inherent band-gaps, and their electrical properties are extremely sensitive to their surroundings, which make them suitable to be used as active materials in field effect

[1] H. Dai. *Acc. Chem. Res.*, **2002,** *35*, 1035-1044.
[2] J. Kong, E. Yenilmez, T. W. Tombler, W. Kim, H. Dai, R. B. Laughlin, L. Liu, C. S. Jayanthi, S. Y. Wu. *Phys. Rev. Lett.*, **2001,** *87*, 106801.

transistors,[3] photovoltaic devices,[4] sensors,[5] etc.[6] Biomedical uses of carbon nanotubes,[7] and nanotube–polymer composites[8] are also particularly active areas of research. Considering all these potential fields of application, significant efforts have been devoted to the chemical modification of SWNTs in order to better exploit their extraordinary properties.[9] A broad variety of strategies have been employed to attach molecular fragments to the surface of SWNTs via covalent[10] and noncovalent methods.[11] Even the interior cavity of SWNTs has been functionalized.[12] Rotaxanes are mechanically interlocked molecules (MIMs) composed of a linear constituent (thread) encapsulated by one or more macrocycles, which cannot escape without the breaking of a covalent bond. Since the macrocycle(s) can move along (shuttling) or around (pirouetting) the thread, rotaxanes have been investigated for the construction of synthetic molecular machines.[13] Besides their dynamic properties, the mechanical link often results in distinct properties, which has spurred interest into mechanically

[3] A. Wurl, S. Goossen, D. Canevet, M. Sallé, E. M. Pérez, N. Martín, C. Klinke. *J. Phys. Chem. C*, **2012,** *116*, 20062-20066.
[4] (a) M. Bernardi, J. Lohrman, P. V. Kumar, A. Kirkeminde, N. Ferralis, J. C. Grossman, S. Ren. *ACS Nano*, **2012,** *6*, 8896-8903; (b) H. Wang, G. I. Koleilat, P. Liu, G. Jiménez-Osés, Y.-C. Lai, M. Vosgueritchian, Y. Fang, S. Park, K. N. Houk, Z. Bao. *ACS Nano*, **2014,** *8*, (3), 2609-2617.
[5] (a) B. Esser, J. M. Schnorr, T. M. Swager. *Angew. Chem., Int. Ed.*, **2012,** *51*, 5752-5756; (b) A. M. Münzer, Z. P. Michael, A. Star. *ACS Nano*, **2013,** *7*, 7448-7453.
[6] For recent reviews, see: (a) J. M. Schnorr, T. M. Swager. *Chem. Mater.*, **2011,** *23*, 646-657; (b) S. Park, M. Vosguerichian, Z. Bao. *Nanoscale*, **2013,** *5*, 1727-1752; (c) C. Wang, K. Takei, T. Takahashi, A. Javey. *Chem. Soc. Rev.*, **2013,** *42*, 2592-2609.
[7] (a) G. Cellot, E. Cilia, S. Cipollone, V. Rancic, A. Sucapane, S. Giordani, L. Gambazzi, H. Markram, M. Grandolfo, D. Scaini, F. Gelain, L. Casalis, M. Prato, M. Giugliano, L. Ballerini. *Nat. Nanotechnol.*, **2009,** *4*, 126-133; (b) M. Adeli, R. Soleyman, Z. Beiranvand, F. Madani. *Chem. Soc. Rev.*, **2013,** *42*, 5231-5256.
[8] (a) J. N. Coleman, U. Khan, W. J. Blau, Y. K. Gun'ko. *Carbon*, **2006,** *44*, 1624-1652; (b) Z. Spitalsky, D. Tasis, K. Papagelis, C. Galiotis. *Prog. Polym. Sci.*, **2010,** *35*, 357-401.
[9] (a) D. Tasis, N. Tagmatarchis, A. Bianco, M. Prato. *Chem. Rev.*, **2006,** *106*, 1105-1136; (b) A. Hirsch. *Angew. Chem. Int. Ed.*, **2002,** *41*, 1853-1859; (c) S. Niyogi, M. A. Hamon, H. Hu, B. Zhao, P. Bhowmik, R. Sen, M. E. Itkis, R. C. Haddon. *Acc. Chem. Res.*, **2002,** *35*, 1105-1113.
[10] (a) C. A. Dyke, J. M. Tour. *J. Phys. Chem. A*, **2004,** *108*, 11151-11159; (b) P. Singh, S. Campidelli, S. Giordani, D. Bonifazi, A. Bianco, M. Prato. *Chem. Soc. Rev.*, **2009,** *38*, 2214-2230.
[11] (a) Y.-L. Zhao, J. F. Stoddart. *Acc. Chem. Res.*, **2009,** *42*, 1161-1171; (b) G. Gavrel, B. Jousselme, A. Filoramo, S. Campidelli. *Top. Curr. Chem.*, **2014,** *348*, 95-126.
[12] (a) A. de Juan, E. M. Perez. *Nanoscale*, **2013,** *5*, 7141-7148; (b) T. Zoberbier, T. W. Chamberlain, J. Biskupek, N. Kuganathan, S. Eyhusen, E. Bichoutskaia, U. Kaiser, A. N. Khlobystov. *J. Am. Chem. Soc.*, **2012,** *134*, 3073-3079.
[13] (a) E. R. Kay, D. A. Leigh, F. Zerbetto. *Angew. Chem. Int. Ed.*, **2007,** *46*, 72-191; (b) D. A. Leigh, E. M. Pérez. *Top. Curr. Chem.*, **2006,** *265*, 185-208.

interlocked materials. Ever since the pioneering work of Jean-Pierre Sauvage,[14] the synthesis of MIMs typically relies on templated methods, in which supramolecular interactions preorganize the submolecular components towards the formation of the mechanical link.[15] We have recently reported the synthesis of rotaxane-type structures in which SWNTs act as threads, introducing the mechanical bond as a new tool for the chemical manipulation of SWNTs.[16] To achieve this, we employed a clipping strategy in which a U-shaped precursor featuring two units of a recognition element for SWNTs was connected through an aromatic spacer, and further decorated with alkene-terminated alkyl spacers of different lengths. In particular, we used p-extended derivatives of tetrathiafulvalene (exTTF), which are known to establish positive noncovalent interactions with SWNTs,[17] to template the ring closing metathesis (RCM) of the U-shaped precursor around the SWNTs, forming mechanically interlocked derivatives of SWNTs (MINTs). MINTs showed remarkable stability, comparable to that of covalently modified nanotubes, while maintaining the native structure of the SWNTs. In order to investigate the scope of the MINT-forming reaction, we decided to test other molecular fragments known to interact with SWNTs. Here, we report that pyrene is a valid recognition motif for the synthesis of MINTs.

[14] (a) C. O. Dietrich-Buchecker, J. P. Sauvage, J. P. Kintzinger. *Tetrahedron Lett.*, **1983,** *24*, 5095-5098; (b) C. O. Dietrich-Buchecker, J. P. Sauvage, J. M. Kern. *J. Am. Chem. Soc.*, **1984,** *106*, 3043-3045.
[15] For reviews, see: (a) J. F. Stoddart. *Chem. Soc. Rev.*, **2009,** *38*, 1802-1820; (b) M. S. Vickers, P. D. Beer. *Chem. Soc. Rev.*, **2007,** *36*, 211-225; (c) C. O. Dietrich-Buchecker, J. P. Sauvage. *Chem. Rev.*, **1987,** *87*, 795-810; (d) For a recent selected example, see D. A. Leigh, R. G. Pritchard, A. J. Stephens. *Nat. Chem.*, **2014,** *6*, 978-982.
[16] A. de Juan, Y. Pouillon, L. Ruiz-González, A. Torres-Pardo, S. Casado, N. Martín, A. Rubio, E. M. Pérez. *Angew. Chem., Int. Ed.*, **2014,** *53*, 5394-5400.
[17] C. Romero-Nieto, R. García, M. Á. Herranz, C. Ehli, M. Ruppert, A. Hirsch, D. M. Guldi, N. Martín. *J. Am. Chem. Soc.*, **2012,** *134*, 9183-9192.

5.2. Results and discussion

The U-shaped precursors of the bispyrene macrocycles (**1–3**, **Figure 1a**) were synthesized by two consecutive Williamson's etherifications from 2,7-dihydroxy-pyrene.[18] Macrocycles **4–6** were synthesized by RCM and show flexible cavities of diameters ca. 1.4–1.8 nm as calculated by molecular mechanics (see the experimental section for synthetic details). We expected the SWNTs to template the macrocyclization of the U-shapes around them through pyrene–SWNT supramolecular interactions (**Figure 1b**). Accordingly, we tested (6,5) and (7,6)-enriched SWNTs as threads, which show diameters of 0.75 nm and 0.88 nm, respectively, and are a good fit for our macrocycles (**Figure 1c**). The SWNTs (5 mg) were suspended in tetrachloroethane (TCE, 5 mL) through sonication and mixed with the corresponding U-shapes **1–3** (2.5 mg) and Grubb's second-generation catalyst at room temperature for 72 h. After this period, samples were filtered through a polytetrafluoroethylene membrane with a pore size of 0.2 mm. The solid was resuspended in CH_2Cl_2 with sonication, and washed profusely with CH_2Cl_2 to remove any unreacted linear precursors, non-interlocked macrocycles, weakly adsorbed pyrene materials, remaining catalyst, etc. This purification stage was repeated three times, after which the samples were dried and subjected to thermogravimetric analysis (TGA) to quantify the degree of functionalization. The results are summarized in **Table 1** (see the experimental section for all TGAs).

[18] A. G. Crawford, Z. Liu, I. A. I. Mkhalid, M.-H. Thibault, N. Schwarz, G. Alcaraz, A. Steffen, J. C. Collings, A. S. Batsanov, J. A. K. Howard, T. B. Marder. *Chem. - Eur. J.*, **2012,** *18*, 5022-5035.

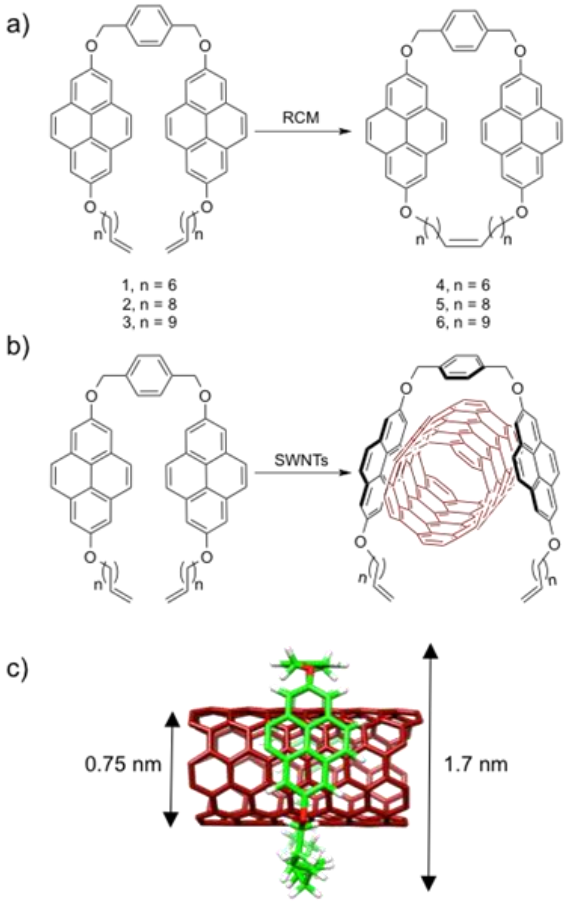

Figure 1. a) Chemical structures of U-shapes **1-3** and macrocycles **4-6**. b) Template effect in the macrocyclization of the U-shapes around SWNTs through pyrene-SWNT interactions. c) Energy-minimized (MM+) model of MINT-(6,5)-**6** showing key distances.

Table 1 Functionalization of the MINT and control samples from TGA.[a]

U-shape	SWNT	MINT	Weight loss (%)[b]
1	(6,5)	MINT-(6,5)-**4**	24 (21)
1	(7,6)	MINT-(7,6)-**4**	25 (21)
2	(6,5)	MINT-(6,5)-**5**	26 (22)
2	(7,6)	MINT-(7,6)-**5**	27 (23)
3	(6,5)	MINT-(6,5)-**6**	27 (25)
3	(7,6)	MINT-(7,6)-**6**	28 (25)

[a] TGAs were run in air at a heating rate of 10 ºC/min. [b] All reactions were run twice, with reproducible results. Numbers in brackets were obtained after refluxing each sample in TCE, as described in the main text.

All samples show a significant weight loss (24–28%) at around 360 ºC corresponding to the pyrene material. This degree of functionalization is similar to that found for exTTF-based MINTs.[16] Although the changes are quantitatively small, for a given type of SWNT the degree of functionalization increases consistently with the size of the macrocycle cavity, for instance MINT-(6,5)-**4** shows a 24% loading compared to 27% for MINT-(6,5)-**6**. The comparison between the types of nanotubes shows that the (7,6)-SWNTs bear more macrocycle loading. Considering that both chiralities fit within the macrocycles, this tendency is most likely due to a more efficient U-shape-SWNT interaction, as it is known that the pyrene–SWNT interaction increases with the increasing SWNT diameter.[19] We also carried out control experiments in which we mixed

[19] (a) S. G. Stepanian, V. A. Karachevtsev, A. Y. Glamazda, U. Dettlaff-Weglikowska, L. Adamowicz. *Mol. Phys.*, **2003,** *101*, 2609-2614; (b) G. Modugno, Z. Syrgiannis, A. Bonasera, M. Carraro, G. Giancane, L. Valli, M. Bonchio, M. Prato. *Chem. Commun.*, **2014,** *50*, 4881-4883.

linear precursor **3** or the corresponding macrocycle **6** with (7,6) SWNTs without Grubb's catalyst, under otherwise identical conditions to the MINT-forming reaction. These samples showed a functionalization of 7 and 5%, respectively, proving that physisorbed **3** and **6** are only a minor part of the pyrene material in the MINT-**6** samples. We have previously observed that MINTs show remarkable stability, comparable to that of covalently modified nanotubes, while maintaining the native covalent structure of the SWNTs.[16] To test the stability of functionalization and remove any remaining noninterlocked pyrene material that might have survived the initial purification process, we subjected all samples to 30 min of reflux in tetrachloroethane (TCE, bp = 147 ºC), followed by a thorough rinse with CH_2Cl_2. TGA of the resulting samples showed a very small decrease in the degree of functionalization (< 4%, numbers in brackets in **Table 1**), confirming the extreme stability of MINTs, and that the supramolecular functionalization of the nanotubes by linear oligomers formed in situ under the RCM conditions is minoritary.[16] Raman spectroscopy (λ_{exc} = 532, 633, and 785 nm) reveals very small changes in the spectra with respect to pristine SWNTs, as expected for the noncovalent functionalization of SWNTs with pyrene-based fragments.[20] In particular, we observed no significant increase in the I_D/I_G ratio and no decrease in the RBM intensity, which confirmed that there is no covalent modification of the SWNTs.[21] We also observed a small shift of the G+ band and a decrease in the relative intensity of the G band.[19a] These changes are summarised in **Table 2** and illustrated by **Figure 2a**, which shows the Raman spectra of the (7,6)-SWNT and MINT-(7,6)-**6** under 785 nm excitation. In this case, the I_D/I_G ratio is 0.05 for the (7,6) SWNTs and 0.06 for MINT-(7,6)-6, while the G^+ band is shifted from 1578 to 1580 cm^{-1} (see the experimental section for all Raman spectra). In the absorption spectra (D_2O, 1% sodium dodecyl sulphate, 298 K, **Figure 2b**), the UV region is dominated by the nanotube

[20] Y. Tomonari, H. Murakami, N. Nakashima. *Chem. - Eur. J.*, **2006,** *12*, 4027-4034.
[21] C. Fantini, M. L. Usrey, M. S. Strano. *J. Phys. Chem. C*, **2007,** *111*, 17941-17946.

absorption, and the characteristic absorption of pyrenes in the 300–350 nm range is not distinguishable, save for an increase in the relative absorption in this region.‡ The S_{22} and S_{11} transitions of the (6,5)-SWNTs are prominent in the vis-NIR, appearing at λ_{max} = 572 and 991 nm for the pristine nanotubes. As expected for an intimate pyrene–SWNT supramolecular interaction, both transitions are red shifted to λ_{max} = 577 and 1006 nm upon derivatization to form MINT-(6,5)-**6**. The S_{22} transition suffers a quantitatively smaller shift due to its higher energy.[22]

Table 2 Selected Raman data for the MINT-**6** samples.[a]

	532 nm		633 nm		785 nm	
Sample	I_D/I_G	G^+	I_D/I_G	G^+	I_D/I_G	G^+
(6,5)	0.06	1572	0.08	1578	0.07	1577
MINT-(6,5)-**6**	0.07	1573	0.09	1579	0.08	1583
(7,6)	0.06	1568	0.07	1584	0.05	1578
MINT-(7,6)-**6**	0.08	1568	0.07	1586	0.06	1580

[a] Average of at least three different Raman spectra. G^+ Raman shifts in cm^{-1}.

‡ The extinction coefficient for pyrenes in an aqueous environment varies between 21000 and 34000 $M^{-1}\cdot cm^{-1}$,(see: H. Siu, J. Duhamel. *J. Phys. Chem. B*, **2008**, *112*, 15301–15312) while it is 4400 M^{-1} cm^{-1} per carbon atom for the S_{11} transition of (6,5)-SWNTs, (see: F. Schöppler, C. Mann, T. C. Hain, F. M. Neubauer, G. Privitera, F. Bonaccorso, D. Chu, A. C. Ferrari, T. Hertel. *J. Phys. Chem. C*, **2011**, *115*, 14682–14686) which shows half the absorption of the 300–400 nm region. At 26% functionalization, we estimate approximately one unit of 6 every 200 SWNT carbon atoms, so the absorption of the SWNTs should be ca. 10 times larger than that of pyrenes.

[22] M. S. Strano, C. B. Huffman, V. C. Moore, M. J. O'Connell, E. H. Haroz, J. Hubbard, M. Miller, K. Rialon, C. Kittrell, S. Ramesh, R. H. Hauge, R. E. Smalley. *J. Phys. Chem. B*, **2003,** *107*, 6979-6985.

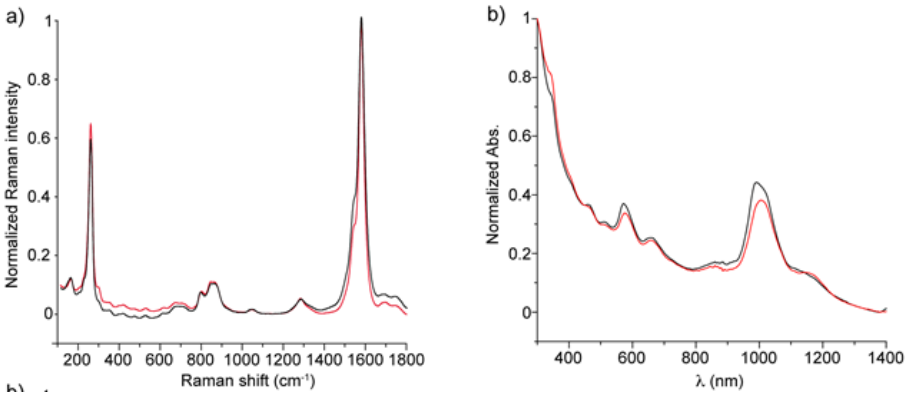

Figure 2. a) Raman spectra (λ_{exc} = 785 nm) of (7,6)-SWNTs (black) and MINT-(7,6)-**6** (red). b) UV-vis-NIR (D_2O, 1% sodium dodecyl sulphate, 298 K) of (6,5)-SWNTs and MINT-(6,5)-**6**.

The photoluminescence excitation (PLE) maps of the (6,5)-enriched SWNTs show an intense peak at λ_{exc} = 565 nm, λ_{em} = 975 nm characteristic of the (6,5) chirality, and residual peaks at λ_{exc} = 643 nm, λ_{em} = 1021 nm and λ_{exc} = 665, λ_{em} = 948 nm, corresponding to (7,5) and (8,3) chiralities. In MINT-(6,5)-**6**, the luminescence of the (6,5) nanotubes is quenched to approximately 40% and suffers a bathochromic shift to λ_{em} = 986 nm, compared to a sample of pristine (6,5) SWNTs with identical optical density (see the experimental section for details). The TGA data, control experiments, and spectroscopic characterization are therefore consistent with the formation of MINTs.[16] High-resolution transmission electron microscopy (HR-TEM) has proven to be a valuable tool to image organic molecules in the vicinity of carbon nanotubes,[23] and we have shown that this is also the case for MINTs.[16] Scrutiny by HR-TEM of samples of MINT-(6,5)-**6** dropcasted from a TCE suspension shows mostly bundled nanotubes with heavily functionalized sidewalls, in agreement with the

[23] E. Nakamura. *Angew. Chem. Int. Ed.*, **2013,** *52*, 236-252.

TGA data. A representative image is shown in **Figure 3a**, where two bundles and an isolated SWNT are distinguishable.

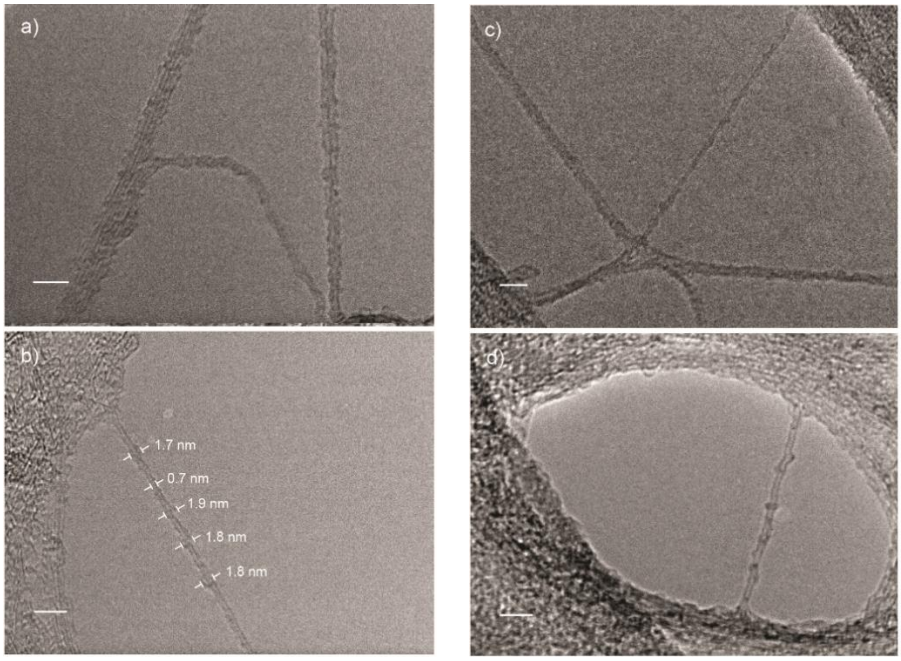

Figure 3. Representative HR-TEM images of MINT-(6,5)-**6**. All scale bars are 5 nm.

Both the bundles and the single nanotube show abundant organic functionalization. For the free nanotube, a diameter of 0.8 nm was measured at its leftmost extreme, where it shows no addends; the derivatized part has a diameter of ca. 2 nm, in good agreement with multiple units of **6**, the first of which is sufficiently detached to be distinguishable. In several instances the nanotubes showed single circular objects with a diameter < 2 nm around them. For example, **Figure 3b** shows a SWNT with a diameter of 0.7 nm in which up to four of these objects are visible. The size and shape of the addends is perfectly consistent with the formation of **6** around the SWNT (**Figure 1c**). **Figure 3c** and **d** further illustrate the formation of rotaxane-type species. In **Figure 3c** a long

SWNT with a diameter of 0.7 nm shows two single objects of 1.8 and 1.7 nm, while in **Figure 3d** we measured diameters of 0.8 and 1.9 nm for the nanotube and the macrocycle, respectively. The role of the nanotube bundles as stoppers is also evident from the micrographs. Note that the discontinuity between the walls of the SWNT and the macrocycles is evident, particularly in **Figure 3b** and **d**. Together with their consistent size of 1.7–1.9 nm this rules out the possibility of them being SWNT imperfections.

4.3. Conclusion

In conclusion, we have proven that pyrene templates the RCM of macrocycles around SWNTs to form MINTs. The results disclosed here suggest that our clipping strategy towards the synthesis of MINTs might be applicable to any molecular fragment that shows sufficiently strong noncovalent interactions with SWNTs, and can be elaborated to synthesize appropriate U-shaped precursors. This broad scope, together with the unique features of MIMs[24] and the interest in the encapsulation of carbon nanomaterials,[25] make the formation of MINTs a particularly attractive method for the noncovalent functionalization of SWNTs.

5.4. Experimental section

General. Reagents were used as purchased. All air-sensitive reactions were carried out under argon atmosphere. Flash chromatography was performed using silica gel (Merck, Kieselgel 60, 230-240 mesh, or Scharlau 60, 230-240 mesh).

[24] (a) E. A. Neal, S. M. Goldup. *Chem. Commun.*, **2014,** *50*, 5128-5142; (b) J. F. Stoddart. *Angew. Chem. Int. Ed.*, **2014,** *53*, 11102-11104.
[25] (a) S. Sato, T. Yamasaki, H. Isobe. *Proc. Natl. Acad. Sci.*, **2014,** *111*, 8374-8379; (b) D. Canevet, E. M. Pérez, N. Martín. *Angew. Chem. Int. Ed.*, **2011,** *50*, 9248-9259; (c) H. Isobe, S. Hitosugi, T. Yamasaki, R. Iizuka. *Chem. Sci.*, **2013,** *4*, 1293-1297; (d) D. Canevet, M. Gallego, H. Isla, A. de Juan, E. M. Pérez, N. Martín. *J. Am. Chem. Soc.*, **2011,** *133*, 3184-3190.

Analytical thin layer chromatographies (TLC) were performed using aluminium-coated Merck Kieselgel 60 F254 plates. NMR spectra were recorded on a BrukerAvance 300 (^{1}H: 300 MHz; ^{13}C: 75 MHz), a BrukerAvance 500 (^{1}H: 500 MHz; ^{13}C: 125 MHz) spectrometers at 298 K, unless otherwise stated, using partially deuterated solvents as internal standards. Coupling constants (J) are denoted in Hz and chemical shifts (δ) in ppm. Multiplicities are denoted as follows: s = singlet, d = doublet, t = triplet, m = multiplet, b = broad. Matrix-assisted Laser desorption ionization (coupled to a Time-Of-Flight analyzer) experiments (MALDI-TOF) were recorded on a HP1100MSD spectrometer and a Bruker REFLEX spectrometer, respectively. Thermogravimetric analyses (TGA) were performed using a TA Instruments TGAQ500 with a ramp of 10 °C/min under air from 100 to 1000 °C. UV-vis-NIR spectrums were performed using a Shimadzu UV-VIS-NIR Spectrophotometer UV-3600. Photoluminescence excitation intensity maps (PLE) were obtained with NanoLog 4 HORIBA. Raman spectra were acquired with a Bruker Senterra confocal Raman microscopy instrument, equipped with 532, 633 and 785 nm lasers. Transmission electron microscopy (TEM) images were obtained with JEOL-JEM 2100F (2.5 Å resolution) instrument.

General Scheme of Synthesis of Compounds

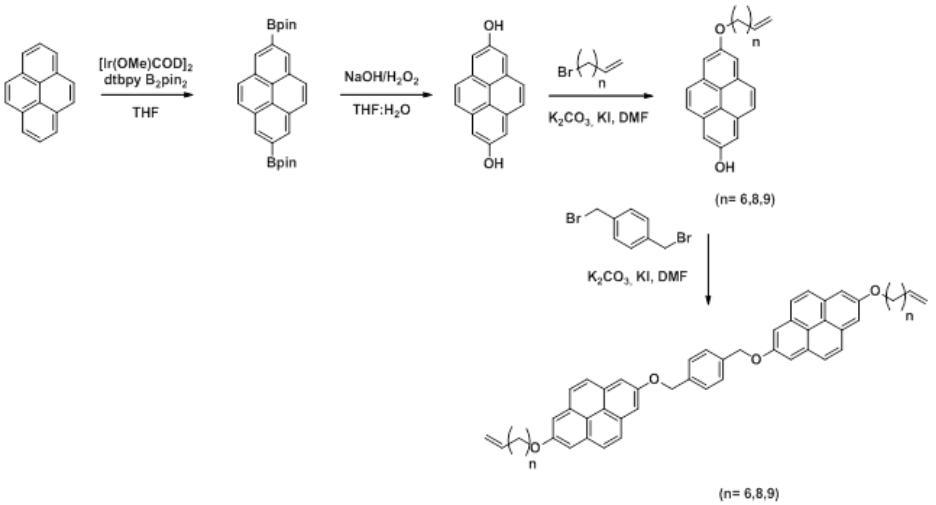

2,7-dihydroxypyrene was synthetized as described in *Chem. - Eur. J.* **2012**, *18*, 5022 – 5035.

General procedure of synthesis of monoalkylated compounds.

2,7-dihydroxypyrene 500 mg (2.14 mmol) was dissolved in 20 mL of dry DMF. Then, 300 mg (2.14 mmol) of dry K_2CO_3, 12.5 mmol) of bromo alkene , and a catalytic amount of KI were added and the mixture heated to reflux for 8 h. The crude reaction was poured into ice-cold 1 M aqueous HCl, and filtrated. The solid was redissolved in CH_2Cl_2 and washed with water (2x), the organic fraction was dried over $MgSO_4$, the solvent evaporated, and the resulting product subjected to column chromatography (CH_2Cl_2) to obtain the pure product as a light brown solid in 16-18% yield.

General procedure of synthesis of lineal receptors.

135 mg (1.04 mmol) of dry K_2CO_3, 56 mg (0.21 mmol) of α−α´ dibromo-p-xylene, and a catalytic amount of potassium iodide were added to a solution of

200 mg (0.52 mmol) of the monoalkylated dihydroxypyrene in 15 mL of dry N,N-dimethylformamide. The solution was heated to 80 ºC for 4 h. The crude reaction was poured into ice-cold 1 M aqueous HCl, and filtrated. The solid was redissolved in CH_2Cl_2 and washed with water (2x), the organic fraction was dried over $MgSO_4$, the solvent evaporated, and the resulting product subjected to column chromatography (CH_2Cl_2) to obtain the pure product as a light brown solid in 58-61% yield.

7-(oct-7-en-1-yloxy)pyren-2-ol

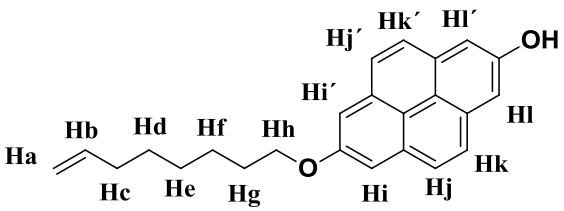

^{1}H RMN ($CDCl_3$, 300 MHz) δ 7.95 (q, *J* = 9.0 Hz, 4H, Hj+j´+k+k´), 7.71 (s, 2H, Hi+i´), 7.62 (s, 2H, Hl+l´), 5.92 – 5.79 (m, 1H, Hb), 5.27 (s,1H, OH), 5.07 – 4.94 (m, 2H, Ha), 4.26 (t, J = 6.5 Hz, 2H, Hh), 2.12 – 2.05 (m, 2H, Hc), 1.99 – 1.90 (m, 2H, Hg), 1.61 – 1.29 (m, 6H, Hd+e+f). ^{13}C NMR ($CDCl_3$, 75 MHz) δ 156.7, 153.0, 139.0, 131.8, 131.5, 127.7, 127.1, 120.1, 120.0, 114.3, 111.8, 111.5, 68.6, 33.7, 29.4, 28.9, 28.9, 26.0. MS m/z calculated for $C_{24}H_{24}O_2$ 344.1, found MALDI 344.2.

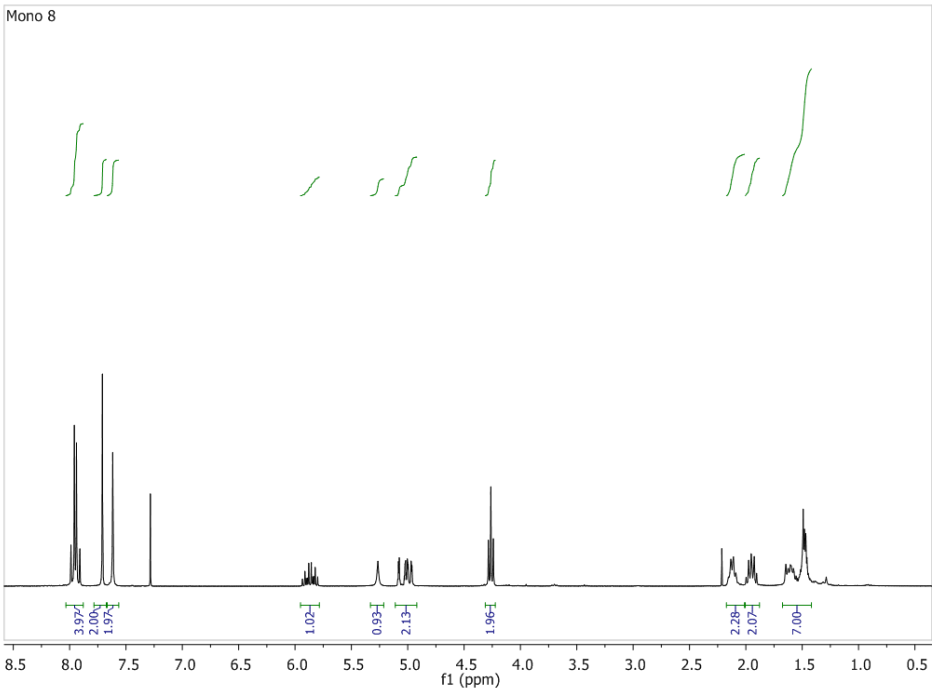
Mono 8
3.97
2.00
1.97
1.02
0.93
2.13
1.96
2.28
2.07
7.00
8.5 8.0 7.5 7.0 6.5 6.0 5.5 5.0 4.5 4.0 3.5 3.0 2.5 2.0 1.5 1.0 0.5
f1 (ppm)

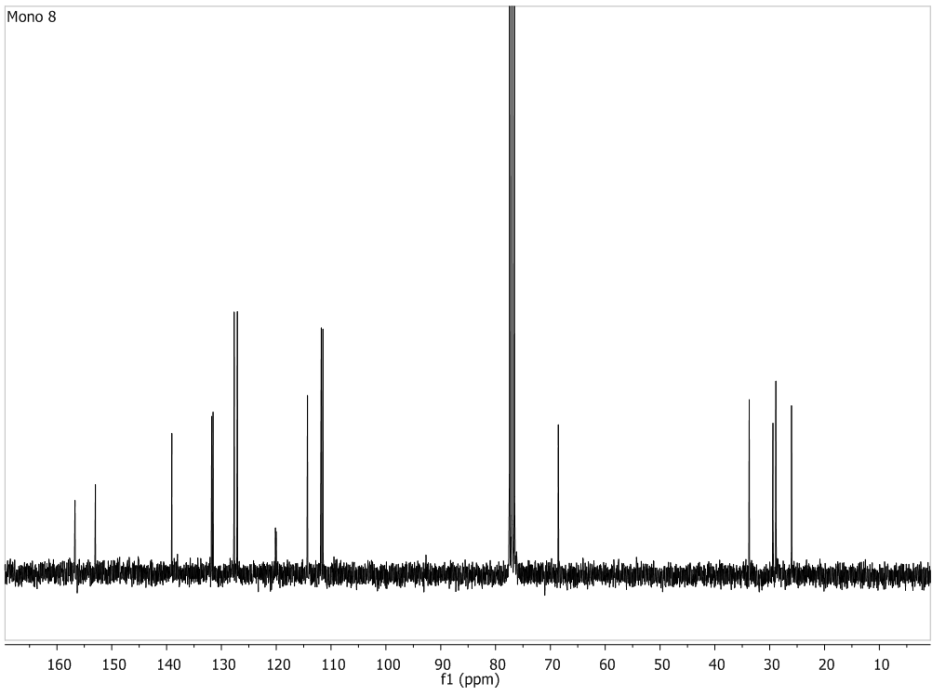
Mono 8
160 150 140 130 120 110 100 90 80 70 60 50 40 30 20 10
f1 (ppm)

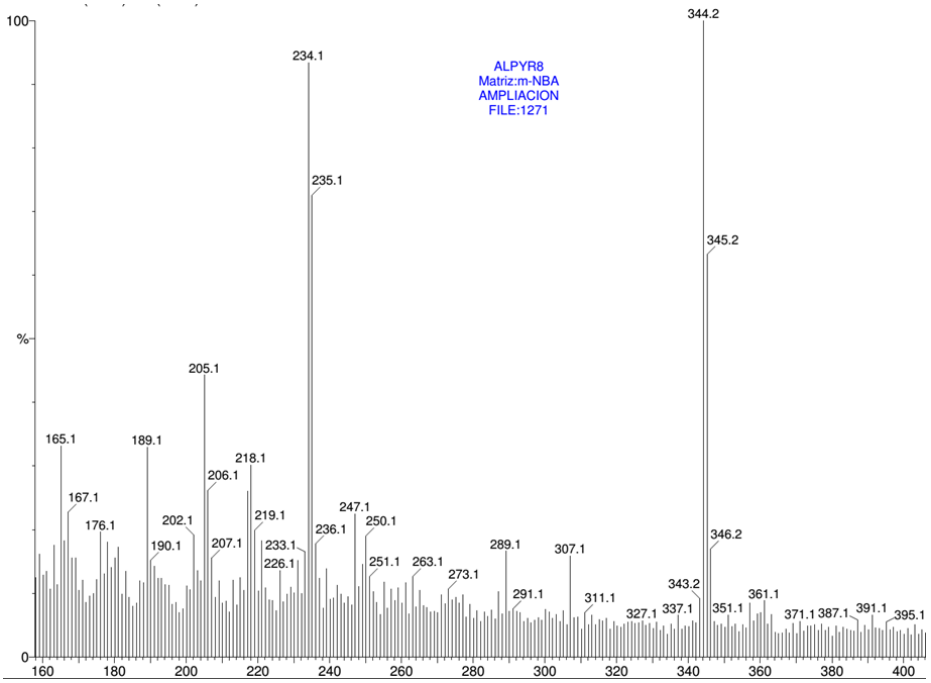

7-(dec-9-en-1-yloxy)pyren-2-ol

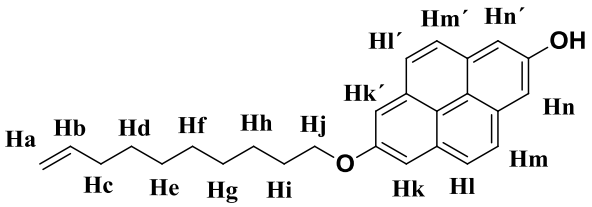

^{1}H RMN ($CDCl_3$, 300 MHz) δ 7.95 (q, *J* = 9.0 Hz, 4H, Hl+l´+m+m´), 7.71 (s, 2H, Hk+k´), 7.61 (s, 2H, Hn+n´), 5.92 – 5.78 (m, 1H, Hb), 5.32 (s,1H, OH), 5.06 – 4.95 (m, 2H, Ha), 4.26 (t, J = 6.5 Hz, 2H, Hj), 2.10 – 2.07 (m, 2H, Hc), 1.97 – 1.92 (m, 2H, Hi), 1.58 – 1.38 (m, 10H, Hd+e+f+g+h) ppm. ^{13}C NMR ($CDCl_3$, 126 MHz) δ: 156.7, 153.0, 139.2, 131.8, 131.5, 127.7, 127.1, 120.16, 120.0, 114.2, 111.8, 111.5, 68.6, 33.8, 29.5, 29.4, 29.1, 28.9, 26.2 ppm. MS m/z calculated for $C_{26}H_{28}O_2$ 372.1, found MALDI 372.3.

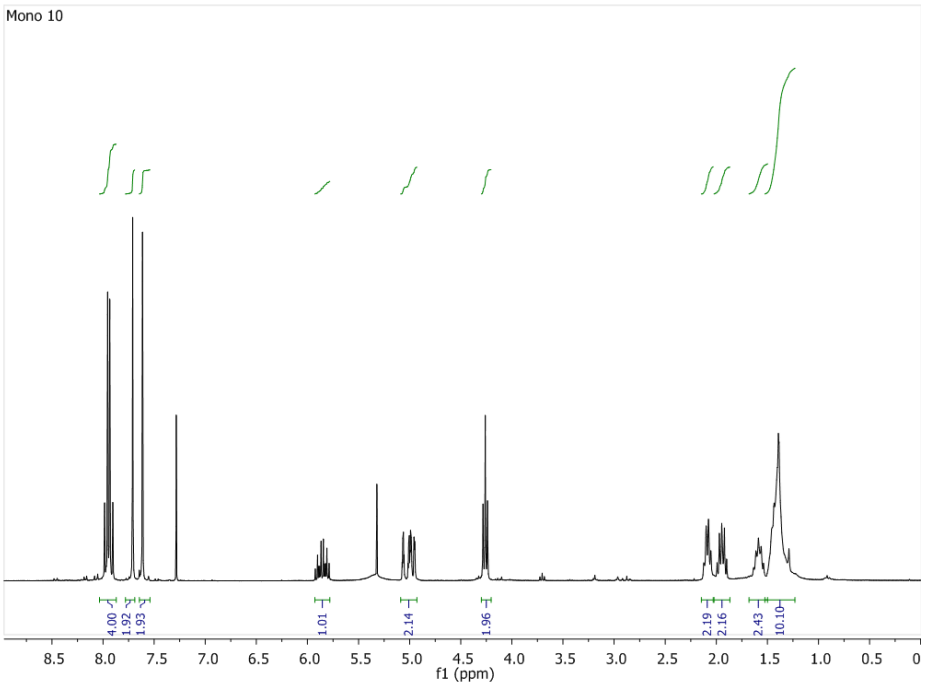
Mono 10
4.00
1.92
1.93
1.01
2.14
1.96
2.19
2.16
2.43
10.10
8.5 8.0 7.5 7.0 6.5 6.0 5.5 5.0 4.5 4.0 3.5 3.0 2.5 2.0 1.5 1.0 0.5 0
f1 (ppm)

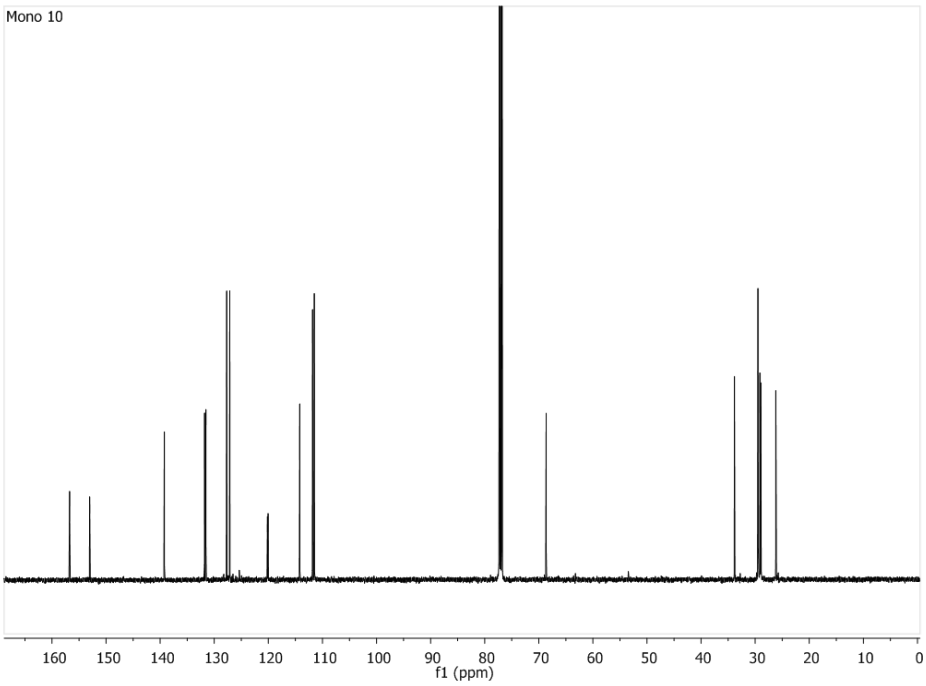
Mono 10
160 150 140 130 120 110 100 90 80 70 60 50 40 30 20 10 0
f1 (ppm)

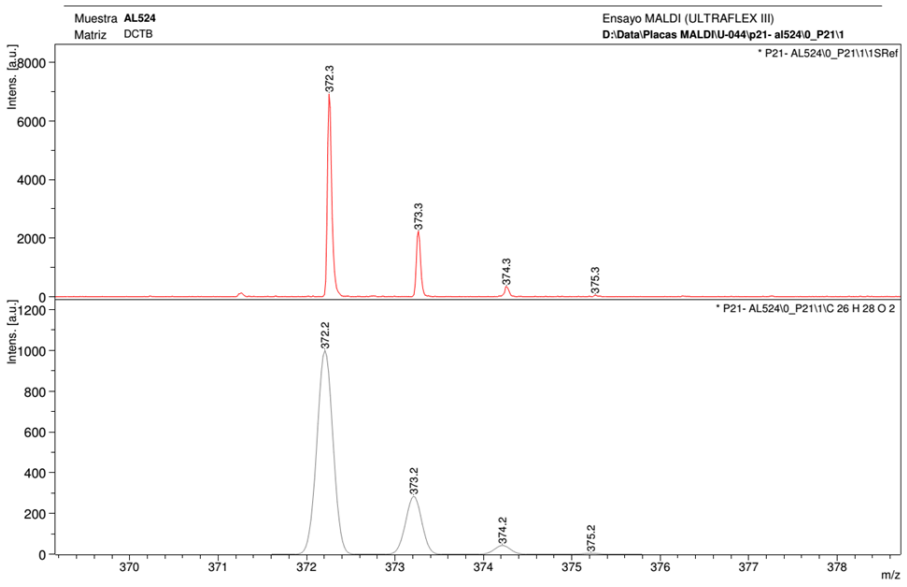

7-(undec-10-en-1-yloxy)pyren-2-ol

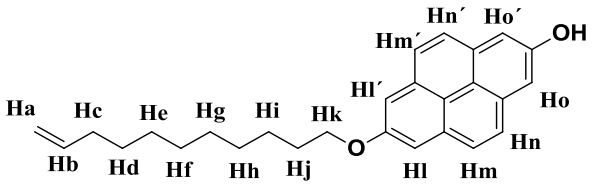

^{1}H RMN ($CDCl_3$, 300 MHz) δ 7.95 (q, *J* = 9.0 Hz, 4H, Hm+m´+n+n´), 7.70 (s, 2H, Hl+l´), 7.61 (s, 2H, Ho+o´), 5.92 – 5.79 (m, 1H, Hb), 5.32 (s,1H, OH), 5.06 – 4.95 (m, 2H, Ha), 4.26 (t, J = 6.5 Hz, 2H, Hk), 2.12 – 2.05 (m, 2H, Hc), 1.99 – 1.90 (m, 2H, Hj), 1.61 – 1.29 (m, 12H, Hd+e+f+g+h+i) ppm. ^{13}C NMR ($CDCl_3$, 126 MHz) δ: 156.7, 153.0, 139.2, 131.8, 131.5, 127.7, 127.1, 120.1, 120.0, 114.2, 111.8, 111.5, 68.6, 33.8, 29.6, 29.5, 29.2, 28.9, 26.2 ppm. MS m/z calculated for $C_{28}H_{30}O_2$ 386.2, found MALDI 386.3.

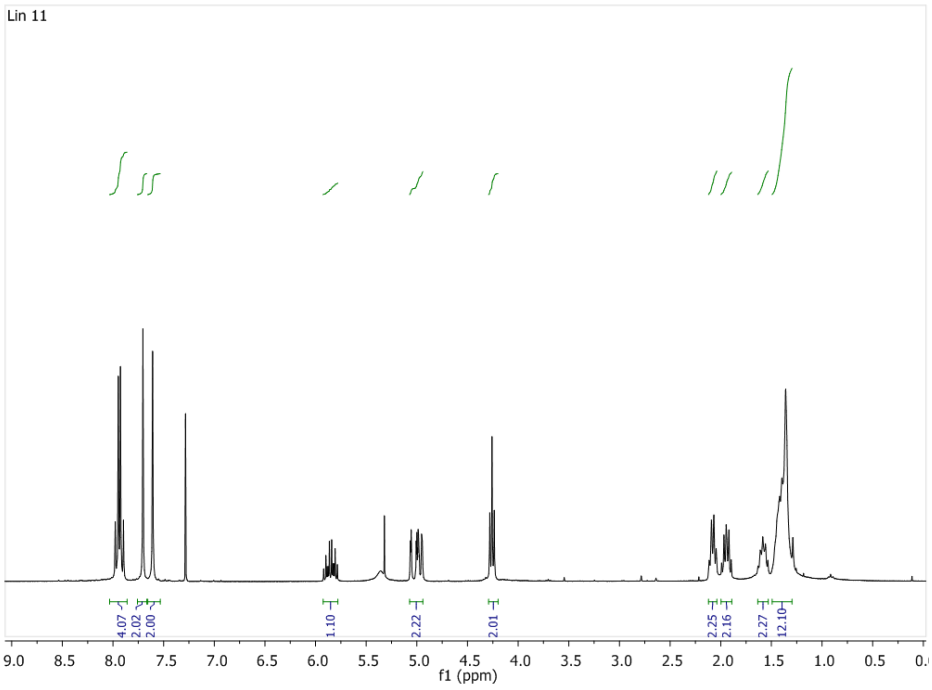
Lin 11
4.07
2.02
2.00
1.10
2.22
2.01
2.25
2.16
2.27
12.10
9.0 8.5 8.0 7.5 7.0 6.5 6.0 5.5 5.0 4.5 4.0 3.5 3.0 2.5 2.0 1.5 1.0 0.5
f1 (ppm)

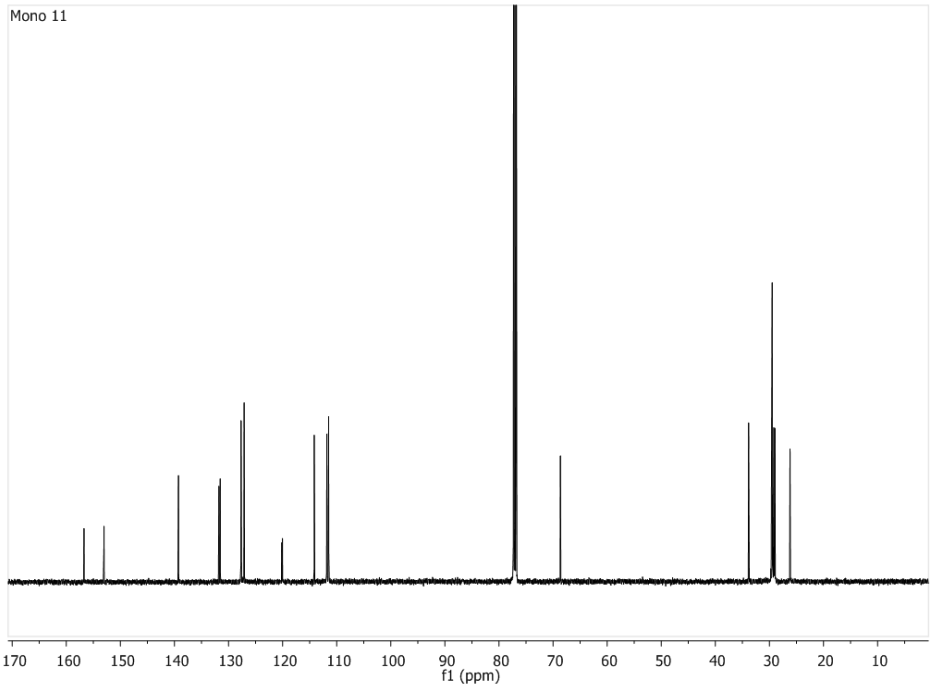
Mono 11
170 160 150 140 130 120 110 100 90 80 70 60 50 40 30 20 10
f1 (ppm)

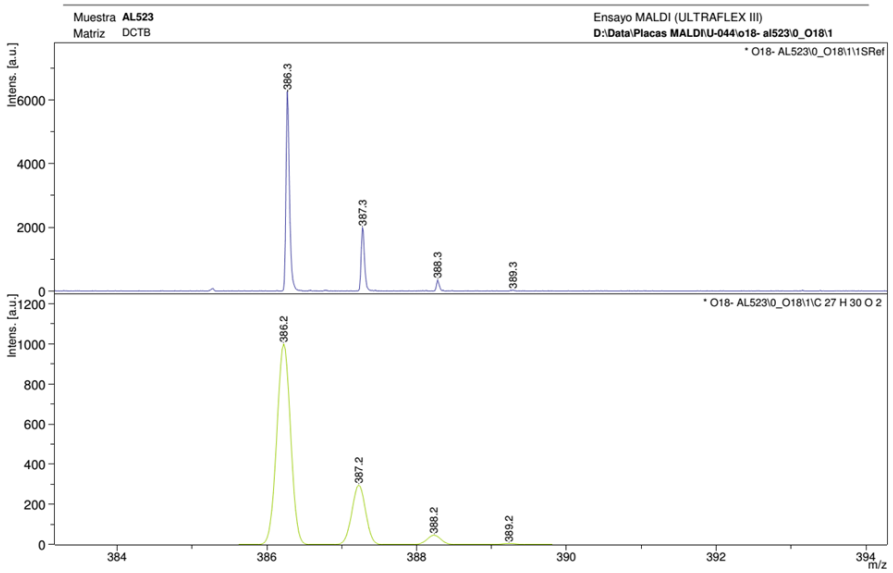

1,4-bis(((7-(oct-7-en-1-yloxy)pyren-2-yl)oxy)methyl)benzene

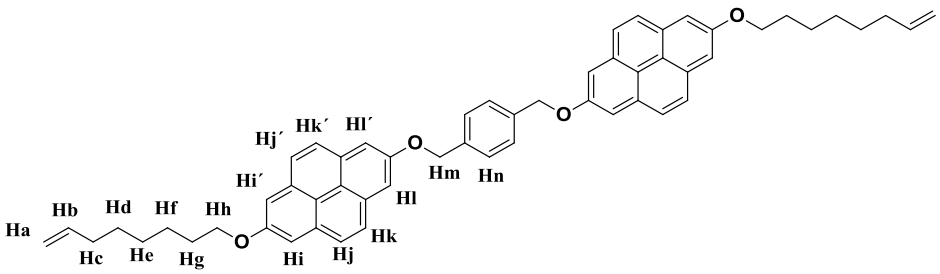

^{1}H RMN ($CDCl_3$, 300 MHz) δ: 7.97 (s, 8H, Hj+j´+k+k´), 7.79 (s, 4H, Hi+i´), 7.71 (s, 4H, Hl+l´), 7.63 (s, 4H, Hn), 5.93 – 5.80 (m, 2H, Ha), 5.40 (s, 4H, Hm), 5.08 – 4.96 (m, 4H, Hb), 4.27 (t, J = 6.5Hz, 4H, Hh), 2.13 – 2.09 (m, 4H, Hc), 2.00 – 1.91 (m, 4H, Hg), 1.63 – 1.58 (m, 4H, Hf), 1.49 – 1.46 (m, 8H, Hd+e) ppm. ^{13}C NMR ($CDCl_3$, 75 MHz) δ: 156.8, 156.3, 139.0, 136.9, 131.6, 131.6, 127.8, 127.5, 127.4, 120.3, 120.0, 114.3, 111.6, 111.4, 77.2, 70.3, 68.5, 33.7,

29.7, 29.4, 28.9, 28.9, 26.0 ppm. MS m/z calculated for $C_{56}H_{54}O_4$ 790.4, found MALDI 790.4.

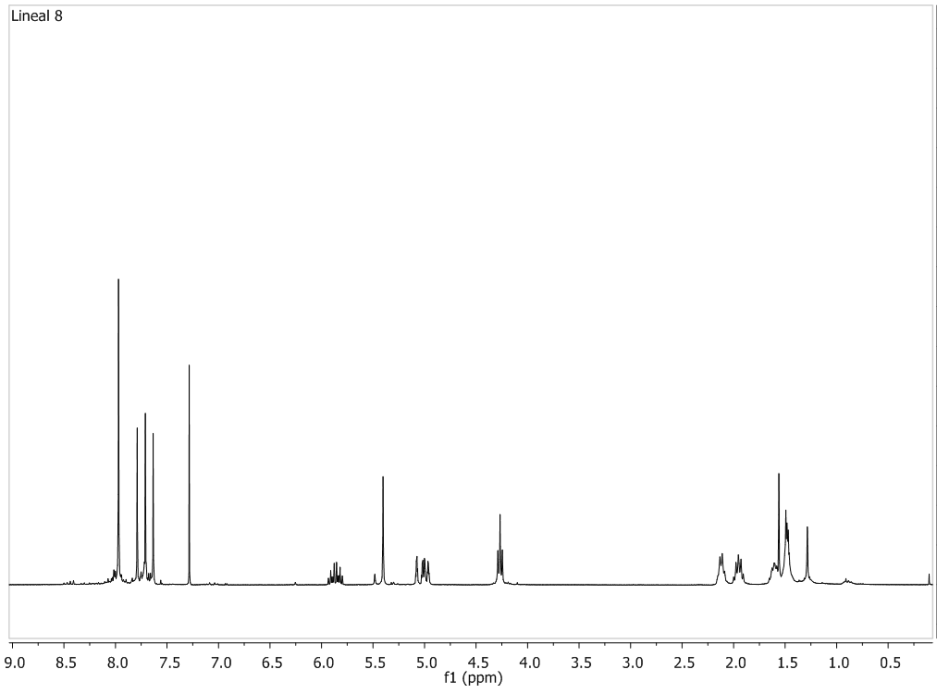

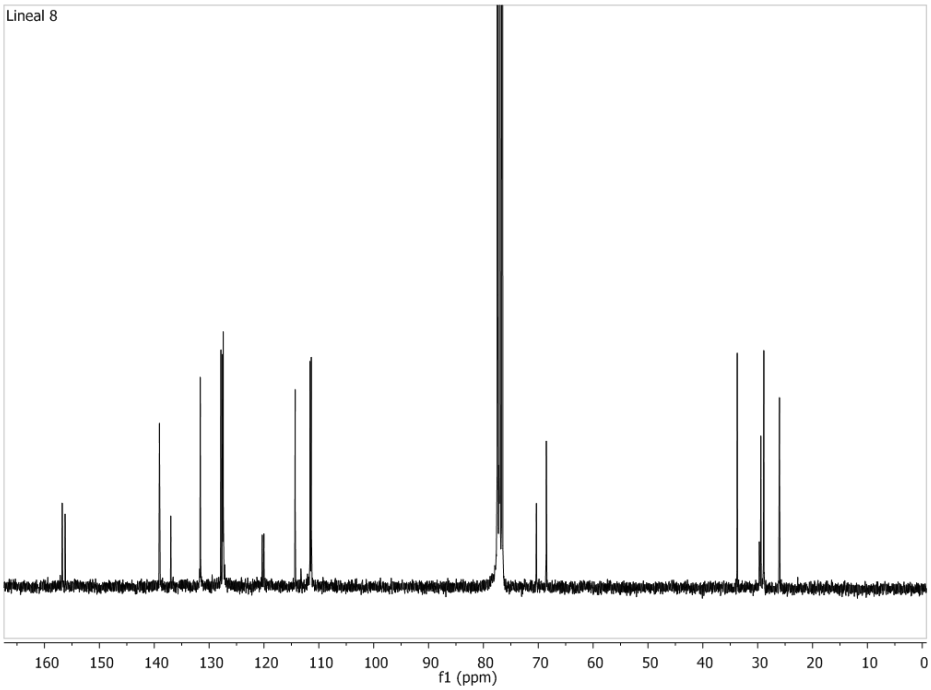
Lineal 8
160 150 140 130 120 110 100 90 80 70 60 50 40 30 20 10 0
f1 (ppm)

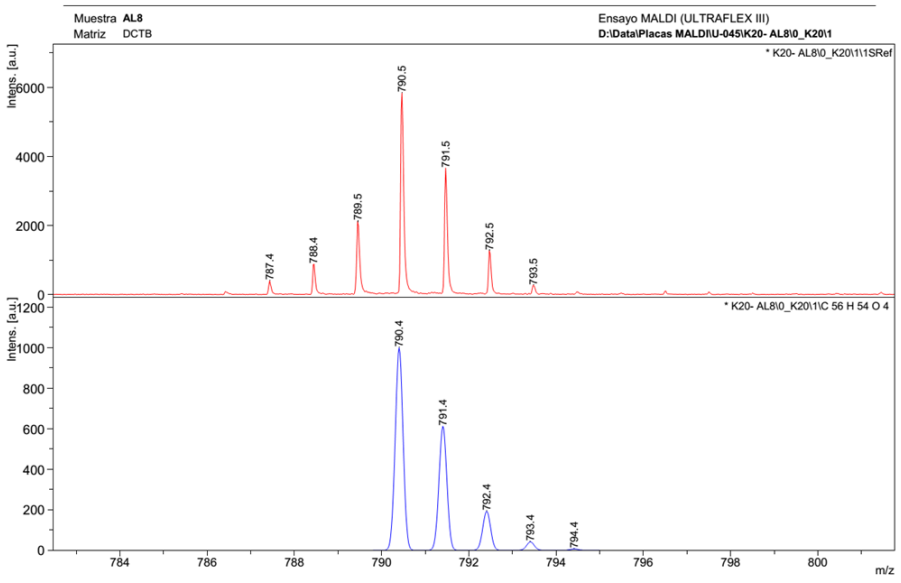
Muestra AL8
Matriz DCTB
Ensayo MALDI (ULTRAFLEX III)
D:\Data\Placas MALDI\U-045\K20- AL8\0_K20\1
* K20- AL8\0_K20\1\1SRef
Intens. [a.u.]
787.4
788.4
789.5
790.5
791.5
792.5
793.5
* K20- AL8\0_K20\1\C 56 H 54 O 4
790.4
791.4
792.4
793.4
794.4
784 786 788 790 792 794 796 798 800
m/z

1,4-bis(((7-(dec-9-en-1-yloxy)pyren-2-yl)oxy)methyl)benzene

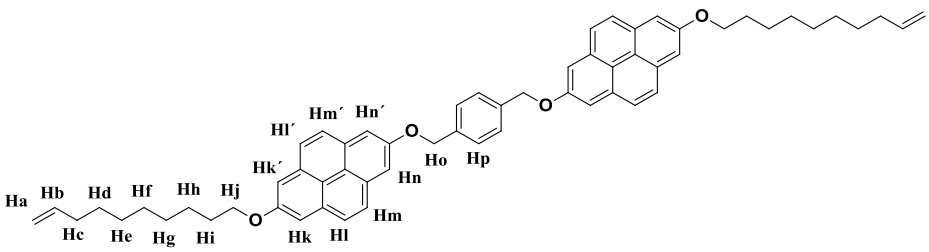

^{1}H RMN ($CDCl_3$, 300 MHz) δ 7.97 (s, 8H, Hl+l´+m+m´), 7.79 (s, 4H, Hk+k´), 7.71 (s, 4H, Hn+n´), 7.63 (s, 4H, Hp), 5.92 – 5.78 (m, 2H, Ha), 5.40 (s, 4H, Ho), 5.06 – 4.94 (m, 4H, Hb), 4.26 (t, J = 6.5Hz, 4H, Hj), 2.11 – 2.05 (m, 4H, Hc), 1.99 – 1.90 (m, 4H, Hi), 1.62 – 1.54 (m, 4H, Hh), 1.45 – 1.39 (m, 16H, Hd+e+f+g) ppm.^{13}C NMR ($CDCl_3$, 126 MHz) δ: 156.8, 156.3, 139.2, 137.0, 131.6, 131.6, 127.9, 127.6, 127.4, 120.3, 120.0, 114.2, 111.6, 111.4, 77.2, 70.3, 68.6, 33.8, 30.9, 29.5, 29.4, 29.1, 28.9, 26.2 ppm. MS m/z calculated for C60H62O4 846.5, found MALDI 846.5.

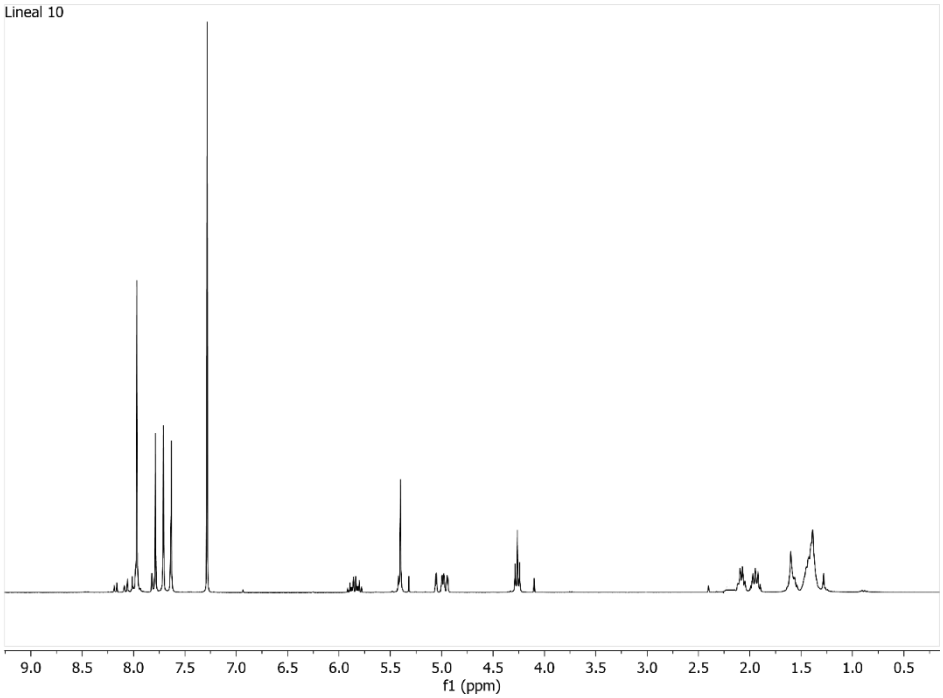
Lineal 10
9.0 8.5 8.0 7.5 7.0 6.5 6.0 5.5 5.0 4.5 4.0 3.5 3.0 2.5 2.0 1.5 1.0 0.5
f1 (ppm)

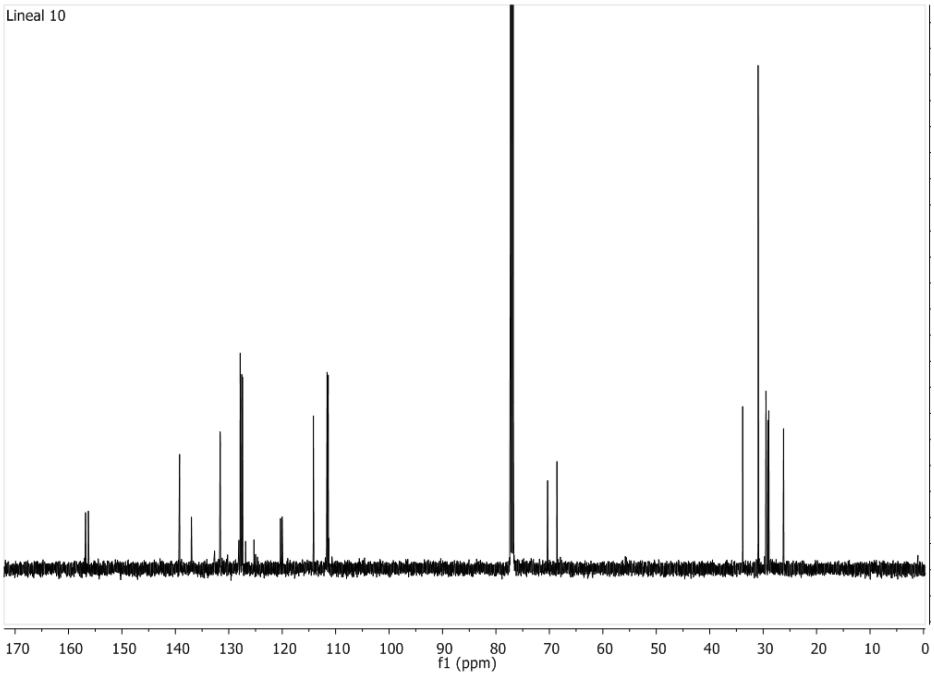
Lineal 10
170 160 150 140 130 120 110 100 90 80 70 60 50 40 30 20 10 0
f1 (ppm)

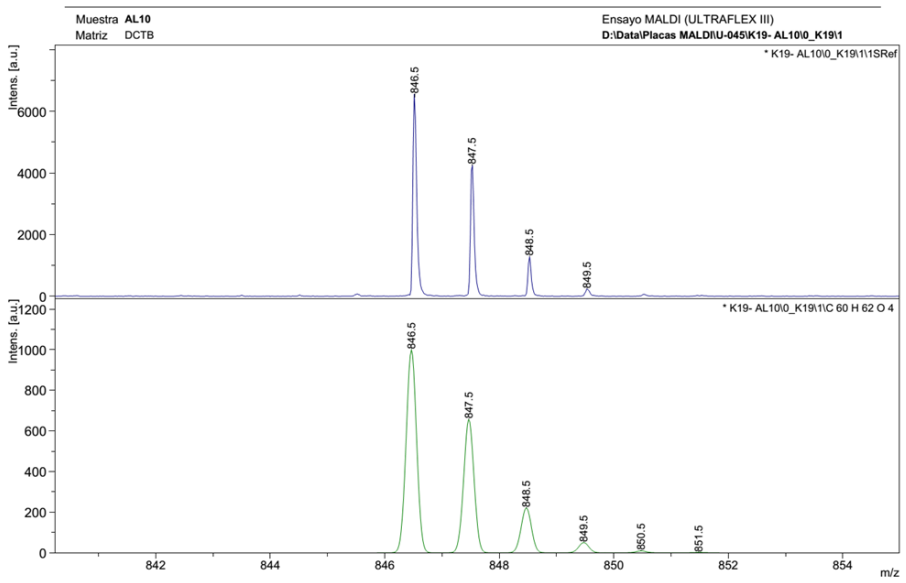

1,4-bis(((7-(undec-10-en-1-yloxy)pyren-2-yl)oxy)methyl)benzene

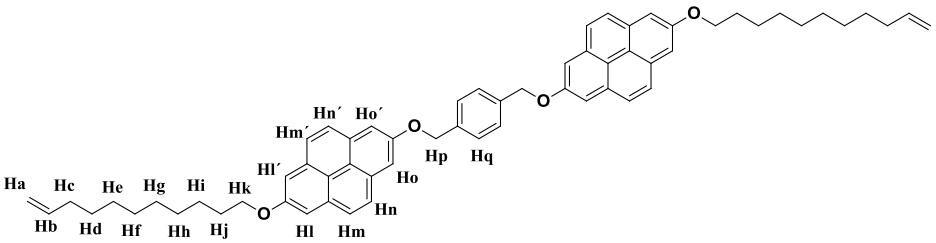

^{1}H RMN ($CDCl_3$, 300 MHz) δ: 7.97 (s, 8H, Hm+m´+n+n´), 7.79 (s, 4H, Hl+l´), 7.71 (s, 4H, Ho+o´), 7.64 (s, 4H, Hq), 5.91 – 5.78 (m, 2H, Ha), 5.41 (s, 4H, Hp), 5.06 – 4.93 (m, 4H, Hb), 4.27 (t, J = 6.5Hz, 4H, Hk), 2.09 – 2.04 (m, 4H, Hc), 1.97 – 1.92 (m, 4H, Hj), 1.59 – 1.54 (m, 4H, Hi), 1.50 – 1.30 (m, 20H, Hd+e+f+g+h) ppm. ^{13}C NMR ($CDCl_3$, 75 MHz) δ 156.8, 156.3, 139.2, 137.0, 131.6, 131.6, 127.8, 127.5, 127.4, 120.3, 120.0, 114.1, 111.6, 111.4, 77.2, 70.3, 68.6, 33.8, 29.6, 29.5, 29.1, 28.9, 26.2 ppm. MS m/z calculated for $C_{62}H_{66}O_4$ 874.5, found MALDI 874.5.

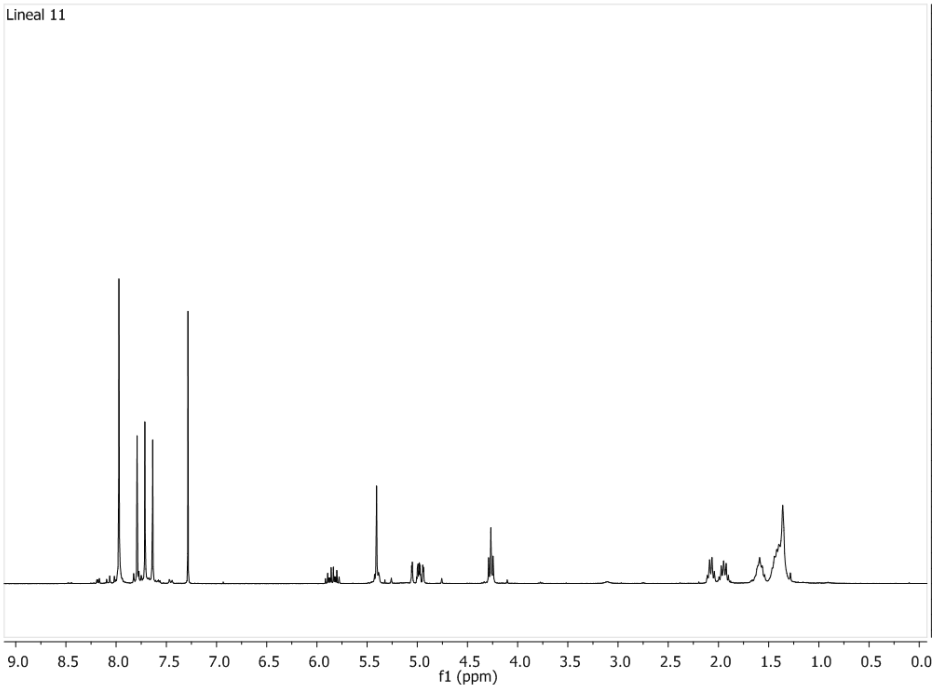
Lineal 11
9.0 8.5 8.0 7.5 7.0 6.5 6.0 5.5 5.0 4.5 4.0 3.5 3.0 2.5 2.0 1.5 1.0 0.5 0.0
f1 (ppm)

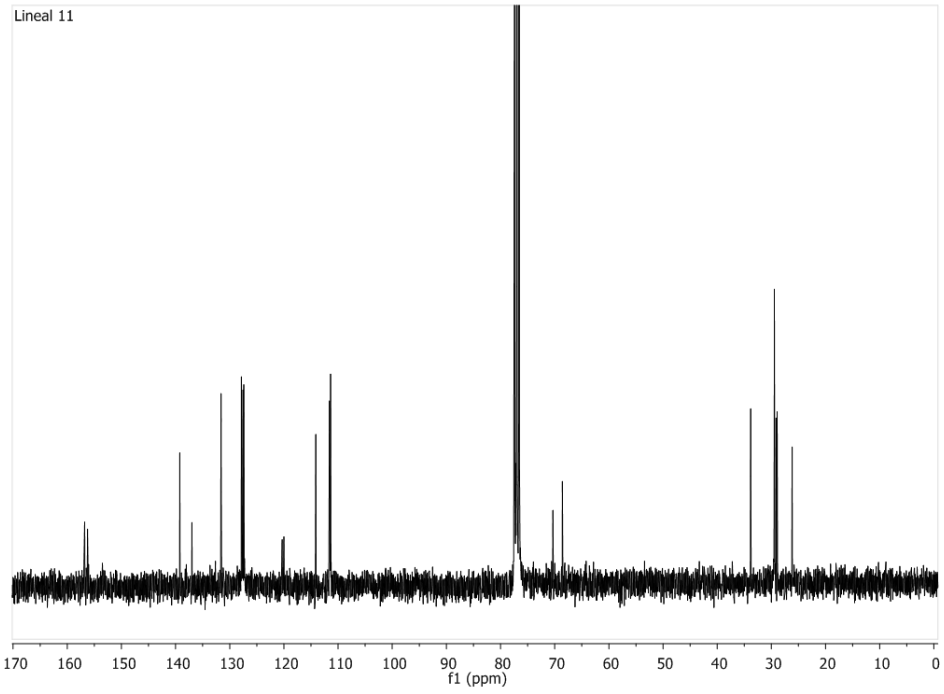
Lineal 11
170 160 150 140 130 120 110 100 90 80 70 60 50 40 30 20 10 0
f1 (ppm)

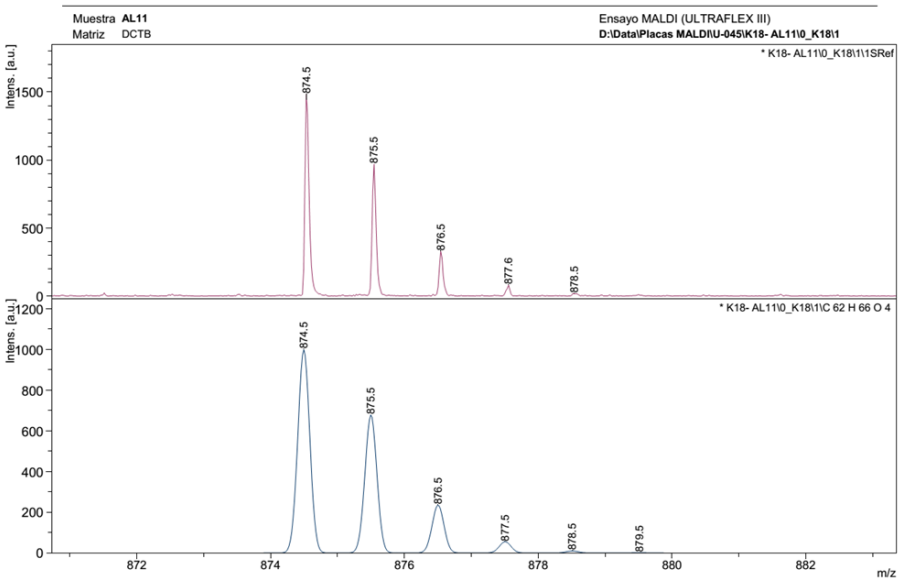

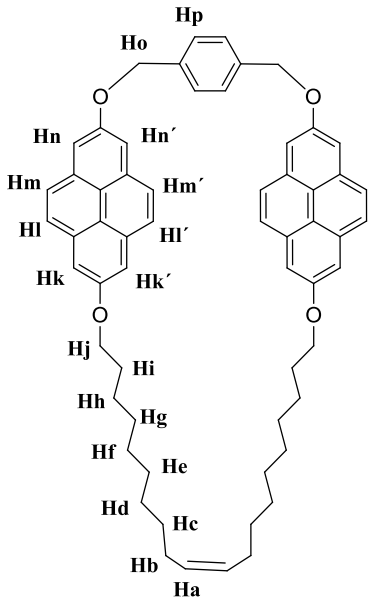

A catalytic amount of Grubb´s 1st generation catalyst was added to a solution of the linear precursor 1 in dry and degassed CH_2Cl_2. The solution was stirred at room temperature and its progress monitored by TLC (Hex:CH_2Cl_2

1:1). The reaction is then stopped, filtered through a pad of Celite, the solvent evaporated under reduced pressure, and the crude subjected to column chromatography silica gel (Hex:CH_2Cl_2 2:1) to obtain the product in 65% yield.

^{1}H RMN ($CDCl_3$, 400 MHz) δ 7.59-7.72 (m, 12H, Hk+k´+l+l´+m+m´), 7.50 (s, 4H, Hn+n´), 7.42 (s, 4H, Hp), 5.45 (s, 4H, Ho), 5.38 (m, 2H, Ha), 4.24 (t, J = 6.5 Hz, 4H, Hj), 1.99 – 1.90 (m, 2H, Hg), 1.35 – 1.26 (m, 24H, Hd+e+f). ^{13}C NMR ($CDCl_3$, 101 MHz) δ 156.7, 155.4, 131.6, 131.3, 130.5, 127.3, 127.2, 112.5, 111.2, 77.3, 77.0, 76.7, 70.2, 68.6, 38.8, 32.4, 29.7, 29.4, 28.9, 26.2. MS m/z calculated for $C_{60}H_{62}O_4$ 846.5, found MALDI 846.5.

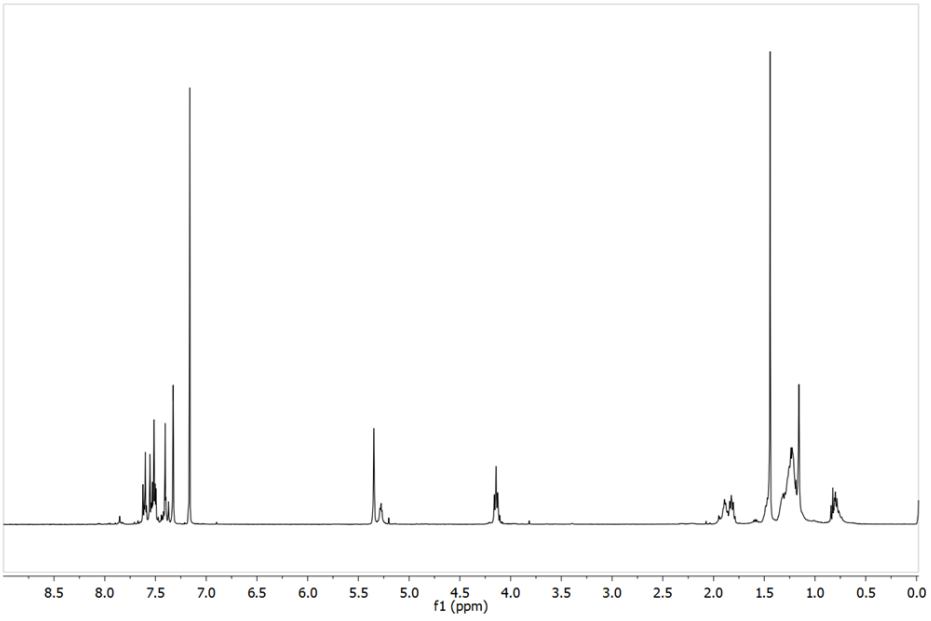

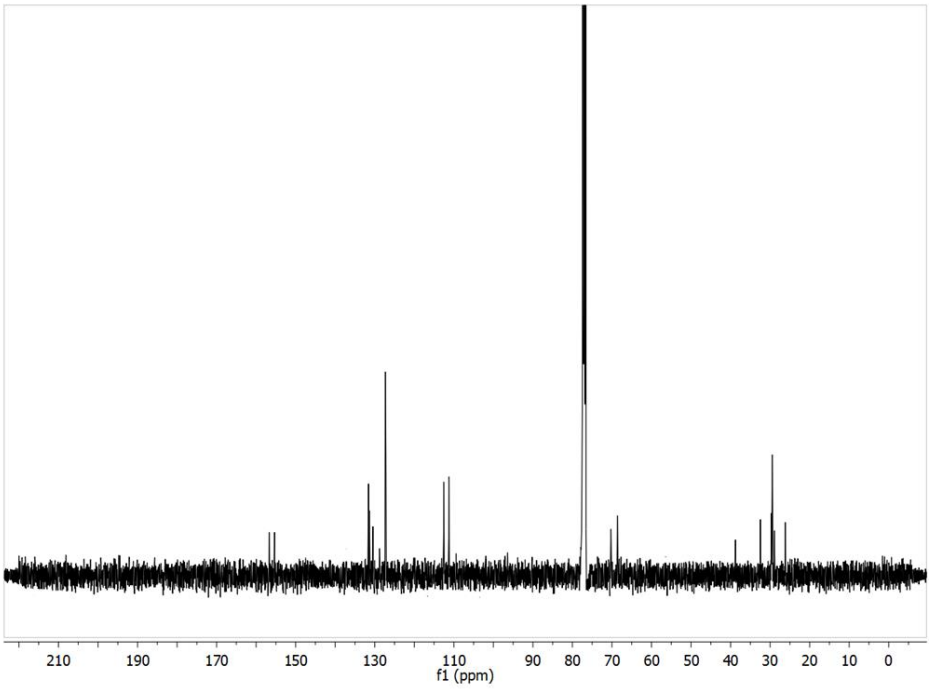
210
190
170
150
130
110
90
80
70
60
50
40
30
20
10
0
f1 (ppm)

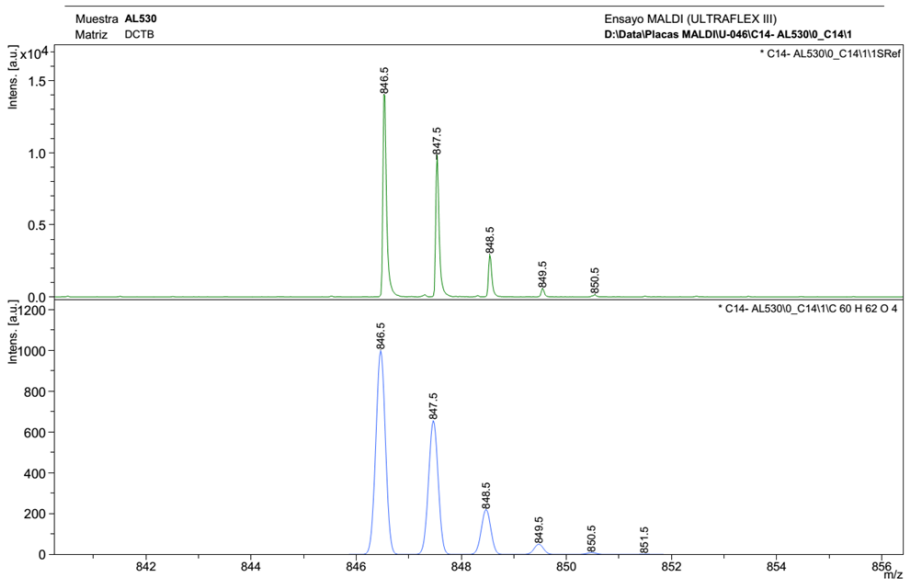
Muestra AL530
Matriz DCTB
Ensayo MALDI (ULTRAFLEX III)
D:\Data\Placas MALDI\U-046\C14- AL530\0_C14\1
* C14- AL530\0_C14\1\1SRef
Intens. [a.u.]
x10^4
1.5
1.0
0.5
0.0
846.5
847.5
848.5
849.5
850.5
* C14- AL530\0_C14\1\C 60 H 62 O 4
Intens. [a.u.]
1200
1000
800
600
400
200
0
846.5
847.5
848.5
849.5
850.5
851.5
842
844
846
848
850
852
854
856
m/z

General procedure for SWNTs functionalization.

The (6,5)- and (7,6)-enriched SWNTs purchased from Sigma Aldrich Co were purified previously. 100 mg of SWNTs were suspended in 70 mL of 35% HCl, and sonicated for 10 min. The mixture was poured in 200 mL of miliQ water and filtered through a polycarbonate membrane of 0.2 μm pore size. The solid was washed with water to neutral pH and then dried in an oven at 350^0C for 30 min. Pristine plasma-purified SWNTs were used without previous purification.

The nanotubes (5 mg) were suspended in 20 mL of tetrachloroethane (TCE) through sonication (10 min.) and mixed with linear precursors 1-3 (2.5 mg), and Grubb's 2nd generation catalyst at room temperature for 72 hours. After this time, the suspension was filtered through a PTFE membrane of 0.2 μm pore size, and the solid washed profusely with dichloromethane (DCM). The solid was re-suspended in 20 mL of DCM through sonication for 10 min. and filtered through a PTFE membrane of 0.2 μm pore size again. This washing procedure was repeated three times.

General procedure for SWNTs functionalization (varying the relative concentration of 3 with respect to SWNTs).

The nanotubes (1 mg/mL) were suspended in TCE through sonication (10 min.) and mixed with linear precursor (0.12 mM, 0.35 mM or 0.83 mM), and Grubb's 2nd generation catalyst at room temperature for 72 hours. After this time, the suspension was filtered through a PTFE membrane of 0.2 μm pore size, and the solid washed profusely with DCM. The solid was re-suspended in 20 mL of DCM through sonication for 10 min. and filtered through a PTFE membrane of 0.2 μm pore size again. This washing procedure was repeated three times.

General procedure for SWNTs Functionalization (control experiments).

The nanotubes (5 mg) were suspended in 20 mL of TCE through sonication (10 min.) and mixed with either linear precursor or macrocycle (2.5 mg) at room temperature for 72 hours. After this time, the suspension was filtered through a PTFE membrane of 0.2 µm pore size, and the solid washed profusely with DCM. The solid was re-suspended in 20 mL of DCM through sonication for 10 min. and filtered through a PTFE membrane of 0.2 µm pore size again. This washing procedure was repeated three times.

General procedure for stability test of functionalized SWNTs.

The functionalized nanotubes (2 mg) were suspended in 5 mL of TCE by sonication for 5 min. and then heated to reflux (bp = 146 °C) for 30 min. The suspension was filtered through a PTFE membrane of 0.2 µm pore size, and the solid washed profusely with DCM. A small de-threading (< 4 %) was observed by TGA.

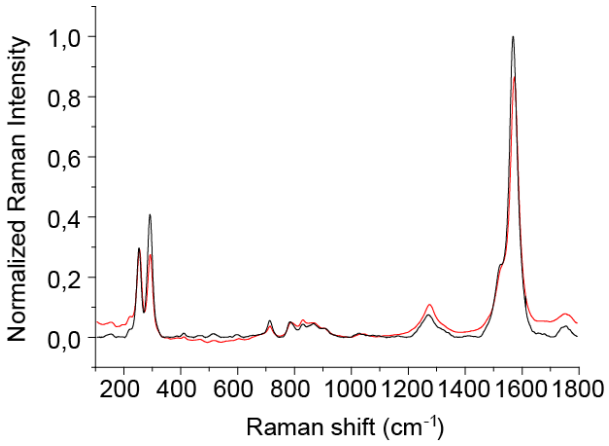

Figure S1. Raman spectra of (6,5)-enriched SWNTs (black) and the corresponding MINT(6,5) (red). The spectra is the average of three different measurements (λ_{exc} = 785 nm).

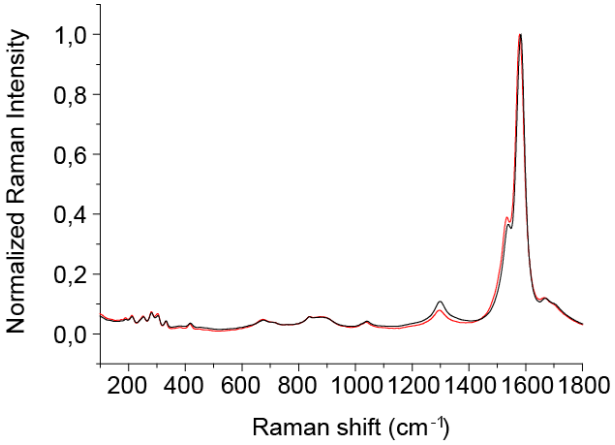

Figure S2. Raman spectra of (6,5)-enriched SWNTs (black) and the corresponding MINT(6,5) (red). The spectra is the average of three different measurements (λ_{exc} = 633 nm).

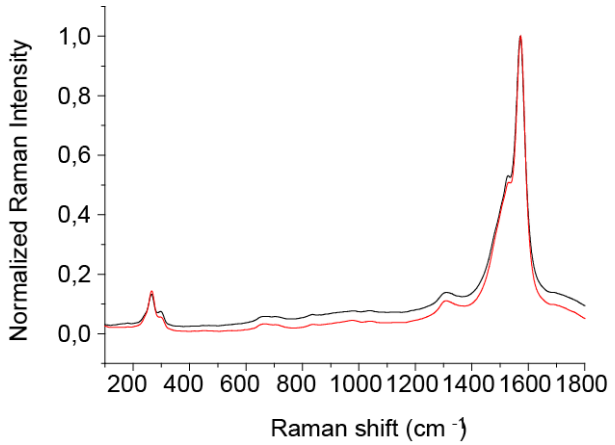

Figure S3. Raman spectra of (6,5)-enriched SWNTs (black) and the corresponding MINT(6,5) (red). The spectra is the average of three different measurements (λ_{exc} = 532 nm).

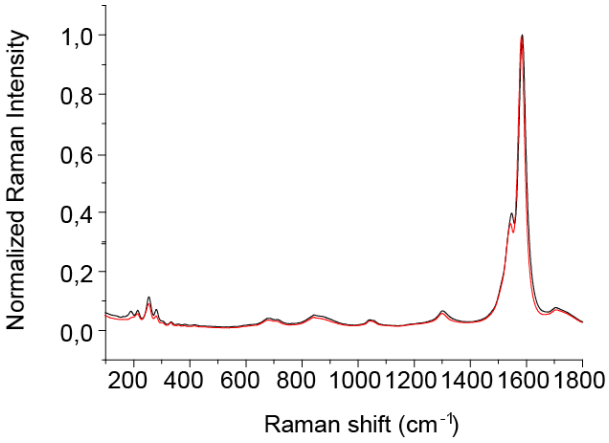

Figure S4. Raman spectra of (7,6)-enriched SWNTs (black) and the corresponding MINT(7,6) (red). The spectra is the average of three different measurements (λ_{exc} = 633 nm).

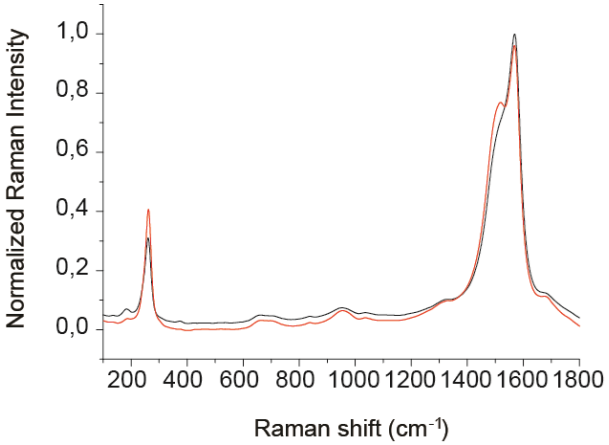

Figure S5. Raman spectra of (7,6)-enriched SWNTs (black) and the corresponding MINT(7,6) (red). The spectra is the average of three different measurements (λ_{exc} = 532 nm).

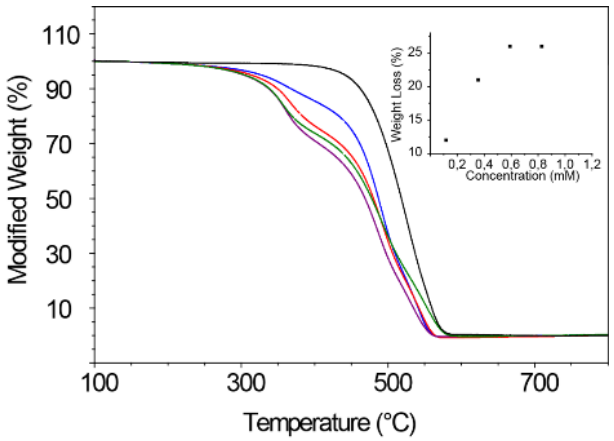

Figure S6. Variation in the degree of functionalization with the relative concentration of macrocycle **6** with respect to that of the SWNTs, as shown by TGA analysis (air, 10 ºC min^{-1}): pristine (6,5)-enriched SWNTs (black), 0.12 mM (blue), 0.35 mM (red), 0.59 mM (green) and 0.83 mM (purple). Inset shows the relative weight loss versus the concentration.

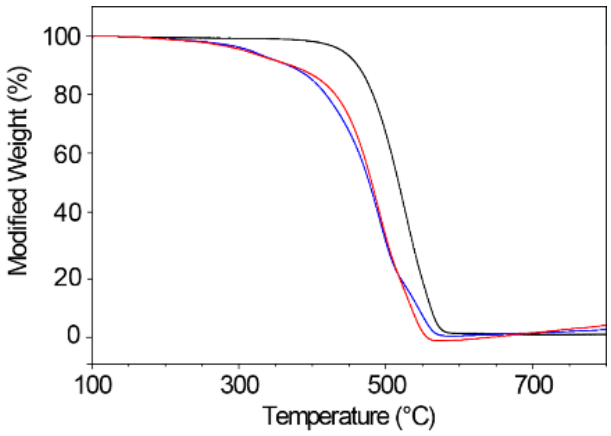

Figure S7. TGA analysis (air, 10 ºC min^{-1}) of: 1 (black), linear receptor control experiment (red) and preformed macrocycle **6** control experiment (blue).

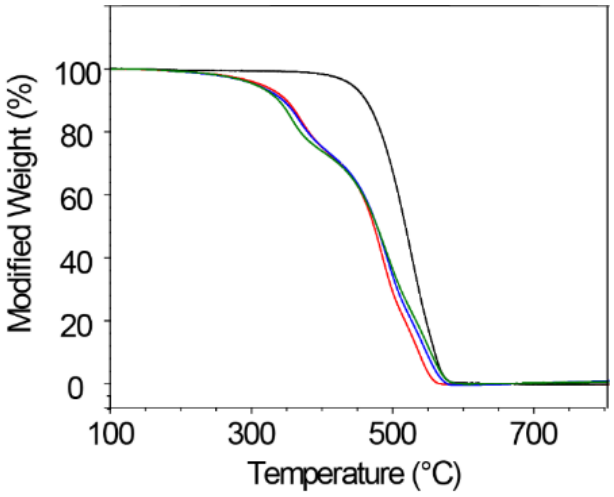

Figure S8. TGA analysis (air, 10 ºC min^{-1}) of pristine (7,6)-enriched SWNTs (black) and the product formed by treatment with **1**, **2** and **3** (blue)(red)(green) and the Grubbs second-generation catalyst in TCE at room temperature for 72 h.

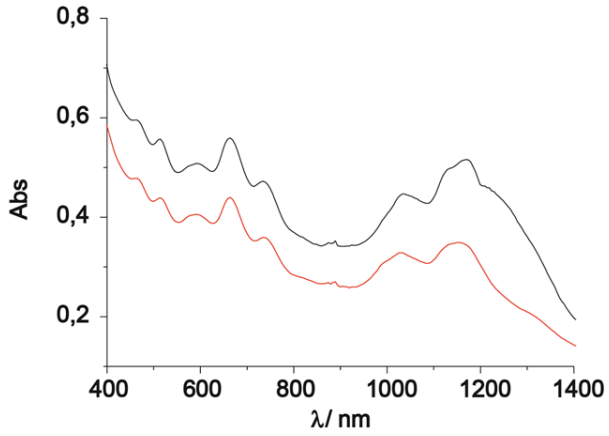

Figure S9. UV/Vis/NIR spectra (D_2O, 1 % sodium dodecyl sulfate (SDS), 298 K) of pristine (7,6)-enriched SWNTs (black) and MINT (7,6)-6(red)

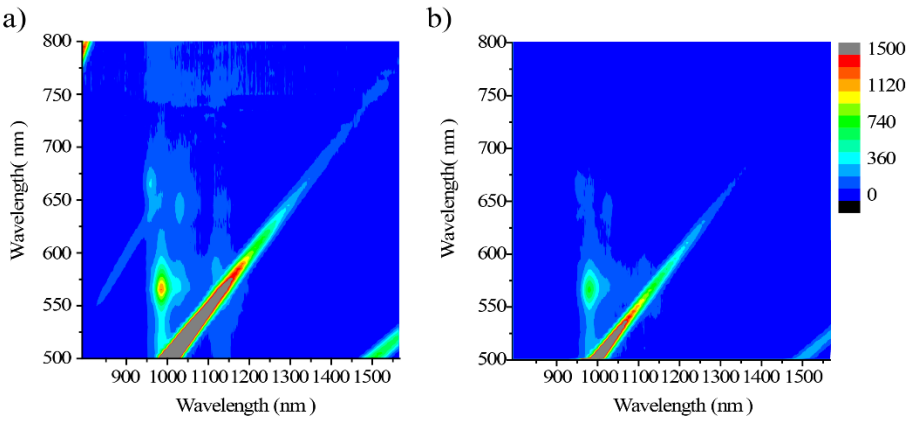

Figure S10. PLE intensity maps (D_2O, 1 % SDS, 298 K) of a) pristine (6,5)-enriched SWNTs and b) MINT(6,5)-**6**.

5.5. References

1. H. Dai. Carbon Nanotubes: Synthesis, Integration, and Properties. *Acc. Chem. Res.*, **2002,** *35*, 1035-1044.
2. J. Kong, E. Yenilmez, T. W. Tombler, W. Kim, H. Dai, R. B. Laughlin, L. Liu, C. S. Jayanthi, S. Y. Wu. Quantum Interference and Ballistic Transmission in Nanotube Electron Waveguides. *Phys. Rev. Lett.*, **2001,** *87*, 106801.
3. A. Wurl, S. Goossen, D. Canevet, M. Sallé, E. M. Pérez, N. Martín, C. Klinke. Supramolecular Interaction of Single-Walled Carbon Nanotubes with a Functional TTF-Based Mediator Probed by Field-Effect Transistor Devices. *J. Phys. Chem. C*, **2012,** *116*, 20062-20066.
4. (a) M. Bernardi, J. Lohrman, P. V. Kumar, A. Kirkeminde, N. Ferralis, J. C. Grossman, S. Ren. Nanocarbon-Based Photovoltaics. *ACS Nano*, **2012,** *6*, (10), 8896-8903; (b) H. Wang, G. I. Koleilat, P. Liu, G. Jiménez-Osés, Y.-C. Lai, M. Vosgueritchian, Y. Fang, S. Park, K. N. Houk, Z. Bao. High-Yield Sorting of Small-Diameter Carbon Nanotubes for Solar Cells and Transistors. *ACS Nano*, **2014,** *8*, 2609-2617.
5. (a) B. Esser, J. M. Schnorr, T. M. Swager. Selective Detection of Ethylene Gas Using Carbon Nanotube-based Devices: Utility in Determination of Fruit Ripeness. *Angew. Chem., Int. Ed.*, **2012,** *51*, 5752-5756; (b) A. M. Münzer, Z. P. Michael, A. Star. Carbon Nanotubes for the Label-Free Detection of Biomarkers. *ACS Nano*, **2013,** *7*, 7448-7453.
6. For recent reviews, see: (a) J. M. Schnorr, T. M. Swager. Emerging Applications of Carbon Nanotubes. *Chem. Mater.*, **2011,** *23*, 646-657; (b) S. Park, M. Vosguerichian, Z. Bao. A review of fabrication and applications of carbon nanotube film-based flexible

electronics. *Nanoscale*, **2013,** *5*, 1727-1752; (c) C. Wang, K. Takei, T. Takahashi, A. Javey. Carbon nanotube electronics - moving forward. *Chem. Soc. Rev.*, **2013,** *42*, 2592-2609.
7. (a) G. Cellot, E. Cilia, S. Cipollone, V. Rancic, A. Sucapane, S. Giordani, L. Gambazzi, H. Markram, M. Grandolfo, D. Scaini, F. Gelain, L. Casalis, M. Prato, M. Giugliano, L. Ballerini. Carbon nanotubes might improve neuronal performance by favouring electrical shortcuts. *Nat. Nanotechnol.*, **2009,** *4*, 126-133; (a) M. Adeli, R. Soleyman, Z. Beiranvand, F. Madani. Carbon nanotubes in cancer therapy: a more precise look at the role of carbon nanotube-polymer interactions. *Chem. Soc. Rev.*, **2013,** *42*, 5231-5256.
8. (a) J. N. Coleman, U. Khan, W. J. Blau, Y. K. Gun'ko. Small but strong: A review of the mechanical properties of carbon nanotube-polymer composites. *Carbon*, **2006,** *44*, 1624-1652; (b) Z. Spitalsky, D. Tasis, K. Papagelis, C. Galiotis. Carbon nanotube-polymer composites: Chemistry, processing, mechanical and electrical properties. *Prog. Polym. Sci.*, **2010,** *35*, 357-401.
9. (a) D. Tasis, N. Tagmatarchis, A. Bianco, M. Prato. Chemistry of Carbon Nanotubes. *Chem. Rev.*, **2006,** *106*, 1105-1136; (b) A. Hirsch. Functionalization of Single-Walled Carbon Nanotubes. *Angew. Chem. Int. Ed.*, **2002,** *41*, 1853-1859; (c) S. Niyogi, M. A. Hamon, H. Hu, B. Zhao, P. Bhowmik, R. Sen, M. E. Itkis, R. C. Haddon. Chemistry of Single-Walled Carbon Nanotubes. *Acc. Chem. Res.*, **2002,** *35*, 1105-1113.
10. (a) C. A. Dyke, J. M. Tour. Covalent Functionalization of Single-Walled Carbon Nanotubes for Materials Applications. *J. Phys. Chem. A*, **2004,** *108*, 11151-11159; (b) P. Singh, S. Campidelli, S. Giordani, D. Bonifazi, A. Bianco, M. Prato. Organic functionalization and characterization of single-walled carbon nanotubes. *Chem. Soc. Rev.*, **2009,** *38*, 2214-2230.
11. (a) Y.-L. Zhao, J. F. Stoddart. Noncovalent Functionalization of Single-Walled Carbon Nanotubes. *Acc. Chem. Res.*, **2009,** *42*, 1161-1171; (b) G. Gavrel, B. Jousselme, A. Filoramo, S. Campidelli. Supramolecular Chemistry of Carbon Nanotubes. *Top. Curr. Chem.*, **2014,** *348*, 95-126.
12. (a) A. de Juan, E. M. Pérez. Getting tubed: mechanical bond in endohedral derivatives of carbon nanotubes?, *Nanoscale*, **2013,** *5*, 7141-7148; (b) T. Zoberbier, T. W. Chamberlain, J. Biskupek, N. Kuganathan, S. Eyhusen, E. Bichoutskaia, U. Kaiser, A. N. Khlobystov. Interactions and Reactions of Transition Metal Clusters with the Interior of Single-Walled Carbon Nanotubes Imaged at the Atomic Scale. *J. Am. Chem. Soc.*, **2012,** *134*, 3073-3079.
13. (a) E. R. Kay, D. A. Leigh, F. Zerbetto. Synthetic Molecular Motors and Mechanical Machines. *Angew. Chem. Int. Ed.*, **2007,** *46*, 72-191; (b) D. A. Leigh, E. M. Pérez. Dynamic Chirality: Molecular Shuttles and Motors. *Top. Curr. Chem.*, **2006,** *265*, 185-208.
14. (a) C. O. Dietrich-Buchecker, J. P. Sauvage, J. P. Kintzinger. New family of molecules: the metallo-catenanes. *Tetrahedron Lett.*, **1983,** *24*, 5095-5098; (b) C. O.

Dietrich-Buchecker, J. P. Sauvage, J. M. Kern. Templated synthesis of interlocked macrocyclic ligands: the catenands. *J. Am. Chem. Soc.*, **1984,** *106*, 3043-3045.
15. For reviews, see: (a) J. F. Stoddart. The chemistry of the mechanical bond. *Chem. Soc. Rev.*, **2009,** *38*, 1802-1820; (b) M. S. Vickers, P. D. Beer. Anion templated assembly of mechanically interlocked structures. *Chem. Soc. Rev.*, **2007,** *36*, 211-225; (c) C. O. Dietrich-Buchecker, J. P. Sauvage. Interlocking of molecular threads: from the statistical approach to the templated synthesis of catenands. *Chem. Rev.*, **1987,** *87*, 795-810; (d) For a recent selected example,see: D. A. Leigh, R. G. Pritchard, A. J. Stephens. A Star of David catenane. *Nat. Chem.*, **2014,** *6*, 978-982.
16. A. de Juan, Y. Pouillon, L. Ruiz-González, A. Torres-Pardo, S. Casado, N. Martín, Á. Rubio, E. M. Pérez. Mechanically Interlocked Single-Wall Carbon Nanotubes. *Angew. Chem., Int. Ed.*, **2014,** *53*, 5394-5400.
17. C. Romero-Nieto, R. García, M. Á. Herranz, C. Ehli, M. Ruppert, A. Hirsch, D. M. Guldi, N. Martín. Tetrathiafulvalene-Based Nanotweezers—Noncovalent Binding of Carbon Nanotubes in Aqueous Media with Charge Transfer Implications. *J. Am. Chem. Soc.*, **2012,** *134*, 9183-9192.
18. A. G. Crawford, Z. Liu, I. A. I. Mkhalid, M.-H. Thibault, N. Schwarz, G. Alcaraz, A. Steffen, J. C. Collings, A. S. Batsanov, J. A. K. Howard, T. B. Marder. Synthesis of 2- and 2,7-Functionalized Pyrene Derivatives: An Application of Selective C—H Borylation. *Chem. - Eur. J.*, **2012,** *18*, 5022-5035.
19. (a) S. G. Stepanian, V. A. Karachevtsev, A. Y. Glamazda, U. Dettlaff-Weglikowska, L. Adamowicz. Combined Raman scattering and ab initio investigation of the interaction between pyrene and carbon SWNT. *Mol. Phys.*, **2003,** *101*, 2609-2614; (b) G. Modugno, Z. Syrgiannis, A. Bonasera, M. Carraro, G. Giancane, L. Valli, M. Bonchio, M. Prato. The supramolecular design of low-dimensional carbon nano-hybrids encoding a polyoxometalate-bis-pyrene tweezer. *Chem. Commun.*, **2014,** *50*, 4881-4883.
20. Y. Tomonari, H. Murakami, N. Nakashima. Solubilizaton of Single-Walled Carbon Nanotubes by Using Polycyclic Aromatic Ammonium Amphiphiles in Water - Strategy for the Design of High-Performance Solubilizers. *Chem. - Eur. J.*, **2006,** *12*, 4027-4034.
21. C. Fantini, M. L. Usrey, M. S. Strano. Investigation of Electronic and Vibrational Properties of Single-Walled Carbon Nanotubes Functionalized with Diazonium Salts. *J. Phys. Chem. C*, **2007,** *111*, 17941-17946.
22. M. S. Strano, C. B. Huffman, V. C. Moore, M. J. O'Connell, E. H. Haroz, J. Hubbard, M. Miller, K. Rialon, C. Kittrell, S. Ramesh, R. H. Hauge, R. E. Smalley. Reversible, Band-Gap-Selective Protonation of Single-Walled Carbon Nanotubes in Solution. *J. Phys. Chem. B*, **2003,** *107*, 6979-6985.
23. E. Nakamura. Movies of Molecular Motions and Reactions: The Single-Molecule, Real-Time Transmission Electron Microscope Imaging Technique. *Angew. Chem. Int. Ed.*, **2013,** *52*, 236-252.
24. (a) E. A. Neal, S. M. Goldup. Chemical consequences of mechanical bonding in catenanes and rotaxanes: isomerism, modification, catalysis and molecular machines for

synthesis. *Chem. Commun.*, **2014,** *50*, 5128-5142; (b) J. F. Stoddart. Putting Mechanically Interlocked Molecules (MIMs) to Work in Tomorrow's World. *Angew. Chem. Int. Ed.*, **2014,** *53*, 11102-11104.

25. (a) S. Sato, T. Yamasaki, H. Isobe. Solid-state structures of peapod bearings composed of finite single-wall carbon nanotube and fullerene molecules. *Proc. Natl. Acad. Sci.*, **2014,** *111*, 8374-8379; (b) D. Canevet, E. M. Pérez, N. Martín. Wraparound Hosts for Fullerenes: Tailored Macrocycles and Cages. *Angew. Chem. Int. Ed.*, **2011,** *50*, 9248-9259; (c) H. Isobe, S. Hitosugi, T. Yamasaki, R. Iizuka. Molecular bearings of finite carbon nanotubes and fullerenes in ensemble rolling motion. *Chem. Sci.*, **2013,** *4*, 1293-1297; (d) D. Canevet, M. Gallego, H. Isla, A. de Juan, E. M. Pérez, N. Martín. Macrocyclic Hosts for Fullerenes: Extreme Changes in Binding Abilities with Small Structural Variations. *J. Am. Chem. Soc.*, **2011,** *133*, 3184-3190.

6. Threading through macrocycles enhances the performance of carbon nanotubes as polymer fillers

Alejandro López-Moreno, Belén Nieto-Ortega, Maria Moffa, Alberto de Juan, M. Mar Bernal, Juan P. Fernández-Blázquez, Juan J. Vilatela, Dario Pisignano, and Emilio M. Pérez, *ACS Nano* **2016,** *10*, 8012-8018.

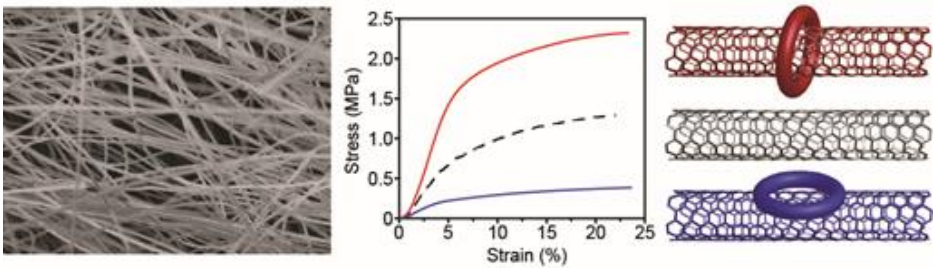

In this work we study the reinforcement of polymers by mechanically interlocked derivatives of single-walled carbon nanotubes (SWNTs). We compare the mechanical properties of fibers made of polymers and of composites with pristine single-walled carbon nanotubes (SWNTs), mechanically interlocked derivatives of SWNTs (MINTs) and the corresponding supramolecular models. Improvements of both Young's modulus and tensile strength of up to 200% were observed for the polystyrene-MINTs samples with an optimized loading of just 0.01 wt.%, while the supramolecular models with identical chemical composition and loading showed negligible or even detrimental influence. This behavior is found for three different types of SWNTs and two types of macrocycles. Molecular dynamics simulations show that the polymer adopts an elongated conformation parallel to the SWNT when interacting with MINT fillers, irrespective of the macrocycle chemical nature, whereas a more globular structure is taken upon facing with either pristine SWNTs or supramolecular models. The MINT composite architecture thus leads to a more efficient exploitation of the axial properties of the SWNTs and of the

polymer chain at the interface, in agreement with experimental results. Our findings demonstrate that the mechanical bond imparts distinctive advantageous properties to SWNT derivatives as polymer fillers.

6.1. Introduction

Carbon nanotubes are extensively used as reinforcing fillers in composites due to their extraordinary mechanical and structural properties. Since the report in this field by Ajayan et al.,[1] several materials where the mechanical and/or electrical properties of polymers have been significantly improved through nanotubes fillers have been demonstrated, and used for different applications,[2] including improved batteries, mechanically reinforced materials,[3] and sensors.[4]

To fully exploit the properties of single wall carbon nanotubes (SWNTs) as fillers in polymer matrices, a lot of research has been addressed to their chemical modification. In this framework, the mechanical bond is very attractive due to its dynamic features,[5] which have allowed for the construction of artificial

[1] P. M. Ajayan, O. Stephan, C. Colliex, D. Trauth. *Science*, **1994,** *265*, 1212-1214.
[2] (a) E. T. Thostenson, Z. Ren, T. W. Chou. *Compos. Sci. Technol.*, **2001,** *61*, 1899-1912; (b) O. Breuer, U. Sundararaj. *Polym. Compos.*, **2004,** *25*, 630-645; (c) P. J. F. Harris. Carbon nanotube composites. *Int. Mater. Rev.*, **2004,** *49*, 31-43; (d) J. N. Coleman, U. Khan, W. J. Blau, Y. K. Gun'ko. *Carbon*, **2006,** *44*, 1624-1652; (e) C. Li, E. T. Thostenson, T.-W. Chou. *Compos. Sci. Technol.*, **2008,** *68*, 1227-1249; (f) B. Arash, Q. Wang, V. K. Varadan. *Sci. Rep.*, **2014,** *4*, 6479; (g) Y. Liu, S. Kumar. *ACS Appl. Mater. Interfaces*, **2014,** *6*, 6069-6087; (h) J.J. Vilatela. Nanocarbon-based composites. In *Nanocarbon-Inorganic Hybrids: Next Generation Composites for Sustainable Energy Applications*, **2014,** 227-254; (i) W. Kong, L. Sun, Y. Wu, K. Jiang, Q. Li, J. Wang, S. Fan. *Carbon*, **2016,** *96*, 1053-1059; (j) G. Liu, Q.-D. Ling, E. Y. H. Teo, C.-X. Zhu, D. S.-H. Chan, K.-G. Neoh, E.-T. Kang. *ACS Nano*, **2009,** *3*, 1929-1937; (k) X. Li, F. Gittleson, M. Carmo, R. C. Sekol, A. D. Taylor. *ACS Nano*, **2012,** *6*, 1347-1356; (l) S. N. Habisreutinger, T. Leijtens, G. E. Eperon, S. D. Stranks, R. J. Nicholas, H. J. Snaith. *Nano Lett.*, **2014,** *14*, 5561-5568; (m) J. Zhu, W. Cao, M. Yue, Y. Hou, J. Han, M. Yang. *ACS Nano*, **2015,** *9*, 2489-2501; (n) Y. Wang, M. Li, Y. Gu, X. Zhang, S. Wang, Q. Li, Z. Zhang. *Nanoscale*, **2015,** *7*, 3060-3066; (o) T. R. Fadel, F. A. Sharp, N. Vudattu, R. Ragheb, J. Garyu, D. Kim, E. Hong, N. Li, G. L. Haller, L. D. Pfefferle, S. Justesen, K. C. Herold, T. M. Fahmy. *Nat. Nanotechnol.*, **2014,** *9*, 639-647.
[3] (a) J. Gao, M. E. Itkis, A. Yu, E. Bekyarova, B. Zhao, R. C. Haddon. *J. Am. Chem. Soc.*, **2005,** *127*, 3847-3854; (b) R. Sen, B. Zhao, D. Perea, M. E. Itkis, H. Hu, J. Love, E. Bekyarova, R. C. Haddon. *Nano Lett.*, **2004,** *4*, 459-464.
[4] (a) J. N. Coleman, U. Khan, Y. K. Gun'ko. *Adv. Mater.*, **2006,** *18*, 689-706; (b) X. Sun, H. Sun, H. Li, H. Peng. *Adv. Mater.*, **2013,** *25*, 5153-5176.
[5] (a) J. F. Stoddart. *Chem. Soc. Rev.*, **2009,** *38*, 1802-1820; (b) E. A. Neal, S. M. Goldup. *Chem. Commun.*, **2014,** *50*, 5128-5142.

molecular machines.[6] The mechanical bond is also very relevant for polymer science: polyrotaxanes, polycatenanes, and supramolecular polymers including mechanically interlocked molecules have all been investigated.[7] The reinforcement effect of B/SiO_x nanocomposites through the formation of interlocked "necklaces" has also been described.[8]

The mechanical link was introduced by some of us as a tool for the chemical manipulation of SWNTs very recently.[9] We used a U-shaped precursor featuring two units of a recognition element for SWNTs connected through an aromatic spacer, and further decorated with alkene-terminated alkyl spacers of different lengths. Using pyrene and π-extended derivatives of tetrathiafulvalene, both of which have high affinity for SWNTs,[10] We could template the ring closing metathesis (RCM) of the U-shaped precursor around the nanotubes, forming mechanically interlocked derivatives of SWNTs (MINTs, **Figure 1a**). Thanks to

[6] (a) J. Berná, G. Bottari, A. Leigh David, M. Pérez Emilio. *Pure Appl. Chem.*, **2007**, *79*, 39-54; (b) E. R. Kay, D. A. Leigh, F. Zerbetto. *Angew. Chem. Int. Ed.*, **2007,** *46*, 72-191; (c) A. Credi, M. Venturi, V. Balzani. *ChemPhysChem*, **2010,** *11*, 3398-3403; (d) J.-P. Sauvage, J.-P. Collin, S. Durot, J. Frey, V. Heitz, A. Sour, C. Tock. *C. R. Chim.*, **2010,** *13*, 315-328; (e) C. J. Bruns, J. F. Stoddart. *Acc. Chem. Res.*, **2014,** *47*, 2186-2199; (f) F. Niess, V. Duplan, J.-P. Sauvage. *Chem. Lett.*, **2014,** *43*, 964-974; (g) E. R. Kay, D. A. Leigh. *Angew. Chem. Int. Ed.*, **2015,** *54*, 10080-10088; (h) S. Erbas-Cakmak, D. A. Leigh, C. T. McTernan, A. L. Nussbaumer. *Chem. Rev.*, **2015,** *115*, 10081-10206.

[7] (a) L. Fang, M. A. Olson, D. Benítez, E. Tkatchouk, W. A. Goddard, III, J. F. Stoddart. *Chem. Soc. Rev.*, **2010,** *39*, 17-29; (b) R. Dong, Y. Zhou, X. Huang, X. Zhu, Y. Lu, J. Shen. *Adv. Mater.*, **2015,** *27*, 498-526; (c) H. W. Gibson, M. C. Bheda, P. T. Engen. *Prog. Polym. Sci.*, **1994,** *19*, 843-945; (d) T. Takata, N. Kihara, Y. Furusho. *Polyrotaxanes and Polycatenanes: Recent Advances in Syntheses and Applications of Polymers Comprising of Interlocked Structures*. **2004**; 1-75; (e) F. Huang, H. W. Gibson. *Prog. Polym. Sci.*, **2005,** *30*, 982-1018; (f) J. P. Coelho, G. González-Rubio, A. Delices, J. O. Barcina, C. Salgado, D. Ávila, O. Peña-Rodríguez, G. Tardajos, A. Guerrero-Martínez. *Angew. Chem., Int. Ed.*, **2014,** *53*, 12751-12755; (g) I.-H. Park, R. Medishetty, J.-Y. Kim, S. S. Lee, J. J. Vittal. *Angew. Chem. Int. Ed.*, **2014,** *53*, 5591-5595; (h) D. Montarnal, N. Delbosc, C. Chamignon, M.-A. Virolleaud, Y. Luo, C. J. Hawker, E. Drockenmuller, J. Bernard. *Angew. Chem. Int. Ed.*, **2015,** *54*, 11117-11121; (i) A. Goujon, G. Du, E. Moulin, G. Fuks, M. Maaloum, E. Buhler, N. Giuseppone. *Angew. Chem. Int. Ed.*, **2016,** *55*, 703-707.

[8] (a) X. Tao, J. Liu, G. Koley, X. Li. *Adv. Mater.*, **2008,** *20*, 4091-4096; (b) H. Ni, X. Li. *Appl. Phys. Lett.*, **2006,** *89*, 053108.

[9] (a) A. de Juan, Y. Pouillon, L. Ruiz-González, A. Torres-Pardo, S. Casado, N. Martín, Á. Rubio, E. M. Pérez. *Angew. Chem., Int. Ed.*, **2014,** *53*, 5394-5400; (b) A. de Juan, M. Mar Bernal, E. M. Pérez. *ChemPlusChem*, **2015,** *80*, 1153-1157; (c) A. López-Moreno, E. M. Pérez. *Chem. Commun.*, **2015,** *51*, 5421-5424; (d) E. Martínez-Periñan, A. de Juan, Y. Pouillon, C. Schierl, V. Strauss, N. Martín, Á. Rubio, D. M. Guldi, E. Lorenzo, E. M. Pérez. *Nanoscale*, **2016,** *8*, 9254-9264.

[10] (a) A. de Juan, A. López-Moreno, J. Calbo, E. Ortí, E. M. Pérez. *Chem.l Sci.*, **2015,** *6*, 7008-7014; (b) A. Wurl, S. Goossen, D. Canevet, M. Sallé, E. M. Pérez, N. Martín, C. Klinke. *J. Phys. Chem. C*, **2012,** *116*, 20062-20066; (c) E. M. Pérez, B. M. Illescas, M. Á. Herranz, N. Martín. *New J. Chem.*, **2009,** *33*, 228-234; (d) C. Romero-Nieto, R. García, M. Á. Herranz, C. Ehli, M. Ruppert, A. Hirsch, D. M. Guldi, N. Martín. *J. Am. Chem. Soc.*, **2012,** *134*, 9183-9192.

the extreme aspect ratio of the nanotubes, which prevents dissociation of the macrocycles from the nanotubes once they are formed around them, MINTs showed stability comparable to that of covalently modified nanotubes, while maintaining the native structure of the SWNTs. Since rotaxanes and pseudorotaxanes are both topologically identical,[11] and the major difference between them is their kinetic stability,[12] we believe our MINT derivatives can be considered mechanically interlocked, despite the lack of explicit stoppers.

To effectively transfer the anisotropic properties of elongated fillers such as SWNTs to composites, a parallel orientation in the matrix and a strong interaction with the polymer are required. In principle, the parallel orientation along the prevalent direction of macromolecular chains can be favored by electrospinning, due to the very high elongational strain rates applied,[13] while the noncovalent interactions between polymer and filler can be tuned chemically. Recently, the groups led by Pisignano and Credi have described that various dynamic properties of rotaxane-type molecules are conserved within electrospun fibers.[14]

Here, we present our results on the influence of the mechanical bond on the mechanical properties of SWNT-based nanocomposites. We incorporate MINTs in polystyrene fibers and study their tensile properties. The merits of the MINT functionalization approach manifest as substantial enhancements in Young's modulus and tensile strength. In comparison, non-interlocked model samples of identical chemical composition show no positive effect.

[11] (a) D. B. Amabilino, L. Pérez-García. *Chem. Soc. Rev.*, **2009,** *38*, 1562-1571; (b) E. Griffiths Kirsten, J. F. Stoddart. *Pure Appl. Chem.*, **2008,** *80*, 485-506.
[12] A. de Juan, E. M. Pérez. *Nanoscale*, **2013,** *5*, 7141-7148.
[13] (a) F. Ko, Y. Gogotsi, A. Ali, N. Naguib, H. Ye, G. L. Yang, C. Li, P. Willis. *Adv. Mater.*, **2003,** *15*, 1161-1165; (b) H. Hou, J. J. Ge, J. Zeng, Q. Li, D. H. Reneker, A. Greiner, S. Z. D. Cheng. *Chem. Mater.*, **2005,** *17*, 967-973; (c)Y. Dror, W. Salalha, R. L. Khalfin, Y. Cohen, A. L. Yarin, E. Zussman. *Langmuir*, **2003,** *19*, 7012-7020.
[14] V. Fasano, M. Baroncini, M. Moffa, D. Iandolo, A. Camposeo, A. Credi, D. Pisignano. *J. Am. Chem. Soc.*, **2014,** *136*, 14245-14254.

6.2. Results and discussion

We utilized two types of macrocycles (**Figure 1b**) and three types of SWNTs of different diameter, length and electronic character. In particular, we used pyrene (**1**) and exTTF (**2**) based macrocycles and (6,5)-enriched nanotubes purchased from Sigma Aldrich Co. (0.7-0.9 nm in diameter, length ≥ 700 nm, mostly semiconducting, 95% purity) denoted as (6,5)-SWNTs, plasma-purified SWNTs (pp-SWNTs) purchased from Cheap Tubes Inc. (0.8-1.6 nm in diameter, length 3-30 μm, mostly metallic, 99 % purity), and shorter COOH functionalized SWNTs (o-SWNTs) purchased from Cheap Tubes Inc. (0.8-1.6 nm in diameter, length 0.5-2.0 μm, mostly metallic, 99 % purity). These various types of samples allowed us to discriminate mechanical reinforcement arising from differences in SWNT length or dispersion quality from those directly due to the MINT functionalization.

The general method for the synthesis of MINTs has been reported elsewhere.[42-45] Briefly, we use a clipping strategy in which a suspension of SWNTs is treated with the adequate bis-alkene U-shape precursor and Grubb's 2nd generation catalyst. After supramolecular association of the U-shape, it can be closed around the SWNT to form MINTs. Non-interlocked macrocycles and U-shapes, oligomers, catalyst, and all other byproducts are removed by extensive washes with dichloromethane. The interlocked macrocycles stay in place without the need for "stoppers" due to the extreme aspect ratio of the SWNTs. All samples used in this study were adequately characterized by standard methods, including TGA, Raman, UV-vis-NIR and TEM. **Figure 1** shows representative examples of TGA curves, Raman spectra and TEM micrographs. TGA evidences that, following MINT-forming reaction, the SWNTs showed organic functionalization between 27 and 43%, keeping stable even after reflux in tetrachloroethane for 30 min. No major shifts and no increase in the I_D/I_G ratio upon functionalization were found in the Raman spectra, confirming that the functionalization is noncovalent. HRTEM allows visualizing individual

macrocycles around the SWNTs in the MINT samples (for comprehensive characterization, including control experiments, please see the experimental section and references 42-45).

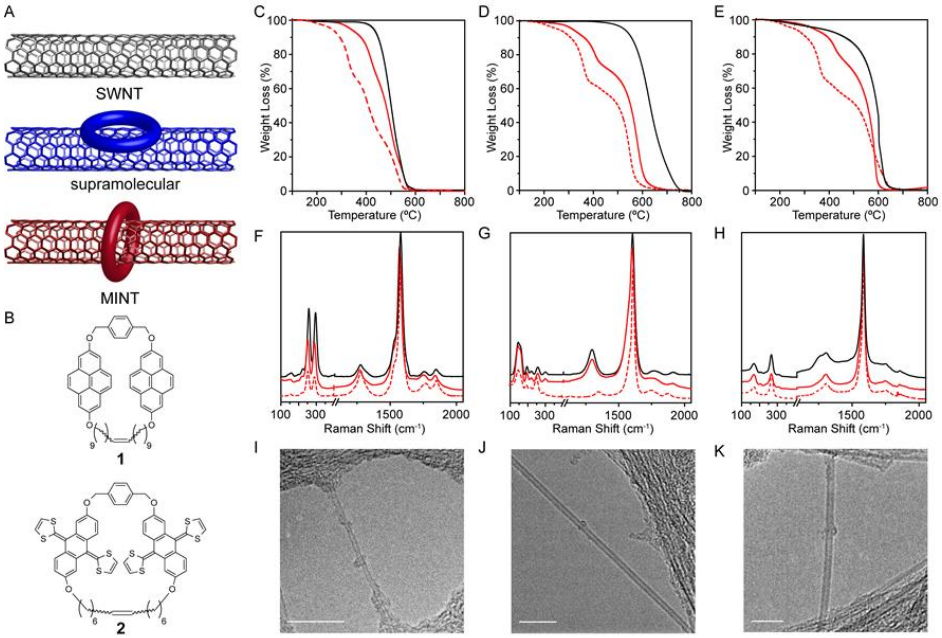

Figure 1. a) Schematic representation of the three fillers investigated: SWNTs, supramolecular associates and MINTs; b) Chemical structure of macrocycles **1** and **2**. c-k) Characterization of MINT derivatives. TGA analysis of c) pristine (6,5)-SWNTs, (black) $MINT_{(6,5)}$-**1** (red) and $MINT_{(6,5)}$-**2** (dashed red); d) pristine pp-SWNTs (black), $MINT_{(pp)}$-**1** (red) and $MINT_{(pp)}$-**2** (dashed red); e) pristine o-SWNTs (black), $MINT_{(o)}$-**1** (red) and $MINT_{(o)}$-**2** (dashed red); Raman spectra of f) (6,5)-SWNTs (black), $MINT_{(6,5)}$-1 (red) and $MINT_{(6,5)}$-**2** (dashed red); g) pp-SWNTs (black), $MINT_{(pp)}$-**1** (red) and $MINT_{(pp)}$-**2** (dashed red); h) o-SWNTs (black), $MINT_{(o)}$-**1** (red) and $MINT_{(o)}$-**2** (dashed red); TEM images of nanotubes (showing macrocycles around nanotubes) in i) $MINT_{(6,5)}$-**2**; j) $MINT_{(pp)}$-**2** and k) $MINT_{(o)}$-**2**. Scale bars are 10 nm. TGAs were run in air at a heating rate of 10 ºC min^{-1}. All Raman spectra are the average of ten different measurements at λ_{exc} = 785 nm.

We prepared suspensions of the SWNT derivatives through ultrasonication. To avoid the presence of aggregates that could affect the mechanical properties, the suspensions were centrifuged and then polystyrene was added. Electrospinning was carried out using a commercially available system, operating with an applied inter-electrode bias of 14 kV and a flow rate of 1 mL h^{-1}. Experimental details and videos of the electrospinning process can be found in the experimental section. The filler loading was optimized to 0.01 wt% respect to polystyrene, since larger loadings lead to defective fibers (experimental section). With this loading, fibers showed seamless and uniform surfaces, without discernable beads or nanotube aggregates. **Figure 2** displays typical scanning electron (SEM) micrographs of fibers made of pristine polystyrene, and of those with o-SWNTs-based fillers, as representative examples (other samples are shown in experimental section).

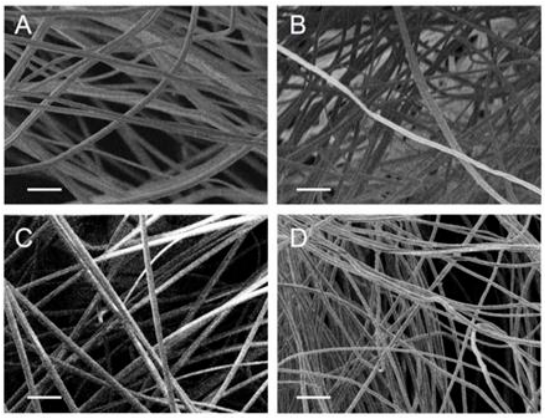

Figure 2. SEM images of: a) Polystyrene fibers; b) o-SWNTs; c) $MINT_{(o)}$-**1**; d) o-SWNTs·**1**. Inset scale: 10 µm.

The diameter distribution of the fibers is within the same range of 1.3-1.8 µm for all samples (**Figure S7**). Pristine polystyrene fibers are slightly thicker

(2.2 ± 0.6 μm) as expected because of the lower solution conductivity.[15] The (6,5)-SWNTs and pp-SWNTs samples are similar to o-SWNTs in structure and size as shown **Figure S8**. The mechanical properties of the fibers were then determined using a dynamic mechanical analyzer (DMA Q800, TA Instruments). Each nanocomposite (n = 3 specimens) was cut into 1×4 cm2 pieces to define samples with thickness 0.15-0.18 mm. All samples had comparable area density (ca. 2.5 mg cm^{-2}) and thus the test specimens had similar linear densities too thus ensuring stable force to stress normalization in measurements. Force-displacement curves were recorded at 1 $N \cdot min^{-1}$ (up to 18 N).

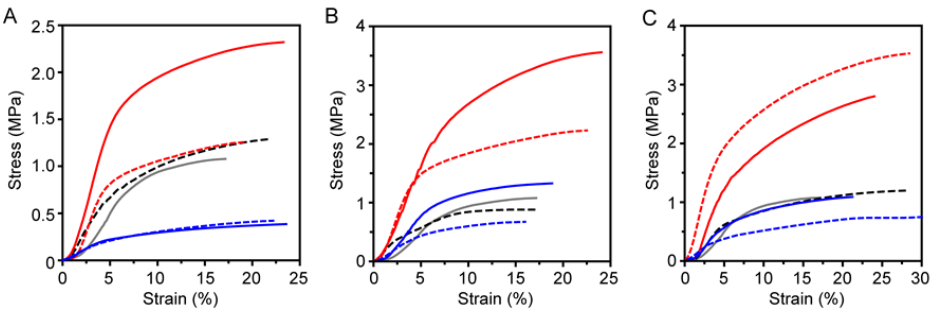

Figure 3. Representative stress/strain curves of a) polystyrene (grey), and its composites with (6,5)-SWNTs (dashed black), $MINT_{(6,5)}$-**1** (red), (6,5)-SWNTs·**1** (blue), $MINT_{(6,5)}$-**2** (dashed red) and (6,5)-SWNTs·**2** (dashed blue); b) polystyrene (grey), and its composites with pp-SWNTs (dashed black), $MINT_{(pp)}$-**1** (red), pp-SWNTs·**1** (blue), $MINT_{(pp)}$-**2** (dashed red) and pp-SWNTs·**2** (dashed blue); c) polystyrene (grey), and its composites with o-SWNTs (dashed black), $MINT_{(o)}$-**1** (red), o-SWNTs·**1** (blue), $MINT_{(o)}$-**2** (dashed red) and o-SWNTs·**2** (dashed blue).

Figure 3 displays stress/strain curves for reference polystyrene (grey) and the nanocomposites explored: with pristine SWNTs (black), SWNTs +

[15] S. Mazinani, A. Ajji, C. Dubois. *Polymer*, **2009,** *50*, 3329-3342.

macrocycle supramolecular complex (blue), and MINT (red) for all types of SWNTs. The MINT samples present substantially higher modulus, yield and tensile strengths than all control samples. Interestingly, in the supramolecular systems the macrocycle reduces dramatically both modulus and strength, suggesting that it acts as a plasticizer that weakens the SWNT/matrix interface. The traditional composite has similar tensile properties to the pure polystyrene matrix, including ductility. The implication is that at this low volume fraction even pure SWNTs are well dispersed, for otherwise in aggregated form they would most likely act as defects that would reduce ductility. This supports the view that the improvement in mechanical reinforcement obtained using the MINT strategy is due to a more efficient stress transfer across the SWNT/polymer interface (*vide infra*). The Young's moduli and tensile strengths of all samples are displayed in **Figure 4** and **Table S1**.

General trends are clearly evidenced. Firstly, the mechanical properties of fibers are only slightly reinforced by pristine SWNTs fillers. Secondly, the use of MINTs leads instead to a significant improvement of both the Young's modulus and the tensile strength in all samples, irrespective of the type of nanotube or macrocycle. Lastly, the supramolecular fillers have negligible or even detrimental effects on the mechanical properties of the polystyrene fibers. For instance, the samples in which pristine (6,5)-SWNTs were used as fillers showed a Young's modulus of (18 ± 1) MPa and a tensile strength of (1.26 ± 0.06) MPa, whereas the pure polystyrene fibers showed (15 ± 1) MPa and (1.09 ± 0.03) MPa, respectively. In contrast, the MINT$_{(6,5)}$-**1** samples showed (32 ± 6) MPa and (2.0 ± 0.3) MPa, that is, a remarkable improvement of 110 % in the Young's modulus and of 80 % in the tensile strength. Meanwhile, the supramolecular filler (6,5)-SWNTs·**1** yielded (7 ± 1) MPa and (0.39 ± 0.03) MPa as Young's modulus and tensile strength, respectively, which implies a variation of −53 % in the Young's modulus and of −64 % in the tensile strength with respect to the pristine polymer.

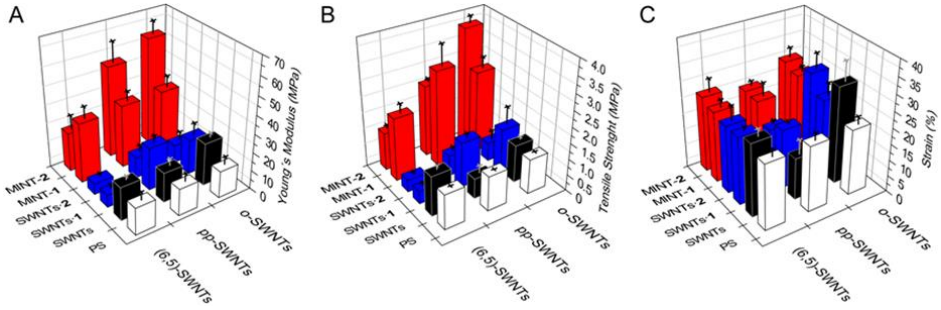

Figure 4. a) Young's modulus of polystyrene (white), SWNTs (black), supramolecular complexes (blue) and MINTs (red) with (6,5)-SWNTs (left), pp-SWNTs (center) and o-SWNTs (right); b) Tensile strength of polystyrene (white), SWNTs (black), supramolecular complexes (blue) and MINTs (red) with (6,5)-SWNTs (left), pp-SWNTs (center) and o-SWNTs (right); c) Strain of polystyrene (white), SWNTs (black), supramolecular complexes (blue) and MINTs (red) with (6,5)-SWNTs (left), pp-SWNTs (center) and o-SWNTs (right).

The trends for macrocycle **2** are identical, although with quantitatively smaller effects. In the case of pristine pp-SWNTs, we observed no significant variation in the Young's modulus and a decrease of −50 % in the tensile strength with respect to polystyrene. Meanwhile, the $MINT_{(pp)}$-**1** and $MINT_{(pp)}$-**2** fillers showed an increase of 130 % and 230 % in the Young's modulus and 170 % and 106 % in the tensile strength, respectively. The supramolecular models showed very small improvements in the case of macrocycle **1** and slightly detrimental effects for macrocycle **2**.

Finally, for the pristine o-SWNTs filled samples, the variation in Young's modulus with respect to polystyrene is of 53 % and of only 8 % in tensile strength. Again, the mechanically interlocked samples lead to a well-defined improvement, offering 130 % and 290 % variations in Young's modulus, and 140 % and 240 % increase in tensile strength for $MINT_{(o)}$-**1** and $MINT_{(o)}$-**2**,

respectively. Just like with the other types of nanotubes, the supramolecular fillers offered no improvements in the mechanical properties over pure polystyrene.

No significant changes were observed in the strain-to-break among samples with the same kind of nanotubes (**Figure 4c**).

Complex effects could be responsible for the improvement observed in the mechanical properties of the composites, including nanoscale friction at the polymer-nanocarbon interface.[16] In order to gain atomic understanding of our system, molecular dynamics (MD) simulations were performed using the AMBER force field,[17] which accounts for dispersion interactions. To mimic our experimental conditions as much as possible, MD calculations were carried out using a (6,5)-SWNT of 400 atoms, to ensure the same SWNT/macrocycle ratio measured experimentally. The polystyrene fiber consisted of 36 residues, which were introduced in a fully extended conformation to emulate the electrospinning conditions. Initial configuration of the composites and computational details are described in the Supporting Information. **Figure 5** shows the equilibrated structures of polystyrene, and its composites with SWNTs, SWNT·**1**, SWNT·**2**, MINT-**1** and MINT-**2**. Due to the flexible backbone, after 0.4 ns a highly-twisted, globular structure is adopted to maximize intramolecular interactions (**Figure 5a**). A similar picture dominates the first frames of the simulations with the nanotube fillers, until polymer-nanotube intermolecular interactions become relevant. Upon stabilization (after approximately 2 ns of simulation time, see the experimental section) we observe very clear differences between the various fillers. The pristine nanotubes allow polystyrene to adopt a globular structure, very similar to that found for pure polystyrene (**Figure 5b**). In the

[16] J. G. Vilhena, C. Pimentel, P. Pedraz, F. Luo, P. A. Serena, C. M. Pina, E. Gnecco, R. Pérez. *ACS Nano*, **2016,** *10*, 4288-4293; (b) K. S. K. Karuppiah, S. Sundararajan, Z.-H. Xu, X. Li. *Tribol. Lett.*, **2006,** *22*, 181-188.
[17] V. Hornak, R. Abel, A. Okur, B. Strockbine, A. Roitberg, C. Simmerling. *Proteins: Struct., Funct., Bioinf.*, **2006,** *65*, 712-725.

supramolecular controls, the fiber tries to maximize short contacts with both macrocycle and SWNT, which results in a slightly more distorted structure (**Figures 5c** and **5d**). Finally, in the MINT samples the positioning of the macrocycles around the nanotubes results in less surface available for interaction with the polystyrene fiber, which reacts by adopting a significantly more extended conformation in order to maximize noncovalent interactions with the SWNT (**Figures 5e** and **5f)**. As a quantitative metric for these observations, we measured the dihedral angles of the polystyrene backbone for each case for a total of 500 frames in the last nanosecond of our simulation (**Figure 5g**). An average of around 130º is found for the MINTs, compared to an average of 95º for the supramolecular compounds and approximately 105º for the polymer-SWNT model. The extended conformation of polystyrene according to MD simulations is more pronounced in the case of MINT-**1** when compared to MINT-**2**, while the results for the supramolecular models are fundamentally independent of the structure of the macrocycle, in direct correlation with experimental results. Polymer chain extension and orientation are established prerequisites to produce strong/stiff polymeric materials, for example in the form of high-performance fibres.[18] The MINT-induced polymer conformation extracted from MD simulations is in line with such arrangement and agrees with the higher degree of reinforcement observed for MINT-containing composites.

[18] (a) H. Staudinger. In *Die Hochmolekularen Organischen Verbindungen - Kautschuk und Cellulose,* **1932**; (b) W. H. Carothers, J. W. Hill. *J. Am. Chem. Soc.*, **1932,** *54*, 1579-1587.

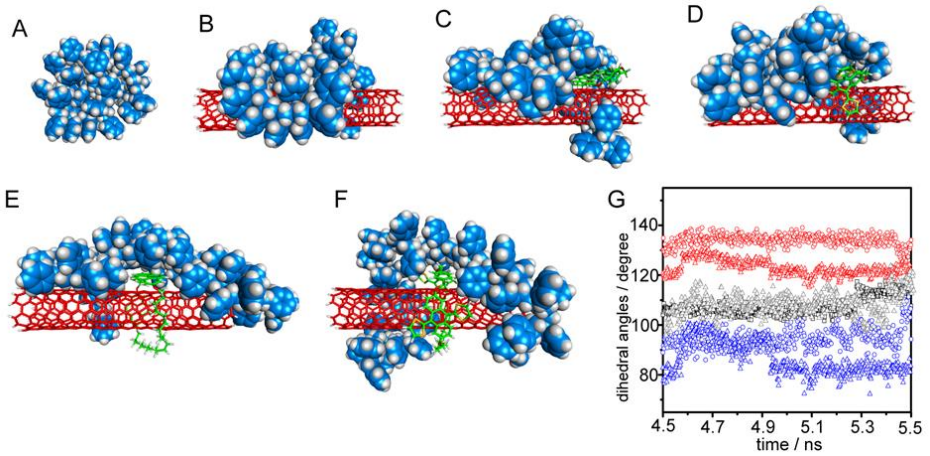

Figure 5. MD snapshots of a) Polystyrene, and its composites with b) SWNTs, c) SWNT·**1**, d) SWNT·**2**, e) MINT-**1**, and f) MINT-**2** after MD simulations. Carbon atoms are shown in red for the SWNTs, green for the macrocycles and cyan for polystyrene. Hydrogens are shown in white, oxygen in red and sulfur in yellow. g) Average dihedral angles of the polystyrene backbone for the last nanosecond of the MD simulation. Color code: polystyrene (grey triangle), and its composites with SWNTs (black square), SWNT·**1** (blue circle), SWNT·**2** (blue triangle), MINT-**1** (red circle), and MINT-**2** (red triangle).

6.3. Conclusions

In summary, we have shown that mechanical interlocking is a strategy to optimize the performance of SWNT fillers with regard to their mechanical properties. Very low loading of 0.01% results in improvement of the Young's modulus and tensile strength of the fibers of over 200%. In comparison, fillers with identical chemical composition but lacking the interlocked architectures showed negligible or even detrimental effects. Moreover, by using up to three different kinds of nanotubes, two macrocycles, and the corresponding supramolecular controls, we have demonstrated that the positive effect is general to the MINTs samples, as the trends hold in all cases under study. MD

simulations show that this effect originates from a superior ability of the MINT samples to induce extended conformation in the polystyrene fibers, which allows for an optimized transfer of stress between matrix and SWNTs.

6.4. Experimental section

(6,5)-enriched nanotubes were purchased from Sigma Aldrich Co. (0.7-0.9 nm in diameter, length ≥ 700 nm, mostly semiconducting, 95% purity), plasma-purified SWNTs (pp-SWNTs) were purchased from Cheap Tubes Inc. (0.8-1.6 nm in diameter, length 3-30 μm, mostly metallic, 99 % purity), and COOH functionalized SWNTs (o-SWNTs) were purchased from Cheap Tubes Inc. (0.8-1.6 nm in diameter, length 0.5-2.0 μm, mostly metallic, 99 % purity). Electrospinning was carried out using a commercially available Spraybase Electrospinning. Thermogravimetric analysis (TGA) was performed using a TA Instruments TGAQ500 with a ramp of 10 °C/min under air from 100 to 1000 °C. Scanning electron microscopy (SEM) micrographs were obtained in a Zeiss EVO HD15 operating at 5 kV. Ultraviolet-visible spectra was obtained in a Varian Cary 50 UV-Vis. Mechanical properties were determined using a dynamic mechanical analyzer (DMA Q800, TA Instruments). Each fibers sample (n = 3 specimens) was cut in 1cm x 4cm rectangular shapes with thickness between 0.15 and 0.18 mm. Stress−strain curves were recorded at a rate of 1 N min−1 (up to 18N).

Linear receptors and MINTs were synthesized as described in references 42-45. The nanotubes (10 mg) were suspended in 10 mL of tetrachloroethane (TCE) through sonication (10 min.) and mixed with linear precursors 1 and 2 (0.01 mmol), and Grubb's 2nd generation catalyst at room temperature for 72 hours. After this time, the suspension was filtered through a PTFE membrane of 0.2 μm pore size, and the solid washed profusely with dichloromethane (DCM). The solid was re-suspended in 10 mL of DCM through sonication for 10 min.

and filtered through a PTFE membrane of 0.2 µm pore size again. This washing procedure was repeated three times.

Composites were prepared by direct suspension of MINTs or pristine nanotubes in dimethylformamide (DMF) by sonication at 20ºC for 12 h and the suspensions were centrifuged at 13150 G for 15 minutes to obtain stable suspensions., following the addition of polystyrene (Mw average 350000) 30 % (w/w) and stirring for 12 hours. In the case of supramolecular samples, pristine nanotubes were suspended in the same conditions and preformed macrocycles were added before polystyrene and the mixture was stirred for 12 h. Concentrations of SWNTs, MINTs, and supramolecular models were matched using UV-Vis spectra at 450 nm of the suspension obtained. The prepared solutions were added to a syringe and pumped at 1 mL h^{-1} with a voltage of 14 kV and constant temperature and humidity. All samples were electrospun over a 10 cm diameter round collector to obtain randomly aligned fibers.

Characterization of MINTs samples

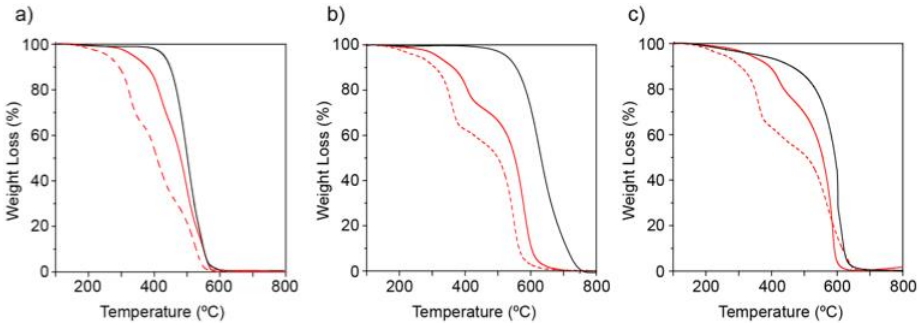

Figure S1. TGA analysis of: a) pristine (6,5)-SWNTs (black), $MINT_{(6,5)}$-**1** (red) and $MINT_{(6,5)}$-**2** (dashed red); b) pristine pp-SWNTs (black), $MINT_{(pp)}$-**1** (red) and $MINT_{(pp)}$-**2** (dashed red). TGAs were run in air at a heating rate of 10 ºC min^{-1}.

TGA of the solid thus obtained showed weight losses of 33% and 41% for MINT$_{(6,5)}$-**1** and MINT$_{(6,5)}$-**2**, 25% and 35% for MINT$_{(pp)}$-**1** and MINT$_{(pp)}$-**2** at approximately 400 °C and 26% and 36% for MINT$_{(pp)}$-**1** and MINT$_{(pp)}$-**2**.

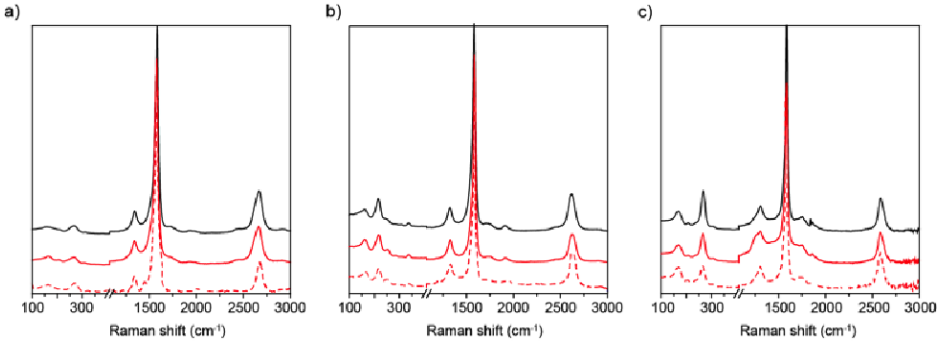

Figure S2. Raman spectra of o-SWNTs (black), MINT$_{(o)}$-**1** (red) and MINT$_{(o)}$-**2** (dashed red): a) λ_{exc} = 532 nm; b) λ_{exc} = 633 nm and c) λ_{exc} = 785 nm All spectra are the average of ten different measurements.

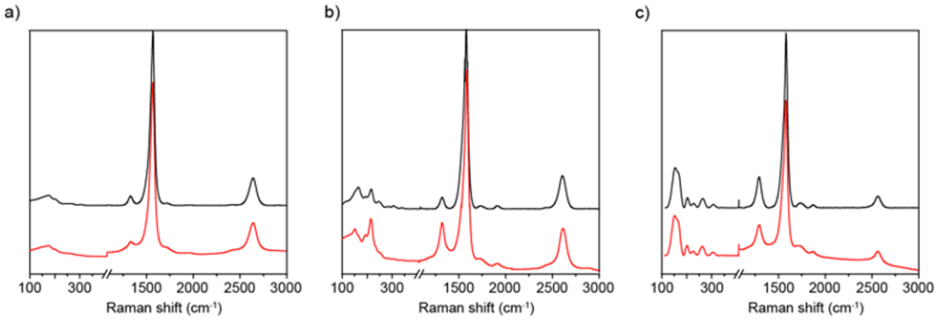

Figure S3. Raman spectra of pp-SWNTs (black) and MINT$_{(pp)}$-**1** (red): a) λ_{exc} = 532 nm; b) λ_{exc} = 633 nm and c) λ_{exc} = 785 nm All spectra are the average of ten different measurements.

Raman spectroscopy (**Figures S2** and S3, λ_{exc} = 532, 633, and 785 nm) reveals no changes in the spectra with respect to pristine pp-SWNTs and o-SWNTs, as expected for the noncovalent functionalization of SWNTs. In particular, we observed no significant increase in the I_D/I_G ratio and no modification in the RBM intensity, which confirmed that there is no covalent modification of the SWNTs.

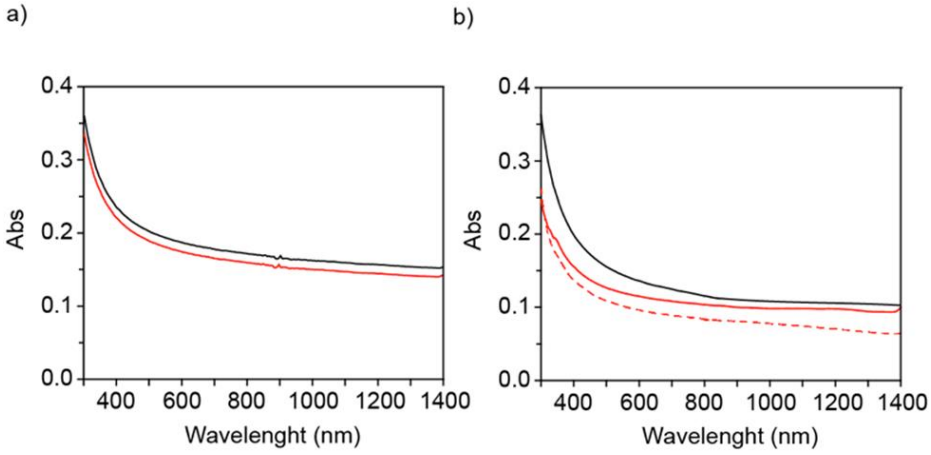

Figure S4. UV/Vis spectra (D_2O, 1% sodium dodecyl sulfate (SDS) , 298 K) of a) pristine pp- SWNTs (black) and $MINT_{(pp)}$-**1** (red); b) o-SWNTs (black), $MINT_{(o)}$-**1** (red) and $MINT_{(o)}$-**2** (dashed red).

In the absorption spectra (D_2O, 1% sodium dodecyl sulphate, 298 K, **Figure S4**), the UV region is dominated by the nanotube absorption in both samples, and the characteristic absorption of pyrenes and exTTF in the 300–350 nm and 300-450 nm range respectively is not distinguishable, save for an increase in the relative absorption in this region.

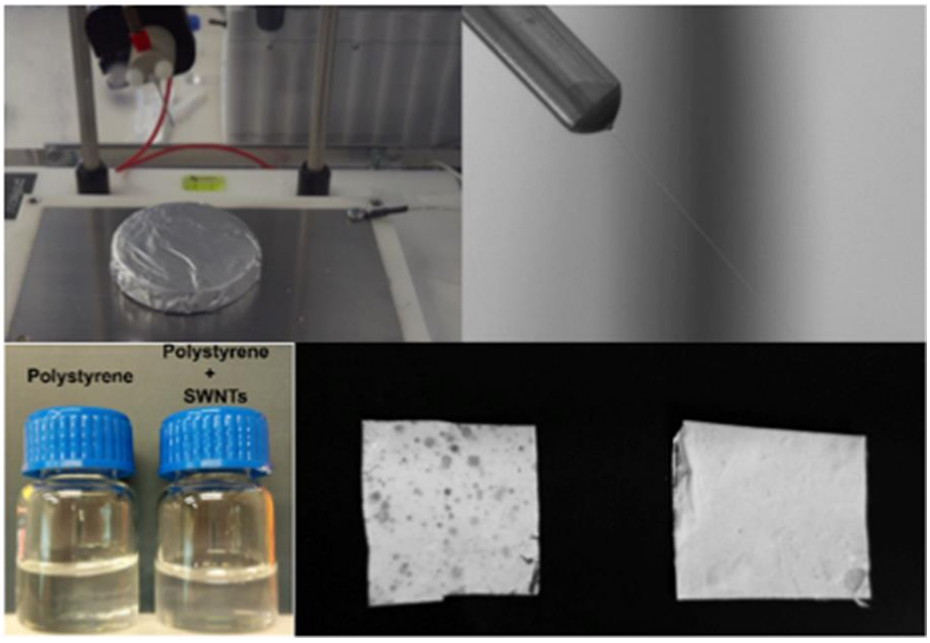

Figure S5. Top Left: Electrospinning setup. Top right: Fiber formation in the needle. Bottom left: Polystyrene and polystyrene/ SWNTs solutions in DMF. Bottom: Defective samples of fibers due to a high concentration of SWNTs (left) and a low fiber density.

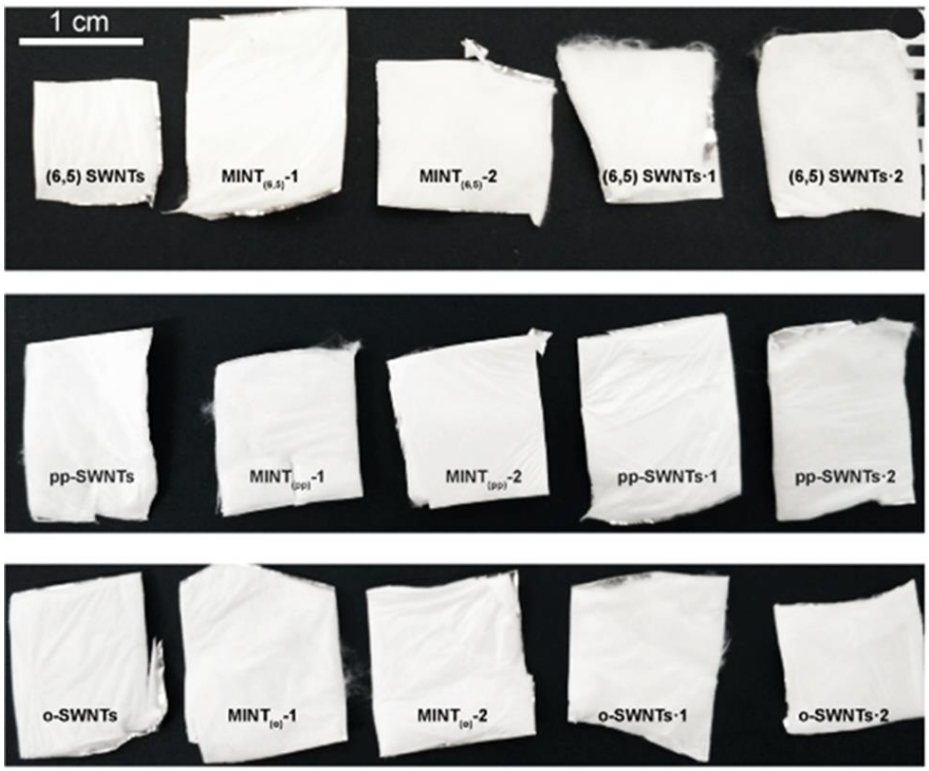

Figure S6. Samples of electrospun fibers. No macroscopic differences are observed.

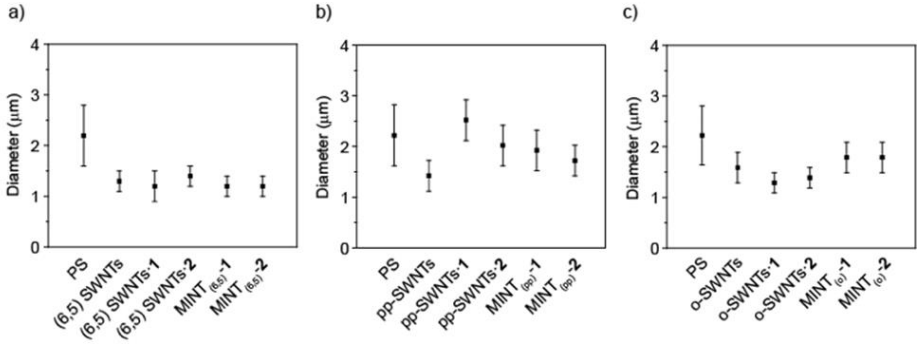

Figure S7. Diameter distribution of: a) (6,5) SWNTs samples; b) pp-SWNTs samples and c) o-SWNTs. Mean of 100 measurements.

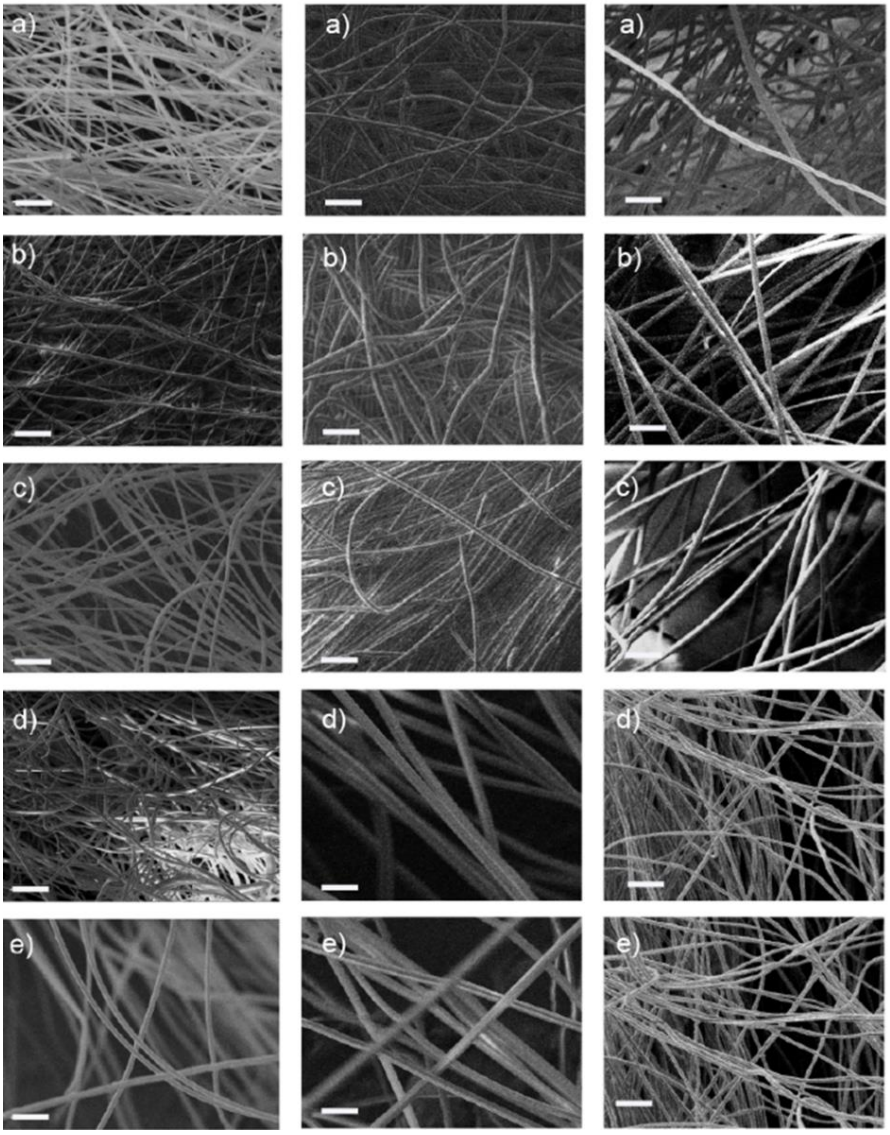

Figure S8. SEM images of (6,5)-SWNTs,pp-SWNTs and o-SWNTs samples. Left: a) (6,5)-SWNTs; b) $MINT_{(6,5)}$-**1**; c) $MINT_{(6,5)}$-**2**; d) (6,5) SWNTs-**1**; e) (6,5)-SWNTs-**2**. Center: a) pp-SWNTs; b) $MINT_{(pp)}$-**1**; c) $MINT_{(pp)}$-**2**; d) pp-SWNTs-**1**; e) pp-SWNTs-**2**. Right**:** a) o-SWNTs; b) $MINT_{(o)}$-**1**; c) $MINT_{(o)}$-**2**; d) o-SWNTs-**1**; e) o-SWNTs-**2.** Inset scale: 10 µm.

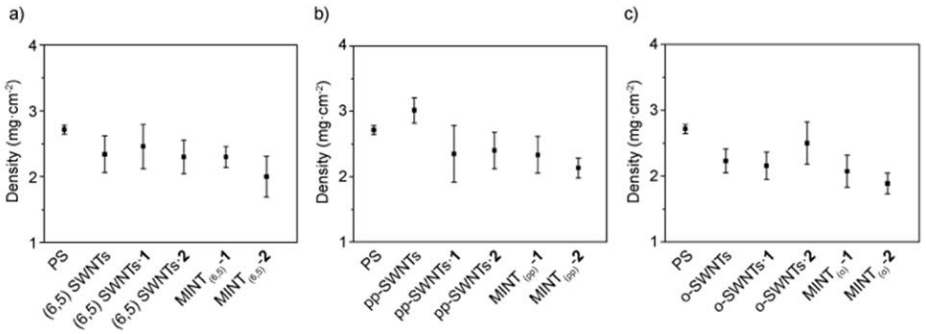

Figure S9. Fiber area density distribution: a) (6,5) SWNTs samples; b) pp-SWNTs samples and c) o-SWNTs. Mean of 7 measurements.

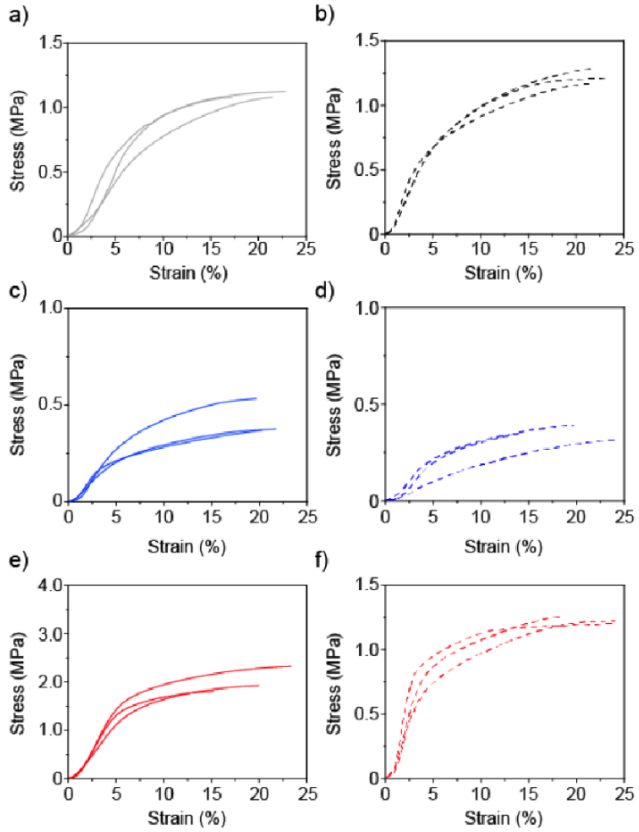

Figure S10. Stress/Strain curve of a) Polystyrene; b) (6,5)-SWNTs; c) (6,5)-SWNTs·**1**; d) (6,5)-SWNTs·**2**; e) $MINT_{(6,5)}$-**1** (red) f) $MINT_{(6,5)}$-**2**.

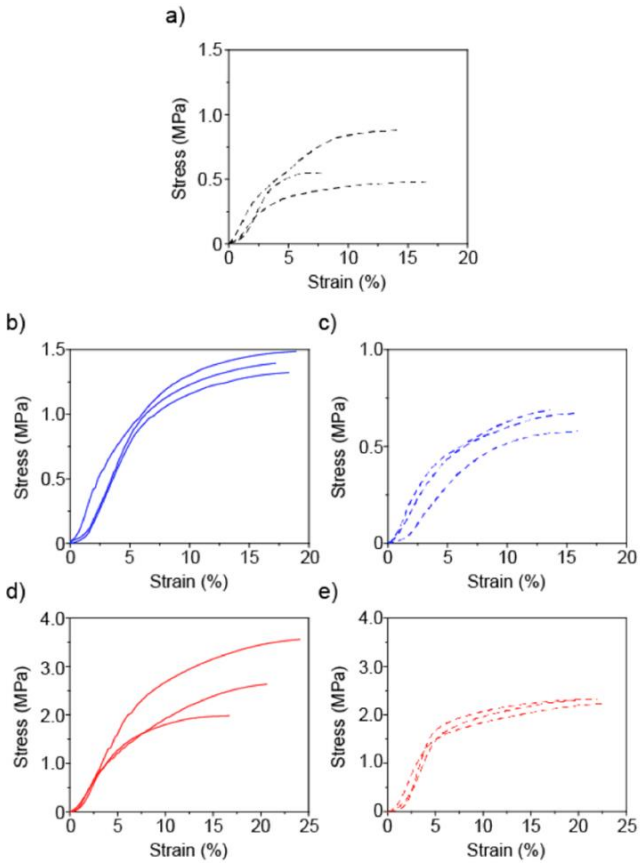

Figure S11. Stress/Strain curve of a) pp-SWNTs; b) pp-SWNTs·**1**; c) pp-SWNTs·**2**; d) $MINT_{(pp)}$-**1**; e) $MINT_{(pp)}$-**2**.

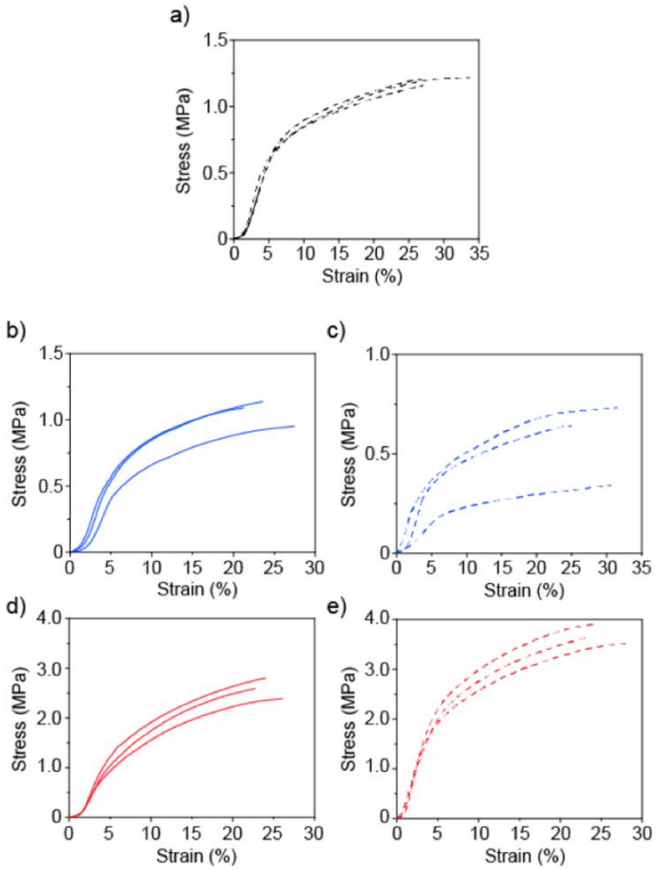

Figure S12. Stress/Strain curve of a) o-SWNTs; b) o-SWNTs·1; c) o-SWNTs·2; d) $MINT_{(o)}$-**1**; e) $MINT_{(o)}$-**2**.

Table S1. Young's Modulus and Tensile Strength in MPa of electrospun fibers.

Sample	Interaction	Young's Modulus/MPa	Tensile Strength/Mpa	Variation /%	
				YM respect PS	TS respect PS
Polystyrene (PS)	-	15±1	1.09±0.03	-	-
(6,5)-SWNTs	-	18±1	1.26±0.06	20	16
$MINT_{(6,5)}$-**1**	Mechanical bond	32±6	2.0±0.3	110	80
1·(6,5)-SWNTs	Supramolecular	7±1	0.39±0.03	-53	-60
$MINT_{(6,5)}$-**2**	Mechanical bond	21±7	1.18±0.08	40	8
2·(6,5)-SWNTs	Supramolecular	6±1	0.37±0.05	-60	-66
pp-SWNTs	-	16±3	0.6±0.2	7	-40
MINT(pp)-**1**	Mechanical bond	34±5	3.0±0.7	130	170
1·pp-SWNTs	Supramolecular	23±4	1.4±0.1	50	30
$MINT_{(pp)}$-**2**	Mechanical bond	50±12	2.25±0.05	230	106
2·pp-SWNTs	Supramolecular	11±3	0.65±0.06	-30	-40
o-SWNTs	-	23±2	1.18±0.02	50	8
$MINT_{(o)}$-**1**	Mechanical bond	35±6	2.6±0.3	130	140
1· o-SWNTs	Supramolecular	19±7	1.4±0.6	30	30
$MINT_{(o)}$-**2**	Mechanical bond	59±7	3.7±0.2	290	240
2· o-SWNTs	Supramolecular	10±4	0.6±0.2	-30	-40

Computational Methods

MD simulations were performed using AMBER 12 software package[19] for all calculations. Following the literature[20] the AMBER99 force field[21] was used to model the SWNT, the polymer and the macrocycles 1 and 2. For missing bonds, angle torsions, or Van Der Waals parameters not included in the AMBER99 force field, the values were transferred from the general AMBER force field (GAFF).[22] The initial structures were minimized using two cycles of

[19] T. A. D. D.A. Case, T.E. Cheatham, III, C.L. Simmerling, J. Wang, R.E. Duke, R., R. C. W. Luo, W. Zhang, K.M. Merz, B. Roberts, S. Hayik, A. Roitberg, G. Seabra,, A. W. G. J. Swails, I. Kolossváry, K.F. Wong, F. Paesani, J. Vanicek, R.M. Wolf, J. Liu,, S. R. B. X. Wu, T. Steinbrecher, H. Gohlke, Q. Cai, X. Ye, J. Wang, M.-J. Hsieh, G., D. R. R. Cui, D.H. Mathews, M.G. Seetin, R. Salomon-Ferrer, C. Sagui, V. Babin, T., S. G. Luchko, A. Kovalenko, and P.A. Kollman. **2012**, *AMBER 12, University of California, San Francisco.*

[20] (a) G. Hummer, J. C. Rasaiah, J. P. Noworyta. *Nature,* **2001,** *414,* 188-190; (b) R. R. Johnson, A. T. C. Johnson, M. L. Klein. *Nano Lett.*, **2008,** *8*, 69-75.

[21] V. Hornak, R. Abel, A. Okur, B. Strockbine, A. Roitberg, C. Simmerling. *Proteins: Struct., Funct., Bioinf.s,* **2006,** *65*, 712-725.

[22] J. Wang, R. M. Wolf, J. W. Caldwell, P. A. Kollman, D. A. Case. *J. Comput. Chem.*, **2004,** *25*, 1157-1174.

conjugated gradient minimization. During the initial cycle, the SWNT was kept in their starting conformation using a harmonic constrains with a force constant of 500 Kcal/mol·Å. This was followed by another minimization cycle where the SWNT was kept a harmonic restraint force constant of 10 Kcal/mol·Å. To allow a slow relaxation of the systems: SWNT-polymer, supramolecular 1 and 2, MINT **1** and **2**, the minimized structures was heated slowly from 0 to 300 K during 0.5 ns (using a 2 fs time step) under of constant-pressure-constant-temperature conditions (NPT). Finally, we carried out 5.0 ns (using a 2 fs time step) of MD simulation in NPT ensemble to equilibrate the system at 300 k. The positions of all SWNT atoms were constrained with a weak 10 Kcal/mol·Å harmonic potential during all MD simulation. In the **Figure S13** we show the calculated potential energy for all studied systems. We observe how the energy increases during the first few ps, corresponding to our heating process form 0 k to 300k, then the energy remains constant and the equilibrium was considered to be reached. Analysis and visualization of MD trajectories were performed with VMD software.[23] In the **Figure S14** we show the initial and the final state of the molecular dynamic simulations conducted.

[23] M. Karplus, J. A. McCammon. *Nat. Struct. Mol. Biol.*, **2002,** *9*, 646-652.

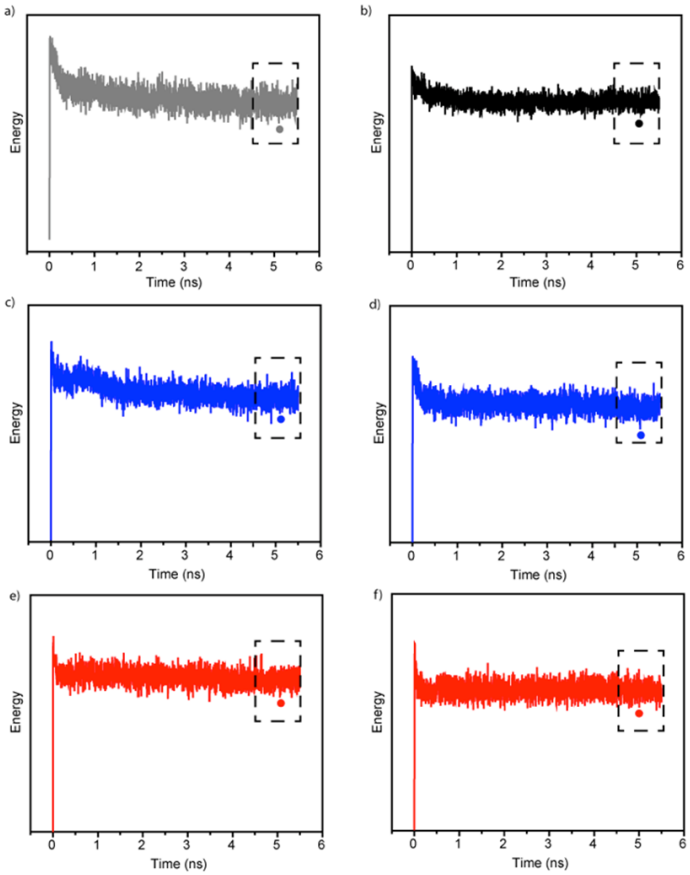

Figure S13. Stabilization energy of a) PS, and its composites with b) SWNTs, c) SWNT·**1**, d) SWNT·**2**, e) MINT-**1** and f) MINT-**2** during the 5.5 ns of MD simulations. The circles indicate the chosen structure for the figure 5. The dashed rectangles remark the chosen snap for the dihedral angle analysis.

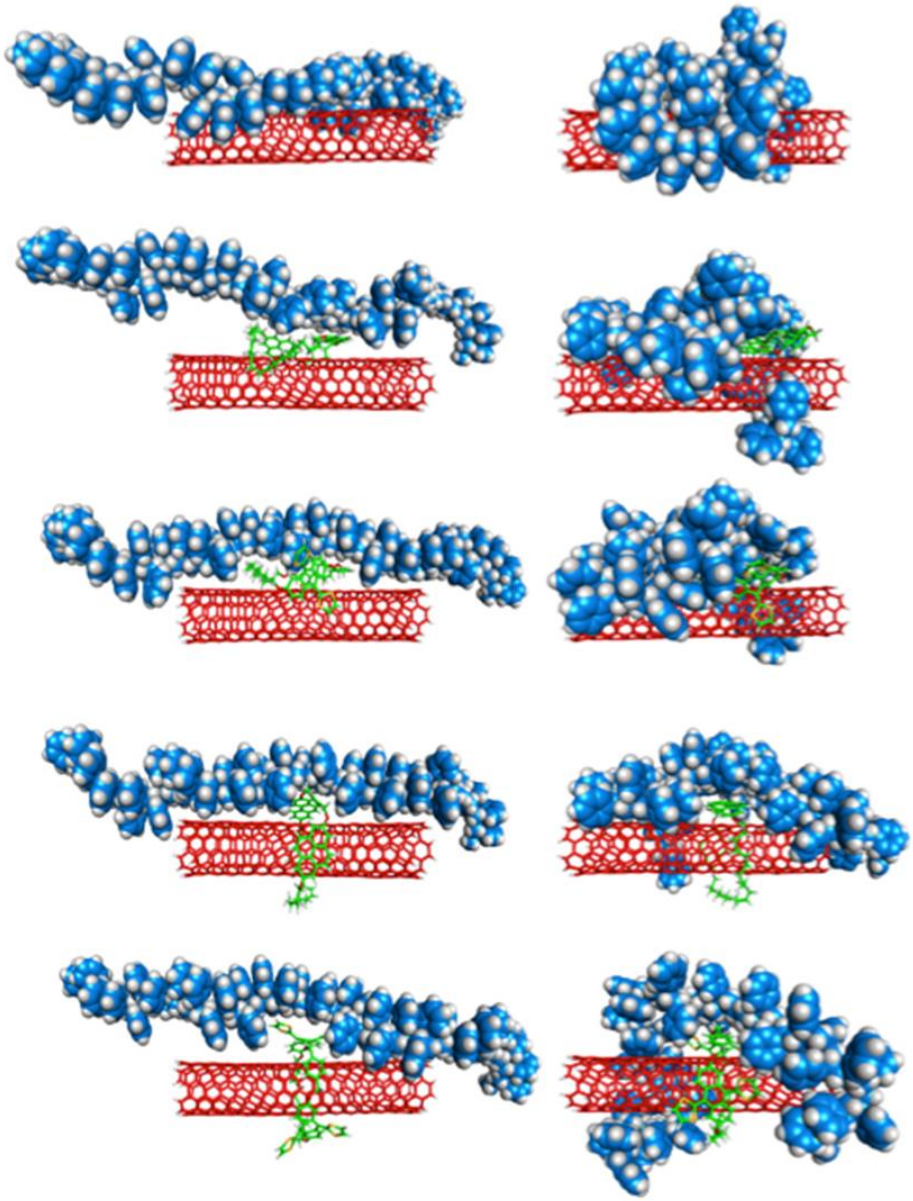

Figure S14. Initial and final state of the MD simulation for the five studied composites.

6.5. References

1. P. M. Ajayan, O. Stephan, C. Colliex, D. Trauth. Aligned Carbon Nanotube Arrays Formed by Cutting a Polymer Resin—Nanotube Composite. *Science*, **1994,** *265*, 1212-1214.

2. (a) E. T. Thostenson, Z. Ren, T. W. Chou. Advances in the science and technology of carbon nanotubes and their composites: a review. *Compos. Sci. Technol.*, **2001,** *61*, 1899-1912; (b) O. Breuer, U. Sundararaj. Big returns from small fibers: A review of polymer/carbon nanotube composites. *Polym. Compos.*, **2004,** *25*, 630-645; (c) P. J. F. Harris. Carbon nanotube composites. *Int. Mater. Rev.*, **2004,** *49*, 31-43; (d) J. N. Coleman, U. Khan, W. J. Blau, Y. K. Gun'ko. Small but strong: A review of the mechanical properties of carbon nanotube–polymer composites. *Carbon*, **2006,** *44*, 1624-1652; (e) C. Li, E. T. Thostenson, T.-W. Chou. Sensors and actuators based on carbon nanotubes and their composites: A review. *Compos. Sci. Technol.*, **2008,** *68*,1227-1249; (f) B. Arash, Q. Wang, V. K. Varadan. Mechanical properties of carbon nanotube/polymer composites. *Sci. Rep.*, **2014,** *4*, 6479; (g) Y. Liu, S. Kumar. Polymer/Carbon Nanotube Nano Composite Fibers–A Review. *ACS Appl. Mater. Interfaces*, **2014,** *6*, 6069-6087; (h) J. J. Vilatela. Nanocarbon-based composites. In *Nanocarbon-Inorganic Hybrids: Next Generation Composites for Sustainable Energy Applications*,E. Dominik R. Schlögl, De Gruyter-GmbH: Berlin, **2014**, pp 227-254. (i) W. Kong, L. Sun, Y. Wu, K. Jiang, Q. Li, J. Wang, S. Fan. Binder-free polymer encapsulated sulfur-carbon nanotube composite cathodes for high performance lithium batteries. *Carbon*, **2016,** *96*, 1053-1059; (j) G. Liu, Q.-D. Ling, E. Y. H. Teo, C.-X. Zhu, D. S.-H. Chan, K.-G. Neoh, E.-T. Kang. Electrical Conductance Tuning and Bistable Switching in Poly(N-vinylcarbazole)−Carbon Nanotube Composite Films. *ACS Nano*, **2009,** *3*, 1929-1937; (k) Li, F. Gittleson, M. Carmo, R. C. Sekol, A. D. Taylor. Scalable Fabrication of Multifunctional Freestanding Carbon Nanotube/Polymer Composite Thin Films for Energy Conversion. *ACS Nano*, **2012,** *6*, 1347-1356; (l) S. N. Habisreutinger, T. Leijtens, G. E. Eperon, S. D. Stranks, R. J. Nicholas, H. J. Snaith. Carbon Nanotube/Polymer Composites as a Highly Stable Hole Collection Layer in Perovskite Solar Cells. *Nano Lett.*, **2014,** *14*, 5561-5568; (m) J. Zhu, W. Cao, M. Yue, Y. Hou, J. Han, M. Yang. Strong and Stiff Aramid Nanofiber/Carbon Nanotube Nanocomposites. *ACS Nano*, **2015,** *9*, 2489-2501; (n) Y. Wang, M. Li, Y. Gu, X. Zhang, S. Wang, Q. Li, Z. Zhang. Tuning carbon nanotube assembly for flexible, strong and conductive films. *Nanoscale*, **2015,** *7*, 3060-3066; (o) T. R. Fadel, F. A. Sharp, N. Vudattu, R. Ragheb, J. Garyu, D. Kim, E. Hong, N. Li, G. L. Haller, L. D. Pfefferle, S. Justesen, K. C. Herold, T. M. Fahmy. A carbon nanotube–polymer composite for T-cell therapy. *Nat. Nanotechnol.*, **2014,** *9*, 639-647.

3. (a) J. Gao, M. E. Itkis, A. Yu, E. Bekyarova, B. Zhao, R. C. Haddon. Continuous Spinning of a Single-Walled Carbon Nanotube−Nylon Composite Fiber. *J. Am. Chem. Soc.*, **2005,** *127*, 3847-3854; (b) R. Sen, B. Zhao, D. Perea, M. E. Itkis, H. Hu, J. Love, E. Bekyarova, R. C. Haddon. Preparation of Single-Walled Carbon Nanotube Reinforced

Polystyrene and Polyurethane Nanofibers and Membranes by Electrospinning. *Nano Lett.*, **2004,** *4*, 459-464.
4. (a) J. N. Coleman, U. Khan, Y. K. Gun'ko. Mechanical Reinforcement of Polymers Using Carbon Nanotubes. *Adv. Mater.*, **2006,** *18*, 689-706; (b) X. Sun, H. Sun, H. Li, H. Peng. Developing Polymer Composite Materials: Carbon Nanotubes or Graphene?, *Adv. Mater.*, **2013,** *25*, 5153-5176.
5. (a) J. F. Stoddart. The chemistry of the mechanical bond. *Chem. Soc. Rev.*, **2009,** *38*, 1802-1820; (b) E. A. Neal, S. M. Goldup. Chemical consequences of mechanical bonding in catenanes and rotaxanes: isomerism, modification, catalysis and molecular machines for synthesis. *Chem. Commun.*, **2014,** *50*, 5128-5142.
6. (a) J. Berná, G. Bottari, A. Leigh David, M. Pérez Emilio. Amide-based molecular shuttles (2001-2006). *Pure Appl. Chem.*, **2007**, *79*, 39-54; (b) E. R. Kay, D. A. Leigh, F. Zerbetto. Synthetic Molecular Motors and Mechanical Machines. *Angew. Chem. Int. Ed.*, **2007,** *46*, 72-191; (c) A. Credi, M. Venturi, V. Balzani. Light on Molecular Machines. *ChemPhysChem*, **2010,** *11*, 3398-3403; (d) J.-P. Sauvage, J.-P. Collin, S. Durot, J. Frey, V. Heitz, A. Sour, C. Tock. From chemical topology to molecular machines. *C. R. Chim.*, **2010,** *13*, 315-328; (e) C. J. Bruns, J. F. Stoddart. Rotaxane-Based Molecular Muscles. *Acc. Chem. Res.*, **2014,** *47*, 2186-2199; (f) F. Niess, V. Duplan, J.-P. Sauvage. Molecular Muscles: From Species in Solution to Materials and Devices. *Chem. Lett.*, **2014,** *43*, 964-974; (g) E. R. Kay, D. A. Leigh. Rise of the Molecular Machines. *Angew. Chem. Int. Ed.*, **2015,** *54*, 10080-10088; (h) S. Erbas-Cakmak, D. A. Leigh, C. T. McTernan, A. L. Nussbaumer. Artificial Molecular Machines. *Chem. Rev.*, **2015,** *115*, 10081-10206.
7. (a) L. Fang, M. A. Olson, D. Benítez, E. Tkatchouk, W. A. Goddard, III, J. F. Stoddart. Mechanically bonded macromolecules. *Chem. Soc. Rev.*, **2010,** *39*, 17-29; (b) R. Dong, Y. Zhou, X. Huang, X. Zhu, Y. Lu, J. Shen. Functional Supramolecular Polymers for Biomedical Applications. *Adv. Mater.*, **2015,** *27*, 498-526; (c) H. W. Gibson, M. C. Bheda, P. T. Engen. Rotaxanes, Catenanes, Polyrotaxanes, Polycatenanes and Related Materials. *Prog. Polym. Sci.*, **1994,** *19*, 843-945; (d) T. Takata, N. Kihara, Y. Furusho. *Polyrotaxanes and Polycatenanes: Recent Advances in Syntheses and Applications of Polymers Comprising of Interlocked Structures*. Springer: Berlin, **2004**; pp 1-75; (e) F. Huang, H. W. Gibson. Polypseudorotaxanes and Polyrotaxanes. *Prog. Polym. Sci.*, **2005,** *30*, 982-1018; (f) J. P. Coelho, G. González-Rubio, A. Delices, J. O. Barcina, C. Salgado, D. Ávila, O. Pena-Rodríguez, G. Tardajos, A. Guerrero-Martínez. Polyrotaxane-Mediated Self-Assembly of Gold Nanospheres into Fully Reversible Supercrystals. *Angew. Chem., Int. Ed.*, **2014,** *53*, 12751-12755; (g) I.-H. Park, R. Medishetty, J.-Y. Kim, S. S. Lee, J. J. Vittal. Distortional Supramolecular Isomers of Polyrotaxane Coordination Polymers: Photoreactivity and Sensing of Nitro Compounds. *Angew. Chem. Int. Ed.*, **2014,** *53*, 5591-5595; (h) D. Montarnal, N. Delbosc, C. Chamignon, M.-A. Virolleaud, Y. Luo, C. J. Hawker, E. Drockenmuller, J. Bernard. Highly Ordered Nanoporous Films from Supramolecular Diblock Copolymers with Hydrogen-Bonding Junctions. *Angew. Chem. Int. Ed.*, **2015,** *54*, 11117-11121; (i) A. Goujon, G. Du, E.

Moulin, G. Fuks, M. Maaloum, E. Buhler, N. Giuseppone. Hierarchical Self-Assembly of Supramolecular Muscle-Like Fibers. *Angew. Chem. Int. Ed*., **2016**, *55*, 703-707.
8. (a) X. Tao, J. Liu, G. Koley, X. Li. B/SiO_x Nanonecklace Reinforced Nanocomposites by Unique Mechanical Interlocking Mechanism. *Adv. Mater.*, **2008,** *20*, 4091-4096; (b) H. Ni, X. Li. Self-assembled composite nano-/micronecklaces with SiO_2 beads in boron strings. *Appl. Phys. Lett.*, **2006,** *89*, 053108.
9. (a) A. de Juan, Y. Pouillon, L. Ruiz-González, A. Torres-Pardo, S. Casado, N. Martín, Á. Rubio, E. M. Pérez. Mechanically Interlocked Single-Wall Carbon Nanotubes. *Angew. Chem. Int. Ed.*, **2014,** *53*, 5394-5400; (b) A. de Juan, M. Mar Bernal, E. M. Pérez. Optimization and Insights into the Mechanism of Formation of Mechanically Interlocked Derivatives of Single-Walled Carbon Nanotubes. *ChemPlusChem*, **2015,** *80*, 1153-1157; (c) A. López-Moreno, E. M. Pérez. Pyrene-based mechanically interlocked SWNTs. *Chem. Commun.*, **2015,** *51*, 5421-5424; (d) E. Martínez-Periñan, A. de Juan, Y. Pouillon, C. Schierl, V. Strauss, N. Martín, Á. Rubio, D. M. Guldi, E. Lorenzo, E. M. Pérez. The mechanical bond on carbon nanotubes: diameter-selective functionalization and effects on physical properties. *Nanoscale*, **2016,** *8*, 9254-9264.
10. (a) A. de Juan, A. López-Moreno, J. Calbo, E. Ortí, E. M. Pérez. Determination of association constants towards carbon nanotubes. *Chem. Sci.*, **2015,** *6*, 7008-7014; (b) A. Wurl, S. Goossen, D. Canevet, M. Sallé, E. M. Pérez, N. Martín, C. Klinke. Supramolecular Interaction of Single-Walled Carbon Nanotubes with a Functional TTF-Based Mediator Probed by Field-Effect Transistor Devices. *J. Phys. Chem. C*, **2012,** *116*, 20062-20066; (c) E. M. Pérez, B. M. Illescas, M. Á. Herranz, N. Martín. Supramolecular chemistry of π-extended analogues of TTF and carbon nanostructures. *New J. Chem.*, **2009,** *33*, 228-234; (d) C. Romero-Nieto, R. García, M. Á. Herranz, C. Ehli, M. Ruppert, A. Hirsch, D. M. Guldi, N. Martín. Tetrathiafulvalene-Based Nanotweezers—Noncovalent Binding of Carbon Nanotubes in Aqueous Media with Charge Transfer Implications. *J. Am. Chem. Soc.*, **2012,** *134*, 9183-9192.
11. (a) D. B. Amabilino, L. Pérez-García. Topology in molecules inspired, seen and represented. *Chem. Soc. Rev.*, **2009,** *38*, 1562-1571; (b) E. Griffiths Kirsten, J. F. Stoddart. Template-directed synthesis of donor/acceptor [2]catenanes and [2]rotaxanes. *Pure Appl. Chem.*, **2008,** *80*, 485-506.
12. A. de Juan, E. M. Pérez. Getting tubed: mechanical bond in endohedral derivatives of carbon nanotubes?, *Nanoscale*, **2013,** *5*, 7141-7148.
13. (a) F. Ko, Y. Gogotsi, A. Ali, N. Naguib, H. Ye, G. L. Yang, C. Li, P. Willis. Electrospinning of Continuous Carbon Nanotube-Filled Nanofiber Yarns. *Adv. Mater.*, **2003,** *15*, (14), 1161-1165; (b) H. Hou, J. J. Ge, J. Zeng, Q. Li, D. H. Reneker, A. Greiner, S. Z. D. Cheng. Electrospun Polyacrylonitrile Nanofibers Containing a High Concentration of Well-Aligned Multiwall Carbon Nanotubes. *Chem. Mater.*, **2005,** *17*, 967-973; (c) Y. Dror, W. Salalha, R. L. Khalfin, Y. Cohen, A. L. Yarin, E. Zussman. Carbon Nanotubes Embedded in Oriented Polymer Nanofibers by Electrospinning. *Langmuir*, **2003,** *19*, 7012-7020.

14. V. Fasano, M. Baroncini, M. Moffa, D. Iandolo, A. Camposeo, A. Credi, D. Pisignano. Organic Nanofibers Embedding Stimuli-Responsive Threaded Molecular Components. *J. Am. Chem. Soc.*, **2014,** *136*, 14245-14254.
15. S. Mazinani, A. Ajji, C. Dubois. Morphology, structure and properties of conductive PS/CNT nanocomposite electrospun mat. *Polymer*, **2009,** *50*, 3329-3342.
16. (a) J. G. Vilhena, C. Pimentel, P. Pedraz, F. Luo, P. A. Serena, C. M. Pina, E. Gnecco, R. Pérez. Atomic-Scale Sliding Friction on Graphene in Water. *ACS Nano*, **2016,** *10*, 4288-4293; (b) K. S. K. Karuppiah, S. Sundararajan, Z.-H. Xu, X. Li. The effect of protein adsorption on the friction behavior of ultra-high molecular weight polyethylene. *Tribol. Lett.*, **2006,** *22*, 181-188.
17. V. Hornak, R. Abel, A. Okur, B. Strockbine, A. Roitberg, C. Simmerling. Comparison of multiple Amber force fields and development of improved protein backbone parameters. *Proteins: Struct., Funct., Bioinfo.*, **2006,** *6*), 712-725.
18. (a) H. Staudinger. In Die Hochmolekularen Organischen Verbindungen - Kautschuk und Cellulose; Springer: Berlin, Heidelberg, 1932; (b) W. H. Carothers, J. W. Hill. Studies of polymerization and ring formation. XV. Artificial fibers from synthetic linear condensation superpolymers. *J. Am. Chem. Soc.*, **1932,** *54*, 1579-1587.
19. T. A. D. D.A. Case, T.E. Cheatham, III, C.L. Simmerling, J. Wang, R.E. Duke, R., R. C. W. Luo, W. Zhang, K.M. Merz, B. Roberts, S. Hayik, A. Roitberg, G. Seabra,, A. W. G. J. Swails, I. Kolossváry, K.F. Wong, F. Paesani, J. Vanicek, R.M. Wolf, J. Liu,, S. R. B. X. Wu, T. Steinbrecher, H. Gohlke, Q. Cai, X. Ye, J. Wang, M.-J. Hsieh, G., D. R. R. Cui, D.H. Mathews, M.G. Seetin, R. Salomon-Ferrer, C. Sagui, V. Babin, T., S. G. Luchko, A. Kovalenko, and P.A. Kollman. **2012**, *AMBER 12, University ofCalifornia, San Francisco.*
20. (a) G. Hummer, J. C. Rasaiah, J. P. Noworyta. Water conduction through the hydrophobic channel of a carbon nanotube. *Nature*, **2001,** *414*, 188-190; (b) R. R. Johnson, A. T. C. Johnson, M. L. Klein. Probing the Structure of DNA−Carbon Nanotube Hybrids with Molecular Dynamics. *Nano Lett.*, **2008,** *8*, 69-75.
21. J. Wang, R. M. Wolf, J. W. Caldwell, P. A. Kollman, D. A. Case. Development and testing of a general amber force field. *J. Comput. Chem.*, **2004,** *25*, 1157-1174.
22. M. Karplus, J. A. McCammon. Molecular dynamics simulations of biomolecules. *Nat. Struct. Mol. Biol.*, **2002,** *9*, 646-652.

CONCLUSIONS

7. Conclusions

i. We have described a method of oxidation of pyrene and other small PAHs, achieving comparable results to other catalytic methods and harsh oxidation procedures. We studied the electron accepting properties of 1,6- and 1,8-pyrenequinones both experimentally and theoretically. We determined that pyrenquinones are better electron acceptor than *p*-benzoquinone.

ii. We have described a method for the determination of association constants between soluble molecules and insoluble and heterogeneous materials. The method is based on the quantitative measurement of the concentration of free host, using TGA, so any host molecule can be evaluated without any approximation.

iii. We have synthesised new U-shaped precursors based on pyrene derivatives and have proven that pyrene templates the RCM of macrocycles around SWNTs to form MINTs, through an extensive characterization with analytical, spectroscopic and microscopic techniques.

iv. We studied the mechanical properties of polystyrene fibers doped with MINTs based on pyrene and exTTF, and we compared these properties with pristine carbon nanotubes and supramolecular derivatives. We incorporated the pristine or modified carbon nanotubes and prepared membranes through electrospinning. Very low loading of 0.01% of MINTs results in improvement of the Young's modulus and tensile strength of the fibers of over 200%. In comparison, fillers with identical chemical composition but lacking the interlocked architectures showed negligible or even detrimental effects.

7. Conclusiones

i. Hemos descrito un método de oxidación de pireno y otros hidrocarburos policíclicos aromáticos, consiguiendo resultados comparables a otros métodos catalíticos u oxidaciones. Además, hemos estudiado las propiedades electroaceptoras de 1,6- and 1,8-pirenequinonas experimental y teóricamente, llegando a determinar que las pirenoquinonas son mejores electroaceptoras que la *p*-benzoquinona.

ii. Hemos descrito un método para determinar constantes de asociación entre moléculas solubles y materiales insolubles y heterogéneos. El método está basado en la medida cuantitativa de la concentración de molécula libre usando TGA, por lo que cualquier molécula puede ser estudiada.

iii. Hemos sintetizado nuevos receptores basados en derivados de pireno y hemos demostrado, mediante una amplia caracterización, que se pueden usar para llevar a cabo la síntesis de nanotubos enlazados mecánicamente mediante una reacción de cierre de anillo.

iv. Hemos estudiado las propiedades mecánicas de MINT basados en pireno y exTTF y las hemos comparado con las de nanotubos de carbono sin modificar y con los complejos supramoleculares correspondientes. Incorporando una pequeña carga (0.01%) de estos tubos a fibras de poliestireno mediante electrospinning se han alcanzado mejoras de hasta un 200% para los MINT. Por el contrario, las muestras preparadas con los complejos supramoleculares, con idéntica composición pero sin las estructuras enlazadas, no presentan mejoras o incluso producen efectos negativos.